Naval Research Laboratory
Washington, DC 20375-5320 NRL/PU/5230--97-320 April 1997

1997 NRL REVIEW

THE NAVY'S CORPORATE LABORATORY –

PROMOTING DISCOVERIES

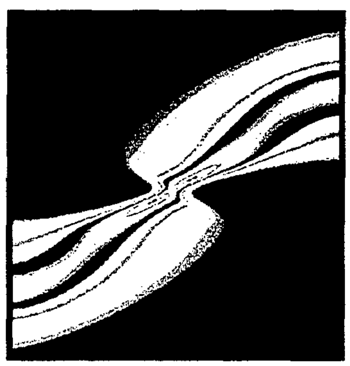

AND SCIENTIFIC ADVANCES

FOR THE NAVAL FORCES OF THE FUTURE

This *1997 NRL Review* introduces you to the Naval Research Laboratory — the Navy's Corporate Laboratory — and focuses on research highlights from fiscal year 1996. In addition, it presents the special honors awarded to NRL employees and describes the programs available to NRL and non-NRL employees. This publication offers an exchange of information among scientists, engineers, scholars, and managers, and it is used as a recruiting tool.

As you read the *NRL Review*, you will become even more aware that the Naval Research Laboratory comprises a dynamic team of scientists, engineers, and support personnel working together to promote the programs that will continue to foster discoveries and scientific advances for the Navy of the future.

General information on the research described in this *NRL Review* may be obtained from the Public Affairs Office, Code 1230, (202) 767-2541. Information concerning Technology Transfer is available from Dr. Richard Rein, head of the Technology Transfer Office, Code 1004, (202) 767-7230. The sources of information on the various nonresearch programs at NRL are listed in the chapter entitled "Programs for Professional Development."

For additional information about NRL, the *Fact Book* lists the organization, key personnel, and major facilities for each division. Further, it contains information about Laboratory funding, programs, and field sites. A copy of the *Fact Book* may be obtained by contacting the Technical Information Division, Publications Branch, Code 5230, (202) 767-2782.

NRL's URL: http://www.nrl.navy.mil/

Cover photo captions (top to bottom):

The temperature field in a turbulent flow beneath a free surface determined from a three-dimensional computer simulation. *Remote Sensing Division*

Table Top Terawatt (T^3) laser system. *Plasma Physics Division*

Spectrum of electronic excitations in a novel metallic state. Color indicates spectral weight and reveals features that reflect an evolving antiferromagnetic state. *Condensed Matter and Radiation Sciences Division*

Col. Tom Leary, Commanding Officer of the Special Purpose Marine Air-Ground Task Force (Experimental) receives training on the Virtual Reality Lab's Virtual Workbench, which was used in Sea Dragon, in the Hunter Warrior exercise. *Information Technology Division*

Quick Reference Telephone Numbers

	NRL Washington	NRL-SSC	NRL-Monterey	NRL CBD
Hotline	(202) 767-6543	(601) 688-5001	(408) 656-4721	(202) 767-6543
Personnel Locator	(202) 767-3200	(601) 688-3390	(408) 656-4731	(410) 257-4000
DSN	297- or 754-	485	878	—
Direct-in-Dialing	767- or 404-	688	656	257
Public Affairs	(202) 767-2541	(601) 688-5328	(408) 656-4708	—

Additional telephone numbers are listed on page 233.

The Navy Unit Commendation

1997 NRL Review

The Navy Unit Commendation was awarded by The Honorable John H. Dalton, Secretary of the Navy, jointly to the military and civilian personnel of NRL and its parent organization, the Office of Naval Research. The award was presented for "unparalleled research and development that significantly contributed to the technological capabilities of current and future Naval forces" during the period January 1992 through July 1996. This award, an unusual distinction for an acquisition activity, further states they "have developed programs that have shaped every aspect of our Naval forces today and are defining the Navy and Marine Corps of the future." Further, they "consistently ensured that the Department of the Navy is at the forefront of scientific knowledge, technology development, and application."

Naval Research Laboratory
Washington, DC 20375-5320

1997 NRL Review

CONTENTS

Preceding Page's Blank

SIMULATION, COMPUTING, AND MODELING

SPACE RESEARCH AND SATELLITE TECHNOLOGY

SPECIAL AWARDS AND RECOGNITION

PROGRAMS FOR PROFESSIONAL DEVELOPMENT

GENERAL INFORMATION

NRL

The Navy's Corporate Laboratory

Mission

To conduct a broadly based multidisciplinary program of scientific research and advanced technological development directed toward maritime applications of new and improved materials, techniques, equipment, systems, and ocean, atmospheric, and space sciences and related technologies.

The Naval Research Laboratory provides

- primary in-house research for the physical, engineering, space, and environmental sciences;

- broadly based exploratory and advanced development programs in response to identified and anticipated Navy needs;

- broad multidisciplinary support to the Naval Warfare Centers;

- space and space systems technology development and support.

Reflections

Reflections ...

from the *Commanding Officer,*

CAPT Bruce W. Buckley, USN

One of the questions that the Commanding Officer and the Director of Research are most often asked to respond to is: why has NRL been so consistently effective as a military research laboratory over its nearly 75-year history? Obviously there are many contributing factors. Some would suggest that our reporting chain to the Secretary of Navy has allowed us to take a somewhat longer term view with respect to the scientific and technical needs of the Department of the Navy. And we have certainly enjoyed the continuous, sustained support of our parent command, the Office of Naval Research, during its past 50 years. Others might suggest that our strong presence in Washington, DC, has historically kept us close to the requirements decision makers. Certainly the quality of the entire workforce and, in particular, the established stature and credibility of our scientists and engineers have been significant factors. And we most often point to the collocation of experts in so many different disciplines that defines the broad-based, multidisciplinary nature of the Laboratory. But perhaps the one most continuous and compelling attribute critical to that success has been the long history of collocation of a strong basic research program with a strong applied research program. This arrangement of sound research being conducted in a very practical atmosphere has been a key ingredient in all of the great achievements of the Laboratory, whether it be the Laboratory's early and seminal work on HF propagation, or its

and the *Director of Research,*

Dr. Timothy Coffey

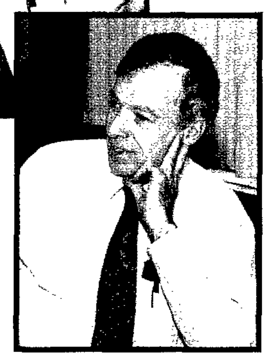

discovery of radar, or its key contributions to what is now the Global Positioning System, or its recent contributions in the area of electronic combat. These contributions would not have occurred had NRL been just a basic research laboratory or had it been just a development laboratory. It has been the collocation not simply of a multidisciplinary workforce, but of a spectrum of work, which ranged from the very basic to the very applied, that has been key to the Laboratory's success. The applied work has provided a significant driver with respect to what basic research should be done. On the other hand, the basic work has enabled possibilities not envisioned by the applied programs. These extremes of basic research and applied programs often find themselves in competition with one another, for resources, for management's attention, or for exposure. In many ways, the real job of NRL management is to ensure that neither of these extremes ever prevails against the other. Were this to happen, the well stream that has been NRL would dry up. It is important as we move through the next few years and adjust to the realities of reduced resources that we not lose sight of what has made NRL a great military research laboratory. The ultimate size of NRL must, of course, depend upon the needs of the Department of the Navy and the Department of Defense. Whatever that size turns out to be, it must include a healthy mix of applied work and basic work if the Laboratory is to retain its historical productivity.

The Naval Research Laboratory

NRL — Our Heritage

Today, when government and science seem inextricably linked, when virtually no one questions the dependence of national defense on the excellence of national technical capabilities, it is noteworthy that in-house defense research is relatively new in our Nation's history. The Naval Research Laboratory (NRL), the first modern research institution created within the United States Navy, began operations in 1923.

Thomas Edison's Vision: The first step came in May 1915, a time when Americans were deeply worried about the great European war. Thomas Edison, when asked by a New York Times correspondent to comment on the conflict, argued that the Nation should look to science. "The Government," he proposed in a published interview, "should maintain a great research laboratory....In this could be developed...all the technique of military and naval progression without any vast expense." Secretary of the Navy Josephus Daniels seized the opportunity created by Edison's public comments to enlist Edison's support. He agreed to serve as the head of a new body of civilian experts — the Naval Consulting Board — to advise the Navy on science and technology. The Board's most ambitious plan was the creation of a modern research facility for the Navy. Congress allocated $1.5 million for the institution in 1916, but wartime delays and disagreements within the Naval Consulting Board postponed construction until 1920.

The Laboratory's two original divisions — Radio and Sound — pioneered in the fields of high-frequency radio and underwater sound propagation. They produced communications equipment, direction-finding devices, sonar sets, and perhaps most significant of all, the first practical radar equipment built in this country. They also performed basic research, participating, for example, in the discovery and early exploration of the ionosphere. Moreover, the Laboratory was able to work gradually toward its goal of becoming a broadly based research facility. By the beginning of World War II, five new divisions had been added: Physical Optics, Chemistry, Metallurgy, Mechanics and Electricity, and Internal Communications.

The War Years and Growth: Total employment at the Laboratory jumped from 396 in 1941 to 4400 in 1946, expenditures from $1.7 million to $13.7 million, the number of buildings from 23 to 67, and the number of projects from 200 to about 900. During WWII, scientific activities necessarily were concentrated almost entirely on applied research. New electronics equipment — radio, radar, sonar — was developed. Countermeasures were devised. New lubricants were produced, as were antifouling paints, luminous identification tapes, and a sea marker to help save survivors of disasters at sea. A thermal diffusion process was conceived and used to supply some of the ^{235}U isotope needed for one of the first atomic bombs. Also many new devices that developed from booming wartime industry were type tested and then certified as reliable for the Fleet.

NRL Reorganizes for Peace: Because of the major scientific accomplishments of the war years, the United States emerged into the postwar era determined to consolidate its wartime gains in science and technology and to preserve the working relationship between its armed forces and the scientific community. While the Navy was establishing its Office of Naval Research (ONR) as a liaison with and supporter of basic and applied scientific research, it was also encouraging NRL to broaden its scope and become, in effect, its corporate research laboratory. There was a transfer of NRL to the administrative oversight of ONR and a parallel shift of the Laboratory's research emphasis to one of long-range basic and applied investigation in a broad range of the physical sciences.

However, rapid expansion during the war had left NRL improperly structured to address long-term Navy requirements. One major task — neither easily nor rapidly accomplished — was that of reshaping and coordinating research. This was achieved by transforming a group of largely autonomous scientific divisions into a unified institution with a clear mission and a fully coordinated research program. The first attempt at reorganization vested power in an executive committee composed of all the division superintendents. This committee was impracticably large, so

in 1949, a civilian director of research was named and given full authority over the program. Positions for associate directors were added in 1954.

The Breadth of NRL: During the years since the war, the areas of study at the Laboratory have included basic research concerning the Navy's environments of Earth, sea, sky, and space. Investigations have ranged widely from monitoring the Sun's behavior to analyzing marine atmospheric conditions to measuring parameters of the deep oceans. Detection and communication capabilities have benefitted by research that has exploited new portions of the electromagnetic spectrum, extended ranges to outer space, and provided a means of transferring information reliably and securely, even through massive jamming. Submarine habitability, lubricants, shipbuilding materials, fire fighting, and the study of sound in the sea have remained steadfast concerns, to which have been added recent explorations within the fields of virtual reality, superconductivity, and biomolecular science and engineering.

The Laboratory has pioneered naval research into space from atmospheric probes with captured V-2 rockets through direction of the *Vanguard* project — America's first satellite program — to involvement in such projects as the Navy's Global Positioning System. Today NRL is the Navy's lead laboratory in space systems research, fire research, tactical electronic warfare, microelectronic devices, and artificial intelligence.

The consolidation in 1992 of NRL and the Naval Oceanic and Atmospheric Laboratory, with centers at Bay St. Louis, Mississippi, and Monterey, California, added critical new strengths to the Laboratory. NRL now is additionally the lead Navy center for research in ocean and atmospheric sciences, with special strengths in physical oceanography, marine geosciences, ocean acoustics, marine meteorology, and remote oceanic and atmospheric sensing. The expanded Laboratory is focusing its research efforts on new Navy strategic interests and needs in the post-Cold War world. Although not abandoning its interests in blue-water operations and research, the Navy is also focusing on defending American interests in the world's littoral regions. NRL scientists and engineers are working to give the Navy the special knowledge and capabilities it needs to operate in these waters.

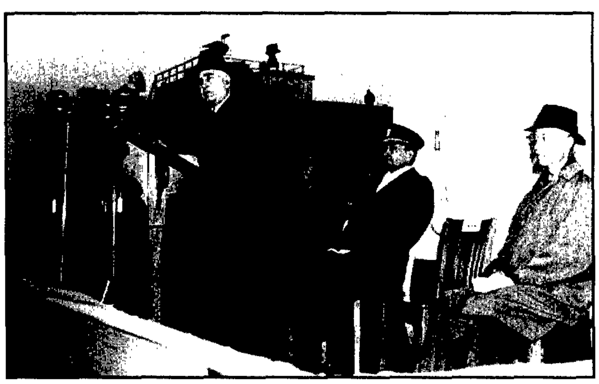

Former Secretary of the Navy, Charles Edison, speaking at the dedication of the bust of his father, Thomas Alva Edison, at the Naval Research Laboratory, on December 3, 1952.

With the conclusion of the Cold War and the rivalries that characterized it, new opportunities for international cooperation have multiplied. The Naval Research Laboratory has become a leader in this regard. This year saw a joint NRL/Russian/Norwegian research expedition aboard the Russian oceanographic vessel *Professor Logachev*. Members of the Marine Physics Branch of NRL's Marine Geosciences Division joined Russian and Norwegian scientists and engineers to explore geological and geophysical characteristics of the Eurasian continental margin and the Knipovich Ridge Valley in the Norwegian-Greenland Sea area. A mud volcano, discovered by a joint 1995 NRL/Norwegian expedition, was now charted in detail. The American/Russian expedition produced a detailed volcanic sonar image, pictures of icelike methane hydrates on the sea floor, and evidence for both methane and a temperature anomaly in the water column above the volcano — the last a phenomenon previously unknown for a warm seep.

On the other side of the physical spectrum, NRL space scientists and engineers were also active this last year. Laboratory astronomers, using the Hubble Space Telescope, detected five optical companion stars orbiting millisecond pulsars. Only two other such systems are known, and three of the companions are among the coolest and oldest white dwarf stars known. Interpretation of the properties of these systems may eventually help set limits on the age of the Milky Way galaxy.

NRL's Trapped Ions in Space (TRIS) detector flew aboard the NASA space shuttle mission STS-76. The TRIS measured a recently discovered belt of energetic cosmic ray nuclei trapped in Earth's magnetic field. This work will eventually help to quantify radiation hazards in space. In related research, an international group of space scientists, including NRL's Dr. Guenter Brueckner, used observations from the Laboratory's Large Angle

Dr. Peter Vogt, Marine Geosciences Division, presents an NRL plaque to Captain Alexander Arutyunov of the Russian research vessel *Professor Logachev* after a research trip to the Norwegian Sea.

Spectro Coronagraph (LASCO) to make the first detections of global, short-term disturbances in the solar corona. The disturbances often produce massive effects on Earth's magnetosphere. The LASCO is a detector on board the European Space Agency/National Aeronautics and Space Administration Solar and Heliospheric Observatory.

LASCO was also used this year to make observations for the first time of a long orbital period comet. The comet Hyakutake was within the LASCO's field of vision between April 29 and May 6. Hyakutake showed three distinct tails, one of which remained aligned with the orbital plane. LASCO also observed the steady diminution of the comet over 4 days, showing its interaction with the solar wind.

Another NRL astronomical detector, the Oriented Scintillation Spectrometer Experiment (OSSE), on board NASA's Compton Gamma Ray Observatory, also made important observations this year. The OSSE observed the eruption of an entirely new X-ray source near the center of our galaxy. The new X-ray pulsar has been officially named GROJ1744-28. It is pulsating at half-second intervals, with bursting rates ranging from 20 bursts per hour soon after its discovery to a later rate of one or two per hour. This is the first time that pulsing and bursting behaviors have been associated with the same X-ray source.

NRL's space engineers and technologists have also been busy this year. Included among their accomplishments have been the design, construction, and deployment of the Tether Physics and Survivability (TiPS) satellite. The TiPS was conceived and constructed in order to research the gravity-gradient dynamics and survivability of a tethered system in space. The satellite was deployed on June 20 in a circular orbit at an altitude of 1022 km.

In the area of environmental sensing, scientists in NRL's Chemistry Division have made progress toward developing a high-sensitivity biosensor for monitoring airborne or waterborne contaminants. The Force Amplified Biological Sensor (FABS) uses ultrasensitive force transducers to detect molecular recognition forces between DNA molecules, metal ions-chelators, antibodies-antigens, or other ligand-receptor molecules. The transducers are sensitive enough to detect the forces between a single pair of molecules. In additional sensor research, researchers at the Center for Bio/Molecular Science and Engineering have developed an antibody-based sensor that can detect explosives at very low levels. The NRL sensor can be used on site and produces results comparable to laboratory analyses.

Researchers in the Laboratory's Navy Technology Center for Safety and Survivability have made progress in the search for nontoxic, inexpensive, biodegradable deicing compounds for jet fuels and wing deicing. Laboratory research has shown that acetals and ketals of reduced sugars represent safe, viable alternatives to the commonly used glycol-based additives. The latter are toxic at the concentrations required for effective deicing and present hazards to both service personnel and the environment.

In the field of radar, a collaborative effort between NRL's Plasma Physics and Radar Divisions has produced a multipurpose microwave beam director by the name of Agile Mirror. It consists of a smooth plasma sheet formed in a low-pressure chamber by a gas discharge. The plasma acts like a conducting metal sheet to microwaves. It is possible to turn the mirror on and off repeatedly and very rapidly and to change the orientation of the mirror between pulses. Multiple high-power microwave sources with the same or different frequency could use a single Agile Mirror beam director. A potential benefit of the mirror is that a radar system might apply it to follow many targets simultaneously while continuing to search for new threats.

Finally, scientists in the Laboratory's Electronics Science and Technology Division, in collaboration with other investigators, have made important strides in wide bandgap electronics technology with the use of silicon-carbide and gallium-nitride semiconductors. The new semiconductors have

Chief of Naval Research, RADM Paul Gaffney presents the prestigious Navy Unit Commendation Award to CAPT Bruce Buckley and Dr. Timothy Coffey.

potential applications in high-temperature sensors, power switching, high-frequency power amplifiers and transmitters, and radiation-tolerant electronics. Wide bandgap semiconductors (as opposed to those of silicon) can operate at temperatures in excess of 400° C and perhaps as high as 600° C.

Technology Transfer: During 1996, NRL's Technology Transfer Office continued its successful efforts at coupling NRL technologies to private companies by establishing new CRADAs and patent-licensing agreements. One illustration of this activity is the patent-licensing agreement between NRL and Lake Shore Cryotronics, Inc. (LSCI) regarding the commercialization of the Quantitative Mobility Spectrum Analysis Algorithm (QMSAA) developed at NRL in collaboration with the University of Western Australia. LSCI and NRL are working to make available to the semiconductor community an analysis software package based on QMSAA, which will significantly enhance the routine characterization of multiple electron/hole densities and mobilities in semiconductors (bulk, thin films, and quantum-well materials and devices). The software package is being developed as a stand-alone product and as an integral component of the LSHall™ system via a recent CRADA.

Similarly, Quantum Magnetics, which licensed the NRL Explosive and Contraband Detector, has established a new CRADA to investigate means for devising and implementing advanced nuclear quadrupole resonance-based (NQR) detection methods as well as developing prototype circuits for testing these concepts. The NRL Explosive and Contraband Detector uses NQR to detect nitrogenous explosives or narcotics carried in luggage, mail, small cargo, or on a person.

In the area of advanced materials, Biocompatible, LTD of Great Britain has recently licensed the NRL controlled-release antifouling coatings technology. Here, microtubules 0.5 μm in diameter and from 10 to 150 μm in length have been shown to be effective for the controlled release of biocides in coatings. During 1996, a CRADA between NRL and Biocompatible, LTD has also been put in place to further investigate the use of microtubules as a controlled-release biocide-delivery system and determine the commercial feasibility of such a product.

While the majority of the CRADAs are with industrial firms, several are also with universities and nonprofit organizations. Recently, a CRADA was established between NRL and the Mid-Atlantic Technology Applications Center (MTAC) with the objective of transferring technology from NRL to companies in the mid-Atlantic states region. MTAC serves as a focus for technologies and scientific engineering expertise within the Federal laboratory system, promoting industrial and economic development in the mid-Atlantic region by assisting private corporations in locating external technology. This CRADA is another example of how NRL-developed technology can be effectively and efficiently transferred into the private sector for use in civilian and commercial applications.

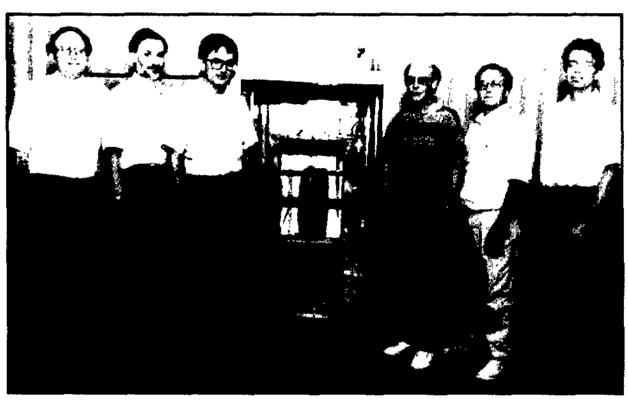

Members of the NRL development team show the research instrument, the Explosive and Contraband Detector, which has been licensed by Quantum Magnetics.

NRL Today

ORGANIZATION AND ADMINISTRATION

The Naval Research Laboratory is a field command under the Chief of Naval Research, who reports to the Secretary of the Navy via the Assistant Secretary of the Navy for Research, Development and Acquisition.

Heading the Laboratory with joint responsibilities are CAPT Bruce W. Buckley, USN, Commanding Officer, and Dr. Timothy Coffey, Director of Research. Line authority passes from the Commanding Officer and the Director of Research to three Associate Directors of Research, a Director of the Naval Center for Space Technology, and an Associate Director for Business Operations. Research is performed in the following areas:

- Systems Directorate
- Materials Science and Component Technology
- Ocean and Atmospheric Science and Technology
- Naval Center for Space Technology.

Through FY 96, NRL operated as a Defense Business Operating Fund (DBOF) activity. As a DBOF activity, all costs, including overhead, were charged to various research projects. Funding in FY 96 came from the Chief of Naval Research, the Naval Systems Commands, other Navy sources; government agencies, such as the U.S. Air Force, Advanced Research Projects Agency, the Department of Energy, and the National Aeronautics and Space Administration; and several nongovernment activities.

PERSONNEL DEVELOPMENT

At the end of FY 96, NRL employed 3600 personnel — 51 officers, 130 enlisted, and 3419 civilians. In the research staff, there are 888 employees with doctorate degrees, 453 with masters degrees, and 594 with bachelors degrees. The support staff assists the research staff by providing administrative, computer-aided design, machining, fabrication, electronic construction,

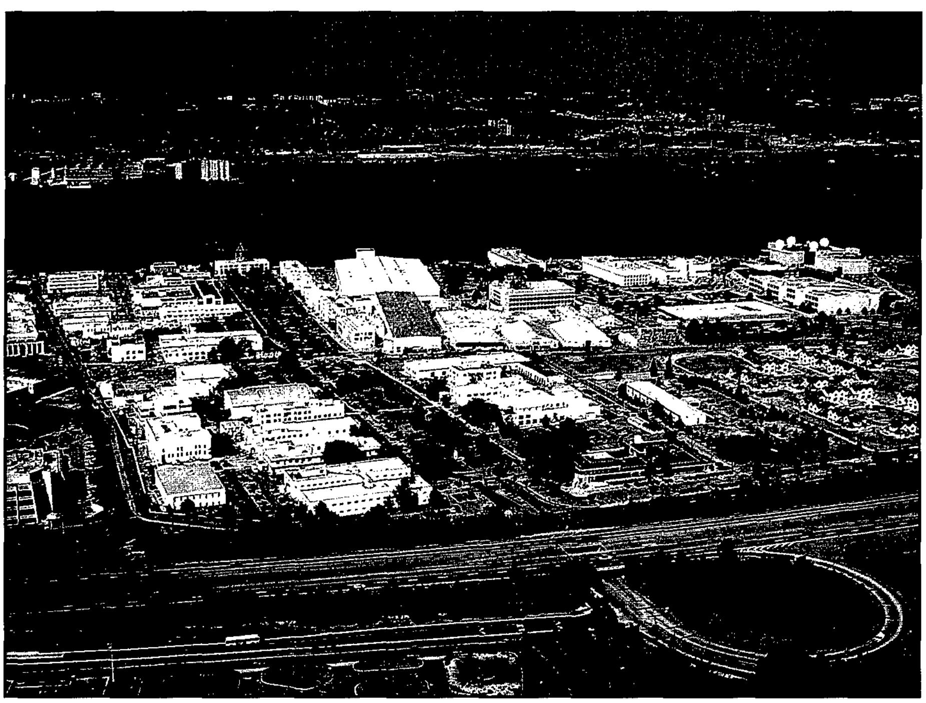

NRL headquarters, located off Interstate 295 in S.W. Washington, D.C., as viewed from the east.

publication, personnel development, information retrieval, large mainframe computer support, and contracting and supply management services.

Opportunities for higher education and other professional training for NRL employees are available through several programs offered by the Employee Development Branch. These programs provide for graduate work leading to advanced degrees, advanced training, college course work, short courses, continuing education, and career counseling. Graduate students, in certain cases, may use their NRL research for thesis material.

For non-NRL employees, several postdoctoral research programs exist. There are also agreements with several universities for student opportunities under the Student Career Experience Program (formerly known as Cooperative Education), as well as summer and part-time employment programs. Summer and interchange programs for college faculty members, professional consultants, and employees of other government agencies are also available.

NRL has active chapters of Women in Science and Engineering, Sigma Xi, Toastmasters International, Federally Employed Women, and the Federal Executive and Professional Association. Three computer clubs meet regularly — NRL Microcomputer User's Group, NeXT, and Sun NRL Users Group. An amateur radio club, a drama group (the Showboaters), and several sports clubs are also active. NRL has a Recreation Club that provides basketball and softball leagues and swim, sauna, whirlpool bath, gymnasium, and weight-room facilities. The Recreation Club also offers classes in martial arts, aerobics, swimming, and water walking.

The Community Outreach Program traditionally has used its extensive resources to foster programs that provide benefits to students and other community citizens. Volunteer employees assist with and judge science fairs, give lectures, and serve as tutors, mentors, coaches, and classroom resource teachers. The program also sponsors African American History Month art and essay contests for local schools, student tours of NRL, a student Toastmasters Youth Leadership Program, an annual holiday party for neighborhood children in December, an equipment/computer transfer program that provides surplus equipment to partnership schools, a book donation program for both students and teachers, and an annual math-science award for high school students. Through the Community Outreach Program, NRL has active partnerships with four District of Columbia public schools and three Aberdeen, Maryland, schools.

NRL has an active, growing Credit Union. Since its creation in 1946, NRL Federal Credit Union (NRL FCU) has grown to serve over 21,000 members. With assets of over $167 million, NRL FCU is a leader in providing innovative financial services. NRL FCU focuses on the tradition of innovation by offering a wide array of no-fee services plus a creative lending program. Winner of the Navy's Distinguished Credit Union Service Award in 1994, NRL FCU is a full-service financial institution.

Public transportation to NRL is provided by Metrobus. Metrorail service is 3 miles away.

For more information, see the *NRL Review* chapter entitled, "Programs for Professional Development."

SCIENTIFIC FACILITIES

In addition to its Washington, D.C. campus of about 130 acres and 102 main buildings, NRL maintains 14 other research sites, including a vessel for fire research and a Flight Support Detachment. The many diverse scientific and technological research and support facilities are described in the following paragraphs.

Research Facilities

Radar

NRL has gained worldwide renown as the "birthplace of radar" and, for a half-century, has maintained its reputation as a leading center for radar-related research and development. An impressive array of facilities managed by NRL's Radar Division continues to contribute to this reputation.

In connection with airborne radar, the division uses a Radar Imaging Facility, employing an inverse synthetic aperture radar (ISAR) deployed either in the air, on the ground, or aboard ship for radar-imaging data collection. There is a space-time adaptive processing (STAP) array and associated processors for the airborne early warning (AEW) area. In connection with ship-based radar, the division operates a Radar Test Bed Facility at the Chesapeake Bay Detachment (CBD), Randle Cliffs, Maryland. Represented are radars and related data-processing facilities for long-range air search, point defense, and surface search. A new

Researchers are setting up an experiment in the Radar Division's Advanced Technology Chamber (ATC). The ATC is capable of operating as a mode-stirred chamber from 200 MHz through 40 GHz, generating high electric field intensity levels; this enables efficient assessment of the effects of shipboard level intensities on hardware and components.

capability for investigating backscatter from surface and volumetric clutter is now operational. Concepts and engineering developments in connection with target identification are explored by using an experimental Cooperative Aircraft Identification (CAI) System. Other installations operated by the division include an Electromagnetic Compatibility (EMC) Facility supported by a mode-stirred chamber, a Radar Signature Calculation Facility for complex electromagnetic radar target modeling, a Compact Antenna Range (operated jointly with the Space Systems Development Department) for antenna design and development, and a Computer-aided Engineering (CAE) Facility.

Information Technology

The Information Technology Division (ITD) is at the forefront of DoD research and development in artificial intelligence, telecommunications, computer networking, human-computer interaction, information security, parallel computation, and computer science.

The division maintains local area computer networks to support its research and hosts test-beds for advanced high-performance fiber-optic network research. These networks make available hundreds of high-performance computers to local and remote users. The ITD research networks connect to NRL's internal network via DS-3 (45 Mbps) links to NSI and via ATM to the ATDnet and AAI. The ATDnet is a metropolitan ATM network with OC-3 (155 Mbps) and OC-12 (622 Mbps) links at NRL. AAI is a CONUS-wide ATM network.

Major shared resources include the systems and networks available in ITD's Center for Computational Science (CCS). The systems include: two CM-500e Connection Machines, one with 256 processors, 32 Gbytes of memory, and rated at 40 Gflops, and the other with 32 processors, 4 Gbytes of memory, and rated at 5 Gflops; a new 43 Tbyte robotic D2 tape storage archiver; a Cray Y-MP EL; a 6 Tbyte file server and archiver; and the Scientific Visualization Laboratory. The CCS manages NICEnet, NRL's local area network, which runs FDDI on the backbone and to some desktops and includes ATM support. NICEnet provides external connections to other networks and the worldwide Internet.

The division facilities also include an Information Security Engineering Laboratory and an experimental facility with special displays, eye and gesture trackers, and speech I/O devices for research in human computer interaction.

The Virtual Reality (VR) Laboratory provides the facilities and expertise to allow NRL scientists to use virtual reality in a variety of scientific investigations. Research areas include: shipboard fire-fighting, simulation-based design, command and control, and scientific visualization. Currently sup-

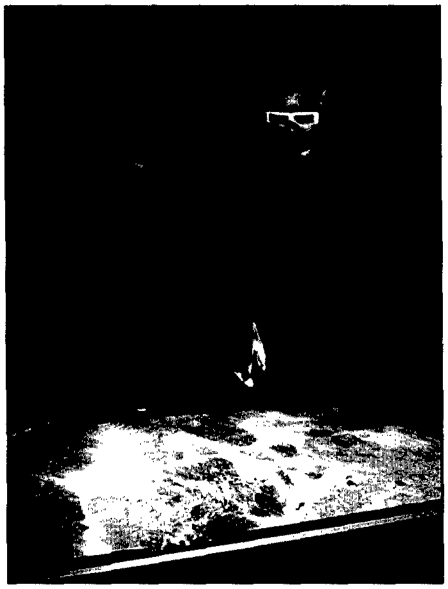

Using the Information Technology Division's Virtual Reality Lab's Responsive Workbench for simulation-based design research, scientists can interact with 3-D models of battlefield terrain.

ported VR technologies include immersive virtual environments using head-mounted displays (HMDs), partially immersive multiuser interaction using the Responsive Workbench, and desktop VR systems. The Responsive Workbench is an interactive 3-D tabletop environment that displays computer-generated, stereoscopic images on the workbench surface. A group of users around the table wears stereoscopic shutter glasses to observe a 3-D image displayed above the tabletop. Several high-speed graphics workstations including Onyx Reality Engine 2 and Infinite Reality computers, and a variety of VR peripherals comprise the VR Lab equipment inventory.

Optical Sciences

The Optical Sciences Division has a broad program of basic and applied research in optics and electro-optics. Areas of concentration include fiber optics, integrated optical devices, signal processing, optical information processing, fiber-optic and infrared sensors, high-power diode lasers, and diode-pumped solid-state lasers.

The division occupies some of the most modern optical facilities in the country. This includes an Ultralow-loss, Fiber-Optic Waveguide Facility using high-temperature infrared glass technology. There is also a Focal-Plane Evaluation Facility to measure the optical and electrical characteristics of infrared focal-plane arrays being developed for advanced Navy sensors. The IR Missile-Seeker Evaluation Facility performs open-loop measurements of the susceptibilities of IR tracking sensors to optical countermeasures. The Large-Optic, High-Precision Tracker system is used for atmospheric transmission and target signature measurements. The High-Energy Pulsed Hydrogen Fluoride, Deuterium Fluoride Laser is used for investigation into a wide variety of research areas including stimulated Brillouin scattering, optical-phase conjugation, and pulsed laser amplification.

There are several Fiber-Optic Sensor Facilities with fiber splicers, an acoustic test cell, a three-axis magnetic sensor test cell, equipment for evaluating optical fiber coatings, and various computers for concept analysis. The Digital Processing Facility is used to collect, process, analyze, and manipulate infrared data and imagery from several sources. The Emittance Measurements Facility performs measurements of directional hemispherical reflectance. Diode-pumped solid-state lasers operate in an eye-safe region of the optical spectrum.

The newest facility is the Infrared Test Chamber, or IR Range, which is an ultradry test chamber used to measure the IR signatures of new surface treatments, scale models, and components used for observables control on ships, aircraft, and missiles.

Electronic Warfare

The scope of research and development at NRL in the field of electronic warfare covers the entire electromagnetic spectrum — from basic technology research, component, and subsystem development — to system design and effectiveness evaluation. Major emphasis is placed on providing the methods and means to counter enemy hostile

actions in all battle phases, from the beginning — when enemy forces are mobilized for an attack — through the final engagement stages. For this purpose, NRL has constructed special research and development laboratories, anechoic chambers, and facilities for modeling and simulation. NRL has also added extensive new facilities where scientists can focus on the coordinated use of all organic defensive and offensive resources now present in the Fleet.

Laboratory for Structure of Matter

The laboratory investigates the atomic arrangements in materials to improve them or facilitate the development of new substances. Various diffraction methodologies are used to make these investigations. Subjects of interest include the structural and functional aspects of energy conversion, ion transport, device materials, and physiologically active substances such as drugs, antibiotics, and antiviral agents. Theoretical chemistry calculations are used to complement the structural research. A real-time graphics system aids in modeling and molecular dynamics studies.

Chemistry

NRL has been a major center for chemical research in support of naval operational requirements since the late 1920s. The Chemistry Division continues its tradition with a broad spectrum of basic and applied research programs concerned with controlled energy release (fuels, fire, combustion, countermeasure decoys, explosives), surface chemistry (corrosion, adhesion, tribology, adsorbents, film growth/etch), advanced polymeric materials (high-strength/low-weight structures, drag reduction, damping, special function), and advanced detection techniques (environment, chemical/biological, surveillance). Facilities for research include a wide range of the modern photon/electron, magnetic- and ion-based spectroscopic/microscopic techniques for bulk and surface analysis; nanometer-scale fabrication and characterization; multiple facilities for materials synthesis and physical/chemical characterization; a 11,400 ft^3 fire-research chamber (Fire I); and a 475-ft ex-USS *Shadwell* (LSD-15) advanced fire-research ship.

The Chemistry Division has been involved in environmental quality studies for many years; some of these efforts have recently coalesced into an Environmental Quality Sciences Section whose mission includes characterization of chemically polluted environments, remediation technologies and evaluations, pollution-prevention strategies for Fleet and shore-side operations, environmental security, and disposal of chemical-warfare agents. Facilities in support of this research are laboratories

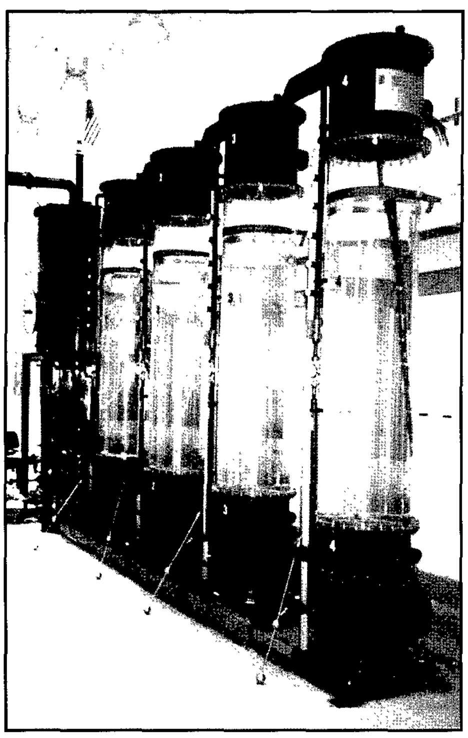

The Chemistry Division's newly established Environmental Quality Sciences Section uses this vertical groundwater circulation well mesocosm located at Aberdeen Proving Ground, Edgewood, Maryland, to study bioremediation of hydrocarbons and chlorinated solvents under both aerobic and anaerobic conditions.

for molecular biology, microbiology, biodegradation assessment, environmental biosensors, and geochemistry. In addition, a mesocosm facility has been established to bridge between laboratory and field work, with controlled scale-up of environmental systems. Located at the Aberdeen Proving Ground, Edgewood, Maryland, it is currently configured to mimic a vertical circulation cell induced in an aquifer by a specific groundwater circulation technology. With that technology, a vertical circular flow pattern in the groundwater is created that transports dissolved contaminants around the circulation well for treatment directly in the well. The mesocosm facility is available for a variety of scientific endeavors. It enables (1) the controlled study of relationships between the effects of an environmental process and the high degree of spatial variability found in natural systems, and (2) the development/validation of hypotheses and/or mathematical models that describe biogeochemical processes.

Materials Science and Technology

NRL has capabilities for X-ray and electron-diffraction analyses and for electron and Auger spectroscopy. Scanning, transmission, and combined scanning-transmission electron microscopes are used to study surface and/or internal microstructures. The division has a secondary ion mass spectrometer for surface analysis that significantly extends the diagnostic capability of the technique. A high-resolution, reverse-geometry mass spectrometer is used to probe reactions between ions and molecules. The Laboratory has a fully equipped fatigue and fracture laboratory, a modern vacuum arc-melting furnace for reactive metals, an ultrasonic gas-atomization system for making metal powders, and hot isostatic press facilities. The Laboratory's cryogenic facilities include dilution refrigerators and superconducting magnetic sensors for measuring ultrasmall magnetic fields. Also available are two molecular beam epitaxy devices for growing thin films.

Laboratory for Computational Physics and Fluid Dynamics

The Laboratory for Computational Physics and Fluid Dynamics is in round-the-clock production for computational studies in the fields of compressible and incompressible fluid dynamics, reactive flows, fluid-structure interaction (including submarine, ship, and aerospace applications), atmospheric and solar magnetoplasma dynamics, application of parallel processing to large-scale problems, such as unstructured grid generation for complex flows, target tracking and correlations for battle management, and other disciplines of continuum and quantum computational physics. The facility is used to develop and maintain state-of-the-art analytical and computational capabilities in fluid dynamics and related fields of physics, to establish in-house expertise in parallel processing and on-line graphical rendering for large-scale scientific computing, to perform analyses and computational experiments on specific relevant problems, and to transfer this technology to new and ongoing projects through cooperative programs.

The Parallel High Performance Computer/Graphics Facility is a heterogeneous high-performance computer system composed of a number of autonomous computers with a composite peak speed equivalent to about 15 Cray 90 processors. The system is coupled directly to the advanced video recording center described below. The main computational engine is comprised of three Intel iPSC/860 Touchstone Gamma parallel supercomputers supported by the hardware and software environment necessary to develop, debug, and benchmark parallel simulations. With multi-Mflop processors as building blocks, the Intel iPSC/860 is a MIMD-distributed memory machine configured as a hypercube. These three machines comprise a block of 224 parallel nodes with a peak computational speed of 18 Gflops with a cross-connected disk farm file system and network connections.

The facility's disk farm also supports three IBM RS/6000 and three DEC AXP high capacity compute-server computers, providing the facility with medium-to-large-scale memory and computational power enabling heterogeneous simulations with a significant scalar component, algorithm development, and diagnostic and postprocessing for large simulations. Special software allows simultaneous use of these computers on a single problem. Access to various other HPCC capabilities around the U.S. is accomplished through this system by using the new DoD high-bandwidth communication networks. A six-processor, 5-Gbyte SGI Onyx provides the division with state-of-the-art high-performance visualization.

A high-quality video studio has been created around a Sony D2 digital recording system, with a coupled Lyon-Lamb animation controller and a large memory Silicon Graphics ONYX workstation.

Through the network, other graphics stations, including the extensive resources of NRL's Visualization Laboratory, can create and record high-quality graphical images of simulation data for analysis and presentation by using digital recording techniques.

Condensed Matter and Radiation Sciences

The Condensed Matter and Radiation Sciences Division is the primary Navy center studying the effects of radiation on materials, electronic equipment, satellites, etc., and the production of thin films on diverse objects. The facilities for production and employment of photons, ions, and hypervelocity projectiles available to the division include:

High-Power Microwave (HPM) Facility: The large anechoic chamber (4.9 m × 4.9 m × 9.8 m) can be used at frequencies ranging from 0.5 to 94 GHz. Effects, susceptibility, and survivability of systems are the major research areas of interest.

Laser Facilities: Pulses of up to several joules are available from one system, while time resolutions down to 30 femtoseconds are produced by another. Synchronized Q-switched oscillators are configured for pump-probe experiments.

Thin-Film Preparation Facilities: The division has several major capabilities for preparation of thin films of advanced materials, such as high-temperature superconductors and active dielectrics. These include ion-assisted evaporation (which produces dense, adherent films), various dc plasma sources (which can etch as well as deposit films), and pulsed laser deposition (for production of chemically complex films).

X-ray Facility: Laboratory X-ray sources, monochromators, detectors, and related equipment are available for X-ray energies from 0.7 to 25 keV and dose rates up to 10^5 rads/s.

Synchrotron Radiation Facility: Intense, monochromatic X-ray photon beams tunable from 10 eV to 12 keV are available from the three beam lines developed by NRL at the National Synchrotron Light Source at the Brookhaven National Laboratory. Environmental target chambers can span a pressure range from 10^{-12} to 10^5 atm and temperatures from 10 to 1500 K.

Ion Implantation Facility: The facility consists of a 200 keV ion implanter with specialized ultrahigh vacuum chambers and associated in situ specimen analysis instrumentation.

3-MeV Tandem Van de Graaff: This facility is used to study charged-particle radiation damage effects such as occur in space, to provide high-sensitivity analysis of materials, and to perform MeV energy implants in materials.

Hypervelocity Impact Facilities: Three facilities are used for ballistics research at speeds exceeding 6 km/s with inert or explosive targets while measuring projectile velocity, orientation, and dynamic projectile-target interaction.

Plasma Physics

The Plasma Physics Division is the major center for in-house Navy and DoD plasma physics research. The division conducts a broad experimental and theoretical program in basic and applied research in plasma physics, which includes laboratory and space plasmas, pulsed-power sources, plasma discharges, intense electron and ion beams, atomic physics, laser physics, plasma

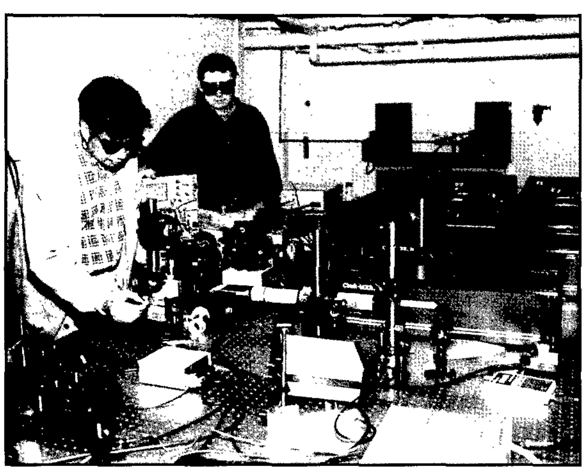

Scientists in the Condensed Matter and Radiation Sciences Division perform time-resolved nonlinear-optical experiments using a titanium:sapphire regenerative amplifier/optical parametric amplifier system that can generate optical pulses of less than 100 fs duration with wavelengths spanning the UV, visible, and infrared spectral regions.

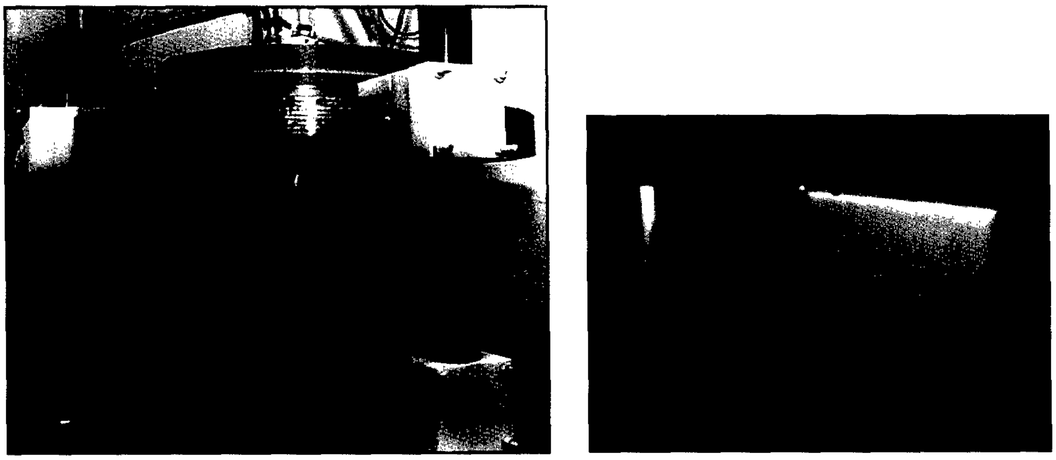

(a) (b)

The Agile Mirror plasma (purple-colored region) (a) is contained within a low pressure (200 mTorr air) chamber. The mirror is formed by a multikilovolt one-dimensional electron beam driven between a linear cathode and a flat plate anode located inside the chamber. A 200-G vertical magnetic field is superimposed by magnetic field coils above and below the plasma. (b) The plasma is shown edge-on (left) and slightly rotated from a side view. The structure at the top is the linear cathode that produces a beam of kilovolt electrons. These electrons ionize the background gas as they stream from the cathode to the anode, forming the plasma sheet. The plasma is sufficiently dense to reflect high frequency microwaves, thereby acting like a plasma mirror.

processing, nonlinear dynamics and chaos, and numerical simulations. The facilities include an extremely high-power laser — Pharos III — for the laboratory simulation of space plasmas and nuclear weapons effects studies, a short pulse, high-intensity Table-Top Terawatt (T^3) laser to study intense laser-plasma, laser-electron beam, and laser-matter interactions. The division also has an 11 m^3 space chamber capable of reproducing the near-Earth space plasma environment and a radar antenna laboratory where the interaction of high-frequency microwaves and a sheet plasma distribution (agile mirror) is studied. The division has developed a variety of pulsed-power sources to generate intense electron and ion beams, powerful discharges, and various types of radiation. The largest of these pulsers — GAMBLE II — is used to study the production of megampere electron and ion beams and for producing very hot, high-density plasmas. Other generators are used to produce particle beams that are injected into magnetic fields and/or cavities to generate intense microwave pulses (e.g., the Relativistic Klystron Amplifier (RKA), in the 1 to 10 GHz regime). A large array of high-frequency microwave sources (35 to 120 GHz) are available to conduct research on microwave processing of advanced ceramic materials.

A major 3 kJ KrF laser facility opened in June 1995. This facility is being initiated to provide intense radiation for studying inertial confinement fusion target heating at short wavelengths (0.25 microns) and high pressure physics.

Electronics Science and Technology

In addition to specific equipment and facilities to support individual science and technology programs, NRL operates the Nanoelectronics Processing Facility (NPF), the Penthouse Processing Facility (PPF), the Laboratory for Advanced Material Synthesis (LAMS), and the EPICENTER. The NPF's mission is to provide service to both NRL and external organizations requiring micro- and nanofabrication processing support. Lithography is a particular strength of the NPF, with definition of feature sizes down to 150 Å possible with an e-beam nanowriter. The NPF can supply items ranging from individual discrete structures and devices to circuits with very-large-scale integration complexity. The recently completed PPF is dedicated to processing III-V semiconductor devices and circuits in addition to serving the hands-on fabrication needs of individual NRL scientists. The PPF uses a single-pass air-ventilation system to minimize human risk to potentially hazardous III-V semiconductor processes and associated chemicals, thereby further meeting existing safety standards. The LAMS' mission is to support NRL programs

that require thin film III-V or refractory semiconductor technology. The LAMS employs organometallic vapor phase epitaxy to synthesize a wide range of thin films such as InSb, InGaP, InP, and GaN. The EPICENTER (a joint activity of the Electronics Science and Technology, Materials Science and Technology, and Chemistry Divisions) is dedicated to the production of multilayer microstructures using in-situ surface analytical techniques in either of two ultrahigh vacuum, molecular-beam-epitaxy growth chambers — one for III-V semiconductors and the other for magnetic materials and II-VI semiconductors.

Bio/Molecular Science and Engineering

The Center for Bio/Molecular Science and Engineering conducts research and development using biotechnological approaches to solve problems for the Navy, DoD, and the nation at large. Problems currently being addressed include advanced material development (for electronic, biomedical, and structural applications), combat casualty care, environmental quality (including pollution cleanup and control), and biological warfare defense. The approach to these problems involves long-term research focused on the study of complex materials systems, coupled with integrated exploratory and advanced development programs. The staff of the center is an interdisciplinary team who performs basic and applied research and development in areas that require expertise in bio- and surface chemistry, biophysics, genetic engineering, cell biology, advanced organic synthesis, solid-state and theoretical physics, and electronics and materials engineering. In addition, the center has many collaborations throughout the Laboratory, at universities, and in industry to ensure that a broad base of the required expertise and critical evaluations are part of the research and development programs. Highlights of the program include the development of liposome-based blood substitutes, the manipulation of biologically derived structures on the nanometer scale, the development of ferroelectric liquid crystal systems with microsecond response times, discovery of an advanced resist system for high-speed, high-density integrated circuits, the patterning of neuronal cells to form neural networks, and the development of biosensors for environmental monitoring.

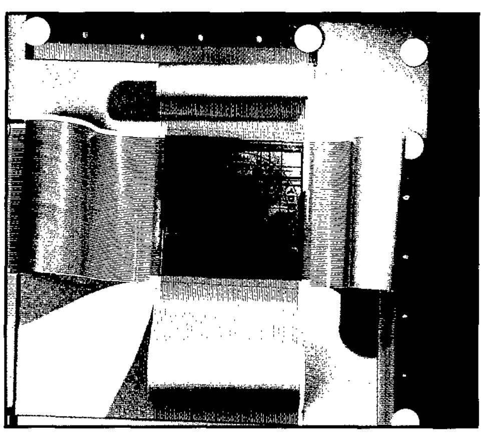

A fully multiplexed reflective liquid crystal display (LCD) using conducting polymer substrates fabricated jointly by the Center for Bio/Molecular Science and Engineering and Kent State University. This is the world's first multiplexed LCD on a plastic substrate.

In October 1994, the center occupied newly renovated laboratories and offices in Building 30. These modern facilities, designed to be used into the next century, include general laboratories for research in chemistry, biochemistry, molecular biology, and physics. Specialized areas include a 600-ft^2 Class 1000 clean room; an advanced Electron Microscope facility; and a Scanning Probe Microscope laboratory. Instrument rooms in the new building provide access to a variety of spectrophotometers (IR, GC-MS, NMR, and UV-Vis) and other equipment used in biochemical or physical analyses of biomaterials. Additional laboratories accommodate an X-ray diffraction instrument, a liquid crystal fabrication facility, and equipment for advanced electronics and biosensor programs.

Acoustics

The Acoustics Division has three integrated acoustic pool facilities supporting research in submarine target characteristics for ASW, submarine acoustic design and quieting, sensors for hull-mounted sonars, and structural acoustics for mine countermeasures. Scaled submarine targets, real mine structures, sensors mounted on hull simulators, and underwater buried objects can all be examined with advanced nearfield holographic and scanning 3-D laser vibrometer systems to measure and visualize the sound fields near a structure, the vibrations of the structure itself, the resulting farfield sound fields, and the physics of the sound-structure-fluid interactions.

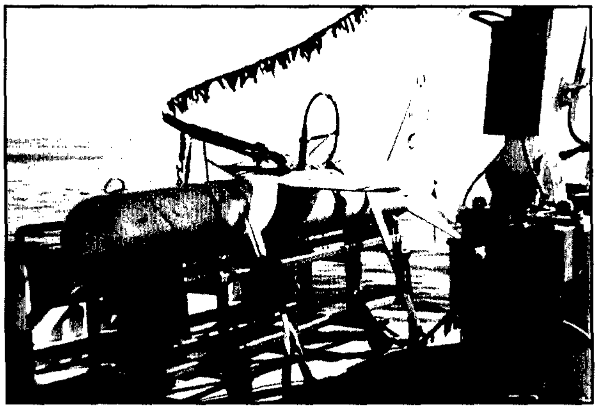

NRL's High-Frequency Acoustics Tow Body System is a high-speed, remotely operated vehicle with acoustic instrumentation to measure high-frequency acoustic properties in shallow water environments.

The division operates several acoustic projectors and receive arrays for the generation and collection of experimental data. Source projectors include five towed XF4 flextensional transducers, two moored WEBB organ-pipe projectors, and a WEBB battery-operated arbitrary-waveform projector system. Receive systems include a moored, 32-element (up to 800 Hz) vertical-array with an RF telemetry system, a 64-element (75 to 600 Hz) towed oil-filled seismic-type array, and a 64-element (100 to 400 Hz) oil-filled array that can either be deployed along the ocean bottom or moored vertically. The 64-element arrays use direct-link cabling to a 64-channel (expendable to 1024 channel), 20 kHz bandwidth data acquisition and processing system. The division also has unique, self-recording digital acquisition buoy systems (DABS) that are used to obtain multichannel (up to 128) acoustic data in the 10 Hz to 5 kHz regime. These systems provide up to 250 Gbytes of data on a single 15-inch reel of 1-in. tape. The division has recently developed the Satellite Vertical Line Array (SLVA) system to collect acoustic and oceanographic data and transmit selected data to a remote shore station in real time. The buoy has a local-area network and computers on board to control the collection, preprocessing, and transmission of data. The multichannel data are sent via high-speed satellite channel at speeds in excess of 1 Mbit/s, using commercial Ku-band satellites.

The division operates high-frequency (up to 600 kHz) acoustic measurement systems to obtain scattering, target strength, and propagation data using bottom-moored instrumentation towers and a high-speed, remotely operated vehicle. These data are used to simulate the performance of weapons and mine countermeasure sonars (including advanced synthetic aperture sonars) in shallow and very shallow water environments.

The Tactical Oceanography Simulation Laboratory (TOSL) is a modeling and simulation architecture consisting of a set of tools for ingesting and processing climatological and real-time environmental data and applying energy propagation models to those data to determine acoustic and nonacoustic propagation loss. TOSL is coupled with a storage repository of environmental data and a wide-area network (WAN), which allow full participation in a distributed simulation environment. TOSL features a high-performance computational capability able to provide real or near-real-time calculations in support of training, war games, operations rehearsal, and other distributed simulation functions.

Remote Sensing

The Remote Sensing Division conducts a program of basic research, science, and applications to develop new concepts for sensors and imaging systems for objects and targets on the Earth, in the near-Earth environment, and in deep space. The research, both theoretical and experimental, leads to discovering and understanding the basic physical principles and mechanisms that give rise to the background environmental emissions and targets of interest and to absorption

The Remote Sensing Division's Free Surface Hydrodynamics Laboratory basin is equipped with a programmable wave-maker, a high-resolution IR camera, laser slope gauges, and a particle image velocimetry system.

and emission mechanisms of the intervening medium. Accomplishing this research requires the development of sensor systems' technology. The developmental effort includes active and passive sensor systems used for the study and analysis of the physical characteristics of phenomena that evolve from naturally occurring background radiation, such as that caused by the Earth's atmosphere and oceans and man-made or induced phenomena, such as ship/submarine hydrodynamic effects. The research includes theory, laboratory, and field experiments leading to ground-based, airborne, or space systems for use in remote sensing, astrometry, astrophysics, surveillance, non-acoustic ASW, improved meteorological/oceanographic support systems for the operational Navy, and the environmental/global climate change initiatives. Special emphasis is given to developing space-based platforms and exploiting existing space systems.

The Navy Prototype Optical Interferometer (NPOI), a major new facility of the Remote Sensing Division, is actually two colocated instruments for making high-angular-resolution optical measurements of stars. Light from widely separated individual siderostats is combined simultaneously to synthesize the angular resolution of a telescope tens to hundreds of meters in diameter. Four siderostats are placed in an array with extremely accurate metrology, to enable very-high-precision measurements of stellar positions (wide-angle astrometry). These measurements are used by the U.S. Naval Observatory to refine the celestial reference frame, determine Earth rotation parameters, and thus satisfy Navy requirements for precise time and navigation data. They also provide determinations of basic astrophysical parameters, such as stellar masses and diameters. Additional relocatable siderostats can be placed out to distances of 250 m from the array center and used to construct very-high-resolution images of stars. These images provide fundamental astrophysical information on stellar structure and activity. When complete, the NPOI will be the most advanced high-resolution imaging optical interferometer in the world.

Oceanography

The Oceanography Division is the major center for in-house Navy research and development in oceanography. It is known nationally and internationally for its unique combination of theoretical, numerical, and experimental approaches to oceanographic problems. Researchers make extensive use of the Maury Oceanographic Library (jointly operated by NRL-Stennis Space Center (NRL-SSC) and the Naval Oceanographic Office), which is recognized as one of the best and most comprehensive oceanographic libraries in the world. The division numerically models the ocean and coastal areas of the world. This modeling is conducted on the Navy's and DoD's most powerful vector and parallel-processing machines. To study the results of this intense modeling effort, the division operates a number of highly sophisticated graphic systems to visualize ocean and coastal dynamic processes. The seagoing experimental programs of the division range worldwide. Unique measurement systems include: towed sensor and advanced microstructure profiler systems for studying micro- and fine-scale ocean structure, an integrated absorption cavity, optical profiler system, and towed optical array for studying ocean optical characteristics, and self-contained bottom-mounted upward-looking acoustic Doppler current profilers for measuring ocean variability. In the laboratory, the division operates an environmental scanning electron microscope and a laser confocal scanning microscope for detailed studies of biocorrosion in naval materials.

Oceanography Division's All Optical Array is shown being deployed for an experiment off the coast of California.

Marine Geosciences

The Marine Geosciences Division is the major center for in-house naval research and development in marine geology, geophysics, geoacoustics, and geotechnology. It is also the Navy's lead activity for mapping, charting, and geodesy research and development. The division has acquired unique instrumentation suites for its studies of the seafloor and its subbottom. These include sidescan sonar systems; deep-towed, low-frequency acoustic-reflection systems; parametric acoustic-swath subbottom-mapping systems; remotely operated vehicles; and electromagnetic mapping sensors. These systems allow studies ranging from sediment classification to mapping of inclusions and changes in the seafloor subbottom structure. The division deploys ocean bottom and subbottom seismometer systems for use in studies ranging from tectonic noise to studies of whale migration. Specialized seafloor probes allow measurement of the water pressure and pressure gradient in sediment pores and acoustic compression and shear wave velocity and attenuation. Laboratory equipment includes a transmission electron microscope with an environmental cell to carry out sediment-fabric and sediment-pollutant adsorption studies.

The Moving-Map Composer Facility, a collection of computers and work stations with associated graphics manipulation software, is used to compress map information onto a CD-ROM for Navy and Marine Corps aircraft digital moving maps. The division also operates the NRL Magnetic Observatory at SSC. This facility includes two specially built wooden buildings with minimal ferrous content and arrays of magnetometers that extend radially from the building. The Magnetic Observatory measures the ambient magnetic field, its changes, and other magnetic phenomena. The observatory is part of a worldwide observing system.

Sea-floor methane hydrate (white patches), fractures (right), and what is probably a species of ca. 20-cm-long bottom-feeding rat-tail fish are shown. Photographed on 1996 NRL-Russian-Norwegian cruise by scientists in the Marine Geosciences Division in 1250-in. water depth, 3 m above seafloor on a mud volcano on continental slope west of Barents Sea. Hydrate on and below seabed explains strong acoustic backscatter observed on earlier NRL-led cruise to this site.

Marine Meteorology

The Marine Meteorology Division is located in Monterey, California. NRL-Monterey (NRL-MRY) performs basic and applied research in the atmospheric sciences relevant to both central-site and shipboard operations. Located adjacent to the Navy's operational weather forecasting center, Fleet Numerical Meteorology and Oceanography Center (FNMOC), NRL-MRY develops global and regional mesoscale data assimilation/forecast systems and other products that provide worldwide environmental support for Navy and joint operations.

NRL-MRY's access to a variety of computer resources helps make this Division one of the premier centers for weather prediction systems and data application research and development. Large mainframes and databases at FNMOC are used to develop and transition operational prediction systems. Secure terminal rooms located throughout NRL-MRY and FNMOC allow for a direct link to classified computer resources. Furthermore, NRL-MRY is networked to the DoD High-Performance Computing Centers, which support research in atmospheric process studies and coupled air-ocean model development. Locally, high-performance workstations are used for shipboard system development, and the John B. Hovermale Visualization Center is designed for the display and interpretation of meteorological data and the development of briefing tools. State-of-the-art satellite receivers allow for local collection of data for applications research in support of the Joint Typhoon Warning Center and other Navy operations.

NRL-MRY has a long-standing tradition for participation in field projects. The Division has been involved in numerous fleet exercises to collect data for 6.2 through 6.4 projects in areas of shipboard forecast systems development and weather-impact assessment.

NRL-MRY is the lead laboratory for the Tactical Environmental Support System (TESS(3)), a workstation-based environmental database and

diagnostic/forecast system designed for shipboard use. Advanced technologies used in development include satellite meteorology, data analysis, advanced numerical modeling techniques, visualization, and artificial intelligence.

Space Science

NRL is the Navy's main laboratory for conducting basic research and development in the space sciences. The Space Science Division conducts and supports a number of space experiments in the areas of upper atmospheric, solar, and astronomical research aboard NASA, DoD, and other Government-agency space platforms. Division scientists are involved in major research thrusts that include remote sensing of the upper and middle atmospheres, studies of the solar atmosphere, and astronomical radiation ranging from the ultraviolet through cosmic rays. In support of this work, the division maintains facilities to design, construct, assemble, and calibrate space experiments. A network of computers, workstations, image-processing hardware, and special processors are used to analyze and interpret space data. Among the division's space science data acquisition and analysis efforts are the following:

- mission operations and data analyses of NRL's Oriented Scintillation Spectrometer Experiment (OSSE) for NASA's Compton Observatory;

- observation of the Sun's interaction with the upper-Earth atmosphere through the Solar Ultraviolet Spectral Irradiance Monitor (SUSIM) experiment in support of NASA's Upper Atmosphere Research Satellite (UARS) and Atmospheric Laboratory for Application and Science (ATLAS) missions; and

- observation and analysis of the evolution and structure of the solar corona from the disk to 0.14 AU. This effort involves acquiring and analyzing data from the Large-Angle Spectrometric Coronagraph and Extreme Ultraviolet Imaging Telescope on the Solar Heliospheric Observatory satellite.

- observation of selected celestial targets in the ultraviolet and X-ray bands by three Advanced Research and Geophysical Observation Satellite (ARGOS) experiments — Global Imaging of the Ionosphere (GIMI), High-Resolution Atmospheric and Auroral Spectroscopy (HIRAAS), and Unconventional Stellar Aspect (USA).

The Space Science Division also operates the BMDO's Background Data Center (BDC) — a center of expertise for backgrounds phenomenology data that provides archival, management, and analysis services, and value-added products for preserving and applying data collected by satellite experimental programs. The BDC's architecture consists of fully functional classified and unclassified processing environments that include operational data processing systems and science analysis stations. Automatic data-processing equipment includes Digital Equipment Corporation (DEC) VMS, and Unix platforms, Sun workstations, Silicon Graphics workstations, Macintoshes, and IBM-compatible personal computers. These platforms support a variety of standard software packages, including Ingres RDBMS, IRAF, IDL, and the World Wide Web application. Unclassified processing environments are linked to scientists throughout the world via the Internet. Data files can be received by or sent from the BDC by using FTP or other protocols.

Space Technology

In its role as a center of excellence for space systems research, the Naval Center for Space Technology (NCST) designs, builds, analyzes, tests, and operates spacecraft, as well as identifies and conducts promising research to improve spacecraft and their support systems. NCST facilities that support this work include large and small anechoic radio frequency chambers, clean rooms, shock and vibration facilities, an acoustic reverberation

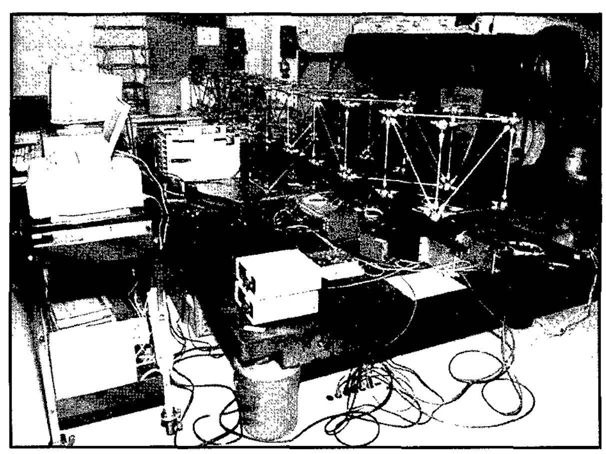

A prototype truss for distributed aperture space sensing is shown undergoing modal testing in the Structures Control Laboratory. The FASTMAST in the background was used on the space shuttle for a tether deployment experiment.

chamber, large and small thermal/vacuum test chambers, control system interaction laboratory, satellite command and control ground stations, fuels test facility, and modal analysis test facilities. NCST has a facility for long-term testing of satellite clock time/frequency standards under thermal/vacuum conditions linked to the Naval Observatory; a 5-m optical bench laser laboratory; and a hologram research laboratory to conduct research in support of the development of space systems.

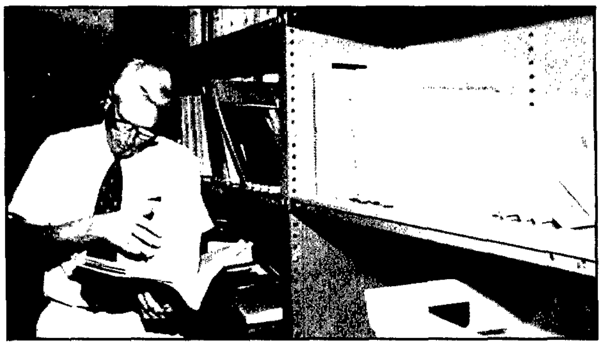

Dean Bundy, NRL archivist, Technical Information Division, reviews a laboratory notebook, one of more than 17,000 such notebooks that are a significant part of NRL's corporate memory.

Research Support Facilities

Technical Information Services

The Ruth H. Hooker Research Library and Technical Information Center contains more than one million items, including journals, books, conference proceedings, and technical report literature. NRL-DC employees, on-site contractors, and ONR personnel can search the Library's computer-based catalogs. The Library provides interlibrary loans, on-line searches, access to CD-ROM and commercial databases, and a full range of reference services. The Library offers desktop availability to its catalogs and databases through its INFONET information system, which may be networked from offices and laboratories as well as from home. A number of these services are also available via the World Wide Web through the Library's InfoWeb interface. The InfoWeb links to the Library's networked document dissemination system called TORPEDO (The Optical Retrieval Project: Electronic Documents Online), offering full-text search capabilities and on-line display and printing of selected journals, research reports, NRL press releases, and reprints. A multiplatform Table of Contents and photocopying service for virtually all the Library's current subscriptions bring journal literature to the desktops of all library users.

Publication services include writing, editing, composition, phototypesetting, publications consultation and production, and printing management. The primary focus is on using computer-assisted publishing technology to produce scientific and technical information containing complex artwork, equations, and tabular material.

The research conducted at NRL requires a diversity of graphic support from the Systems/Photographic Branch, such as technical and scientific illustrations, computer graphics, design services, photographic composites, calligraphy, display panels, sign making, and framing. A high-end workstation provides and delivers a new level of electronic airbrushing and photographic retouching. Photographic services include still-camera coverage for data documentation both at NRL and in the field. Photographic images can also be captured with state-of-the-art digital cameras and still video. A photographic laboratory offers custom processing and printing of black and white and color films. Quick-service color prints are also available. Video services include producing video reports of scientific and technical programs. A video studio and editing facility with high-quality Beta Cam and digital video editing equipment are available to support video production. The NRL Exhibits Program develops and produces displays, audio-visual material, and multimedia programs for presentation at technical meetings, conferences, and symposia. The Visual Design/Imaging Center offers high-quality output from computer-generated files in EPS, Postscript, PICT, TIFF, Photoshop, and PowerPoint. The Captivator film recorder produces high-resolution 35-mm slides, viewgraphs, and negatives. Photographic quality color prints and viewgraphs are available from Kodak dye-sublimation printers. High-resolution scanning to a Macintosh or PC disk is available. The Linotron imagesetter produces gray-scale prints and transparencies at 1693 dots per inch.

The Administrative Services Branch collects and preserves archival correspondence, memoranda, reports, research problem files, and scientific notebooks that together constitute the bulk of the Laboratory's corporate memory. These documents are retained at the Washington National Records Center, from which they can be retrieved. The Administrative Services Branch is also responsible for the management of NRL's mail services and disposition of NRL's active records.

FIELD STATIONS

NRL has acquired or made arrangements over the years to use a number of major sites and facilities for research. The largest facility is located at the Stennis Space Center (NRL-SSC), in Bay St. Louis, Mississippi. Others include a facility at the Naval Postgraduate School in Monterey, California (NRL-MRY), and the Chesapeake Bay Detachment (CBD) in Maryland. Additional sites are located in Maryland, Virginia, Alabama, and Florida.

Flight Support Detachment (NRL FSD)

Located aboard the Patuxent River Naval Air Station in Lexington Park, Maryland, NRL FSD operates and maintains five uniquely configured P-3 Orion turboprop aircraft as airborne research platforms. The FSD conducts single aircraft, worldwide detachments in support of a wide range of scientific research.

In FY 96, NRL FSD provided flight support for diverse research programs, including Project Birdseye, involving hydroacoustic research; Airborne Multisensor Pod System, a multisensor data collection system; Airborne Geophysical Sensor Suite (AGSS), involving data and gravimeter testing to detect variations in the ocean floor; MAKO, an ECM study of received signals; Fly's Eye, an infrared threat warning system; Phils, an advanced camera group; Real Aperture Radar (RAR); Laser Airborne Depth Sounding (LADS); and Integrated Electronic Warfare System (IEWS), a system that simulates radars of various surface and airborne platforms.

The NRL FSD aircraft are the sole airborne platforms for numerous projects, such as bathymetry, electronic countermeasures, gravity mapping, and radar development research. The detachment has an impressive safety record of over 53,000 accident-free flight hours amassed over a 33-year period.

Chesapeake Bay Detachment (CBD)

CBD occupies a 168-acre site near Chesapeake Beach, Maryland, and provides facilities and support services for research in radar, electronic warfare, optical devices, materials, communications, and fire research. Because of its location high above the Chesapeake Bay on the western shore, unique experiments can be performed in conjunction with the Tilghman Island site, 16 km across the bay from CBD. Some of these experiments include low clutter and generally low-background radar measurements. By using CBD's support vessels, experiments are performed that involve dispensing chaff over water and radar target characterizations of aircraft and ships. Basic research is also conducted in radar antenna properties, testing of radar remote-sensing concepts, use of radar to sensor ocean waves, and laser propagation. CBD also hosts facilities of the Navy Technology Center for Safety and Survivability, which conducts fire research on simulated carrier, surface, and submarine platforms.

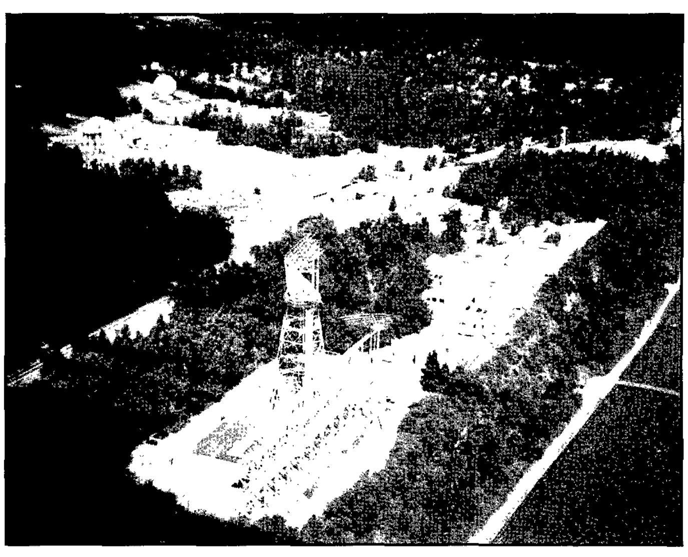

Aerial view of NRL's Chesapeake Bay facility located near Chesapeake Beach, Maryland.

Marine Corrosion Test Facility

Located on Fleming Key at Key West, Florida, this facility offers an ocean-air environment and clear, unpolluted, flowing seawater for studies of environmental effects on materials. Equipment is available for experiments involving weathering, general corrosion, fouling, and electrochemical phenomena, as well as coatings, cathodic protection devices, and other means to combat environmental degradation.

Naval Research Laboratory-Stennis Space Center (NRL-SSC)

NRL-SSC, a tenant activity at NASA's Stennis Space Center, is located in the southwest corner of Mississippi, about 50 miles northeast of New Orleans, Louisiana, and 20 miles from the Mississippi Gulf Coast. NRL-SSC encompasses over 200 square miles of land area, including a perimeter buffer zone to insulate surrounding civilian communities from the noise of rocket-engine testing by NASA. Other Navy tenants at NRL-SSC include the Commander, Naval Meteorology and Oceanography Command and the Naval Oceanographic Office, who are major operational users of the oceanographic and atmospheric research and development performed by NRL. The Naval Oceanographic Office provides access for NRL researchers to one of the Navy's largest supercomputers. This unique concentration of operational and research oceanographers makes NRL-SSC the center of naval oceanography and the largest such grouping in the Western world.

NRL-SSC provides administrative and business operations support for NRL's Center for Environmental Acoustics, Remote Sensing Applications Branch, Oceanography Division, and Marine Geosciences Division. NRL-SSC occupies over 200,000 square feet of research, computation, laboratory, administrative, and warehouse space. Facilities include a number of large antennas to receive available oceanographic and meteorological satellite data, a Magnetic Observatory building constructed of nonferrous materials in an electromagnetically quiet area of NRL-SSC, a Pattern Analysis Laboratory, a Map Data Formatting Facility, a water-wave channel, and numerous laboratories for acoustic and oceanographic computation, instrumentation, analysis, and testing. Special areas are available for constructing, staging, refurbishing, and storing sea-going equipment.

Marine Meteorology Division Monterey, California (NRL-MRY)

Located in Monterey, California, as a tenant activity of the Naval Postgraduate School (NPS), this facility is collocated with the Navy's operational Fleet Numerical Meteorology and Oceanography Center (FNMOC) to support development of numerical atmospheric prediction systems and related user products. NRL-MRY's mission has broadened considerably in recent years to include basic research and development and to provide support to other customers. Collocation with FNMOC allows NRL-MRY easy access to a large classified vector supercomputer mainframe. This access provides real-time global atmospheric and oceanographic databases for research on-site and at other NRL locations. Interfaces to the Defense Research and Engineering Network and Defense Simulation Internet have also been established. Locally, NRL-MRY has multiprocessing Digital Equipment Corporation and Silicon Graphics Inc. workstations and data archives that allow in-house researchers to conduct numerical weather-prediction experiments, data processing, simulation, and visualization studies.

NRL-MRY's experience extends to mesoscale and shipboard atmospheric prediction systems. A third-generation Navy system — the Tactical Environmental Support System (TESS(3)), developed for the Space and Naval Warfare Systems Command, is installed on-site and has undergone various upgrades to provide substantial improvements in system performance and capability and automatic product generation and display. TESS(3) is functioning as an R&D testbed for new tactical/environmental decision aids (TDAs/EDAs), object-oriented databases, and Motif/X Windows-user interfaces. State-of-the-art graphics workstations (SGIs), network file-servers (Suns), and tactical (HP) systems have been acquired for use by researchers. Environmental components of future shipboard systems are currently being developed. In addition, the effects of the atmosphere on weapons, sensors, and platforms are being evaluated with primary emphasis on electromagnetic/electro-optic aerosols, and modeling and simulation impacts.

Other Sites

Some field sites have been chosen primarily because they provide favorable conditions to operate specific antennas and electronic subsystems and are close to NRL's main site. Pomonkey,

Maryland, a field site south of NRL, has a free-space antenna range to develop and test a variety of antennas. The antenna model measurement range in Brandywine, Maryland, has a 4.6-m diameter turntable in the center of a 305-m-diameter ground plane for conducting measurements on scale-model shipboard and other antenna designs. A site on the cliffs overlooking the Chesapeake Bay provides an over-the-water range of approximately 10 miles to Tilghman Island.

Midway Research Center

The Midway Research Center (MRC) is located on a 158-acre site in Stafford County, Virginia. Located adjacent to the Quantico Marine Corps' Combat Development Command, the MRC has 10,000 square feet of operations and administration area and three precision 18.5-m-diameter parabolic antennas housed in 100-ft radomes. The MRC, under the auspices of the Naval Center for Space Technology, provides NRL with state-of-the-art facilities dedicated solely to space-related applications in naval communications, navigation, and basic research.

Research Platforms

Mobile research platforms contribute greatly to NRL's research. These include five P-3 Orion turboprop aircraft and one ship, the ex-USS *Shadwell* (LSD-15), birthed in Mobile Bay, Alabama. The ex-*Shadwell* is used for research on fire-suppression techniques on-board ship.

NRL in the Future

In order to provide preeminent research for tomorrow's Navy, NRL must maintain and upgrade its scientific and technological equipment to keep it at the forefront of modern research facilities. The physical plant to house this equipment must also be state of the art. NRL has embarked on a Corporate Facilities Plan to accomplish these goals. This plan and future facility plans are described below.

THE CORPORATE FACILITIES INVESTMENT PLAN (CFIP)

The CFIP is a financial spending plan to provide modern research facilities at NRL by the year 2000. The plan calls for both Congressional and Laboratory investment and is updated and altered as changes occur in scientific emphasis and Congressional attitude. During the past 5 years, Congressionally approved military construction (MILCON) funds were used to construct the new Electro-Optics Laboratory and a high-bay facility for the Naval Center for Space Technology. MILCON funds have been approved in the FY 97 Congressional budget for the construction of an Ocean Acoustics Research Laboratory building at NRL-SSC. Future MILCON funds have also been requested for the construction of a Nano Science Research building at NRL-DC.

To complement these efforts, overhead funds have been used to renovate and upgrade laboratory and support areas in several existing buildings. Modern laboratory facilities have recently been provided for the Center for Bio/Molecular Science and Engineering, the Materials Science and Technology Division, the Remote Sensing Division, and the Acoustics Division. Work that is currently in progress will provide new facilities for the Information Technology Division and the Radar Division.

In parallel with efforts to upgrade laboratory buildings to the most modern standards, those buildings that were built during World War II and which do not lend themselves to renovation are being demolished. This will provide space for the construction of future MILCON buildings, and it will also reduce the Laboratory's overhead costs.

Information Technology

The Information Technology Division's Center for Computational Science is awaiting delivery of two scalable, multiple-instruction multiple-data (MIMD) computer systems, which have Global Shared Memory (GSM) and Nonuniform Memory Architectures (NUMA). These systems are part of the Distributed Center (DC) at NRL that is funded by the DoD High Performance Computing Modernization Program (HPCMP). The systems will be used to continue innovative exploration and evaluation of massively parallel processing (MPP)

technology for the solution of significant military-relevant problems relating to computational and information science. The systems will allow for continuing research into heterogeneous parallel processing with the NRL Thinking Machines Corporation CM-500e systems and other computational assets.

Information Technology's Virtual Reality Laboratory will expand its facilities to include a large-scale, fully immersive Cave — a room-sized, multiuser, high-resolution 3-D visual and audio environment that projects computer-generated images onto three walls and the floor to create a shared virtual environment. The Cave provides true perspective viewpoint tracking for a single-user and collaborative viewing for as many as 10 other users. This technology promises to provide greatly improved capabilities for scientific visualization and virtual environments.

Plasma Physics

The division has established a new facility for research on high-frequency microwave processing of advanced ceramic materials. It features a unique, tunable (60 to 120 GHz) quasi-optical gyrotron, 35 and 94 GHz fixed-frequency gyrotrons, and a 6 kW, 2.45 GHz industrial microwave source. The facility is being used to investigate the scientific basis for understanding and controlling microwave processes, such as sintering/densification, coating, and joining, for low-loss, refractory ultrafine-grain polycrystalline ceramic materials.

Electronics Science and Technology

Important division emphasis is focused on the continual upgrading of the Nanoelectronics Processing Facility (NPF) and the Penthouse Processing Facility (PPF) and expanding activities in the nanoelectronics, heterostructures, and vacuum electronics science and technology programs. The Laboratory for Advanced Material Synthesis Facility will continue to upgrade its organometallic vapor-phase epitaxy equipment to meet program needs for thin-film semiconductors. Upgrades include safer and more environmentally benign processing and waste-disposal techniques. The EPICENTER (a joint activity of the Electronics Science and Technology, Materials Science and Technology, and Chemistry Divisions) will continue to provide new insight into epitaxial semiconductor growth processes. Knowledge of these growth processes will be used for improved control of film properties for use in the electronic devices of tomorrow.

Ocean Acoustics Research Laboratory

NRL's Ocean Acoustics Research Laboratory (MILCON Project P-006), a 52,000-square-foot building, will place 90% of NRL-SSC in one closely located area. This project will provide secure laboratory and computing facilities for research and development in ocean science and technology. Completion and occupancy should occur by the end of 1999.

Vacuum Ultraviolet Space Instrument Test Facility

The Space Science Division facilities include an ultraclean solar instrument test facility in Building A-13 on the main NRL campus. The new facility is designed to satisfy the rigorous contamination requirements of state-of-the-art solar spaceflight instruments. The facility has a 400-square-foot Class 10 clean room and a large Solar Coronagraph Optical Test Chamber (SCOTCH). This completely dry-pumped, 550-cubic-foot vacuum chamber is maintained at synchrotron levels of cleanliness. Solar instrumentation up to 1 m in diameter and 5 m in length may be physically accommodated in the chamber. The instrument's optical performance is probed and calibrated with a variety of visible and XUV sources mounted on the chamber's 11-m beamline. The optical testing and characterization of the Large-Angle Spectrometric Coronagraph (LASCO) instrument for the European Space Agency's Solar Heliospheric Observatory satellite was conducted in this chamber. Coronagraph stray-light characterization was carried out by mounting a set of baffles in the main beamline, illuminating the instrument with a simulated solar beam, and measuring the residual radiation. A stray light background measurement of 10^{-12} was successfully measured in the LASCO C3 channel. Coronagraph calibration was carried out by installing back-illuminated calibrated opals in front of the instrument entrance aperture. Instrument polarization properties were analyzed by using a variety of polarizers installed in a wheel located between the opal and the instrument. The wheel was remotely controlled from outside the chamber. Instrument Mueller matrices were verified

with a 12-in. diameter, two-plate partial polarizer. Calibration and focus of XUV solar instrumentation are accomplished by exposing the instrument to an XUV windowless collimator at the end of the tank. The facility also has a small thermal bake/vacuum test chamber used for vacuum conditioning and thermal testing of spaceflight components and subassemblies. Both the SCOTCH and the small test chamber are instrumented with temperature-controlled quartz-crystal monitors and residual gas analyzers for real-time, quantitative measurements of volatile contamination.

Remote Sensing

To validate numerical and theoretical efforts ongoing within the Remote Sensing Division, extensive hierarchical-coupled experiments are planned within a new, Free-Surface Hydrodynamics Laboratory. This laboratory will be used to study free-surface turbulence interactions, wave-generation phenomena, jet-flow phenomena, vorticity dynamics, and free-surface/surfactant interactions. Of particular importance is the detailed study of surfactant materials, both in shear and surface wave flows. State-of-the-art diagnostic tools are available, such as Langmuir film balance to measure the properties of surface films, hot-wire and laser-Doppler anemometry, together with the new quantitative flow techniques of laser speckle, particle tracking, and particle image velocimetry. The laboratory is also equipped with an IR camera with a 20×10^{-3} K resolution. These experimental diagnostic techniques use high-powered lasers, high-tolerance optical lenses, and extensive ultra-high-resolution video-imaging hardware and PC-based computerized systems. Further computational assets consist of powerful graphical computer work stations, the NRL Connection Machine, and other off-site CRAY supercomputer systems.

Marine Geosciences

The Marine Geosciences Division will greatly enhance the capabilities and quality of seafloor sediment fabric analyses through completion of purchase, installation, and staff training for a 300 kV transmission electron microscope (TEM) and accompanying environmental cell (EC) in FY 97. The TEM-EC will be housed in a specially built facility imparting a null effect on the functioning of the TEM-EC electronics. The new facility will improve transition of developed capabilities and sediment fabric understanding to applied issues of acoustic and shock-wave propagation, mine burial, and mine countermeasures.

REHABILITATION OF SCIENTIFIC FACILITIES

Specialized facilities are being installed or upgraded in several of the research and support divisions.

Flight Support Detachment

NRL's Flight Support Detachment (FSD) has continued to improve both capabilities and diversity among its aircraft platforms. Aircraft 153442 was transferred to Lockheed Martin to undergo extensive modification to install a "roto-dome" antenna and full AEW radar system. These modifications will support the Navy's Theater Air Defense programs, while providing a testbed for advanced EW radar research. Additionally, Aircraft 154589 and 154587 received updates to enhance interoperability and support pod-based research programs, such as the Advanced Multipod System (AMPS) and the Integrated Electronic Warfare System (IEWS). These upgrades and modifications will ensure that NRL will have the finest airborne research capabilities well into the next century.

Information Technology

The Information Technology Division continues to upgrade its local area network and research into high-performance network testbeds, including ATM/SONET technology. The 256-processor CM-500e massively parallel computer has been upgraded to 400 Gbytes of storage in the Scaled Disk Array and now has an Extended Control Processor tied in with an SCI ring that will include an SCI-ATM gateway in the future. Two additional scalable massively parallel systems will arrive in late 1996, which will allow for continued research into heterogeneous parallel processing in connection with the existing two NRL CM-500e systems and will provide an alternative globally shared-memory programming paradigm. The need for additional facilities to supplement research in virtual environments and Global Grid demonstrations will lead to gradual development of a demonstration/Virtual Reality and conference center in

Building 34. An upgrade for the Human-Computer Interaction Laboratory will integrate and enhance its video and audio presentation and recording capabilities.

Materials Science and Technology

Renovation is in progress for Building 3, which is composed of two of the original five buildings at NRL, to contain modern laboratories for studies of thin-film deposition and characterization, superconducting materials, magnetic materials, and other materials science projects. The new space will feature the most modern molecular beam epitaxy and other materials synthesis and processing equipment, an up-to-date fatigue and fracture laboratory, and state-of-the-art diagnostic equipment, including electron microscopes, spectrometers, and electron and X-ray diffraction equipment. The renovated building will also contain office and laboratory space for approximately 70 technical personnel.

Plasma Physics

A state-of-the-art short-pulse (<1 ps), high-intensity (>1 TW) Table-Top Terawatt (T^3) laser has been in operation for a variety of physics studies. The T^3 laser will be upgraded to boost its power to >20 TW. This will provide a facility to do fundamental physics experiments in intense laser-plasma interactions and intense laser electron beam interactions.

A low-frequency (300 MHz to 10 GHz), high-power microwave facility that uses a relativistic klystron concept is being upgraded to produce multigigawatt coherent radiation pulses.

A compact spectral imager, which records 2-D images of scenes with up to 500 spectral bands and 500 pixel spatial resolution, has been developed. This hyperspectral imager can be deployed on aircraft or on the ground for remote-sensing applications.

Electronics Science and Technology

The Electronics Science and Technology Division continues to upgrade and expand its capability in nanofabrication science. As a result, renovation is in progress in Building 208 to establish the Joint Laboratory for Proximal Probe Nanofabrication. This laboratory will serve as a resource for the characterization of electrical and mechanical properties of nanostructures, for establishing the limits to high-resolution material patterning, and for process development leading to advanced nano-device fabrication. The following capabilities will initially reside in this new laboratory: controlled ambient scanning probe lithography, high-vacuum scanning tunneling microscopy, in-situ high-resolution etch diagnostics, nanostructure electrical characterization, and atomic-force microscopy.

Highlights of NRL Research in 1996

Tubule-based Radar-absorbing Composites

Signature Technology Office

In recent years, the need to develop low-cost, high-performance radar-absorbing materials (RAM) has become increasingly important. Preliminary results of the Tubule-based Radar-absorbing Composites Program have demonstrated several RAM concepts to address these needs. A novel class of RAM designs has been developed that are competitive with current low-observable treatments. The overall development of tubule-based RAM composites has led to a patent application, which was sealed in October 1996. These accomplishments were achieved by several breakthroughs during FY 96: techniques to disperse water-based copper-coated tubules in composite panels (12 in. × 12 in.), the extension of the spherical-based percolation theory to cylindrical geometries, and RAM calculations based on measured properties indicating a class of light-weight, high-performance tubule RAM composite. Preliminary results indicate that tubule-based radar-absorbing composites may form the basis of next-generation, lower-cost, lighter-weight, high-performance, low-observable treatments to address the Navy's needs.

An Electronic Countermeasure to Microwave Intrusion Sensors

Signature Technology Office

A novel electronic device has been developed that renders microwave intrusion detectors ineffective within its area of control. The device was designed to exploit this weakness, and a "breadboard" demonstration was constructed and tested. This device was found to dramatically reduce the effectiveness of the sensor. A sensor, which normally would detect an intruder, failed to detect a person walking normally within the sensors' direct field of observation. Initiation of the countermeasure device's signal does not cause an alarm, and its removal leaves the sensors' performance unchanged. The device is amenable to redesign into a compact, unobstrusive and even more effective field unit. This electronic countermeasure will be important for forces in the field and for special operations.

ROTHR Small Boat Search Algorithms

Radar Division

The Navy Relocatable Over-the-Horizon Radar (ROTHR) is presently being used to track small aircraft that may be delivering illegal drugs to the U.S. mainland. The waveforms used have short dwell periods since aircraft have enough velocity to separate them from the clutter in Doppler space. A potential solution has been proposed. It is a variation of super-resolution, and it works against simulated targets. A potential algorithm has been devised and tested successfully against simulated in-phase and quadrature (I&Q) waveforms containing synthetic targets. The algorithm successfully extracts the targets that are initially buried in the Bragg lines. Since I&Q data will now be available from the ROTHR (located in Virginia), it will be possible to test this algorithm against real targets using real radar data. If successful, the technique would allow enhanced use of an expensive Navy asset with little additional investment over what has been planned.

AN/SPQ-9B Radar Program

Radar Division

The AN/SPQ-9B radar concept maintains AN/SPQ-9 radar MK 86 gun-fire control-system support while adding a low-cost, quality, sea-skimmer detection capability in a heavy-clutter environment, that currently does not exist. The concept provides significantly increased sensitivity and improved ability to detect targets in clutter while maintaining current operating modes. The AN/SPQ-9B Advanced Development Model is being used to test new design concepts, software algorithms, and various radar interfaces to reduce development risk and to recommend improvements to the production design. NRL is currently developing new sidelobe canceller algorithms for the AN/SPQ-9B. In support of work, additional receivers and jammers have been built to allow the collection of data to test the canceller. The AN/SPQ-9B radar is scheduled for installation on the DD 963, LHA, DDG 993, CVN 76, and the CG 47 ship classes.

Advances in Perception, Action, and Learning in Mobile Robots

Information Technology Division

The Navy Center for Applied Research in Artificial Intelligence's project in perception, action, and learning has contributed to the design of future autonomous systems by extending and integrating recent results in machine perception, behavior-based control, task planning, and machine learning. Results were tested on mobile robots performing cooperative and competitive tasks. Long-term goals include answering fundamental questions such as: Can a robotic system learn how much perceptual detail is required for particular behaviors? Can it learn to adapt to unexpected changes in its sensor/motor capacities? The algorithms and software architectures developed under this project will transition directly to the Machine Learning task at NRL, which is developing software tools that enable autonomous vehicles and other systems to adapt to their operational environment.

Onion Routing

Information Technology Division

The use of a packet or circuit-switched network should not require revealing who is talking to whom. The Onion Routing project developed a flexible communications infrastructure that is resistant to both eavesdropping and traffic analysis. Onion routing accomplishes this by removing information from the data stream. In a packet-switched network, packets have a header used for routing and a payload that carries the data. The header reveals the source and destination of the packet. Even if the header were obscured, the packet could still be tracked as it moves through the network. Encrypting the payload is similarly ineffective because the goal of traffic analysis is to identify who is talking to whom and not to identify directly the content of that conversation. We have designed and implemented a prototype system that provides anonymous connections that can be used by a wide variety of unmodified Internet applications, such as World Wide Web browsing, electronic mail, remote login, and file transfer.

Chalcogenide Fibers Enable Delivery of High-Power Mid-IR Laser Radiation

Optical Sciences Division

NRL has demonstrated high-power transmission through chalcogenide glass fibers using both continuous wave (CW) and pulsed-IR laser sources. Up to 7.3 W of CW laser power at 5.4 μm and 500 MW/cm^2 peak power density from a pulsed laser at 3.48 μm were successfully launched into sulfide glass-clad fiber. Antireflection (AR) coatings have been applied to fiber endfaces to reduce the reflection loss from 17% to less than

1% per endface. A new method to fabricate fiber connectors has been developed that improves AR coating adhesion and high average power throughput. A method to smooth the far-field speckle distribution at the fiber output has been developed for IR countermeasures applications. With recently achieved low optical losses and higher strength obtained for chalcogenide fibers, the following applications have become attainable: IR countermeasures and laser threat-warning systems, fiber for focal plane arrays, and IR chemical sensors.

64-Channel All-Optical Deplorable System (AODS) Array

Optical Sciences Division

Recently NRL's All-Optical Deplorable System (AODS), using a combination of wavelength and time division multiplexing (WDM/TDM), has demonstrated the transmission of 64 fiber-optic hydrophone signals over a single fiber. The AODS concept uses batteries to power four optical wavelengths, each carrying 64 TDM channels, supporting 256 fiber optical hydrophones. The two-node AODS system was successfully deployed and tested in 1996. System deployment took less than 1 day, and the array survived for 5 months. The AODS 2 node test demonstrated that 64-channel fiber-optic hydrophone array system could be built, deployed, and tested in an at-sea environment. This system will provide a small, compact, rapidly deplorable undersea surveillance system for shallow water applications.

Vectored Infrared Personnel Engagement and Returnfire (VIPER)

Tactical Electronic Warfare Division

A perimeter defense system (VIPER) has been developed and demonstrated that detects a hostile infrared muzzle flash and then communicates to the user precise location data for counterfire. The system provides rapid detection of muzzle flash at or beyond weapon effective range against all weapons tested to date and provides sniper alert prior to bullet impact. Peacekeeping operations and expeditionary warfare have become important functions for the U.S. Navy and Marine Corps, and as such, direct engagements with land forces are increasingly likely. In many such scenarios, the sniper problem will be critically important because of the nonuniformed enemy who engages in harassment-type operations for political and military reasons. In man-portable, vehicle-mounted, and aircraft versions, VIPER will be an immediate military response to any type of gun flash, denying the enemy a free-fire capability. It may also be applied to non-military uses —for example, DEA, FBI, SWAT, and Secret Service operations.

Practical Method for Performing Quantum Crystallographic and Ab Initio Calculations for Molecules and Macromolecules

Laboratory for the Structure of Matter

Recently, a method for combining experimental information from crystallography with ab initio quantum mechanics was established. Examination of the mathematics of quantum mechanics has led to "fragment" calculations that provide access to macromolecules. The time required for the fragment calculations increases linearly with the complexity of the molecular structure of interest. A way was found to divide very large molecules into fragments that are a feasible size to compute. With an appropriate way to combine the results for the fragments, it is possible to obtain ab initio wave functions for very large molecules. A current study involves the membrane active antibiotic that transports potassium ions across a gate, which could explain why the experiment shows that one potassium ion at a time is transported and why a potential is required to facilitate the transport. The fragment method can revolutionize the use of quantum mechanics to determine such properties as electron density distributions, charges on atoms, molecular energies, and electrostatic potential.

Multisensor Towed Array Detection System (MTADS)
Chemistry Division

Unexploded ordnance (UXO) is arguably the most serious and prevalent environmental problem currently facing DoD facility managers. It is the environmental issue that will be the most expensive to mitigate and remediate. Often UXO is located with other environmental threats, including ordnance explosive waste, chemical waste, and other toxic and hazardous materials. Current techniques for UXO detection, site characterization, and remediation are slow, labor intensive, and inefficient. Typical detection and characterization technologies involve hand-held detectors operated by walking explosives ordnance or civilian technicians. NRL is developing a multisensor detection system that will extend and refine ordnance detection technology to more efficiently characterize ordnance and explosive waste sites. The successful deployment and commercialization of MTADS will provide state-of-the-art technology in environmental ordnance remediation for use by all branches of DoD.

Low-Solar-Absorbance Paint
Chemistry Division

NRL has produced a new formulation for the Navy's standard shipboard topside paint that reflects solar energy, thus diminishing the accumulation and reradiation of heat. Infrared gray-body radiation from ship hulls and superstructures arises from the intrinsic heat of the ship. Some of this heat arises from on-board machinery, but a principal heat source is the absorbance of solar radiation by Navy haze-gray paint. Paint that reflects solar radiation reduces heat buildup, thereby increasing crew comfort and endurance and reduces reradiation of infrared energy. This upgrade will be invisible to ship's forces, to maintenance personnel, and to environmental and worker safety officers, because the physical properties of the new coating will be identical to the old. The new formulation was approved for use by the Navy Environmental Health Center, Norfolk, Virginia.

Pulsed-Laser Deposition of Collagen and Collagen-Hydroxyapatite Composites
Condensed Matter and Radiation Sciences Division

Pulsed-laser deposition (PLD) has been used to deposit thin films of hydroxyapatite that are more highly pure and crystalline than films deposited by other methods (for example, plasma spraying). For biomedical applications, it is of interest to duplicate the chemistry and structure of bone as closely as possible. The accomplishment of PLD of collagen has applications itself for wound healing wherein the collagen film could serve as a scaffold for the regeneration of skin for burn victims. Collagen-hydroxyapatite composites may prove to have better biocompatibility as coatings for orthopedic implants due to their closer duplication of the structure and composition of natural bone. This is the first demonstration of the phenomenon on "crystal tectonics," the chemical construction of organized architectures resulting from organic surface chemistry associated with biomineralization during a thin-film deposition process.

Density Functional Studies of Skutterudite Thermoelectrics
Condensed Matter and Radiation Sciences Division

Thermoelectric devices used as solid-state coolers or electrical power generators have no moving parts, are extremely reliable, do not require the use of refrigerants, and can be scaled from small cooling devices to full-scale room or ship coolers. On the other hand, existing devices have lower energy efficiencies imposed by the thermoelectric performance of known materials. Thermoelectric materials with higher performance are being sought. To this end, electronic structures, phonon frequencies, and transport properties of

Skutterudite and filled-Skutterudite materials were studied using first-principle calculations. Beside a new understanding of the electronic structures of binary Skutterudites, the main features of which have now been confirmed, these studies led to the suggestion that filled Skutterudites, $CeFe_4Sb_{12}$ and $CeFe_4As_{12}$ might be good thermoelectric materials, particularly with n-type dopants. Subsequent to our calculations, an experimental group at the Jet Propulsion Laboratory synthesized Co-doped $CeFe_4Sb_{12}$ and found the material to have a dimensionless figure of merit ZT of 1.4. This value exceeds the performance of any previously known thermoelectric material. This material will be suitable for power-generation applications.

Evolution of the Electronic Excitation Spectrum of an Incipient Antiferromagnet

Condensed Matter and Radiation Sciences Division

The role of antiferromagnetic spin correlations in the normal state of the high-temperature superconductors and related antiferromagnetic materials was investigated using a Hubbard model and a finite-temperature Green's function technique. Numerical calculations were performed using large-scale parallel-architecture DoD high-power computing facilities. A simplified model for interacting electrons in copper-oxygen planes was used to study how the electronic excitation spectrum evolves as the antiferromagnetically ordered state is approached with decreasing temperature and increasing interaction strength. The resulting electronic excitation spectrum shows structures in the metallic state that are "shadows" of an antiferromagnetic ground state, excitations near the Fermi energy that are qualitatively different from those of an ordinary metal, and the formation of a gap at the magnetic zone boundary. These results yield valuable insight into the role of electronic interactions in classes of materials and provide a basis for the extension of the finite-temperature theoretical approach used here to more detailed and accurate models of electronic excitation and magnetic and superconducting states in real materials. The many possible applications include fast electronic devices such as Rapid Single-Flux Quantum logic devices and superconducting transistors and signal transmission lines.

Sheath-coupled Cross-field Ion Transport in Magnetized Discharges

Plasma Physics Division

NRL has shown that the spatially dependent sheath potential drop plays a critical role in cross-field diffusion of ions in a magnetized plasma discharge contained within a conducting vessel. The sheath potential adds a term that is mathematically similar to a viscosity, dissipating nonuniformities in the cross-field ion flux. This effectively suppresses internal cross-field plasma diffusion due to ion pressure variations, as well as waves associated with ion pressure. It was shown analytically and computationally that the dominant contribution to the plasma potential is due to the spatially dependent sheath potential drop associated with the electron flow. This type of reactor is in use at NRL as an etcher and is the major focus of the Plasma Processing Advanced Research Initiative. Other examples include helicon plasma-processing sources and certain fusion devices.

A 230 Watt S-Band SiGe Microwave Power Heterojunction Bipolar Transistor (HBT)

Electronics Science and Technology Division

A SiGe HBT microwave power transistor has demonstrated significant improvements over a state-of-the-art silicon bipolar microwave power transistor and has achieved the highest power and highest efficiency S-band microwave power transistor ever reported. Small-signal microwave transistors fabricated using this technology have achieved f_T of 113 GHz and f_{max} of 160 GHz; prior to this work, no results had been

reported for SiGe HBT for high power microwave operation. The peak efficiency of the SiGe HBTs was 50% compared to less than 35% for the silicon transistors. The results represent a performance improvement of over 30% in power and efficiency. The primary applications for the SiGe microwave power transistor technology is for solid-state microwave power sources for active-aperture radars and microwave communication systems. Potential system applications include AEGIS, JTIDS, and MIDS.

Low-Frequency Dielectric Constants of Semiconductors

Electronics Science and Technology Division

A new method for making accurate determinations of low-frequency dielectric constants of materials has been developed. Low-frequency dielectric constants often are determined by extrapolating accurate near-IR values with the Lyddane-Sachs-Teller (LST) relation. Published data suggest that this relation is accurate to approximately 1%, but an accuracy of greater than 1% is desired for some applications. NRL has developed an experimental technique that uses spectroscopy from the near IR into the submillimeter region that can determine both the dielectric constant and confirm the LST relation. Understanding the properties of semiconductors used in commercial and military systems is essential for future material and device improvement. The most fundamental properties, such as the dielectric constant, enter into many electrical and optical-device characteristics and are used in calculations of carrier-transport properties and impurity and defect characteristics. Potential applications include electric, optical, and theoretical properties of semiconductors and the devices made from them.

Sub-10 nm-sized Metal/Oxide Quantum Devices

Electronics Science and Technology Division

A new fabrication technique has been developed that can produce true nanometer-scale metal/oxide-based quantum devices with precisely controlled electrical properties. The fabrication process uses an electrically conducting atomic-force-microscope (AFM) tip to locally anodize thin metal films. Real-time in situ device measurements are used as feedback to guide the anodization. Such a spatially local anodization process, combined with the in situ electrical measurements, allow NRL to fabricate sub-10-nm-sized metal/oxide devices with precisely controlled electrical properties. This approach is used to fabricate the smallest possible device, a one-atom metallic wire. This accomplishment is significant because it demonstrates a means for controllably fabricating true nanometer-sized devices by using a simple process with widely available equipment. These features make this a promising candidate for a room-temperature-operational quantum transistor, and we are using this novel fabrication technique to explore such metal/oxide-based nanoelectronics.

Improved Vertical Array Performance in Shallow Water with a Directional Noise Field

Acoustics Division

A new array processor — the matched-beam processor — was developed to improve the rejection of surface-generated noise fields in acoustic beamformers. The matched-beam processor exploits directionality of the noise field to separate high-angle surface noise from low-angle target signals. Source position in range and depth is obtained by combining a fan of complex acoustic beams in a matched-field sense. This new processor is a hybrid with the most desirable properties of a conventional beamformer (directionality) and a matched-field processor (localization). Higher array gain and better localization performance with matched-beam processing means we can identify a target farther away (or equivalently, a quiet target) with better confidence for a given array configuration. The better performance with a submerged target is significant because it may be difficult to detect targets by other means.

Effect of Median Stability on High-Frequency Sound Propagation in Shallow and Very Shallow Water

Acoustics Division

New-generation mine-countermeasure systems are being developed that are based on the synthetic-aperture-sonar (SAS) concept. The performance of these systems is limited by the spatial and temporal stability of the medium in which they operate. NRL has conducted the first high-frequency acoustics measurements in very shallow water (10 m) to determine the effect of the medium on SAS performance. Results demonstrate that the acoustic phase variability is a result of small-scale variations in the ocean thermal microstructure that increases with acoustic frequency and occurs with a period that corresponds to the ocean swell. These data will be used to predict SAS processing gains based on selected environmental parameters. Accurate measurements of the effects of the medium on SAS performance in very shallow water are a first step toward developing a reliable prediction model for these environments. The U.S. Navy and DARPA are developing prototype SAS systems to be used in mine-countermeasure applications in very shallow water. This work is in direct support of this development program.

Remote Sensing of the Ocean Surface Wind Vector Using Passive Microwave Polarimetry

Remote Sensing Division

The global ocean surface wind speed and direction are essential information facts for short-term weather forecasts and warnings, climatology, and oceanography studies in both the civilian and military sectors. Historically, spaceborne scatterometers have provided global ocean surface wind vector information. Preliminary retrieval algorithms using neural network algorithms have demonstrated that the first three Stokes parameters (I, Q, and U) at 19 and 37 GHz can be used to retrieve the ocean surface wind direction. The development of models to reduce the measured brightness, temperatures, and Stokes parameters to surface emissivities has begun. This is integral to the development of the Navy's capability to measure the ocean surface wind speed and direction. The advent of passive microwave polarimetry makes meeting the Navy's operational requirement for winds technically and fiscally feasible.

Ocean Surface Slope Measurement by Polarimetric SAR

Remote Sensing Division

The topographic effect associated with ocean surface features, such as current fronts, eddies, and surface deformation due to the underlying geoid, can be measured with radar altimeters to an accuracy of a few centimeters. A new technique based on the polarization signature of Bragg scattering has been developed that uses polarimetric synthetic aperture radar (SAR) to measure the slope in the along-track direction over a two-dimensional ocean surface. The significance of this accomplishment is that the remote sensing of the ocean surface by SAR does not need to rely on backscatter intensity modulation alone as a marker of ocean features. A new, independent parameter is now available to detect and characterize ocean features such as convergent fronts, surface manifestations of internal waves, and bathymetric features. The technique is also significant for its potential ability to remotely sense and discriminate between classes of ocean features.

Discovery of a New Supernova Remnant at the Galactic Center

Remote Sensing Division

Wide-field, low-frequency imaging have revealed a new supernova remnant (SNR) in the center of our Galaxy. With the exception of SGR-A East, the new source G0.33+0.04 is now the closest identified SNR to the Galactic center. There are a host of observations from radio wavelengths to gamma ray energies that

support the hypothesis that the supernova birthrate near the Galactic center is, or has recently been, much higher than inferred elsewhere in the Galaxy. The new discovery provides important evidence in support of this hypothesis. The division's work in this area has demonstrated that the once formidable problem of three-dimensional image deconvolution is now a tractable problem when addressed with modern, scaled processing-computing algorithms.

Forced Upper Ocean Dynamics

Oceanography Division

Using an advanced air-sea hydrodynamical-biodynamical model in situ and remote measurements, the response of the Indian Ocean to the annual monsoonal cycles has been accurately described for the first time. This work showed that the nutrient-rich waters are advected far offshore by intense mesoscale eddies and jets that carry upwelled water from the continental shelf. The biodynamical-hydrodynamical model accurately described the succession, population densities, and bioluminescence distributions that evolve as a result of the upwelling and advection. NRL's coupled model accurately describes the predictive relationship between the hydrodynamics and ecosystem responses. Spatial and temporal relationships of the physical environment and pelagic ecosystem can be predicted for the Arabian Sea.

Surfzone/Mine Interaction Program — Torrey Pines Field Experiment

Marine Geosciences Division

As part of a program to understand and predict the behavior of antitank mines placed on a beach, a field experiment was held at Torrey Pines State Beach, California. Instrumentation to capture the relevant hydrodynamic conditions was emplaced in a cross-shore-oriented array and included current meters and wave gages. Movement of the mines was monitored through video-image processing. Three varieties of mines were placed on the beach face at low tide and were then monitored for movement or burial during the rising tide phase. Tests were also conducted in which mines were buried just below the surface and were then monitored for "unburial" as the wave action reached their position. This program is expected to provide a capability to assess whether mines expected to be encountered are likely to have migrated to some predictable location and whether or not burial due to scour is likely. This program represents the only surfzone mine study being conducted within NATO.

Derivation of Atmospheric Winds from Geostationary Satellite Water-Vapor Imagery

Marine Meteorology Division

Geostationary satellite imagery has been used to supplement the atmospheric data void over remote locations. Algorithms that infer wind speed and direction by tracking individual clouds from one image to another have been adapted to sequential water-vapor images. Tracking water-vapor gradients can provide high-density upper-level wind observations even in cloud-free regions. This effort calculates the wind vector from sequential imagery and assigns a height by checking the measured radiance against model estimates of the thermal field. This research and development project was the first in the world to routinely exploit water-vapor imagery in this manner. The Navy is the first institution to make use of this new data source, which has led directly to improved warnings and forecasts for tropical cyclones impacting Navy resources around the globe.

Army Airborne Command and Control System (A2C2S)

Space Systems Development Department

The A2C2S is a UH-60 helicopter-based command and control (C2) mission kit that will serve as a corps, division, or maneuver brigade commander's airborne tactical command post. The system will feature situational awareness that fosters a commander's common view of the battlefield; it will also include voice and data equipment that provides battlefield information processing and connectivity equivalent (via a tactical internet) to ground tactical command posts and battle command vehicles. The A2C2S Program now is authorized officially to begin development of Engineering Design Models for the objective system. During war, the situational awareness ability will enable the war fighter to exercise C2 "on the move" for assigned and attached elements and to coordinate with adjacent supported and supporting forces. In addition, during operations other than war, the system will provide accurate connectivity to embassy, law enforcement, maritime, civil and/or other humanitarian information/communication networks.

NaSBE, Sodium Sulfur Battery Experiment

Space Systems Development Department

The department has developed a flight experiment to demonstrate the performance capability of a newly developed sodium sulfur (NaS) electrochemical battery in the absence of gravity. Sodium sulfur batteries have the potential for much higher energy density and specific energies than currently used nickel hydrogen and nickel cadmium batteries. This is especially valuable on space vehicles. The experiment will demonstrate that these cells will operate in space and enable others to use this new, state-of-the-art battery technology. In addition, the lightweight, low-volume NaS cells will reduce the mass and volume of many military and commercial spacecraft.

Advanced Fiber-Optic Sensing Program

Spacecraft Engineering Department

High-quality fiber Bragg grating strain sensor arrays have been fabricated and surface-mounted on aluminum honeycomb composite panels. Instrumentation for interrogating 16 multiplexed sensors for static strain measurements has been developed, and static measurements have been made. A breadboard instrumentation system has been developed and the system was used in the vibration testing of a spacecraft structural deck. An algorithm has been developed for real-time calculation and display of two-dimensional surface deformation of the plate from strain measurements by 16 fiber Bragg gratings, with the capability to run with over 32 sensors. This program will demonstrate the unique capabilities and advantages of fiber-sensor technology for spacecraft engineering/monitoring applications and will develop space-qualified flight and laboratory high-bandwidth sensor systems that are lightweight, low-cost, low-power dissipators, multiplexable, electromagnetic interference immune, highly sensitive, and long-term reliable.

Meet the Researchers

Dr. Ben H. Cantrell is head of the Radar Characteristics Branch, Radar Division, and has served in this capacity for over 9 years of his 25-year career at NRL. The branch performs basic and applied research, radar analyses, experimental systems development and testing, conducts experiments, and provides support to the Navy in their programs. Dr. Cantrell has formulated and initiated numerous programs over the last few years. These include a new shipboard sea skimmer radar, SPY-1 radar improvements in clutter rejection and identification, radar operation without sensitivity time control, multiple-interval clutter rejection by magnetrons, and high-stability receiver/exciter equipment. The SPS-49A and the SPQ-9B programs have transitioned to production and preproduction, respectively. Advanced Development Models (ADMs) were developed, constructed, and tested by researchers under Dr. Cantrell's direction and, in both cases, orders-of-magnitude improvements in clutter rejection were achieved. Dr. Cantrell also works with numerous Government agencies in various ways to provide direction of research and development for the Navy. He was recently a key participant in an effort to lay out a Navy radar road map for the next 10 years.

"My career at NRL has provided me the opportunity to serve the Navy in the area of national defense. Along with my colleagues at NRL, industry, and other government agencies, we have had the opportunities to develop new technologies to provide orders-of-magnitude improvements in our defense equipment. I feel fortunate to have been able to play a role in these technology developments."

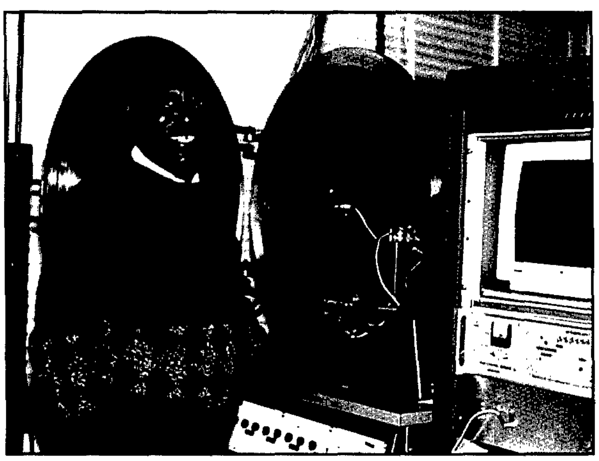

Mr. Fredrick Danzy is an electronics engineer in the Space Applications Branch of the Space Systems Development Department (SSDD) in the Navy Center for Space Technology. He heads the branch's Project Analysis Unit and the Precision Clock Evaluation Facility. Mr. Danzy serves as a team leader in the development, test, and evaluation of precision timing systems for satellite applications. He has played a major role in the development of the atomic clocks used in the Global Positioning System (GPS). He is currently responsible for a new initiative for design enhancements and characteristics evaluation methodology for the next generation of atomic clocks for future GPS satellites.

"The SSDD's Precision Clock Evaluation Facility is a unique NRL resource, particularly in the development, test, and evaluation of high-precision timing devices for satellite applications. The accomplishments of the facility have resulted in significant improvements in the performance and operating characteristics of atomic frequency standards developed for DoD spaceborne-, sea-, and ground-based applications."

Dr. Ruth H. Preller is section head of the Coastal and Semi-Enclosed Seas Section within the Oceanography Division at Stennis Space Center. Section scientists focus on the development of numerical models and their application to the study of ocean processes and to ocean nowcasting and forecasting in coastal seas. This is largely accomplished through the use of the resources provided through DoD High Performance Computing Centers. Projects within the section rely on techniques using data in conjunction with numerical models, both in terms of model validation and data assimilation. Dr. Preller's current research activities are focused on the application of numerical models to environmental problems in the Arctic Ocean, as well as on modeling processes in the shallow semi-enclosed seas of the western Pacific "rim" region.

"My professional experience at NRL has been both interesting and challenging, mainly due to the ever-changing nature of my job. This experience has focused on the application of numerical models to problems in ocean circulation. These applications have ranged from modeling the circulation of semi-enclosed seas, such as the Mediterranean Sea and the Yellow Sea, to modeling the growth and decay of the ice cover in the Arctic. One of the most gratifying aspects of my work at NRL is the opportunity to carry a project out from its early stages of basic research through to advanced development and finally to the implementation of models into operational Navy forecast systems. Working at NRL has provided me not only with the opportunity to address challenging research issues but also the knowledge that this work can lead to the improved success of Navy operations."

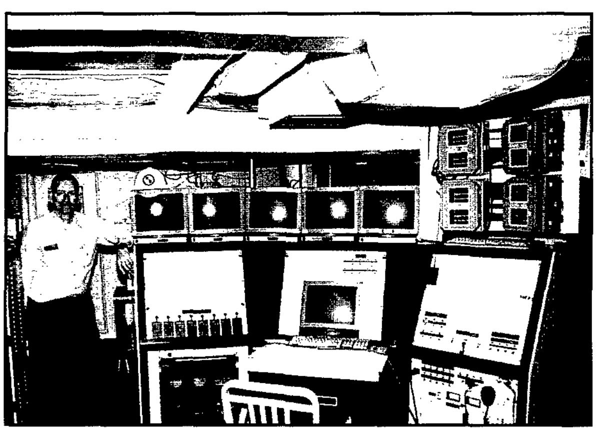

Dr. Frederick W. Williams is director of the Navy Technology Center for Safety and Survivability, Chemistry Division. He is also technical director of the ex-USS *Shadwell* (LSD-15), the Navy's full-scale damage-control fire fighting research ship based in Mobile, Alabama. The ex-*Shadwell* is a 457-ft, 10,000-ton Landing Ship Dock. The center conducts broad-based combustion and fuels research spanning from basic to applied work; further, it maintains intermediate-scale fire research facilities at NRL's Chesapeake Bay Detachment (CBD). Among the unique facilities at CBD is the worlds largest pressurizable submarine fire test chamber. Recent advances at the center include environment-friendly fire-fighting agents as replacements for halon, advanced fire-fighting doctrine under reduced manning, fire-hardened insulation and electrical cables, advanced simulation models for fire and smoke spread in ships, and fixed suppression systems for submarines.

"It is becoming more apparent that immediate relevance is important in our workplace. It is also important for us to keep in mind that basic principles give us our firm foundation on which we build our relevance. NRL has afforded me the opportunity to work across all facets of the R&D world, from the very basic to the direct Fleet support. As we move into a new century, I look forward to having our center continue to play an active role in Navy survivability."

Featured Research

Modeling the Dispersion of Radioactive Contaminants in the Arctic

R.H. Preller and P.G. Posey
Oceanography Division

International attention has been drawn to the fact that a substantial amount of radioactive waste was dumped into the shallow waters of the Kara Sea by the former Soviet Union. This issue raised both national and international environmental concern. From the national point of view, the United States is interested in the possible impact this dumping may have on the fishing industry along the northern coast of Alaska. Results from a coupled ice-ocean model, which is part of the U.S. Navy's Polar Ice Prediction System 2.0 (PIPS 2.0), are used to determine the preferred pathways taken by radioactive waste dumped into the shallow water of the Arctic seas. Based on reports from the former Soviet Union, model simulations incorporate the release of radionuclides at the locations of known dumpsites, including the major rivers that empty into the Kara Sea. The coupled model allows for the calculation of preferred pathways taken by the radionuclides, either suspended in the water column or trapped in sediment contained in the sea ice. Model results show that neither the ocean nor the sea ice provides a rapid transport pathway to the Alaskan coast.

INTRODUCTION

Countries making use of nuclear power are posed with the question of how to safely dispose of the resultant radioactive waste. One option that has been used by many of these countries is the dumping of radioactive waste into the deep ocean. Disposing of this waste into deep waters limits its possible contamination of the ecosystem. In September 1991, public attention was drawn to information presented at a Greenpeace conference concerning the disposal of radioactive waste by the former Soviet Union. Indications were that substantial amounts of radioactive waste had been disposed of in the shallow waters of Russian Arctic seas. In October of 1992, the President of the Russian Federation formed a commission to investigate issues relating to the disposal of radioactive waste at sea. The Commission's report, now referred to as the White Book (or the Yablokov Report [1]) was released to the public in 1993. It documented the dumping of both liquid and solid radioactive waste into the shallow waters of the Kara and Barents Seas from 1959 to 1992. This news raised international concern for the safety of local and distant fishing grounds. In particular, the United States was concerned with the possibility that the radioactive waste might be transported from the Kara Sea to the northern coast of Alaska.

A group of scientists was organized by the Office of Naval Research, under a congressionally authorized program called the Arctic Nuclear Waste Assessment Program (ANWAP), to investigate the environmental issues raised by the dumping of this waste. A major emphasis of this program was the gathering of data, both historical and new, to gain a better understanding of the past and present states of the environment in the affected Arctic seas. Several scientists from NRL's Radiation Effects and the Marine Physics Branches played a major role in gathering these data. A key research issue in this program was the study of potential transport pathways for the radioactive waste once released into the water column or surrounding sediments. Could the radioactive waste be carried away from the dumpsites into adjacent regions and contaminate the local food chain? If so, how, and which would be the dominant pathways? Scientists from NRL's Ocean Dynamics and Prediction Branch proposed to investigate these potential pathways by applying the ice-ocean model used as the basis of the Navy's sea-ice forecasting system, the Polar Ice Prediction System 2.0 (PIPS 2.0). The PIPS 2.0 seemed ideal for such a study since it

covered the region of interest, contained mechanisms for studying the transport of contaminated waste both through the ocean and sea ice and was advanced enough to be applied immediately to the problem.

THE MODEL

The PIPS 2.0-coupled ice-ocean model was developed by NRL to forecast ice conditions for the sea-ice-covered regions of the Northern Hemisphere. As a result, the numerical model extends from the North Pole southward to approximately 30°N latitude. The model uses a horizontal grid resolution of approximately 0.25° and has 15 levels to define the vertical structure of the ocean. Figure 1 represents the model domain and the horizontal grid structure.

The two numerical models that serve as the basis of the PIPS 2.0 are the Hibler Ice model [2,3] and the Bryan and Cox ocean model [4]. The ice model calculates ice drift, ice thickness, and ice concentration or the percentage of ice cover over an area. The ocean model calculates ocean temperature, salinity, and currents. The two models are coupled by exchanging heat and salinity fluxes, as well as interfacial stresses defined by the interaction of winds, ice motion, and ocean currents [5]. The ocean model was designed to simultaneously calculate multiple passive tracers. Temperature and salinity fields are calculated in this manner. This capability was extended to the calculation of radionuclides as such a passive tracer. This technique allows for the release of radionuclides into the model at a specified rate with a specified half-life. Once released, the radionuclides are transported by the processes of advection and diffusion.

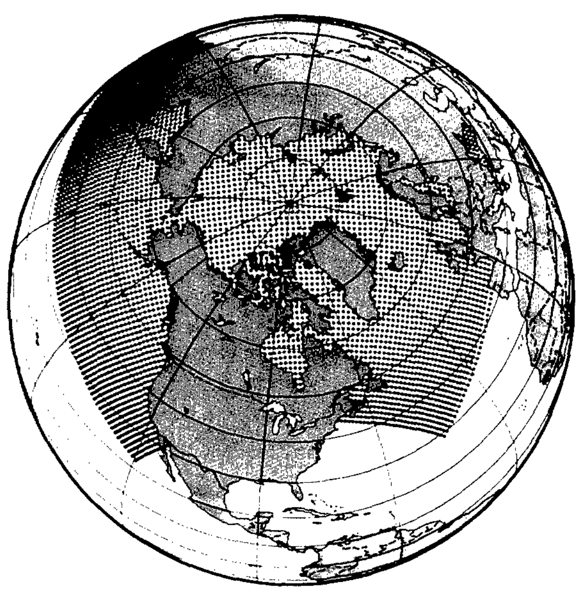

Fig. 1 — The horizontal grid and the model domain used in the Polar Ice Prediction System 2.0 (PIPS 2.0). Every fourth grid point of the model is plotted.

The coupled-ice-ocean model, run on a Cray C90 computer, is initialized with climatological temperature and salinity data derived from a database created by Levitus [6]. The model is also initialized with an estimate of the average ice thickness and concentration for winter. The ocean's bathymetry is derived from the Navy database, DBDB5. This model also includes fresh-water runoff from the eight major rivers of the Arctic. Two of these rivers, the Ob and Yenisei, each as large as the Mississippi, flow into the Kara Sea.

When the model is numerically integrated out in time, it is forced by atmospheric heat fluxes and surface stresses (winds) derived from the U.S. Navy's global atmospheric model — called the Navy Operational Global Atmospheric Prediction System (NOGAPS) — developed by the Marine Meteorology Division of NRL. During the numerical integration, the model evolves an ocean thermal structure and ocean circulation, as well as ice motion and ice cover based on these forcing fields.

MODEL SIMULATIONS

The model was used to investigate the dispersion of radioactive waste dumped into the Arctic Ocean by first studying methods of transport in the ocean and then adding the possibility of transport via sea ice into the calculation. To do this, the first model simulations were carried out with the ocean model alone. These simulations were run for anywhere from 10 to 30 years, using the NOGAPS atmospheric forcing. Several model simulations were carried out using different source locations and release rates for the dumped radioactive waste. These source locations and release rates were based on the data provided by the Russian White Book [1]. For lack of more detailed information, release rates were taken as constant values and calculated from the total amount of waste dumped and the period of time over which it was dumped. Two of the dominant isotopes released in the discarded waste were ^{137}Cs (137 cesium) and ^{90}Sr (90 strontium). These isotopes were appropriate for the model simulations since each has the characteristics of a passive tracer and a half-life of approximately 30 years.

Table 1 — Anthropogenic Radionuclide Budget of the Barents and Kara Seas Ecosystem, 1961-1990 [1]

Source of Long-Lived Radionuclides	Barents Sea		Kara Sea		Ecosystem as a Whole		
	Activity		Activity		Activity		Contribution
	kCi	TBq	kCi	TBq	kCi	TBq	%
1. Atmospheric fallout	100	3700	70	2600	170	6300	6.2
2. River runoff†	6	200	33	1200	39	1400	1.4
3. Contributions from Gulf Stream System†	200	7400	—	—	200	7400	7.3
4. Dumping of solid and liquid RW†	13	480	16	600	30	1100	0.7
5. Sinking of SRW with SNF†	—	—	2300*	85300*	2300*	85100	84.4
6. Underwater and surface nuclear explosions	. . . (No data) . . .						
Total (upper limit)	319	11780	2419	89700	2739	101300	100

*Expert estimate of the upper limit of activity at the time of disposal.
†Sources dumped directly into the ocean.

Table 1 shows the dominant sources of radioactive waste and their contribution to the total radioactivity for the Kara and Barents Seas. Common units of radioactivity are the curie (Ci), defined as the number of disintegrations per minute equivalent to one gram of radium, or 3.7×10^{10} disintegrations per second, and the becquerel (Bq), defined as one disintegration per second. Figure 2 shows the location of these sources. Solid waste dumped into the Kara Sea included containers, ships, barges, and submarines containing nuclear reactors. Liquid waste was discharged directly into the ocean water, predominantly into the Barents Sea. Numerical model simulations were carried out for the sources dumped directly into the ocean (marked as Sources 2 to 5 in Table 1). Atmospheric fallout was not included in this study.

The largest contribution to the total inventory of dumped radioactive waste comes from the source called solid radioactive waste (SRW), with spent nuclear fuel (SNF). This waste consists of sunken objects, such as nuclear reactors, which were dumped in the shallow bays and inlets along the coast of Novaya Zemlya Island, in the Kara Sea. Reactor compartments were encased in a substance called furfurol, which was estimated to restrict contact with the sea water for anywhere from 100 to 500 years. Thus it was estimated that this source, though large, might not be an immediate environmental hazard. Numerical model simulations, which were made assuming that this source was actually leaking, produced levels of radionuclides in the Kara Sea one to two orders of magnitude larger than those recently observed. The conclusion was that this material is, indeed, still well sealed within the furfurol mixture. A similar experiment was conducted using the low-to-intermediate level solid and liquid radioactive waste, listed as Source 4 in Table 1. Model simulations showed that the levels of radioactivity in the Kara Sea in this case were an order of magnitude less

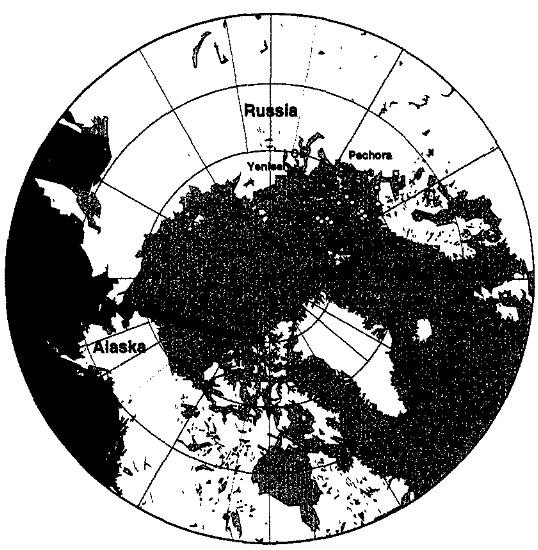

Fig. 2 — The locations of dump sites for radioactive waste, taken from the Yablokov Report [1]. Solid radioactive waste appears as a green square. Liquid radioactive waste appears as a yellow circle, and nuclear reactors appear as red stars.

than those observed. These results indicated that this source plays a minor role in the existing contamination of the area.

The third simulation used the runoff from the Ob and Yenisei Rivers in the Kara Sea and from the Pechora River in the Barents Sea as a source of radionuclides. Figure 3 shows the ocean currents and the level of radioactivity for the upper 30 m of the ocean at the end of 30 years of model integration, representing the period from 1963 to 1992. The ocean currents shown in this figure agree well with the observed surface circulation of the Arctic and its marginal seas. The highest levels of radioactivity, represented by the color scale, are found in the vicinity of the mouths of the Kara Sea rivers. The average value for radioactivity in the Kara Sea is approximately 10 Bq/m^3, which is in good agreement with observations in this region made in the early 1990s. Modeled levels of radioactivity along the Alaskan coast are approximately four orders of magnitude less then those found in Kara Sea and do not appear in this figure. This simulation indicates that the waste dumped into the rivers plays a dominant role in the contamination of the Kara Sea but has little effect on the Alaskan Coast.

A fourth simulation was run using the liquid waste discarded from the British nuclear reprocessing plant at Sellafield, located in the Irish Sea. Figure 4 shows the levels of ^{137}Cs discarded at this facility from 1950 to 1993. For comparison, the total amount of radioactivity discarded from the Ob, Yenisei, and Pechora Rivers was approximately 1400 TBq (10^{12} becquerels) over a 30-year period. Levels of discharge peaked during the mid-1970s and were greatly reduced after the mid-1980s. For this simulation, the Sellafield source was relocated to the northernmost limits of the Irish Sea. The Irish Sea is small when compared to the PIPS 2.0 domain and, therefore, not well resolved. By placing the source to the north, radionuclides can be carried north by the currents, in agreement with observations. Figure 5 shows the ocean circulation and levels of radioactivity in the upper 30 m of the ocean at the end of a 23-year model integration using the release of radionuclides depicted in Fig. 4 for the period 1970 to 1992. Note that the highest levels of radioactivity are found in the North Sea, along the coast of Norway, and in the Kara and Barents Seas. Levels in the Kara Sea are similar to those derived from the case using the rivers as a source. In addition, this simulation shows levels of radioactivity along the Alaskan coast to be approximately two orders of magnitude less than those observed in the Kara Sea and three orders of magnitude less than those found near the source.

These last two simulations indicate that the Sellafield source has been a dominant contributor to the radioactivity observed in the eastern Arctic over the last 20 years and has provided more radioactivity to the Alaskan coast than the Kara Sea sources.

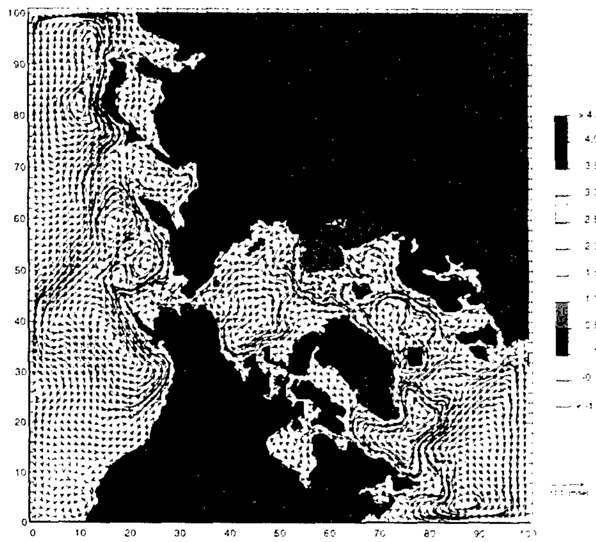

Fig. 3 — PIPS 2.0 ocean currents and levels of radioactivity for the upper 30 m of the ocean at the end of the 30th year of model integration using river runoff as the contaminant source. The color scale for radioactivity is logarithmic (1.0 = 10^1 = 10) in units of Bq/m^3. The scaled current vector is 10 cm/s.

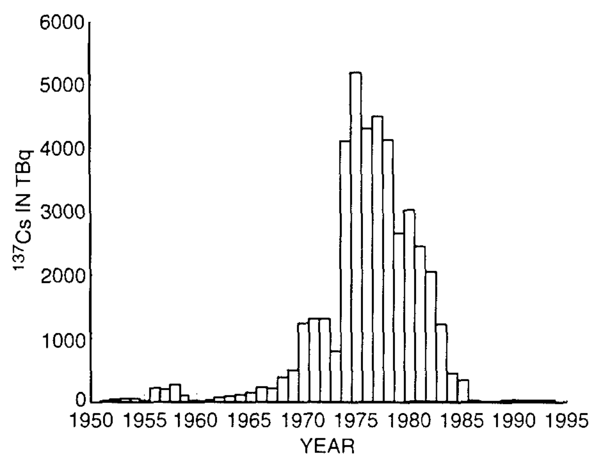

Fig. 4 — Annual releases of ^{137}Cs from the Sellafield nuclear reprocessing plant, taken from Kershaw and Baxter [7].

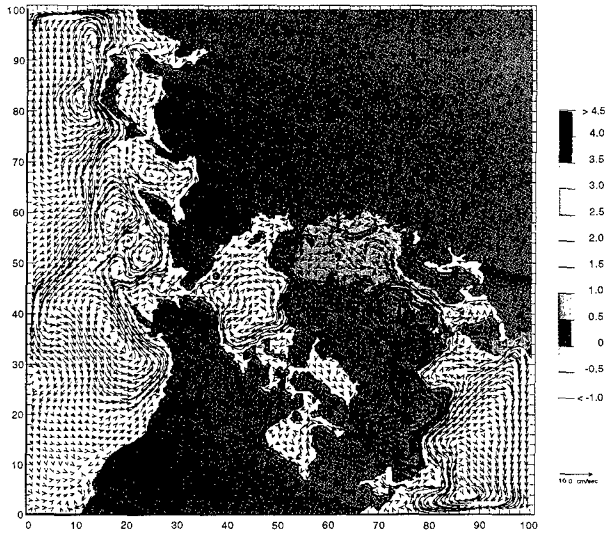

Fig. 5 — PIPS 2.0 ocean currents and levels of radioactivity for the upper 30 m of the ocean at the end of the 23rd year of model integration using the Sellafield discharge as the contaminant source. The color scale for radioactivity is logarithmic in units of Bq/m^3. The scaled current vector is 10 cm/s.

TRANSPORT PATHWAYS — OCEAN

The model simulations have identified key surface-transport pathways from source locations in the Kara and Barents Seas and from the Sellafield source into other parts of the Arctic. Figures 6 and 7 show surface levels (upper 30 m) of radioactivity from the two cases previously described but earlier in the simulation, at years 7 and 6, respectively. Using a different color scale to represent the level of radionuclides enhances the visualization of the transport pathways. Figure 6 shows three dominant pathways from sources located at the river mouths in the Kara and Barents Seas. The first pathway (1) runs from the Ob and Yenisei Rivers northward out of the Kara Sea, across the northern boundary of the Barents Sea, through the Fram Strait into the East Greenland Sea. The second pathway (2) runs from the rivers eastward into the Laptev Sea. The third pathway (3) is from the Pechora River into the Barents Sea, around the southern tip of Spitzbergen, and into the East Greenland Sea.

Figure 7 shows that the dominant surface pathway from the Sellafield source (1) follows the North Atlantic extension of the Gulf Stream into the Norwegian current north along the Norwegian coast. The current then splits, part entering the Barents Sea (2) and part turning north and west along the western coast of Spitzbergen (3) where it then meets with the southward-moving current through the Fram Strait and continues south along the East Greenland coast. The pathway into the Barents Sea is the dominant route into the Kara Sea. An additional (although shorter pathway) is from the Sellafield source location directly into the North Sea.

TRANSPORT PATHWAYS — SEA ICE

The Russian Arctic shelves are known as the dominant location for sea-ice generation in the Arctic. Ice formed in these shallow regions often entrains sediments. Contaminants, including radionuclides, may attach to the fine-grained sediments

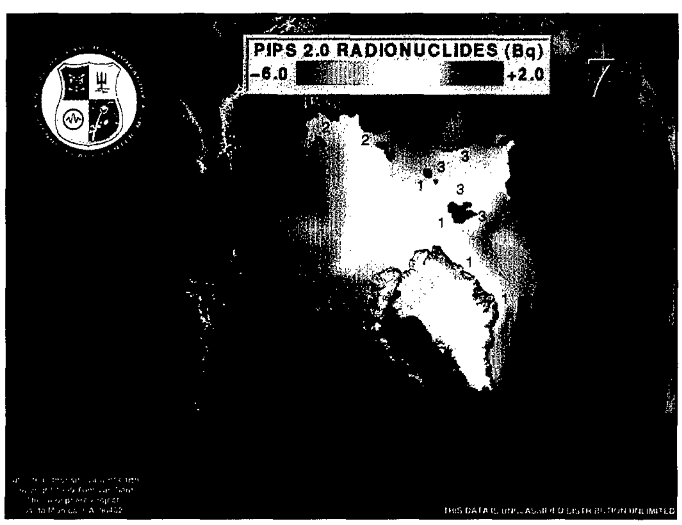

Fig. 6 — PIPS 2.0 radioactivity for the upper 30 m of the ocean during the 7th year of model integration, using river runoff as a contaminant source. The color scale is logarithmic in units of Bq/m^3. Numbers indicate the three dominant pathways taken by the released contaminants.

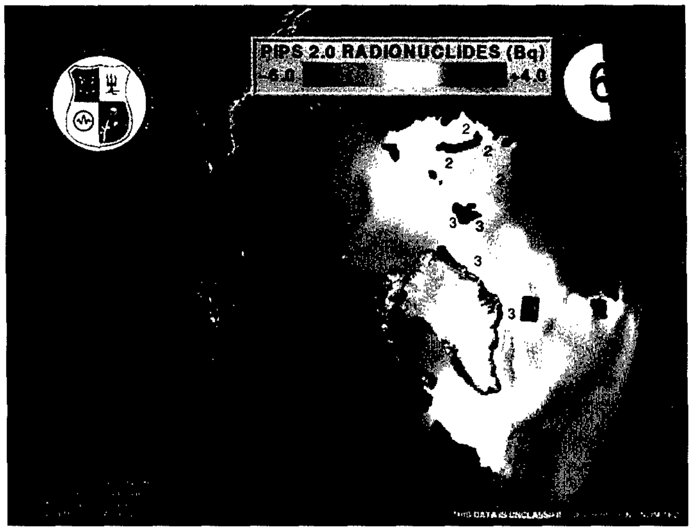

Fig. 7 — PIPS 2.0 radioactivity for the upper 30 m of the ocean during the 6th year of model integration using the Sellafield discharge as a contaminant source. The color scale is logarithmic in units of Bq/m^3. Numbers indicate the three dominant pathways taken by the released contaminants.

found in these locations. If sea ice forms in a region of known radioactive waste dumping (such as near the mouths of rivers or along the coast of Novaya Zemlya), it may entrain contaminated sediments. Sea-ice motion is more directly dominated by wind forcing than ocean circulation, which is also affected by thermodynamic processes and topographic steering of currents. As such, sediment-laden sea ice may travel along a different path than the underlying ocean currents. The PIPS 2.0 coupled ice-ocean model was used to investigate these sea-ice transport pathways.

The PIPS 2.0 was run from November 1991 through December 1995 using the atmospheric heat fluxes and winds stresses from NOGAPS. Ice-drift data from the model simulations were used to calculate the trajectories for specific parcels of sea ice. The ice parcel's trajectory begins during the fall freeze-up period, when the possibility exists for contaminated sediment to become trapped in the newly forming sea ice. The sea ice is then allowed to drift until it either encounters a land boundary or until it melts. Several such trajectories were calculated for parcels of ice that formed near the dumpsites along the coast of Novaya Zemlya or near the river mouth/estuaries in the Kara Sea. Ice-parcel trajectories were initiated in the fall of each year from 1991 to 1994. Assuming that the sediments remain contained in the sea ice, the end of the trajectory is the location at which the radionuclides are released back into the water column with the sediment. Each of the ice parcels that formed along the Novaya Zemlya coast during these 4 years melted in the Kara Sea during the following summer. This implies that sea ice does not provide a transport mechanism out of the Kara Sea for the contaminants dumped along the coast of Novaya Zemlya. Ice that formed during the fall of 1992 and 1994 in the estuary of the Ob River was able to travel out of the Kara Sea and into the northern part of the Barents Sea where it melted during the following summer.

Figure 8 shows the paths taken by two parcels of ice originating in the estuary of the Yenisei River during the fall freeze-up period for each year. The large differences in these trajectories from year to year indicate the strong interannual variability of the winds that drive the ice motion. During some years, the ice never travels outside of the Kara Sea (Fig. 8(a)), while during other years it may travel far into the Barents Sea (Fig. 8(b) and Fig. 8(d)) and even well into the East Greenland Sea (Fig. 8(c)). Although these pathways are similar to the ocean pathways described in Fig. 6, the ice parcels often reach their final destination sooner than a "parcel" of ocean water originating in the same location. Note also that during this 4-year period, none of the ice parcels was transported into the western Arctic and, therefore, never approached the northern coast of Alaska.

SUMMARY

The coupled ice-ocean model developed by NRL and used as the basis of the U.S. Navy's Polar Ice Prediction System 2.0 (PIPS 2.0) has been used to simulate possible pathways taken by radioactive contaminants released into the Arctic seas. Model results indicated that the dominating source of oceanographic contamination for the Arctic are the rivers that empty into the shallow coastal regions and the contaminants that were released from the

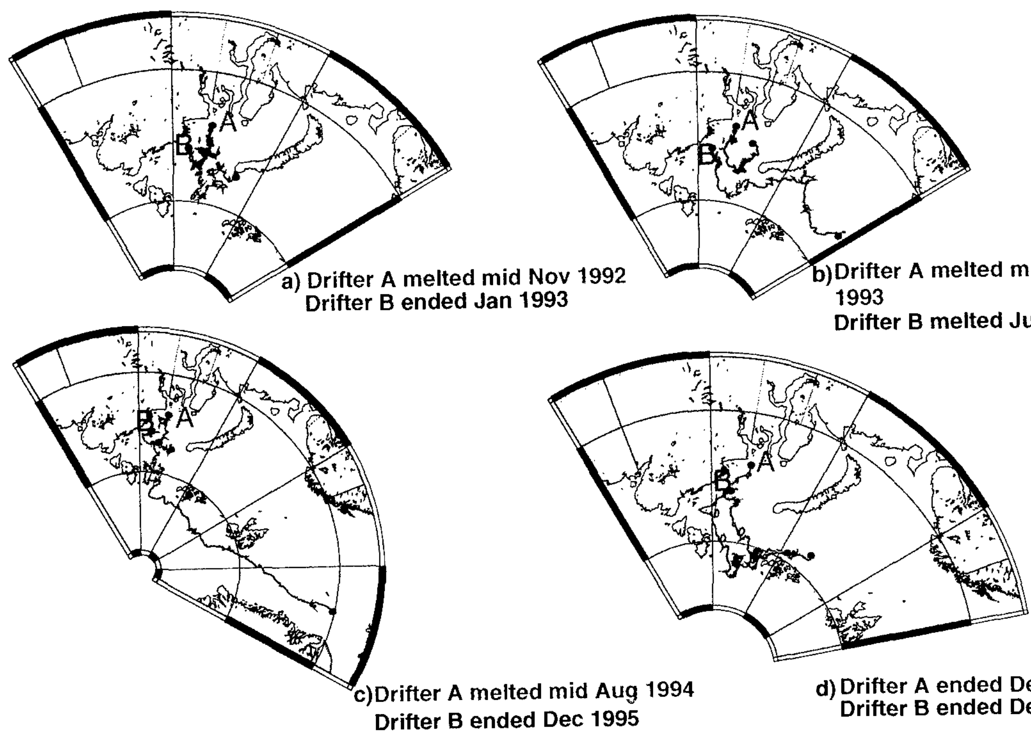

Fig. 8 — PIPS 2.0 trajectories for two parcels of sea ice originating in the Yenisei River estuary in November of (a) 1991, (b) 1992, (c) 1993, and (d) 1994. The month, year, and reason for the termination of each trajectory is given.

Sellafield nuclear-reprocessing plant located in the Irish Sea. Neither of these sources produced a large impact on the level of radioactivity along the Alaskan coast. Sea ice was shown to provide a rapid transport mechanism for contaminated sediments located in the vicinity of the river estuaries in the Kara Sea to more distant locations. Finally, with the reduction of contaminant dumping at Sellafield, the Arctic rivers remain as a dominant source of contamination for the Arctic region. Rivers are often used as a dumpsite for many types of waste that may prove as, or more, dangerous to the environment in the future than radioactive contaminants.

ACKNOWLEDGMENT

We acknowledge the contributions made to the coding of the coupled ice-ocean model performed by Dr. Abe Cheng, of Sverdrup Technology, Inc.

[Sponsored by ONR]

REFERENCES

1. A.V. Yablokov, V.K. Karasev, V.M. Rumyantsev, M.Y. Kokeyev, O.I. Petrov, V.N. Lystsov, A.F. Yemelyanenkov, and P.M. Rubtsov, "Facts and Problems Related to Radioactive Waste Disposal in Seas Adjacent to the Territory of the Russian Federation," translated by P. Gallager and E. Bloomstein (Small World Publishers, Inc., Albuquerque, 1993).

2. W.D. Hibler III, "A Dynamic Thermodynamic Sea Ice Model," *J. Phys. Oceanogr.* **9**, 815-864 (1979).

3. W.D. Hibler III, "Modeling a Variable Thickness Sea Ice Cover," *Mon. Wea. Rev.* **108**, 1943-1973 (1980).

4. M. Cox, "A Primitive Equation, Three-Dimensional Model of the Ocean," GFDL

Ocean Group Technical Report 1, Geophysical Fluid Dynamics Laboratory, Princeton, N.J. (1984).

5. A. Cheng and R. Preller, "The Development of an Ice-Ocean Coupled Model in the Northern Hemisphere," NRL/FR/7322--95-9627 (1996).

6. S. Levitus, "Climatological Atlas of the World Ocean," NOAA Professional Paper 13, National Oceanic and Atmospheric Administration (Geophysical Fluid Dynamics Laboratory), Princeton, N.J. (1982).

7. P. Kershaw and A. Baxter, "Sellafield as a Source of Radioactivity to the Barents Sea," Proceedings in Radioactivity and Environmental Security in the Oceans: New Research and Policy Priorities in the Arctic and North Atlantic, Woods Hole, Massachusetts, pp. 91-104 (1983). ■

THE AUTHORS

[illegible]

[illegible]

High Density Nonvolatile Computer Memory

G.A. Prinz and K.M. Bussmann
Materials Science and Technology Division

The draw-down in defense forces following the end of the Cold War has placed added demands on the remaining personnel. It is now imperative that technology provide the tools to make the existing forces as efficient and effective as possible, and this is nowhere more important than in the processing of information in the battlefield environment. Satellite reconnaissance, aircraft navigation, missile guidance, and shipboard data handling all demand prodigious amounts of information storage. These demands are ever increasing and often cannot be met with current off-the-shelf technology. In the area of computer memory, the requirements of radiation hardness, resistance to single-event upset, electromagnetic interference, power outages, and low power drain for portable electronics all present challenges for the Navy. NRL scientists are developing a new technology to address this challenge — high density nonvolatile computer memory based upon the giant magnetoresistance (GMR) effect.

GIANT MAGNETORESISTANCE EFFECT

GMR, as first reported in France in 1988 [1], was observed in a materials system pioneered at NRL in the early 1980s, namely epitaxial films of Fe on GaAs. The resistance change associated with GMR is much greater than the more well-known anisotropic magnetoresistance (AMR) found in ferromagnetic metals discovered by Lord Kelvin in 1857. GMR was first observed in epitaxial, multilayered films of Fe and Cr grown on GaAs and has since been demonstrated in a variety of materials systems grown using a multitude of techniques. The effect is illustrated in Fig. 1, which shows a cross section of iron layers separated by nonferromagnetic chromium spacer layers. The spacer layers in the first experiments were such that each Fe layer was forced into antiparallel alignment with its neighboring Fe layers, if there were no externally applied magnetic field. (This is brought about by oscillatory exchange coupling that causes the Fe layers to be parallel or antiparallel, depending on the thickness of the Cr spacer layer — a related subject that we do not pursue here.) At zero applied field, the moments in the Fe layers are all antiparallel to each other. The resistance of the multilayers is measured to be R_0, the subscript referring to the applied magnetic field. If a magnetic field is applied causing the magnetic moments of the Fe layers to become parallel, the resistance is then measured to be R_∞, a value significantly *lower* than R_0. The quantity $(R_0 - R_\infty)/R_\infty$ is termed the GMR of the multilayer, and the original work showed this to be ~ 80% at low temperatures — a factor of 20 larger than conventional AMR. Since the first work, GMR values of over 200% have been measured in Co/Cu multilayers at 4.2 K and 80% at room temperature, and efforts at obtaining even higher values are continuing. GMR has also been demonstrated in dual ferromagnetic multilayers like Co/Cu/Fe/Cu where the Cu spacer layers are thick enough to eliminate exchange coupling and allow independent rotation of the ferromagnetic layers. In this system, one may take advantage of the fact that the magnetic moments of the Fe layers rotate at a lower applied field than the Co layers — a result of the lower coercivity of Fe. In such a system, we can generate parallel alignment at high fields (low resistance) and antiparallel alignment at intermediate fields (high resistance) in which we switch the Fe but not the Co. Clearly, if individual elements could be fabricated that allowed easy placement of the element into each of these two states at will and if they could be addressed electrically in large, dense arrays, one would have the basis for a random

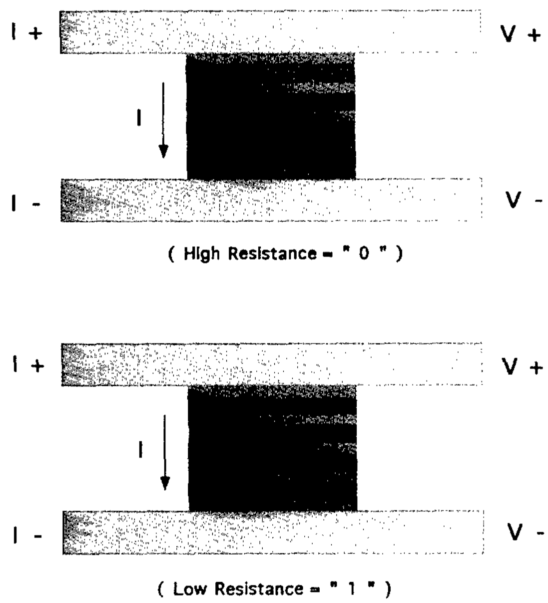

Fig. 1 — The two configurations of the magnetic moments in a multilayered sample to obtain high resistance (antiparallel) and low resistance (parallel).

access, nonvolatile storage system. This type of system is the focus for the development of GMR magnetic memory at NRL.

The physical basis for the effect lies in the fact that electrical currents in ferromagnetic metals are spin polarized. Although this property is predicted by the quantum-mechanical description of itinerant electron ferromagnetism, it attracted little attention from the scientific community until the discovery of GMR. This may be seen readily from Fig. 2, which is a representation of the distribution of energy states of d-electrons in ferromagnetic Co compared to nonmagnetic Cu. The exchange splitting of the spin states in Co creates an imbalance in the number of spin-up electrons (majority) and spin-down electrons (minority). This gives Co a net magnetic moment, making it ferromagnetic. More importantly for electrical transport devices, however, is the fact that at the top of the distribution, called the Fermi level (E_F), there is also an imbalance in the number of spin-up and spin-down electrons. In this figure, they are 100% polarized; that is, there are no down-spin electrons at the Fermi level. In real materials, this extreme case has not yet been observed, although a number of laboratories are pursuing such a half-metallic compound. On the other hand, Cu shows no imbalance, and the electrons at E_F are unpolarized. Since the electric current generated in a metal by an applied voltage is composed of those electrons near E_F, we see that the current in a ferromagnetic metal is polarized, but in a normal metal, it is not. If we now join these metals into a multilayered film, we can obtain the device represented in Fig. 3. Here the current flowing from the Co is spin-polarized and can readily enter the Cu layer since there are states for both up and down spins at E_F in Cu. In attempting to enter the second ferromagnetic layer, however, the electrons will have states available only at E_F, if the magnetic moment of the second layer is parallel to the first. If they are antiparallel, there are no states available, and the electrons will be reflected. This is the physical basis for the observed resistance changes. Notice that the effect is much like crossed polarizers for light, but in this case, a 180° misalignment stops the transmission rather than the 90° value seen for polarized light.

A convenient theoretical model has been developed to describe the electrical transport through a magnetic multilayer; this is shown schematically in Fig. 4. It is assumed there are two electrical currents supported by the materials: one polarized spin-up and the other spin-down. (If the current were 100% polarized, of course, only one of these would exist.) It is further assumed that these two currents never mix: that is, there is no mechanism to "flip" a spin into its opposite state. This is a good assumption for the types of magnetic multilayers discussed here where the spin-flip decay length λ_{SF} is ~ 1000 Å at room temperature, a value larger than the thickness of the device. Note that λ_{SF} is much larger than the collision mean-free path that generates resistance in the Drude model, often of the order of 10 Å, and this accounts for the robust nature of spin transport in certain multilayer systems. The original polarization established by the ferromagnetic material will decay

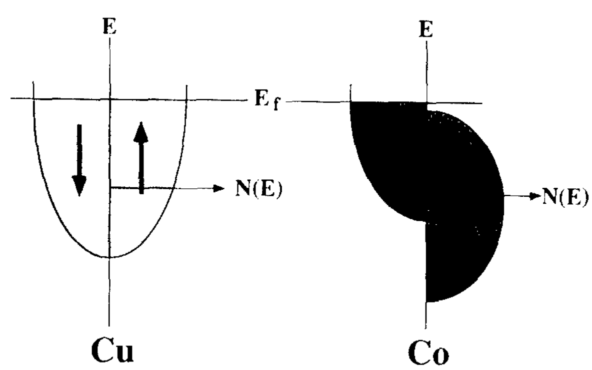

Fig. 2 — Energy states available to electrons in a normal metal (Cu) and a ferromagnetic metal (Co) when specifying the orientation of the spin angular momentum.

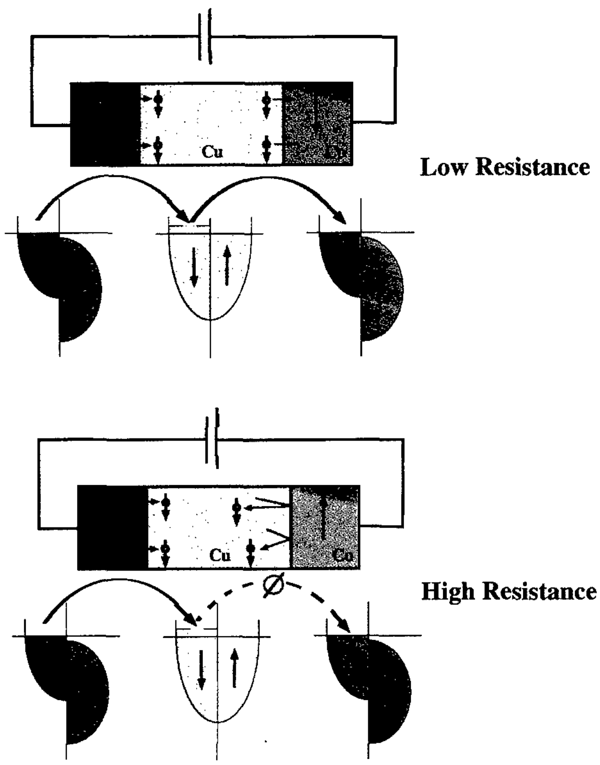

Fig. 3 — The effect of relative magnetic moment orientation on electron transport between two ferromagnetic metals through a thin normal metal film.

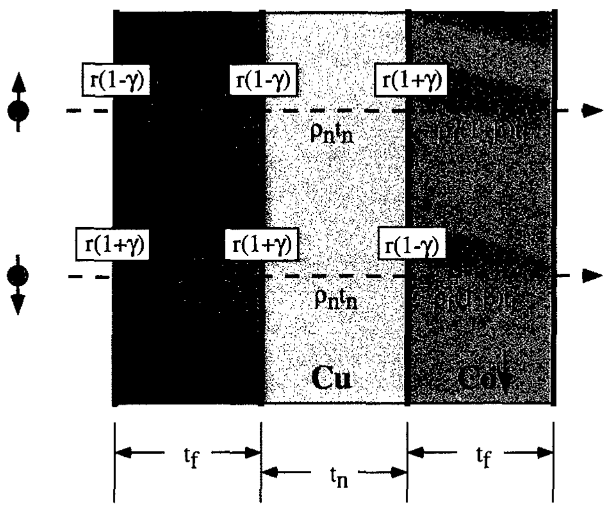

Fig. 4 — The series resistance encountered by spin-polarized currents when passing through a multilayered structure of ferromagnetic and normal metal films.

away as $e^{-x/\lambda_{SF}}$. Under these assumptions, the electrical current will encounter bulk resistance (modeled as resistivity ρ) within the layers and interface resistance (modeled as $r_{N/F}$) where the layers meet. To account for the GMR, the bulk resistances of the ferromagnetic layers are multiplied by a parameter $1 \pm \beta$. The plus sign in this expression is associated with an electron of spin opposite to the magnetization of the bulk ferromagnet in which it is passing; the minus sign is associated with an electron of spin parallel to the bulk magnetization. A down-spin electron passing through a ferromagnetic material of up magnetization thus experiences a resistance proportional to $\rho(1 + \beta)$ and an up-spin electron, a resistance of $\rho(1 - \beta)$. The interface resistance is modeled in a completely analogous manner using the parameter $1 \pm \gamma$. In the absence of magnetism, β and γ both would be zero. Modeling GMR then becomes a matter of experimentally determining the values of β and γ, along with interface and bulk resistivities of the nonferromagnetic and ferromagnetic metals.

If one considers the two cases of low resistance (all moments parallel) and high resistance (alternating moments antiparallel), one can use this model to write down the change in resistance for N multilayers of area A between those two states. One obtains

$$R_0 - R_\infty = \frac{N\{\rho_F t_F \beta + 2\,\gamma r\}^2}{A(\rho_F t_F + 2r + \rho_N t_N)} .$$

From this we see that the effect is additive in that the more layers N we have, the greater the effect. Also, the smaller the area, the larger the effect, because resistance increases as a wire becomes thinner. Finally, the spin asymmetry parameters γ and β are in the numerator, so to maximize the effect, one wants them to be as large as possible. Typical values of these parameters are: $\beta_{Co} = 0.50$; $\gamma_{Co/Cu} = 0.76$; $r_{Co/Cu} = 0.21\ f\Omega m^2$; $\rho_{Co} = 6.5\ \mu\Omega cm$; $\rho_{Cu} = 0.7\ \mu\Omega cm$.

DEVICE FABRICATION

At NRL, devices based upon these physical ideas have been fabricated. Figure 5 shows an optical micrograph of a single device, and Fig. 6 shows an array of such devices, ranging in size from 100 $\times$ 100 μm^2 down to 1 $\times$ 1 μm^2. Shapes of squares and circles are evident. Studies of single elements on test chips of this type have confirmed that the two-current model is valid and has also shown that these devices become useful at sizes below ~ 3 $\times$ 3 μm^2 where the resistance becomes sufficiently high. This illustrates the useful scaling properties of these devices. At large sizes, their resistance is too

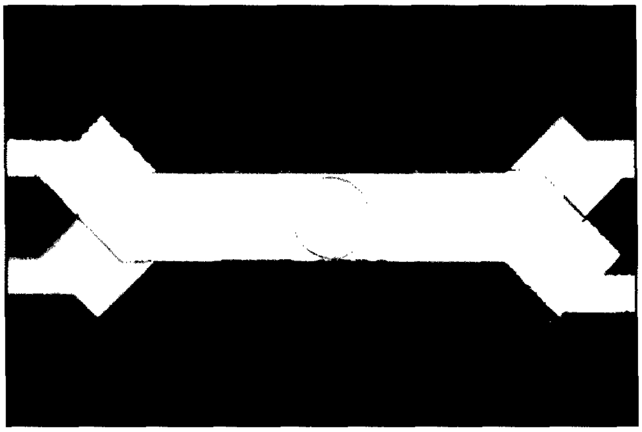

Fig. 5 — Optical micrograph of a typical memory element viewed perpendicular to the film plane. The top metallization is Al, the bottom is Cu and the surrounding blue is Si_3N_4. The stack location is revealed by a circular ring.

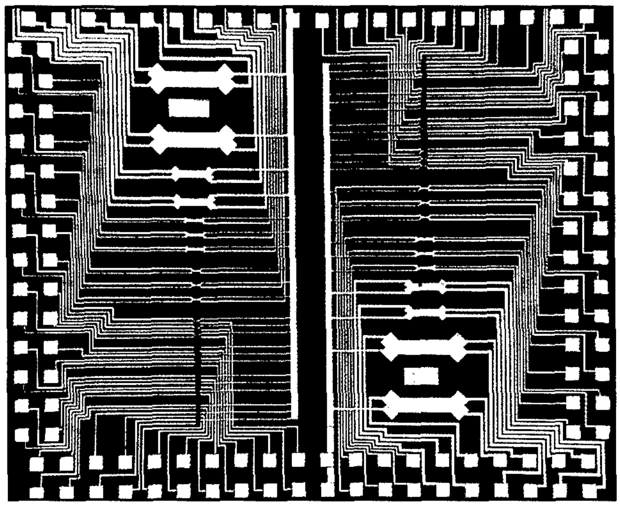

Fig. 6 — A test chip containing an array of elements having circular and square multilayer stacks ranging from 100 μm down to 1 μm in dimension.

low, but as they are made smaller and their packing density increases, the resistance becomes high enough to be practical. Devices containing 100 layers of Co/Cu at the dimension of 0.01 μm × 0.01 μm will have a projected resistance of 600 Ω and a packing density of 1 Gbit/cm^2.

During 1997, NRL will be fabricating the first functional memory arrays using this approach. Figure 7 illustrates the basic storage element. It consists of small (0.6 μm × 0.1 μm) patterned stacks of magnetic multilayer material connected in an up-and-down serpentine fashion to form a sense line. Two consecutive stacks form a single bit, and a 1-cm sense line contains 5×10^3 bits. Information is stored and read out by applying small pulsed magnetic fields to align or unalign the magnetic moments in the stacks. These magnetic fields are created by sending small current pulses down the electrical lines shown immediately above and below the magnetic stack elements. The detailed operational protocol is too lengthy for this article, but the elements are fabricated to retain information in the absence of any applied power. Power is required only to store information or to interrogate a bit by measuring its resistance. Each bit is individually addressable. The total array thus becomes a nonvolatile random access memory. It is immune to external disturbance (radiation, power failures, etc.) except for large external magnetic fields that can be easily shielded with proper packaging of the array. It retains its information indefinitely much like magnetic disks one finds in a personal computer and only draws power during read or write.

An example of a test array under fabrication at NRL is shown in the mask design of Fig. 8. The density is 1 Mbit/cm^2. Current program goals require a transfer of this technology to industry for commercial product availability in fiscal year 2001.

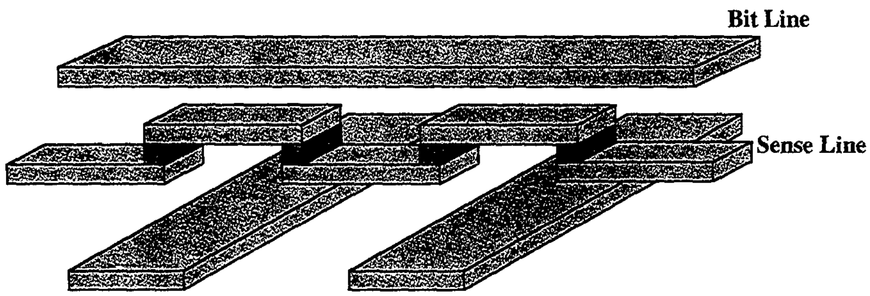

Fig. 7 — Representation of the fundamental elements of a memory array showing the multilayered magnetic stacks in red and the copper leads in orange. Two stacks form one memory bit. The word lines and bit lines provide magnetic fields to read and write the bits.

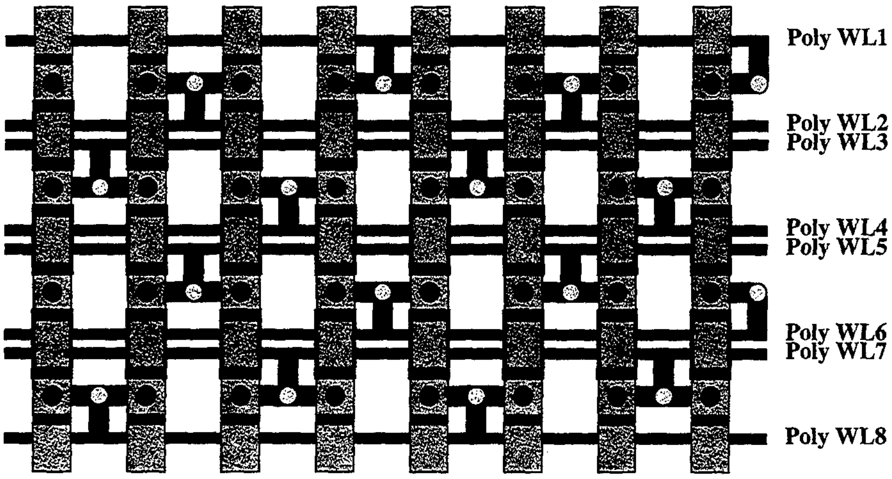

Fig. 8 — Representation of the memory architecture under development. Multilayered magnetic stacks are in red, the serpentine sense lines viewed from above run vertically. Switching transistors to select a particular element are shown in blue. They are activated by the polysilicon lines running horizontally, shown in black. The word and bit lines above and below the sense lines are not shown for clarity.

This technological development stems directly from the long-term ONR-NRL investment in magnetic materials research. As described in an earlier *NRL Review* article [2], thin-film research in magnetic materials at NRL dates back over 20 years. Without that investment, developments such as this and others originated at NRL that apply magnetic materials to meet Navy challenges would not have been possible.

[Sponsored by DARPA and ONR]

REFERENCES

1. M.N. Baibich, J.M. Broto, A. Fert, F. Nguyen Van Dau, F. Petroff, P. Etienne, G. Creuzet, A. Friederich, and J. Chazelas, "Giant Magnetoresistance of (001)Fe/(001)Cr Magnetic Superlattices," *Phys. Rev. Lett.* **61**, 2472 (1988).

2. J.J. Krebs, *1993 NRL Review*, "Ultrathin Magnetic Film Research at NRL," pp. 67-73. ■

THE AUTHORS

GARY A. PRINZ is currently chief scientist for planar magnetism and head of the Magnetic Multilayers Program at the Naval Research Laboratory, in Washington, D.C. He received his Ph.D. degree in physics in 1966 from Johns Hopkins University and joined NRL in 1967. He has been active in the field of solid-state magnetism for 30 years and has published over 150 papers in this area. Starting in 1980, he pioneered the epitaxial growth of magnetic materials on semiconductors. In recognition of that contribution, he was presented the Sigma Xi Applied Physics Award in 1983, was elected a Fellow of the American Physics Society in 1984, and was elected to the Johns Hopkins Society of Scholars in 1991. He has delivered more than 80 invited lectures at national and international meetings, universities, and research laboratories in North America, Europe, and Asia. He currently serves as advisory editor to the *Journal of Magnetism and Magnetic Materials*; program chairman for the 1996 Conference on Magnetism and Magnetic Materials; chairman of the Management Advisory Committee, National Consortium for Microwave Ferrites; organizer of the National Consortium for Applications of Giant Magnetoresistance; and was guest editor for the April 1995 issue of *Physics Today*, which was devoted to magnetoelectronics, and in which he authored the article "Spin Polarized Electronics."

KONRAD M. BUSSMANN graduated in 1984 from the University of Minnesota, Minneapolis, with BEE and BME degrees in electrical engineering and mechanical engineering. He began work at Texas Instruments, Inc. in Dallas, Texas, in the fall of 1984 where he worked as an electrical design engineer in the company's Defense Systems and Electronics Group. He began postgraduate work at the University of Texas at Austin in the fall of 1987. His initial work centered on the development of low-temperature magnetic force microscopy of high-T_c superconductors using the Meissner effect to modulate the response of a magnetic cantilever. He completed his dissertation under Prof. J.B. Goodenough, studying narrowband phenomena in various transition-metal oxides using magnetometry, thermoelectric power, and low-temperature specific heat measurements; he received a Ph.D. degree in physics in the fall of 1994. Dr. Bussmann came to the Naval Research Laboratory in December of 1994 as a National Research Council Associate and has focused since that time on the experimental problems of current perpendicular to the plane transport in magnetic multilayers. Other studies at NRL include the development of lithographic processing techniques for magnetic materials, epitaxial growth of Co/Cu multilayers on (100) diamond, and investigations of the magnetic coupling at NiO/Co and NiO/NiFe interfaces. He is a member of the American Physical Society.

Flight of the Biosensor

G.P. Anderson, F.S. Ligler, and D.A. Stenger
Center for Bio/Molecular Science and Engineering

P.T. Davidson, R.J. Foch, and J.F. MacKrell
Tactical Electronic Warfare Division

Currently, there is no way remotely to identify an aerosolized biological warfare threat. In 1995, an International Task Force (ITF-24) named the potential for putting a biological warfare agent detection system on a remotely piloted airborne vehicle as the most important step in the development of effective detection systems for biological warfare agents. To address this requirement, the Defense Advanced Research Projects Agency (DARPA) funded NRL's Center for Bio/Molecular Science and Engineering (CBMSE) and Tactical Electronic Warfare Division (TEWD) to automate a sensor for biological warfare agents and integrate it with a miniaturized air sampler onto a small, remotely operated aircraft. This team was responsible for designing, integrating, and testing a detection system, including the fiber-optic biosensor, an air sampler, automated fluidics unit, and a remotely piloted aircraft.

INTRODUCTION

On January 29, 1996, NRL demonstrated an airborne detection system using a small testbed aircraft that carried an air collector integrated with an automated fluidics unit and biosensor and a radio transceiver to downlink the data to a computer on the ground. This was 1 month after an expert panel from the unmanned air vehicle (UAV) community released a draft report saying it would be at least 3 years before such a system could be constructed. In September 1996, the team flew several aircraft with various modifications of the sampling and identification system during the Joint Field Trials III (JFT III) at Dugway Proving Grounds, Utah. During these trials, both aerial and ground-generated aerosols of a harmless bacteria were disseminated, simulating a biological warfare attack. The NRL airborne detection system successfully collected the bacteria from the air, identified the bacteria, and relayed the information to an operator on the ground.

BACKGROUND

Over the last decade, CBMSE had developed the technology to perform rapid immunoassays with a fiber-optic biosensor. A small, four-channel fiber-optic fluorimeter — the Analyte 2000 — was built by Research International (RI) in collaboration with NRL to provide the Navy with a portable device capable of performing multiple manual assays. In 1994, the Office of Naval Research (ONR) funded a pilot project to explore automated fluidic systems for a variety of NRL biosensors.

The TEWD has been conducting research to advance the technologies needed for the development of unmanned aircraft for electronic warfare missions since the mid-1970s. These technologies include electric propulsion, advanced composite structures, low Reynold's number aerodynamics for long endurance, low speed flight, and advanced digital avionics and flight control systems. Using these technologies, TEWD has developed and demonstrated several prototype mission aircraft, including the Flying Radar Target (FLYRT), an RF decoy for ship's self-defense and the Self-Navigating Drone Expendable, Recoverable (SENDER), a 4-ft wingspan expendable aircraft capable of carrying a 2.5 lb payload for a distance of 100 nmi. In addition, TEWD operates several inexpensive, generic, testbed aircraft that are capable of carrying a variety of payload weights and sizes for in-flight verification of payload operation. These testbed aircraft were well suited for the initial demonstration of the biological warfare agent detection mission.

FIBER-OPTIC BIOSENSOR

The first step in the project was to demonstrate the feasibility of operating the biosensor in the air. The Analyte 2000 [1], NRL's custom-built fluidics unit, and an all-glass impinger (AGI) used to collect airborne particles, were integrated into a small Telemaster aircraft operated by TEWD. A successful demonstration of this airborne biosensor was accomplished in January 1996.

Both the NRL-built fluidics unit and a fluidics control module built by RI operate under on-board microprocessor control and perform repetitive immunoassays. These fluidics units remove liquid from the air sampler and pump it over the optical probes. The probes are coated with antibodies directed toward the threat agents. When a sample containing that particular agent is brought into contact with the probes, that agent is bound to the fiber surface. The probes are then washed with buffer to remove any unbound material. Next, the presence of agent is interrogated by cycling a solution of fluorescently labeled antibody over the probes. While the probes are being interrogated, the sampler is automatically refilled, and the next sample is collected. The assay cycle is repeated every 5 min. Data are constantly transmitted to the ground for immediate interpretation by the ground crew.

Results from early flight tests of the biosensor payload indicated a number of areas where improvement was needed. First, an improved sampler was required to replace the AGI. Impingers collect only a few liters of air per minute. Since the aircraft would typically be flying far from the agent release point, the number of particles per liter of air would have diffused to the point that this sampling rate would not enable the collection of a detectable amount of agent. To solve this problem, we resolved to develop a cyclone air sampler driven by the ram air produced by the plane in flight at 30 to 40 mph. The only cyclone already developed that was small enough to consider putting on the plane was the Portable High-Throughput Liquid-Absorption Air Sampler (PHTLAAS)[2] developed by the Army at the Edgewood Research Development and Engineering Center (ERDEC). A PHTLAAS, modified to run on ram air, was tested in the ERDEC wind tunnel but was too large for integration with the aircraft. Two other approaches were taken to obtain an effective air sampler; NRL built several versions of ram-air-driven cyclones based on the larger British Aerojet model [3], and RI also provided NRL with a small, ram-air-driven cyclone. All of these cyclones were tested in the ERDEC wind tunnel for the ability to collect protein aerosols. It was found that both the NRL and RI designs were twice as efficient as the modified PHTLAAS and were many times better than the AGI.

Another feature that required modification was the size of the optical probes. An optical probe with a 12.5-cm sensing region was used for the ground-based system. The total probe length was nearly 22 cm, making insertion into the aircraft difficult. A total probe length of 10 cm was desired. This allowed the probes to be placed directly on top of the Analyte 2000. It also permitted the probes to be compatible with the RI fluidics control module. The major difficulty in producing shorter probes was that their smaller length made them incompatible with NRL's existing optical-probe tapering equipment. The tapering apparatus was subsequently modified to allow the simultaneous tapering of 96 probes at a time. This also permitted preparation of more consistently tapered probes. The apparatus used for the immobilization chemistry was also modified. To accommodate the short probes, a new apparatus was assembled to permit simultaneous coating of all 96 probes. This provided a large number of identically prepared probes for field testing. Both the probes and the fluorescently labeled antibody were lyophilized, making them stable for extended storage without refrigeration. In the field, they could be rehydrated easily and made ready for use.

Two types of fluidics control modules were developed for use with the remotely piloted vehicles. An improved version of the fluidics module designed at NRL and first flown in January 1996 was the primary unit used in the field trials. The main improvement was to replace the small solenoid pump with a peristaltic pump. Although it increased the weight of the unit, it also greatly improved its reliability. The solenoid pump was easily fouled, pumped weakly, and was susceptible to valve clogging. Once this change was made, the units operated flawlessly. The main limitation of the NRL fluidics unit was that it operated independently of the Analyte 2000. Since it would have required an additional radio transceiver to fully control the fluidics unit, the immunoassay cycle was started while on the ground and run continuously until the aircraft was recovered; then the unit was turned off. This is practical with the fiber-optic biosensor since it can test numerous negative samples without changing probes and is also sensitive to the increasing concentration of analyte.

The RI fluidics control module was the second fluidics unit tested at the joint field trials. This unit was fully integrated with the Analyte 2000, thus both units were fully controlled by the same ground computer. The RI fluidics unit differs from the NRL unit because it encloses the fibers in a disposable molded plastic card with microfabricated valves that prevent fouling of pumps by dirty samples. Fluids are driven through the system using pneumatic pressure rather than a peristaltic pump. Figure 1 shows the Analyte 2000 fiber-optic biosensor, the RI fluidics control module, the RI cyclone air sampler, and a laptop computer for receiving data.

SWALLOW AIRCRAFT

TEWD was tasked to design and build a custom unmanned aircraft for the biosensor mission. The aircraft, named Swallow (Fig. 2), features electric propulsion in a pusher configuration to eliminate the possibility of aircraft fuel contaminating the sample and allows the payload to be located in the nose of the aircraft for sample collection. The Swallow's wingspan is 15 ft, and gross takeoff weight is 60 lbs. The nose payload capacity is 10 lbs. The Swallow is powered by a 1500 W brushless dc electric motor, driving a five-bladed propeller. NiCad batteries were used during JFT III, enabling a 15-min flight duration. Future plans for the Swallow include operating with $LiSO_2$ batteries to enable 2-h endurance.

Two Swallow aircraft were fabricated and integrated with the payload for testing at JFT III. For these tests, Swallow was operated as a remotely piloted vehicle with the pilot in the loop. Since the tests were conducted at night, the pilots wore night-vision goggles (NVGs), and the aircraft were equipped with NVG-compatible lighting for the pilots to distinguish aircraft attitude. A mission aircraft would incorporate a Global Positioning System-navigated, digital autopilot system for autonomous operation along preprogrammed waypoints.

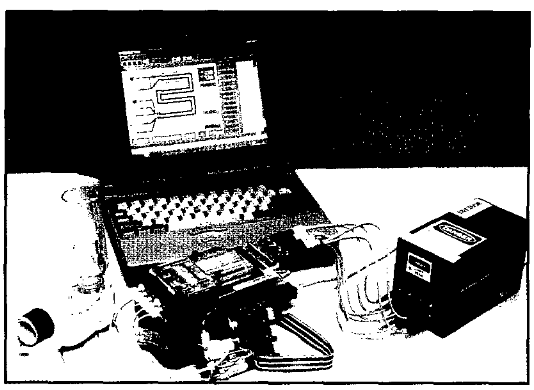

Fig. 1 — The Analyte 2000 fiber-optic biosensor, with the fluidics control module and RI air-particle collector.

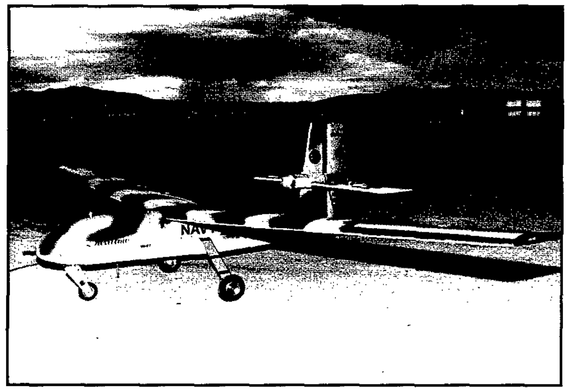

Fig. 2 — The Swallow 1 was the first all-electric vehicle to carry the fiber-optic biosensor payload to detect biological agents.

JOINT FIELD TRIALS

The Swallow biosensor system was demonstrated during JFT III, held at Dugway Proving Grounds in September 1996. The primary purpose of the JFT III was to provide an opportunity for biosensor developers to demonstrate their system's capability in a simulated bio-warfare environment. The test set-up was geared toward static sensor assemblies that were located on fixed test stands at the Tower Grid test site. Disseminations of the simulant were directed toward the static display. The UAV operations were considered secondary to the main purpose of the tests. Many disseminations were conducted under weather conditions (wind, lightning, and high humidity), which — while acceptable for static testing — precluded safe operation of the prototype aircraft. The biosensor was flown during 11 of the 26 disseminations.

Two Swallow aircraft, two 12-ft (wingspan) Telemaster testbed aircraft, one 8-ft Telemaster testbed aircraft, and the biosensor payloads were transported to Dugway. During the last week of August 1996, operational readiness tests were performed. On the two nights when the weather was suitable for testing, the 8-ft Telemaster — which carried an air-particle sizer — was flown, primarily for pilot familiarization with the test site.

For the first week of actual testing, the Analyte 2000, NRL fluidics unit, and the NRL cyclone-air-particle collector were integrated into one of the

large Telemaster aircraft. The initial flight tests produced negative results. The aircraft was flown through the expected location of the disseminated cloud, but the biosensor did not register a detection. Postflight inspection revealed that the air-particle collector was dry, indicating that the fluid sample was evaporating. Additionally, it was decided that the inlet to the collector was too close to the fuselage. After modifications were made to relocate the air inlet to a position outside of the propeller slipstream and reduce the diameter of the collector outlet to decrease liquid loss, the system operated successfully during all subsequent flights. Figure 3 shows the results of the next four flights in comparison to a standard curve for *Bacillus globigii* obtained in the laboratory. The most impressive positive detection of the trials occurred during Test 21 when only 0.5 lb of bacteria was released during an aerial dissemination.

Both Swallow aircraft were successfully flight demonstrated during the second week of September 1996. The NRL fluidics unit was integrated into Swallow 1 and the RI fluidics unit into Swallow 2. Both aircraft were equipped with the RI cyclone. Unfortunately, neither flight resulted in a positive detection. Swallow 1's flight was cut short due to RF interference with the command link to the aircraft. Swallow 2's flight lasted 10 min, but the wind blew the cloud across the static test site well to the west of pilot's visual range.

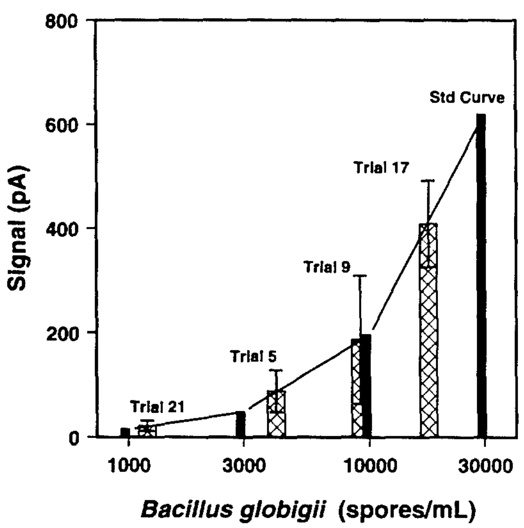

Fig. 3 — Positive flight test results obtained by the Analyte 2000, NRL fluidics unit, and the NRL air-particle collector flown on the Telemaster for each of the four trials undertaken following modification of the air-particle collector.

CONCLUSION

The data from JFT III confirm that an airborne biosensor packaged for integration with a small UAV operating at very low altitude is a feasible, near-term capability. The only requirement is funding for production. The biosensor is already small enough to be carried on currently fielded or projected UAV systems; however, the high cost of these UAV systems must be balanced against the mission requirement of extremely low-altitude collection where the aircraft may be exposed to ground fire, terrain, and obstacles. The Swallow aircraft is a low-cost, sensor-specific platform capable of meeting the mission requirements.

A return to the Joint Field Trials in 1997 will focus primarily on testing the Swallow with an improved sampler, greater flight endurance, and autopilot control to allow operation at greater range.

ACKNOWLEDGMENTS

We thank these CBMSE and TEWD personnel, without whom success would have been impossible: Jim Whelan, Joe Czarnaski, Dave Cuttino, John Hardgrove, Hiedi Liss, Keeley King, Chris Bovais, Ron Gilman, Mark Haupt, Rudy Monteleone, and Greg Page. We also thank the personnel at Dugway Proving Grounds for their support and Dan Weber at ERDEC for his help with air-particle collector testing.

REFERENCES

1. J.P. Golden, E.W. Saaski, L.C. Shriver-Lake, G.P. Anderson, and F.S. Ligler, "A Portable Multichannel Fiber Optic Biosensor for Field Detection," *Opt. Eng.*, in press.

2. S. Zaromb, R. Torres, A. Birenzvige, A. Akinyemi, and F. Wrede, "Measurements of the Collection Efficiency of a Portable High-Throughput Liquid-Adsorption Aerosol Sampler," *Proc. ERDEC Scientific Conference on Chemical Defense Research* **SP-024**, 61 (1993).

3. S.L. Upton, D. Mark, E.J. Douglass, D.J. Hall, and W.D. Griffiths, "A Wind Tunnel Evaluation of the Physical Sampling Efficiencies of Three Bioaerosol Samplers," *J. Aerosol Sci.* **25**, 1493-1501 (1994). ■

THE AUTHORS

GEORGE P. ANDERSON received the B.S. degree (1981) and Ph.D. degree (1986) in biochemistry from The Ohio State University. His thesis research focused on the chemical modification of the electron transport protein plastocyanin to define binding sites. As a postdoctoral fellow at The Ohio State University College of Medicine, he studied the mechanism of platelet activation by antibodies via the Fc receptor. He joined the Center for Bio/Molecular Science and Engineering at the Naval Research Laboratory in 1991 and has been working on the development and testing of the fiber-optic biosensor for biological warfare defense.

FRANCES S. LIGLER is currently head of the Biosensors and Biomaterials Laboratory in the Center for Bio/Molecular Science and Engineering at the Naval Research Laboratory and a DoD senior scientist. She earned a D.Phil. from Oxford University, Oxford, England, and completed postdoctoral fellowships at the University of Texas Health Science Centers at San Antonio (biochemistry) and Dallas (immunology). After 5 years in academic research, she spent 5 years in industry (DuPont) and then joined NRL in 1985. Dr. Ligler has published approximately 100 patents and full-length articles in scientific journals. She is the winner of the National Drug Control Policy Technology Transfer Award, the Chemical Society Hillebrand Award, and three NRL Edison Awards for Patent of the Year. She cochairs several sensor meetings for the Society for Photo-optical Instrumentation Engineers and was the elected chair of the 1994 Gordon Research Conference on Bio/Analytical Sensors. She is on the editorial boards of the *Journal of Biomedical Optics*, *Genetic Engineering*, and *Applied Biochemistry & Biotechnology*.

DAVID A. STENGER graduated from Wheeling College in 1984 (biology/physics) and received his Ph.D. degree in biophysics from the State University of New York (Buffalo) in 1989. The emphasis of his thesis research was the physical/chemical properties of cell membranes, particularly under the influence of applied electric fields. He joined the Naval Research Laboratory as an ONT Postdoctoral Fellow in 1989 and joined the NRL staff in 1990. Dr. Stenger is a member of the Laboratory for Biosensors and Biomaterials in the Center for Bio/Molecular Engineering and acts as the principal investigator for projects dealing with: (1) generic detection of chemical and biological warfare agents using neural cells as detector elements, (2) precision lithographic patterning of cultured hippocampal and cortical neurons, and the transduction of electrical signals using optical methods and solid state electronics, (3) application of biologically derived neural algorithms to Navy applications, and (4) rapid prototyping and testing of autonomous sensor systems. Dr. Stenger is an author on more than 40 refereed papers and patents.

PEGGY T. DAVIDSON joined NRL's Tactical Electronic Warfare Division following graduation from Texas A&M University in May 1986, with a B.S. degree in aerospace engineering. She was previously employed by NRL as a summer hire before her senior year at Texas A&M. Ms. Davidson received an M.S. degree in aerospace engineering from the University of Maryland in May 1992, while working full time at NRL. Presently, Ms. Davidson is the head of the Aerodynamics and Flight Research Unit for the Vehicle Research Section where her work focuses on the development of small, unmanned aircraft for electronic warfare (EW) applications. She is the NRL project manager for the ONR-sponsored Eager Advanced Technology Demonstration (ATD), a $12M RF decoy development and demonstration effort and is the flight test director for all of the section's research programs. Ms. Davidson received an NRL Special Act Award in 1991 for her participation in quick-reaction EW efforts to support Fleet activities prior to and during Desert Storm. Ms. Davidson is a member of the Board of Trustees for the Association for Unmanned Vehicle Systems International (AUVSI) and is the technical chairperson for the AUVSI '97 symposium. She is also a member of the American Institute for Aeronautics and Astronautics (AIAA).

RICHARD J. FOCH joined the Naval Research Laboratory's Tactical Electronic Warfare Division as an aerospace engineer in 1979, following graduation from the Florida Institute of Technology with a B.S. degree in mechanical engineering. He received an M.S. degree in aerospace engineering from the University of Maryland in 1985 while working full time at NRL. Since 1985, Mr. Foch has been head of the Offboard Countermeasures Branch's Vehicle Research Section. Mr. Foch has led several quick-reaction electronic warfare (EW) efforts to support Fleet activities prior to and during Desert Storm, for which he received the Meritorious Civilian Service Award in 1989 and an NRL Special Act Award in 1991. Under his leadership, the Vehicle Research Section has developed and demonstrated numerous unmanned aircraft for EW applications, including the Low Altitude/Airspeed Unmanned Research Aircraft (LAURA), the Flying Radar Target (FLYRT), the Self-Navigating Expendable, Recoverable (SENDER), and the Swallow airborne test platform for NRL's biosensor. Mr. Foch is a member of the Association for Unmanned Vehicle Systems International (AUVSI), the Experimental Aircraft Association (EAA), the Academy of Model Aeronautics (AMA), and the American Institute for Aeronautics and Astronautics (AIAA).

JOSEPH F. MACKRELL graduated from the University of Notre Dame with a B.S. degree in aeronautical engineering in 1984 and joined the Tactical Electronic Warfare Division's Offboard Countermeasures Branch. While in the Vehicle Research Section, Mr. MacKrell supported its ongoing research into low speed/low Reynolds number aerodynamics. In 1986, Mr. MacKrell was assigned to the Airborne Active Electronic Decoy (AAED) program, which was developed by NRL and led to the AN/ALE-50 Towed Decoy Countermeasures System. Mr. MacKrell was instrumental in the development of the Quick Reaction Time (QRT) countermeasures pod and supported Fleet introduction of this system in 1993 in the Persian Gulf. In 1994, Mr. MacKrell was assigned to a 1-year tour at the Technical Support Group (TSG), an N3/5-sponsored organization operating at the Office of Naval Intelligence (ONI) in Suitland, Maryland. Upon his return, Mr. MacKrell managed the design and development of Swallow, an electric-powered, low-altitude biosensor platform. He is currently the program manager for the 1997 SKUNKWORKS project.

Acoustics

64-Channel All-Optical Deployable Array

C.K. Kirkendall, A.R. Davis, A. Dandridge,
and A.D. Kersey
Optical Sciences Division

Over the past few years, littoral warfare has become a concern to the U.S. Navy. The perceived threats are no longer restricted to the open ocean but exist in the harbors, straits, and narrow seas of the world. This need, coupled with advances in signal-processing capabilities, has spurred the development of rapidly deployable shallow water acoustic arrays for broad area surveillance and antisubmarine warfare (ASW) applications. The All-Optical Deployable System (AODS) array, which uses fiber-optic technology to detect undersea acoustics, has been developed by NRL to meet the Navy's newest need. The AODS concept is shown in Fig. 1.

The deployability of an array is driven by the number and size of the "lumps" on the array cable. The sensors themselves generally are small enough not to be a problem. The power plant, on the other hand, is significantly larger than the array cable and determines the deployability of the array. Conventional array technologies use active sensors, which require power, and the associated large lumps to be distributed throughout the array. Fiber-optic hydrophone technology uses significantly less power than conventional approaches, and since the sensor array is completely passive, power is required in only two locations, drastically improving deployability.

The AODS system concept uses both wavelength division and time division multiplexing (WDM/TDM) to transmit 256 sensing channels over a single fiber. Four optical wavelengths, each with 64 TDM channels, are used to achieve the 256 channels/fiber. The number of TDM channels per wavelength is limited by the required system signal-to-noise ratio, while the number of wavelengths is limited by the diversity of distributed feedback (DFB) sources. Array spans on the order of 100 km and array standoffs to a shipboard or shore-based monitoring station of 100 km are achievable.

In May 1996, the AODS system concept was validated when two 32-element hydrophone arrays were deployed and tested at sea. For this test, two wavelengths were used, each with only half of their TDM channels populated to reduce the cost of the test. The 64 individual hydrophone sensors from the two acoustic arrays were transmitted to a shore-based monitoring station over a single fiber, thus demonstrating an order of magnitude improvement in channels/fiber density over previous field-deployed systems. Fully populating the TDM channels of four wavelengths would realize a further factor of four improvement.

System Description: Figure 2 shows a block diagram of the system, with insets of the actual hardware used in the validation test. The continuous-wave output of each laser is pulsed by an optical switch with a duty cycle to provide for 64 TDM channels. An erbium-doped fiber-optic amplifier is used to amplify the pulses by greater than 20 dB. The amplified optical pulses interrogate the forward-coupled hydrophone array [1]. The acoustic array itself is totally passive. After interrogation of the arrays, the two wavelengths are combined and optically amplified in the telemetry node (TN) for transmission to the monitoring station (MS). In this test, due to the reduced-array

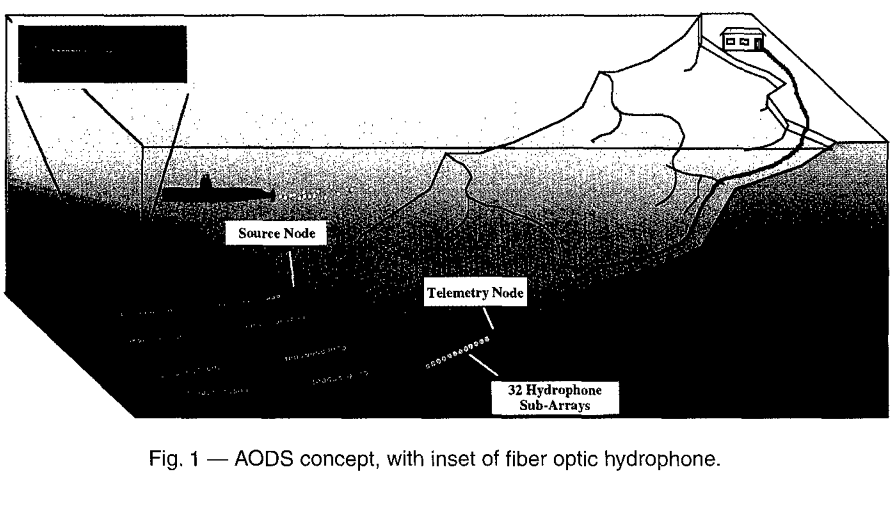

Fig. 1 — AODS concept, with inset of fiber optic hydrophone.

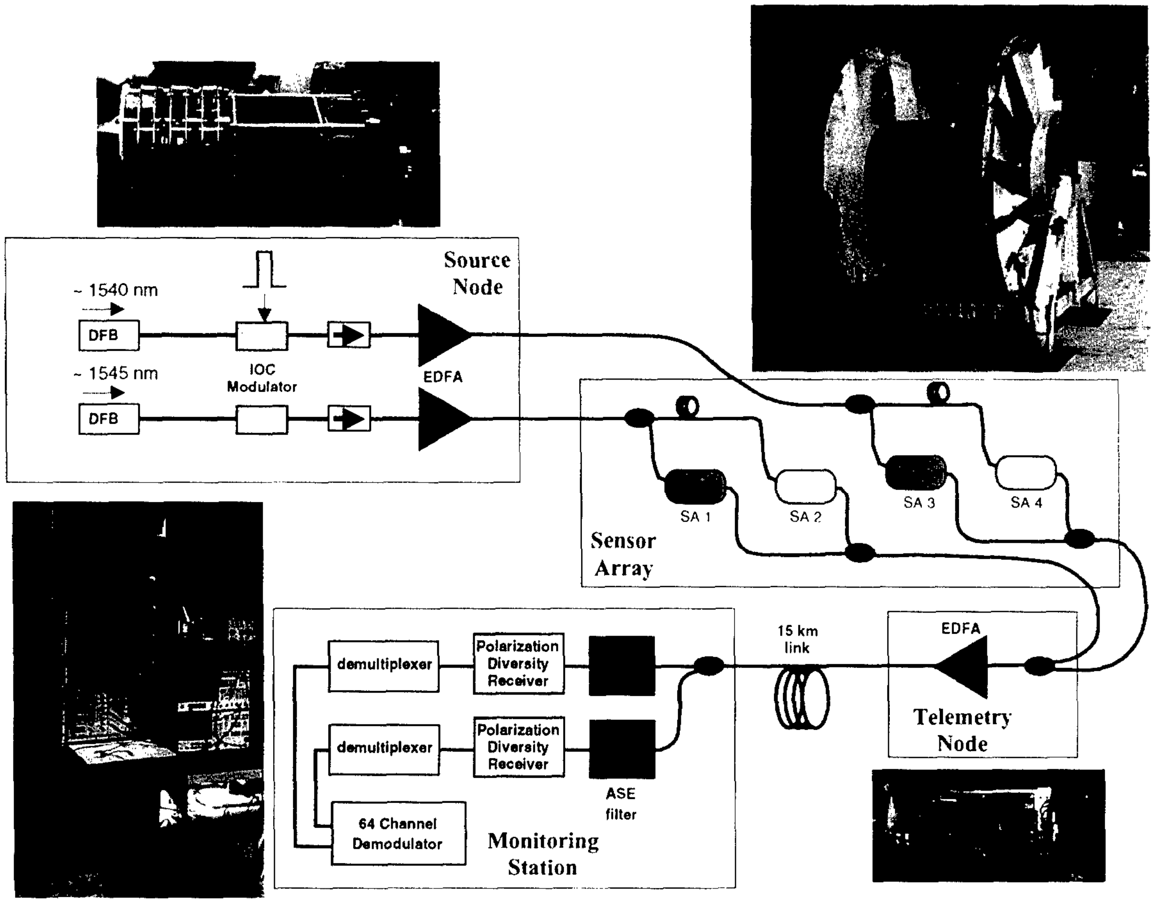

Fig. 2 — AODS block diagram.

span and relatively short standoff, the TN is configured to have a low gain (~ 1). In the MS, a pair of tunable optical wavelength filters selects the two wavelengths and filters out the amplified spontaneous emission (ASE) noise generated by the optical amplifiers. A polarization diversity receiver overcomes the polarization-induced fading of the optical signals (a characteristic of interferometric fiber optic sensors). The signal is then demultiplexed and demodulated to recover the sensors' acoustic signals, which are digitized and archived in a data acquisition system.

Results: In May 1996, two 32-element horizontal line arrays were deployed off the coast of San Diego, California, in conjunction with the shallow-water evaluation cell experiments (SWellEX). The experiments were designed to determine the passive detection limits of submarines in littoral waters and included 160 h of towed source and 40 h of USS *Dolphin* (AGSS-555) as calibrated target data. Sophisticated real-time signal-processing hardware used the AODS array to detect and track sea-going vessels. Typical single-sensor ambient acoustic data from 5 MHz to 6 kHz are shown in Fig. 3. The peaks near 55 MHz are due to changes in hydrostatic pressure from surface waves while the spurs from 60 to 400 Hz are due to a calibrated source tow during the SWellEX test. In Fig. 4, the crosscorrelation between two sensors clearly shows a target passing the array. The target travels from endfire through broadside to endfire before fading away.

Conclusion: We have leveraged NRL's extensive experience in fiber-optic sensor systems to develop and demonstrate a hybrid WDM/TDM hydrophone array that meets the Navy's broad-area surveillance/ASW requirements. The all-optical technology offers significant advantages over conventional approaches in power, size, weight, and overall deployability.

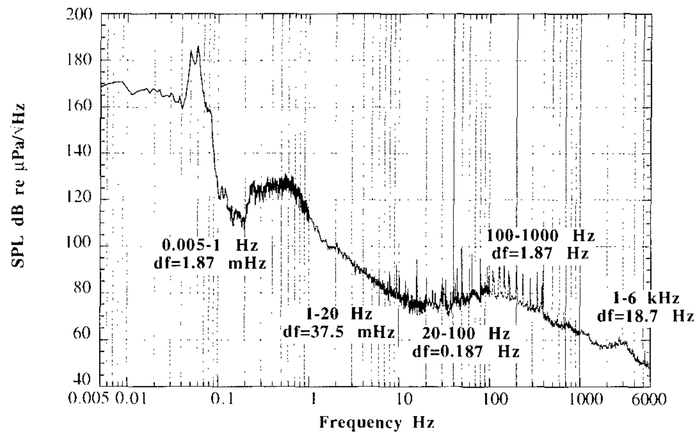

Fig. 3 — Ambient acoustic spectrum (data pieced together from multiple fast Fourier transforms to maintain frequency resolution over entire span).

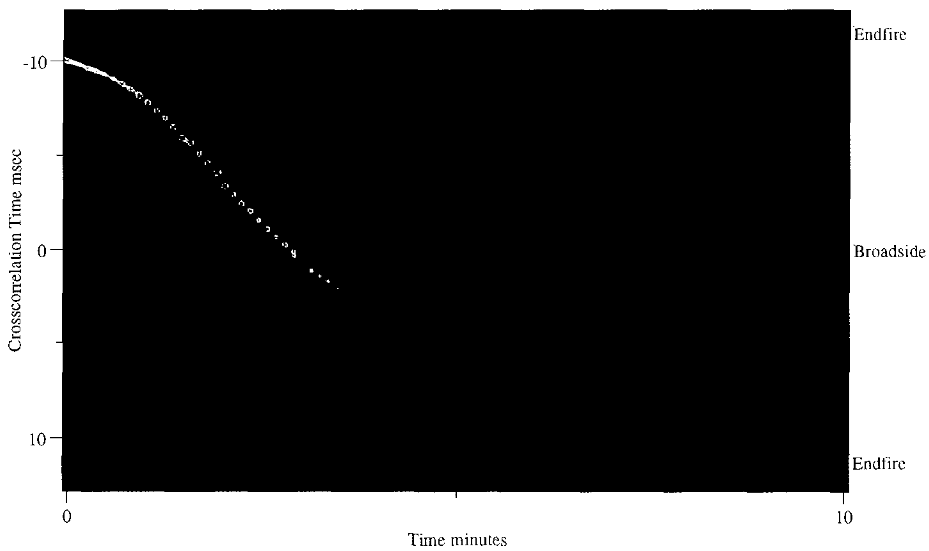

Fig. 4 — Crosscorrelation of a passing vessel.

Acknowledgments: The Naval Command, Control and Ocean Surveillance Center, Research, Development, Test and Evaluation Division was responsible for developing the data-acquisition system, the deployment scheme, and pressure housings used in the sea test of the AODS system.

[Sponsored by SPAWAR]

Reference

1. A.D. Kersey, A. Dandridge, A.R. Davis, C.K. Kirkendall, M.J. Marrone, and D.G. Gross, "64-Element Time-Division Multiplexed Interferometric Sensor Array with EDFA Telemetry," OFC'96 Technical Digest **2**, pp. 270-271. ■

Influence of Subsurface Bubbles on Acoustic Scattering

R.C. Gauss, P.M. Ogden, and M. Nicholas
Acoustics Division

When operating in the world's oceans, acoustic interaction with the sea surface can limit an active sonar's performance by masking desired signals or by creating false targets. The dynamic nature of the air-sea boundary complicates attempts to model this interaction. As the winds and seas increase, waves begin to break, entraining air in the form of subsurface bubbles. Under these conditions, both the air-sea interface and bubble clouds can contribute to the acoustic reverberation

and clutter. A key goal of Navy ocean acoustic-scattering research is to develop a set of easily measured environmental parameters for use by the Fleet as inputs for improving their sonar-system prediction modeling.

Background: From 1987 through 1996, the Space and Naval Warfare Systems Command (SPAWAR) conducted a series of at-sea experiments, known as the Critical Sea Tests (CST), to improve the Navy's understanding of environmental acoustics and its impact on low-frequency sonar performance. Using a variety of systems and waveforms, short-range measures of the strength, spectral, spatial, and temporal characters of acoustic surface interaction were obtained in the open ocean under well-documented conditions for a range of acoustic frequencies and sea states. These measured scattering quantities were correlated to environmental measures of the air-sea boundary conditions such as wind speed, wave spectra, and bubble parameters. Long-range surface reverberation experiments complemented these short-range tests, furnishing the link between the basic scattering mechanisms and the reverberation important to an active sonar system.

Scattering Strength Characteristics: In the CST program, high-quality measurements using both signal, underwater sound (SUS) explosive charges, and controlled waveforms characterized the strength of the backscattered signal as a function of the acoustic frequency (50 to 1500 Hz), the grazing angle (the angle of ensonification with respect to the scatterer), and environmental descriptors of the boundary conditions, such as wind speed. By comparing predictions of well-established, physics-based theories of air-water interface scattering, the measurement results demonstrated that subsurface bubbles and not the interface drive the acoustic backscatter at most frequencies and wind speeds.

To empirically characterize the dependence of surface scattering strength (SSS) on frequency, grazing angle, and environmental descriptors, a number of multidimensional, multiparameter, nonlinear fits were performed on the entire CST SUS data set (Fig. 5). The resulting new SSS prediction algorithm, the Ogden-Nicholas-Erskine algorithm, has much higher confidence levels than the Chapman-Harris empirical formula, which had been the Navy standard model for over 30 years. The best correlation of SSS with environmental descriptors was provided by wind speed back-averaged over 1 h. Figure 5 illustrates that while SSS depends fairly smoothly on the grazing angle, there are distinct regimes to the wind-speed dependence. The first rise at low wind speeds coincides with the appearance of whitecaps (due to breaking waves) on the ocean surface. As the winds and seas increase, the levels continue to rise quickly. Finally, at high sea states, there is evidence of a limit to scattering strengths, most likely due to deeper bubbles attenuating the acoustic energy on its path to and from the higher air-content bubbles near the surface that dominate the scattering process.

One of the major issues answered by NRL is the appropriateness of using scattering strengths derived from short-range measurements as performance-model inputs when predicting long-range reverberation for controlled waveforms. Figure 6 illustrates a forward-modeling approach where short-range SSS values were used to predict reverberation levels out to long range over all azimuths. That these levels (bottom image) generally agree well with measured long-range reverberation levels (top image) demonstrate that the new

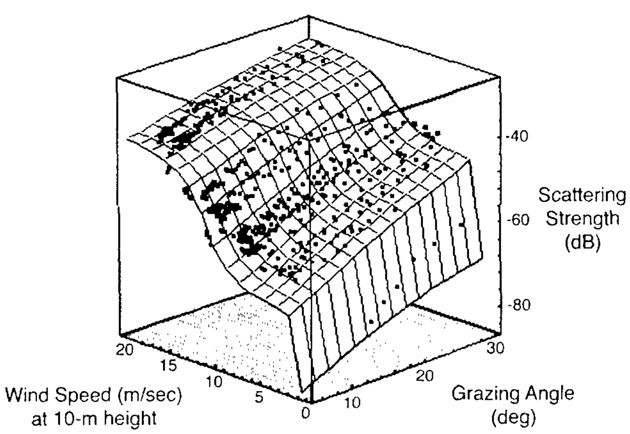

Fig. 5 — An illustration of the performance of the Ogden-Nicholas-Erskine algorithm (grid) vs surface scattering strengths measured during seven CST experiments (points) for a representative range of frequencies (474-560 Hz).

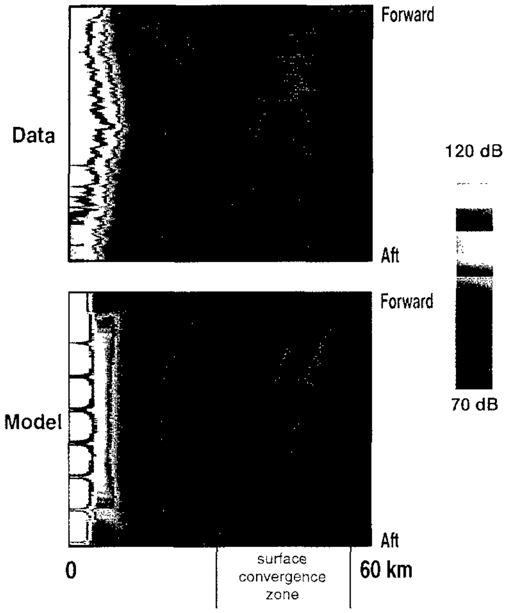

Fig. 6 — Data-model comparisons for distant surface reverberation. The data represent returns out to 60 km for all azimuths following transmission of a 12-s continuous wave signal at 920 Hz during high sea-state conditions.

empirical algorithm described above can be used with confidence in making estimates of the interference due to surface interaction for the signals and ranges of interest to the Navy.

Spectral Characteristics: In addition to having an effect on the received level, the moving sea surface induces Doppler shifts in acoustic signals. When whitecaps are present, these excursions from the carrier frequency have been shown to be correlated not with wind speed but with the mean orbital speed of the surface gravity-wave spectrum. This is consistent with scattering from bubble clouds being passively advected by the waves. This circular motion leads to the bubble cloud alternately advancing and receding from the receiver, causing a Doppler shift in the signal. This is illustrated in Fig. 7(a), where a time history of backscattering from individual bubble clouds shows sinuous patterns consistent with the hypothesized spectral spreading mechanism. At long range, a sonar typically ensonifies many such clouds so that the spectral envelope of these shifts will determine the frequency structure, as is illustrated in Fig. 7(b). The fact that the average frequency shift is at zero Doppler (i.e., at the carrier frequency) is corroborating evidence for the dominant role subsurface bubbles play in scattering from the air-water boundary zone.

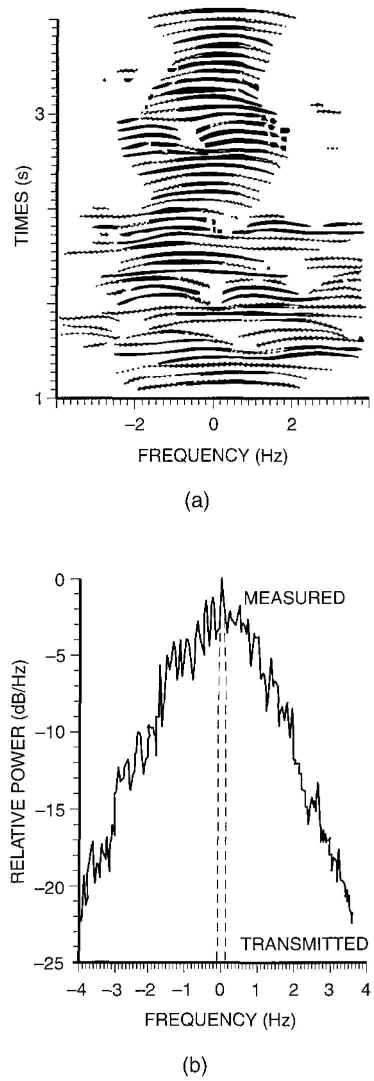

Fig. 7 — (a) Short-range, normalized spectral history for a single, short-duration continuous transmission at 920 Hz showing the wander in time about the carrier frequency. The solid, dashed and dotted lines represent the 3, 6, and 10 dB down-spreads of each spectrum. (b) Long-range, normalized spectrum representing an average of 12-s continuous transmissions at 920 Hz from the convergence zone shown in Fig. 6 (top). Note the considerable broadening in frequency relative to the transmitted waveform, which is represented by the dashed curve.

Significance: Recent work by NRL has led to the most important advances in our understanding of low-frequency (50–1500 Hz) acoustic scattering from the sea surface in over 30 years. The Navy now has a considerably more reliable capability for predicting the effects of the sea surface on sonar performance; moreover, these predictions use

easily obtained environmental parameters: wind speed (surface scattering strength) and wave spectra (spectral spreading). We have also advanced the understanding of the physics responsible for the observed scattering characteristics; this, in turn, will lead to a better theoretical description of the scattering process.

While much progress has been made for the open seas, there is still exciting work ahead. For example, while 1-h back-averaged wind speed furnished the best environmental fit to all the CST SSS data, we know that short-term wind history is not the whole story, as significant differences were found between CST-4 and CST-7 SSS results at similar wind speeds. Resolving issues such as this will be of particular importance for Navy operations in shallow water, where larger, more persistent bubble populations occur.

[Sponsored by ONR and SPAWAR]

References

1. P.M. Ogden and F.T. Erskine, "Surface and Volume Scattering Measurements Using Broadband Explosive Charges in the Critical Sea Test 7 Experiment," *J. Acoust. Soc. Am.* **96**(1), 2908-2919 (1994).

2. M. Nicholas, P.M. Ogden, and F.T. Erskine, "Improved Empirical Descriptions for Surface Backscatter," SPAWAR CST/LLFA-WP-EVA-30, Space and Naval Warfare Systems Command, Arlington, VA, September 1995.■

Supersonic Acoustic Intensity — A Key to Source Identification

E.G. Williams, B.H. Houston, and J.A. Bucaro
Acoustics Division

Introduction: The location of radiating "hot spots" (a region on a vibrating structure that radiates to the farfield) on the surface of a vibrator is crucial to the Navy, providing critical information for the effective application of quieting techniques, thereby decreasing the vulnerability of the structure to detection. A new quantity — supersonic acoustic intensity — provides a quantitative means to locate these hot spots by removing the nonradiating components of the nearfield intensity using special signal-processing techniques, leaving only the radiating (supersonic) components. It provides the power-per-unit area radiated by the hot spots and, thus, can be used to rank the contributions of the hot spots to the total radiated power.

Theory: The power-flow-per-unit area (time averaged over a cycle) out of a body is measured by the normal component of the acoustic Poynting vector, a quantity called the normal acoustic intensity. It can be computed from a knowledge of both the pressure and normal velocity on the body. When the structural wavelengths of the normal velocity on the outer surface of this body are small compared to the acoustic wavelength (as is dominantly the case in submarines), the resulting radiation is in "short circuit," that is, the flow of the energy circulates back into the shell and very little is pumped into radiation away from the shell. In the face of this very strong short circuit, the small, uncancelled component is obscured. It is this latter component that characterizes the strength of the accompanying region as a farfield source — that is, as a "hot spot" on the shell.

Using basic signal processing techniques, one can remove this short-circuited component leaving only the radiating residue. This is done by removing (using a spatial fast Fourier transform (FFT) and a low pass filter) the wavelength components that are smaller than the acoustic wavelength (the short-circuited components) in both the surface pressure and surface normal velocity. The resulting intensity I, ($I = 1/2\,\Re(pv^*)$), is called the supersonic intensity [1]. It turns out that the circulation of the intensity is removed in this process, leaving only the positive outgoing components and, thus, uncovering the farfield source strength of the region. Most important is the fact that the integral of the normal component of the supersonic intensity over the whole surface of the shell (this gives the total radiated power $\Pi = \iint I\,dA$ in watts) is equal to the integral of the normal component of the actual intensity (with all its circulating fields). This equality to the actual total power radiated gives credibility and meaning to the supersonic intensity.

There is one undesirable but unavoidable effect of this filtering process. The resulting supersonic intensity has a resolution limited to one-half the acoustic wavelength. Thus, acoustic sources within this distance will be averaged over and will not appear as distinct entities.

Experiment: Using the laboratory for structural acoustics — a state-of-the-art acoustic measurement facility at NRL — pioneering experi-

ments were carried out using nearfield acoustical holography (NAH) to study radiation from a scale model of a submarine hull. This scale model was constructed using advanced modeling techniques in order to create high fidelity, welded regular and king frames with simple attached internal structures. Many of the frames were bridged with chock plates, which formed foundations for mounting isolated ballast trays and the attachment of small electromagnetic shakers. Figure 8 is a photograph of the completed shell. Figure 9 shows the inside of the shell with some of the "simple" structure. The trays along the keel are ballast trays. Small cylindrical tubes of rubber, which were carefully designed to simulate real isolators, isolated the actual tray from the mounting plates bridging the ribs. During the experiment, the trays were loaded with lead ballast to provide the scaled internal weight of a submarine. The individual sections (shown in Fig. 9(a)) were joined with realistic king frames, as can be seen in Fig. 9(b).

Experiments were carried out using NAH [2] to reconstruct the unfiltered surface pressure, normal velocity, and normal acoustic intensity over the complete cylindrical surface of the shell. The shell was excited into vibration by an axial shaker driving a thrust block mounted at the center of a chock that was welded between two adjacent frames. Data were collected over the frequency range of 5 to 50 kHz. At any frequency over the whole frequency band, the reconstructed, unfiltered intensity showed the dominating circulation of the field as explained above, with energy flowing in and out of the shell every half-structural wavelength. We then processed these data to derive the normal supersonic intensity by filtering out the small wavelength components as prescribed. The resulting filtered intensity was then averaged over 3 kHz bands to help illuminate the coherent sources, averaging out the incoherent ones.

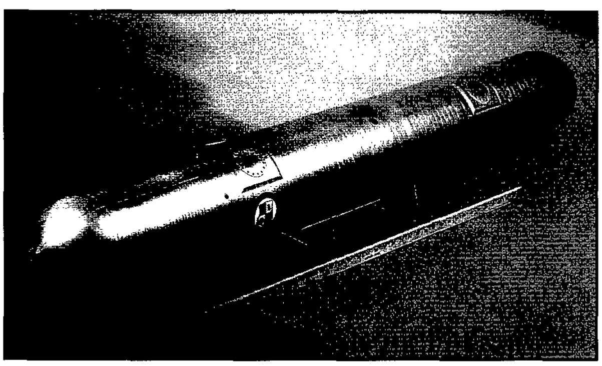

Fig. 8 — Completed scaled shell model.

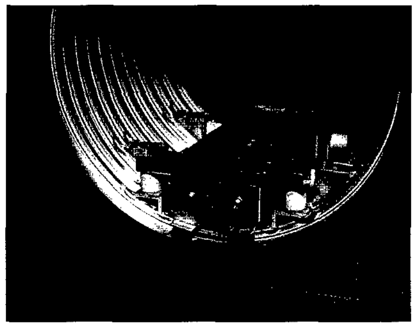

(a)

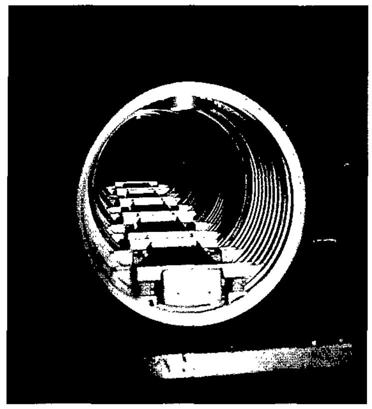

(b)

Fig. 9 — (a) Isolated ballast tray shown inside one of the bays of the shell. The tray is mounted on two vertical and two horizontal isolators (rubber cylinders) that are attached to the regular tee frames on the hull with bridging plates; (b) five such sections joined with king tee frames.

We present one such result in Fig. 10 for the frequency band at 18.5 kHz. At the top of the figure is a side view of the shell showing the 8 king frame locations, indexed to the color picture, with 11 regular frames in between. The location of the shaker is shown (axial force). In the color map, the supersonic intensity is shown color coded to level, as indicated in the key at the bottom of the figure. Each color represents an increment of 1 dB intensity. NAH provides the intensity over the complete surface of the shell. In the display, this intensity has been unwrapped, slicing open the data at the keel of the shell, as indicated on the axis labels. Using the key, the largest intensity sources on the shell were ranked and labeled on the table at the right of the figure. The small white rectangles indicate the location of bridging plates across the regular frames with those close to the keel used for support of the ballast trays. The vertical white lines mark the boundaries of the king frames.

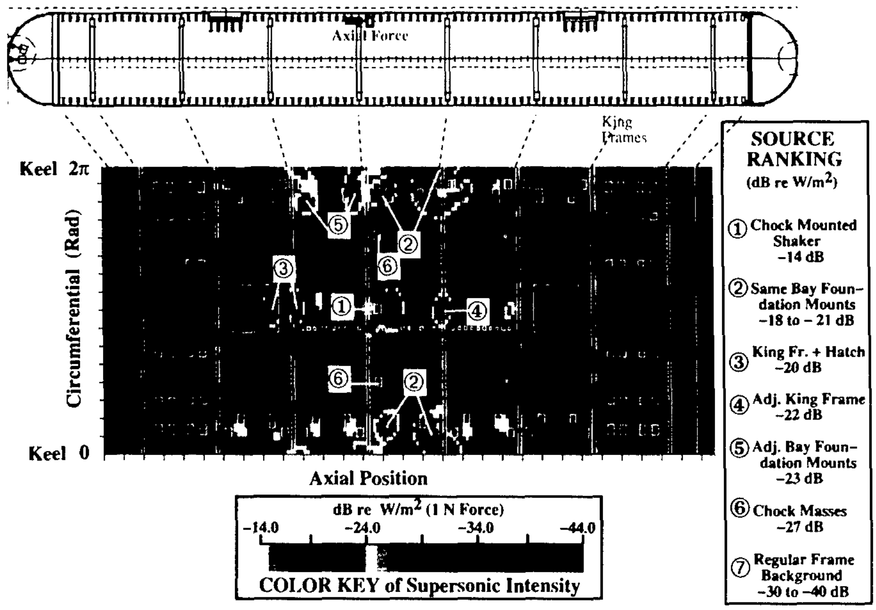

Fig. 10 — Color-coded supersonic intensity over the complete cylindrical surface of the model showing the source strength of regions (hot spots) that radiate to the farfield. The data are unwrapped as indicated. Highest intensity levels are ranked and related to internal structure.

Analysis: The maximum supersonic intensity was located directly above the shaker on the hull. As the key indicates, it has a level of −14 dB re watt per-square meter for a newton of force at the driver. The second strongest peak intensity was found at the locations of the foundation mounts for the ballast trays in the same bay (region bounded by king frames) as the shaker. As Fig. 9 shows, the entire keel is covered with these ballast trays, and one can see the "hot spots" arising from their chock mounts at the keel positions in Fig. 10. The trays were isolated from the hull by rubber mounts. Other source intensities are indicated in the table. Note that peak intensities are displayed for the ranking procedure. One could rank the actual power radiated from the different regions by integrating the intensity over some local area and then ranking the different regions according to radiated power.

It is also significant that (in Fig. 10) the background intensity levels are generally in the −30 to −34 dB range (green) even though there are no lumped structures here. The hot-spot effect of the regular frames, however, cannot be discounted with regard to source levels, since the frames disrupt the nonradiating flexural waves traveling in the axial direction, thereby resulting in local radiation at the frame locations. But since the acoustic wavelength is about the distance between six frames, the discrete source nature is averaged out, resulting in a smooth background level. Also it is clear that the total radiated power from each bay decreases as we move away from the shaker. Clearly, as energy radiates from the shell, less is left over to travel to farther out regions of the shell.

The source ranking results illustrate the disadvantageous effect of mounting vibration sources without isolation directly to the hull, as shown by the axial shaker in Fig. 10. Perhaps surprising is the fact that the passive plates that bridge the regular frames provide the second highest source levels, only 5 dB below the active source.

With the combination of the construction capability of high-fidelity scale models and the source ranking capability, NRL is positioned for dramatic gains in characterizing, locating, and ranking the farfield radiation from internal structures on submarines and surface ships.

[Sponsored by ONR]

References

1. E.G. Williams, "Supersonic Acoustic Intensity," *J. Acoust. Soc. Am.* **97**, 121-127 (1995).

2. E.G. Williams, B. Houston, and J.A. Bucaro, "Broadband Nearfield Acoustical Holography for Vibrating Cylinders," *J. Acoust. Soc. Am.* **86**, 674-679 (1989). ■

Chemical/Biochemical Research

Lysozyme Diffusion in the Vicinity of Crystal Surfaces

K.B. Ward, S. Gorti, and W.M. Zuk
Laboratory for the Structure of Matter

Introduction: We have used a novel microscopic dynamic light-scattering technique to investigate the physical chemical characteristics of protein molecules in the vicinity of protein crystal surfaces. Using the microscope laser light-scattering (MLLS) technique [1], we can investigate the existence and levels of protein aggregation near the surfaces of crystals. We have used an MLLS apparatus to observe the diffusion of lysozyme molecules close to the surface of a crystal under solution conditions that promote its growth [2]. The motive for the preliminary research was to determine the efficacy of MLLS to measure accurately the size distribution of lysozyme molecules within the depletion zone of crystals. That is, for a long time it had been hypothesized that an imbalance in the rates of lysozyme attachment onto crystals vs solution diffusion gives rise to a "depletion zone" surrounding a crystal of sufficient size. Since MLLS is capable of measuring the size distribution of molecules within small sampling volumes (~ 8 μm^3), we assumed that the method should enable us to determine changes in the observed lysozyme diffusion coefficients within the depletion zone in the vicinity of the 110 face of a lysozyme crystal when compared with lysozyme diffusion coefficients in bulk solution.

Materials and Methods: Figure 1 is a schematic diagram of the MLLS apparatus. The MLLS design utilized focusing optics that allowed for light exiting the laser to interface with a single-mode optical fiber. The optical fiber serves as a light guide whose "output" end, coupled to a micro-lens, focused the laser light exiting the optical fiber within a specified region of the solution that was at the focal plane of the microscope. The basic components and configuration of the remainder of the MLLS apparatus include: (1) a microscope objective collects the scattered light that was magnified 32X; (2) a microscope eyepiece with an embedded optical fiber collects scattered light within an ~ 7.8 μm^2 sampling area and guides the light to a photo multiplier tube; (3) an amplifier-discriminator converts the analog ac photo current into a digital transistor-transistor logic (TTL) pulse train; (4) a counter measures the number of photon counts that are detected per second; (5) a correlator computes the intensity correlation function from the TTL pulse train; and (6) a computer stores and analyzes the intensity correlation function of the scattered light, as well as the number of photon counts/s that were observed. In the current configuration, the scattered light-sampling volume detected by MLLS was ~ 8 μm^3, determined by the magnification power (32X) and the depth of focus of the microscope objective (~ 1 μm; based on a numerical aperture of 0.40), and the core diameter of the embedded optical fiber (50 μm).

Experiments were conducted using hen egg-white lysozyme. Lysozyme crystals were grown in 100-ml capillaries from a solution containing 40 mg/ml protein, 5% sodium chloride, and 0.08 M sodium acetate. The lysozyme crystals were bathed in a filtered solution containing 30 mg/ml lysozyme, 5% sodium chloride, and 0.08 M sodium acetate, promoting slow growth of the crystals. The capillaries were placed on the sample stage of the MLLS apparatus. Using the microscope objective, the laser beam was focused adjacent to a 110 face of a crystal. The position of the detector fiber was then adjusted to place it directly over the laser beam, collecting scattered light 90° to the incident beam.

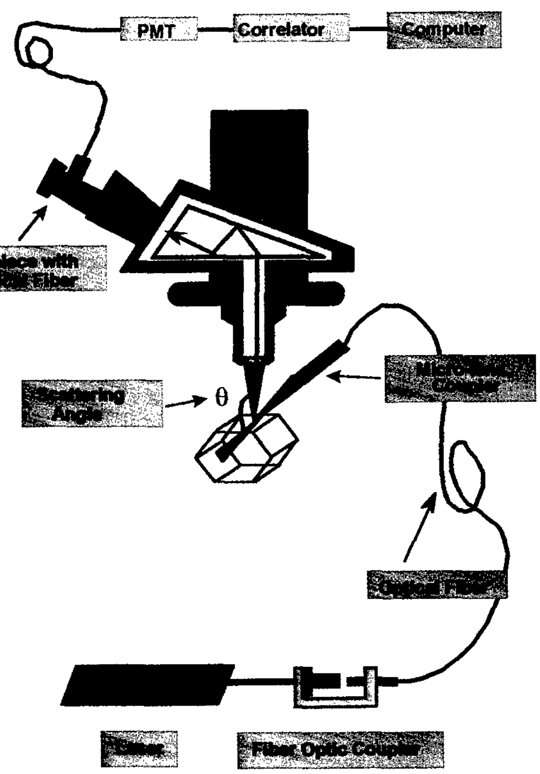

Fig. 1 — Simple schematic of a microscope laser light-scattering (MLLS) apparatus.

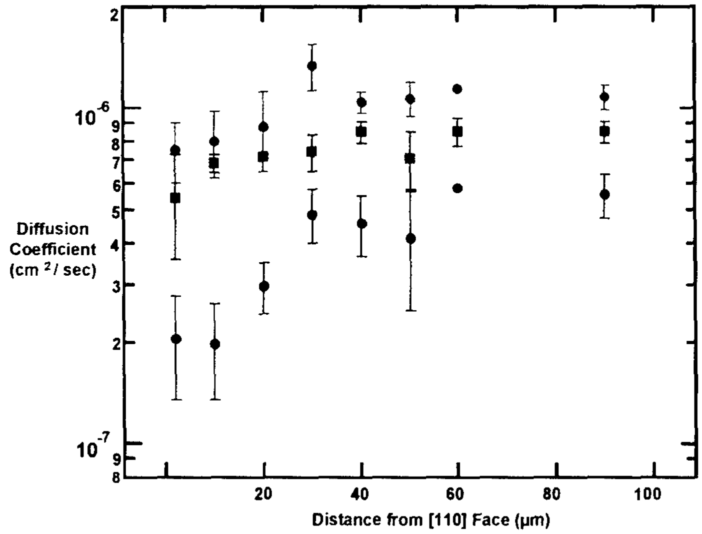

Fig. 2 — Diffusion of lysozyme in the vicinity of a [110] crystal face.

Results and Discussion: As predicted, MLLS was fully capable of measuring a change in the observed diffusion coefficient of lysozyme molecules as a function of distance away from the 110 face of a lysozyme crystal. Namely, MLLS data evidenced an increase in the size of lysozyme aggregates (depicted by the decrease in the cumulative or the "slow" diffusion coefficients) in the vicinity of the crystal surface when compared with the bulk solution diffusion characteristics of lysozyme molecules. Figure 2 shows a plot of the observed diffusion coefficients of lysozyme molecules within the depletion zone of a lysozyme crystal. The dependence of observed protein diffusion coefficients as a function of distance away from the lysozyme crystal 110 face is shown. The red squares represent the averaged diffusion coefficients of lysozyme molecules obtained from the analyses of intensity correlation functions by Koppel's method of cumulants, where the existence of only one population of scatterers in solution is assumed. Alternatively, the green and blue circles represent the diffusion coefficients of "fast" and "slow" groups of lysozyme molecules obtained by analyses of light-scattering data using the assumption that a bimodal population of scatterers exists in solution. The value for the fast diffusion coefficient represents the Brownian motion of lysozyme monomers, whereas the slow diffusion coefficient represents the motions of the larger lysozyme aggregates. Regardless of the assumption used to analyze the scattered light intensity correlation functions, the overall trend that the averaged diffusion coefficient (red squares) and the slow diffusion coefficient (blue circles) both decrease in the vicinity of the crystal surface is evidenced. These results may be interpreted to indicate that a specific species of lysozyme aggregates are absent from the depletion zone as they become attached to the crystal surface.

[Sponsored by NASA]

References

1. I. Nishio, T. Tanaka, S.-T. Sun, Y. Imanishi, and S.T. Ohnishi, "Hemoglobin Aggregation in Single Red Blood Cells of Sickle Cell Anemia," *Science* **220**, 1173 (1983).

2. S. Gorti, W.M. Zuk, K.B. Ward, T. Tanaka, and H. Yang, "Lysozyme Diffusion in the Vicinity of Crystal Surfaces," *Acta Cryst D*, in preparation. ■

Exploiting Microbiology to Enhance Biodegradation of Hydrocarbon-contaminated Environments

B.J. Spargo,[1] R.B. Coffin,[1] M. Montgomery,[2]
J. Jones-Meehan,[1] and C. Kelley[1]
[1]*Chemistry Division*
[2]*GeoCenters, Inc.*

Introduction: Decades of material storage, on-going shipboard and shore activities, and indiscriminate dumping have driven the Department of Defense to explore innovative technologies

to address environmental contamination of groundwater, soil, sediment, and marine environments. The extent of contamination and increasing regulatory requirements has placed considerable emphasis on the development of cost-effective remediation strategies. The Office of Naval Research (ONR), the Strategic Environmental Research and Development Command (SERDP), and the Environmental Strategic Testing and Certification Program have supported innovative technologies to address these needs. The Environmental Quality Sciences group of NRL's Chemistry Division has been challenged to assess several of these technologies with creative approaches. Of particular interest is the assessment of biological treatment technologies (bioremediation), especially those that enhance natural biodegradation processes through nutrient and/or oxygen addition and/or increased availability of the contaminants to microorganisms.

In our research, we have focused on assessment strategies that combine ecological, geochemical, and microbiological studies. For example, the ability of native microorganisms to degrade contaminants to nontoxic forms has been examined using a technique called mineralization. This technique determines the rate and extent to which bacteria convert the carbon in a contaminant chemical(s) to carbon dioxide and more microbial biomass (bacteria grow at the expense of the contaminant carbon). Ecological methods that have been used include measuring bacterial productivity and tracking specific microorganisms by using genetic probes. These analyses have been further coupled to geochemical studies by using state-of-the-art stable carbon-isotope methods to trace the degradation of contaminant into microorganism biomass and mineralized carbon.

Our approach for enhancing biodegradation activity in the field has been to overcome environmental limitations to the growth of microorganisms that are catalyzing the biodegradation processes. In contaminated sites, the presence of high concentrations of organic matter often creates an oxygen or nitrogen demand that cannot be accommodated by natural renewal processes. By using innovative techniques, we have shown that physically adding nitrogen and/or oxygen in the field effectively overcomes this limitation. In other cases where the contaminants are in a form unavailable to the bacteria, such as adsorbed to soil or sediment particles, the addition of surfactants has significantly increased bioavailability and thereby enhanced biodegradation. Finally, in environments where certain metabolic activities of the microorganisms are lacking, microencapsulated bacteria have been successfully used to augment natural microbial populations.

Field Studies/Applications: Methods to monitor the degradation of contaminants in the laboratory cannot always be applied directly to the field. Basic research studies in microbiology, ecology, and oceanography have provided protocols that are specific for field application. For example, measures of bacterial abundance and productivity in contaminated groundwater must be done through the use specialized sampling wells. Figure 3 shows productivity measurements made during a bioremediation demonstration. Since the effect of aerating groundwater and improving bioavailability through enhanced groundwater circulation on contaminant degradation cannot be measured directly, productivity measurements can provide surrogate measures of microbial activity enhancement. While no single method can describe biodegradation, when taken together, these methods support an overall view of the bacterial processes occurring in the ecosystem. This is depicted in Fig. 4, as it might apply to the fate of polycyclic aromatic hydrocarbons (PAHs) (contaminants from petroleum fuel spills) in estuarine sediments.

A new and promising method for monitoring the direct degradation of contaminants by bacteria is the use of stable carbon isotope ($\delta^{13}C$) values. With the combined technologies of gas chromatography and isotope ratio mass spectrometry, simultaneous compound identification and stable isotopic analyses can be accomplished. This capability allows for the resolution of hydrocarbon pollutants within complex environmental mixtures. In the past, a primary problem in monitoring the effectiveness of bioremediation efforts was the ability to measure the degradation rate of individual compounds and to relate the disappearance of targeted compounds to bacterial activity. By coupling indirect measurements, such as bacterial productivity with $\delta^{13}C$ values found in representative fractions of the carbon pool, we can now trace the flux of pollutant carbon through natural bacterial assemblages in many different types of environments. Furthermore, the proportion of indigenous versus contaminant compounds that are metabolized can be determined.

FEB 1995

MAY 1995

SEPT 1995

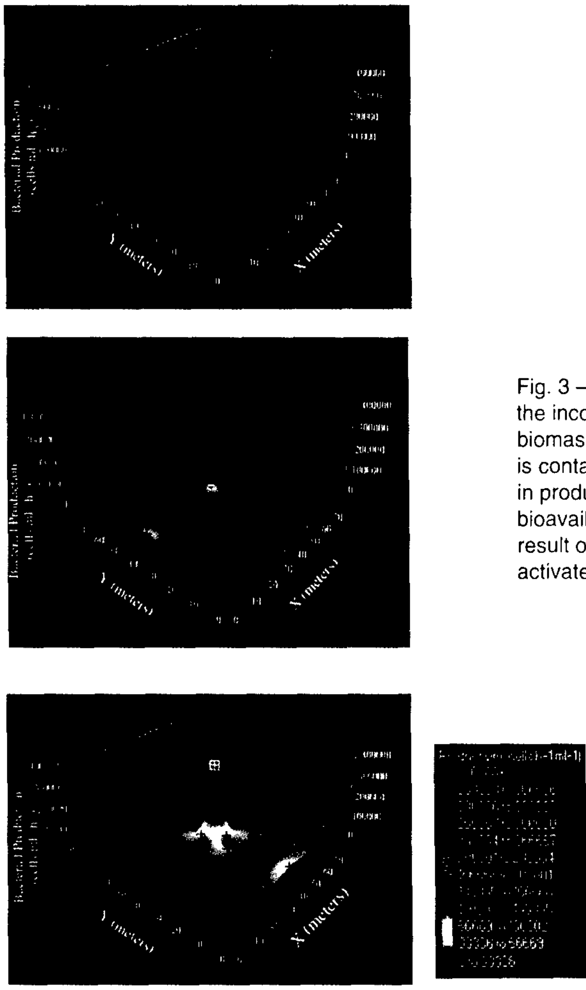

Fig. 3 — Measurements of bacterial production (using the incorporation of radio-labelled leucine into bacteria biomass) in samples taken from a groundwater site that is contaminated with PAHs and creosote. The increase in productivity with time occurs because of improved bioavailability of the contaminants to bacteria as a result of groundwater recirculation wells that were activated in February 1995.

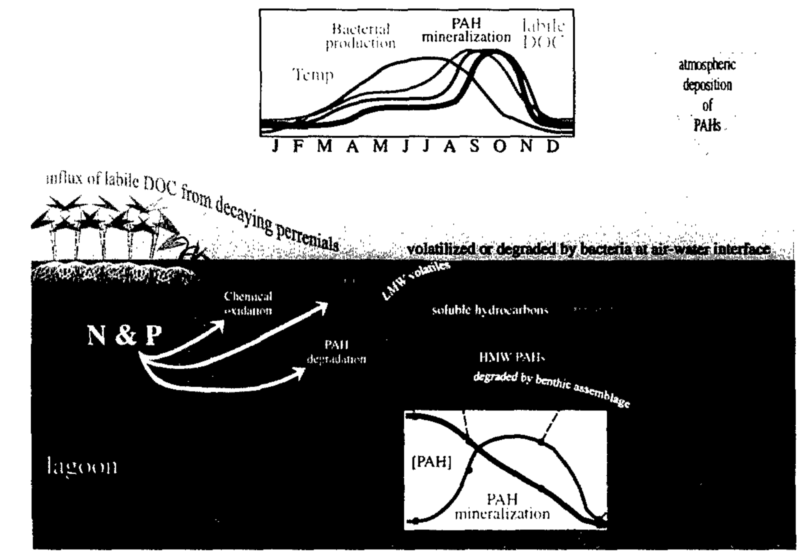

Fig. 4 — Conceptual model of the environmental dynamics of PAHs originating from contamination of groundwater with petroleum. The PAHs distribute into different components of the ecosystem, and degradation of the PAHs, as shown by their disappearance and mineralization, is affected by ecosystems processes on a seasonal basis and the availability of nitrogen and phosphorous nutrients.

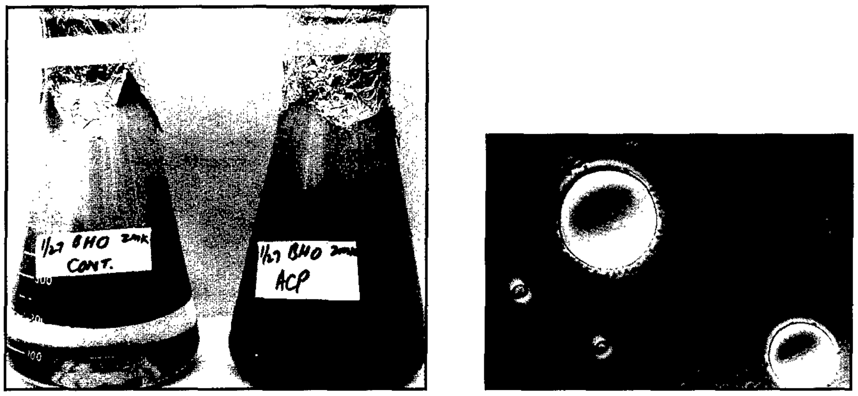

(a) (b)

Fig. 5 — Demonstration of the biosurfactant capability of certain microorganisms; (a) the flasks contain oil on water, and in the flask on the right, a bacterial culture that produces a biosurfactant was added. Note the greater emulsification of the oil, making it more available to the bacteria, as seen by the association of bacteria with the large oil droplets shown in the right panel (b).

Enhancement/Nutrient Additions: Many of the contaminants are hydrophobic and tend to bind to particles, such as soil and sediment particulates, making them less available to the microorganisms for degradation. To increase bioavailability, we have used chemical and physical perturbations such as synthetic and biological surfactants (chemical) and groundwater circulation (physical) in large-scale field demonstrations to increase bioavailability of the contaminants (Fig. 5). These technologies are being applied to shipboard oil/water separators, collection holding and transfer (CHT) tanks, subsurface gasoline spills, and creosote lagoons.

We are currently studying encapsulation as a mechanism to deliver agents to enhance biodegradation at contaminated sites. Nutrients, including inorganic nitrogen and phosphorus compounds, and oxygen can be encapsulated in agarose beads and delivered to the contaminated area, where the nutrients are slowly released. In a similar manner, bacteria isolated from the environment and found to degrade specific contaminants also can be encapsulated and delivered back to the site in higher concentrations and in a form that assures degradative activity over extended periods. This encapsulation technology is being field tested with a bacterium that degrades high molecular weight PAHs at a contaminated salt marsh site.

Summary: The combination of direct (stable isotopes and mineralization) and indirect (bacterial productivity and abundances) measurements allows us to determine the amount of biologically mediated contaminant degradation that is occurring in a field system. We can then determine the fate of the pollutants in the environment and evaluate the effectiveness of clean-up efforts. With additions of nutrients or surfactants to increase bioavailability, we can further manipulate and optimize the system to facilitate greater biodegradation.

Acknowledgments: The excellent scientific contributions and experimental competence of Lt. Thomas Boyd (USN) and Rachael Owlett are gratefully acknowledged.

[Sponsored by SERDP, ONR, NAVSEA, and NAVFAC] ■

Explosives Detection by Nuclear Quadrupole Resonance (NQR)

A.N. Garroway,[1] M.L. Buess,[2] J.P. Yesinowski,[1] J.B. Miller,[1] and K.J. McGrath[1]
[1]*Chemistry Division*
[2]*Sachs/Freeman Associates*

The detection of bulk quantities of concealed explosives is a significant problem of concern to the Department of Defense and to organizations responsible for aviation and other types of security. Nuclear quadrupole resonance (NQR) of ^{14}N nuclei offers a novel approach to detecting explosives such as RDX (Fig. 6) and illicit substances and contraband containing nitrogen [1]. Almost all solid explosives contain nitrogen and, hence, are amenable to ^{14}N NQR detection. Because the

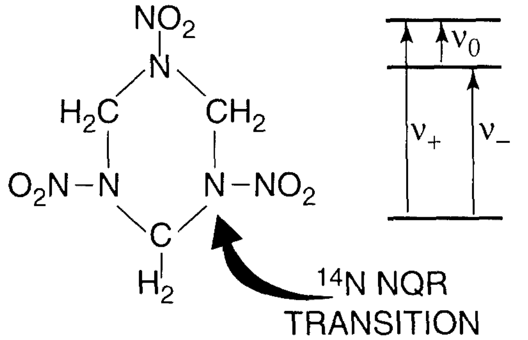

Fig. 6 — Molecular structure of RDX and schematic ^{14}N nuclear energy level diagram in zero magnetic field showing three possible NQR transitions.

NQR frequencies are a unique characteristic of a particular solid chemical compound, there are no false alarms from the NQR signals of other substances. In addition to its specificity, a second advantage of NQR is that no costly magnet is required, in contrast to nuclear magnetic resonance (NMR) methods. Here we describe how NQR can be applied to explosives detection and show results from a laboratory prototype demonstration conducted at the Federal Aviation Administration Technical Center.

Technical Background: NQR spectroscopy is a solid-state magnetic resonance method in which radio-frequency (RF) irradiation is used to excite transitions between different energy levels of the appropriate nuclei. Many stable nuclear isotopes, including the 100% naturally abundant ^{14}N nucleus, have nuclear spin quantum numbers greater than one-half that result in a splitting of the nuclear levels in the absence of a static magnetic field. This splitting is created by asymmetries in the distribution of electronic charge surrounding the nucleus and, hence, is sensitive to the specific chemical and crystallographic environment of that nucleus. Figure 6 also shows schematically the three energy levels of a ^{14}N nucleus. The established technique of ^{14}N NQR *spectroscopy* involves locating and interpreting one or more of the three transition frequencies labeled in the diagram. The technique of NQR *detection*, which has been developed to a great extent at NRL, involves measuring the intensity of a specific known NQR transition to quantify the amount of substance present. The ^{14}N NQR transition frequencies in the explosive compound RDX occur at 1.8, 3.4, and 5.2 MHz. The resonances are sharp, typically a few hundred Hz wide. Thus, by looking for the nitrogen signal at one of the NQR frequencies of RDX, only nitrogen in RDX will be detected, with no interference from nitrogen in such benign forms as wool. The detection of the RDX signal at 3.4 MHz (as described below) is carried out by applying continuous trains of phase-shifted RF pulses separated by intervals of a few milliseconds in a steady-state, free-precession sequence and obtaining the NQR signal in the intervals between pulses. The detection sensitivity can be improved by lengthening the total duration of the experiment; the practical goal is a determination of the presence or absence of the explosive RDX within 6 s.

NRL Prototype NQR Detector for RDX: The successful development of this prototype involved technical advances in a number of areas [2]: (1) designing efficient large-volume RF coil circuits that produce adequate RF field intensities with minimal power; (2) optimizing RF pulse sequences for signal detection with low RF fields while minimizing acoustic artifacts, using both an experimental and theoretical understanding of the NQR "spin dynamics" of the ^{14}N nucleus; (3) finding ways to minimize the undesirable effects of a "dead time" immediately following the RF pulse during which the extremely weak NQR signals cannot be observed; and (4) developing data-processing algorithms for identifying weak signals in the presence of artifacts and a noisy background. One important early discovery was that pure ^{14}N NQR could be performed at much lower RF field strengths than typical for pulsed solid-state NMR, with the fortunate consequence that 1 kW, rather than tens of kilowatts, provided sufficient field strength even when using a large detector coil.

Figure 7 shows the 300-l RF NQR coil accommodating a large suitcase. Not shown are a 1 kW RF amplifier and a small rack of electronics controlled by a personal computer. Experiments using this prototype NQR-RDX detector demonstrate that the ^{14}N NQR signal intensity from C-4 and Semtex-H, two military explosives containing RDX, can be detected in a piece of luggage containing 50 lb of miscellaneous items. Furthermore, the NQR signal intensity is observed to be linear in the RDX content, as expected. It is also significant that the geometry of the explosive does not matter; both bulk and sheet forms have been detected equally well. Figure 8 shows statistical results from repeated tests of the same piece of luggage, both without ("clean") and with C-4 explosive ("threat").

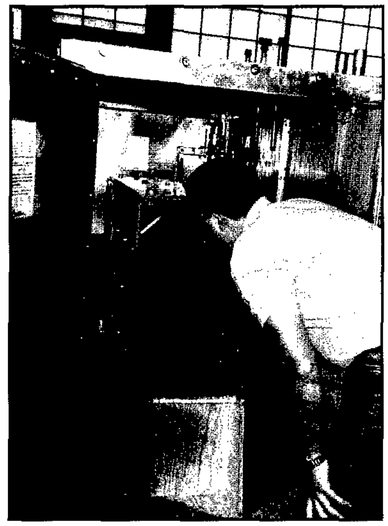

Fig. 7 — The NRL NQR-RDX detector coil loaded with a large suitcase. The large metal cabinet with door provides shielding from electromagnetic interference. The 300 l (10 ft^3) detection volume in this prototype is many orders of magnitude larger than those typically used for NQR spectroscopy experiments.

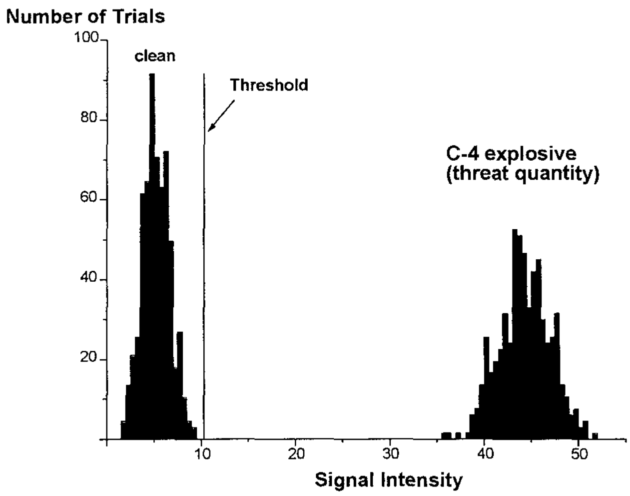

Fig. 8 — Statistical trial histogram showing ^{14}N NQR signal intensity from a 50-lb piece of luggage, either "clean" or packed with a "threat" quantity of the explosive C-4. The adjustable threshold value for the detector was set to provide a 1% false alarm rate (vertical line). Note the excellent distinction between "safe" (clean) and "alarm" (threat) conditions.

The threshold level (vertical line) has been set to yield a 1% false alarm rate. The differing shapes of the experimental distribution are as theoretically expected. The good signal-to-noise ratio of the RDX detector (16:1) results in a large separation between the two cases and a correspondingly high RDX detection probability.

Future Development: The successful demonstration of a prototype NQR-RDX detector has led to the commercialization of such a device through the NRL Technology Transfer Program. Further work continues in exploring new methods for improving the detection sensitivity, minimizing interferences from artifacts, observing at multiple frequencies, and detecting other explosives such as HMX, PETN, TNT, and ammonium nitrate.

[Sponsored by FAA, Office of Special Technologies (DoD), and DARPA]

References

1. A.N. Garroway, M.L. Buess, J.P. Yesinowski, and J.B. Miller, "Substance Detection Systems (1993), *SPIE Proceedings 2092*," 318-327 (1994).

2. M.L. Buess, A.N. Garroway, and J.B. Miller, U.S. Patent 5,233,300; M.L. Buess, A.N. Garroway, and J.P. Yesinowski, U.S. Patent 5,365,171; M.L. Buess, A.N. Garroway, and J.B. Miller, "NQR Detection Using a Meanderline Surface Coil," *J. Magn. Reson.* **92**, 348-362 (1991); J.P. Yesinowski, M.L. Buess, A.N. Garroway, M. Ziegeweid, and A. Pines, "Detection of ^{14}N and ^{35}Cl in Cocaine Base and Hydrochloride Using NQR, NMR and SQUID Techniques," *Anal. Chem.* **34**, 2256-2263 (1995). ■

Low-Solar-Absorbance Paint

R.F. Brady, Jr., and J.D. Adkins
Chemistry Division

D.S. Fraedrich
Tactical Electronic Warfare Division

Infrared gray-body radiation from ship hulls and superstructures arises from the intrinsic heat of the ship. Some of this heat arises from on-board machinery, but a principal heat source is the absorbance of solar radiation by Navy haze gray paint. A paint that reflects solar radiation would reduce heat buildup, thereby increasing crew comfort and endurance and reducing reradiation of infrared energy (Fig. 9).

Formulation: A new formulation for haze-gray ship topside enamel that reflects a large proportion of incident solar energy has been developed by altering the pigment portion of the paint. Carbon black, which absorbs solar energy throughout the visible and infrared spectral regions, is replaced by a mixture of red, yellow, and blue pigments. These colors mix to form a gray color in the visible region of the spectrum. However, they are transparent in the infrared and do not interfere with the infrared reflectivity of titanium dioxide, a highly reflective white material, which is the principal pigment in the paint. This formulation successfully preserves the low-visibility haze-gray color and reflects several times more energy than carbon black in the infrared region. The new formulation has been approved for use by the Navy Environmental Health Center, Norfolk, Virginia. This upgrade will likely go unnoticed by paint applicators, maintenance personnel, and environmental and worker safety officers because the physical properties of the new coating are identical to those of the old.

Testing: Following laboratory and outdoor exposure testing, the paint was applied to the USS *Dextrous* (MCM 13) in April 1995 at its home port in Corpus Christi, Texas. Measurements by the Advanced Techniques Branch of the Tactical Electronic Warfare Division demonstrate a 4° C reduction in surface temperatures during summertime operations in the Gulf of Mexico. The ship has since relocated to the Persian Gulf where the coating's solar reflective properties reduce heat buildup and increase crew comfort.

The Naval Sea Systems Command (NAVSEA) is supporting work to convert all manufacturing and Navy stocks of haze-gray enamel (Military Specification MIL-E-24635) to the low-solar-absorbance formulation. The Advanced Techniques Branch and the Materials Chemistry Branch, Chemistry Division, are working with NAVSEA and with manufacturers of this enamel to produce industrial quantities of this paint.

Applications: The primary application of this paint will be to all topside and freeboard surfaces of ships now painted haze gray. In addition, many topside structures are painted bright white to reduce heat buildup; these include weapons lockers and the Phalanx close-in weapons systems (CIWS). NAVSEA is making stringent efforts to reduce contrast on ships, but these white structures are conspicuous. In August 1996, in Tucson, Arizona,

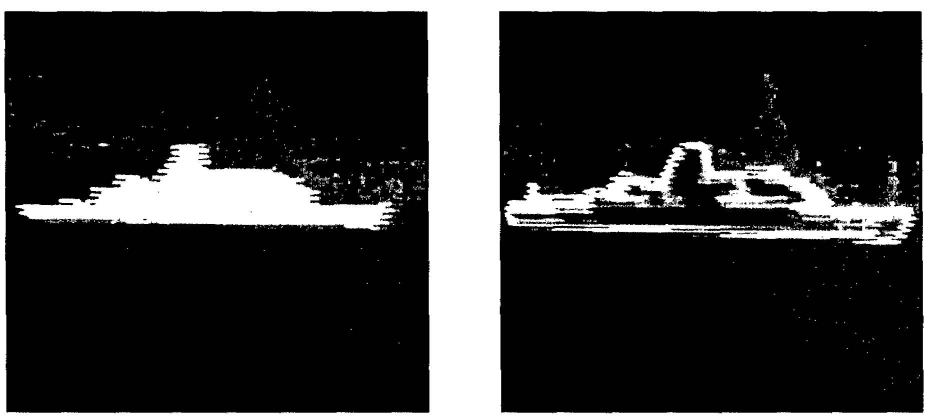

(a) (b)

Fig. 9 — Infrared photographs of sister MCM-class ships (a) with and (b) without the low-solar-absorbance paint.

this low-solar-absorbance paint was tested on a CIWS enclosure. Although internal temperatures were somewhat higher than for a white paint, the temperature did not build to a point to cause failure. Present plans call for putting this paint on one CIWS structure on a ship and evaluating its long-term performance in tropical weather at sea.

This paint is being tested by the Naval Surface Weapons Center, Carderock, Maryland, for use during the Advanced Technology Demonstration (ATD) of the advanced enclosed mast/sensor. Also, low-solar-absorbance nonskid deck coatings are being developed with funding from the AEGIS Program Office. The first ship to be delivered with this coating (in the Spring of 1997) will be the next new AEGIS cruiser; all topside and freeboard surfaces of this ship are scheduled to be coated with the low-solar-absorbance coating.

Summary: A new paint that will reduce the collection and reradiation of solar infrared energy is being introduced to the Fleet. Compared to the paint it replaces, this paint absorbs less solar radiation, increases crew comfort and endurance, and reduces reradiation of infrared energy.

[Sponsored by the AEGIS Program Office, NAVSEA]

References

1. R.F. Brady, Jr. and L.W. Wake, "Principles and Formulations for Coatings with Tailored Infrared Properties," *Prog. Org. Coat.* **20**, 1-25 (1992).

2. L.V. Wake and R.F. Brady, Jr., "Formulating Infrared Coatings for Defence Applications," Technical Report MRL-RR-1-93, Materials Research Laboratory, Australia, March 1, 1993.

3. J. Dries, D. Fraedrich, and S. Surko, "Infrared Ship Signature Reduction using Low-Solar-Absorbance Paint," Proceedings of the 41st Annual Joint Electronic Warfare Conference, 1996. ■

Electronics and Electromagnetics

Affordable Phased Array Using Radant Lens

J.B.L. Rao and P.K. Hughes II
Radar Division

Background: Phased array antennas can steer transmitted and received signals without mechanically rotating the antenna. Each element of a phased array is connected to a phase shifter, which determines the phase of the signal at each element to form a beam at the desired angle. A typical phased array may have several thousand elements and requires that many phase shifters and drivers. The complexity of the corresponding control circuitry and the feed network can increase rapidly with the size of the phased array. The phase shifters, their control circuitry, and the feed network account for the major hardware costs in a phased array antenna. A few years ago, a study was performed by NRL on ways of obtaining two-dimensional scanning at low-cost [1]. In that study, a hybrid approach of combining a slotted waveguide array with a Radant lens was identified as a low-cost approach to a phased array. Since then, a slotted waveguide array was acquired that can phase scan in the azimuth plane. Recently, a contract was awarded to procure a Radant lens that will be added to the front of the slotted waveguide array to obtain scanning in the elevation plane. This approach avoids using a phase shifter behind each radiating element and simplifies beam steering using row-column controls, which reduce the phased array cost.

Slotted Waveguide Array: A slotted waveguide array, which is a modified version of a production series (AN/TPQ-36) built by the Hughes Aircraft Company, has been acquired. The modified version [2] uses high-power phase shifters and a monopulse feed network, and it can phase scan in the azimuth plane.

Radant Lens: The basic principle on which the Radant lens operates was demonstrated by Radant Technologies, Inc. [3] under a contract to Rome Laboratory. NRL tested the lens in the compact range, and the results indicated the potential for an affordable phased array by using this technology. NRL is investigating the feasibility and practicality of using a Radant lens to electronically scan the beam in a tactical Navy shipboard radar. A number of technological issues (insertion loss, operational bandwidth, sidelobes, etc.) will be addressed as the properties of this antenna are characterized. The Radant lens is constructed from a diode-controlled medium, as Fig. 1 shows. In the lens, the electric field is constrained to propagate between parallel metal plates. In between the plates, the medium is constructed from strips of metal with cross-connected diodes on a dielectric support layer. The principle of operation is that the phase shift through this medium changes when the diodes in one strip are turned on or off. The amount of metalization controls the amount of phase shift per diode strip. The phase shift results from selectively switching between the two diode states via some digital bias control circuitry. The phase delay achieved is modulo 360°. The simplest configuration is an E-plane scanning lens in which beam scanning results from a linear phase gradient along the E-plane dimension. A simple Radant lens provides one-dimensional electronic beam scanning. Two-dimensional scanning can be achieved by cascading two Radant lenses or using one Radant lens in a hybrid configuration. Figure 2 illustrates the hybrid phased array using a Radant lens in front of a slotted waveguide array [4].

Summary: An affordable phased array is described. The array uses a hybrid approach by combining a slotted waveguide array with phase shifters to scan the beam in the azimuth plane and a Radant lens placed in front of the slotted array to scan the beam in the elevation plane. The proposed approach avoids using a phase shifter behind each radiating element and simplifies beam

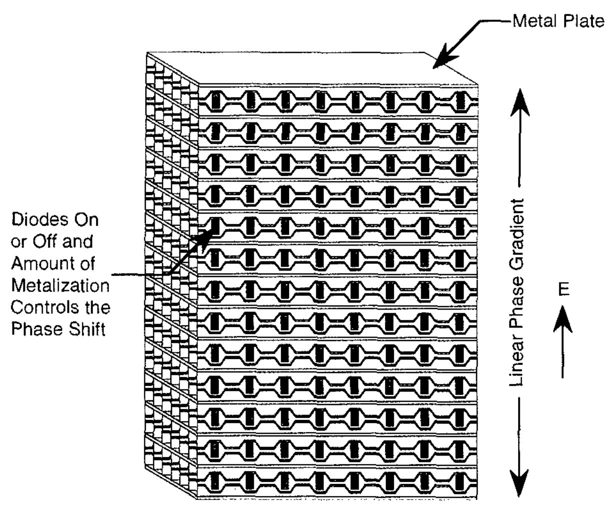

Fig. 1 — Radant lens configuration.

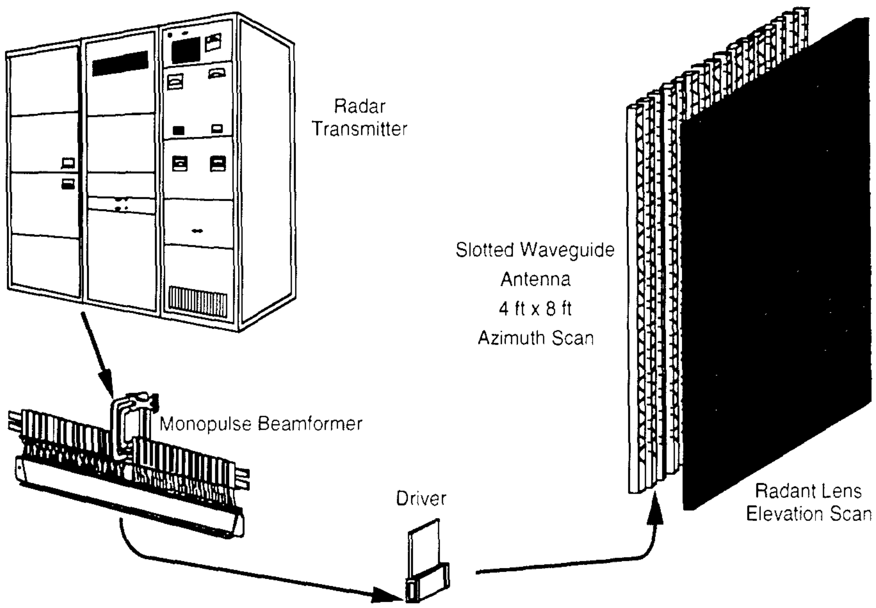

Fig. 2 — Hybrid phased array using Radant lens.

steering using row-column controls, which reduce the phased array cost. The production cost of the proposed array is estimated to be less than one-third of a similar size array using a phase shifter behind each radiating element.

[Sponsored by ONR]

References

1. J.B.L. Rao, T.C. Cheston, and A.A. Moffat, "X-Band Phased Array Antenna Options for One- and Two-Dimensional Scanning," NRL Memorandum Report 6846, July 1991.

2. J.B.L. Rao, T.C. Cheston, J.B. Evins, A.A. Moffat, and P.K. Hughes, "One-Dimensional Scanning X-Band Phased Array for an Engagement Radar," NRL Memorandum Report 7853, June 1996.

3. J. Leibinger, "Demonstration of Two-Axis Electronic Scanning by a Hybrid Radant-TM Lens Array," RL-TR-91-201, Rome Laboratory, Hanscom AFB, Boston, Massachusetts, Sept. 1991.

4. J.B.L. Rao, P.K. Hughes, G.V. Trunk, and J.C. Sureau, "Affordable Phased Array for Ship Self-Defense Engagement Radar," IEEE/ Proceedings of the 1996 National Radar Conference, Ann Arbor, Michigan, May 13-16, 1996. ■

Research and Development of Micro-Air Vehicles for Electronic Warfare

R.J. Foch and K.G. Ailinger
Tactical Electronic Warfare Division

Introduction: Recent advances in microwave monolithic integrated circuits (MMIC) and micro-electromechanical systems (MEMS) technology are making miniature sensors and payloads practical for many applications and enabling the research and development of small autonomous machines. Micro-Air Vehicles (MAVs) capable of carrying these miniature payloads are now being developed at NRL that have wingspans of 15 to 20 cm, masses of 30 to 60 g, and flight speeds of 5 to 15 m/s. Potential military and civilian uses for MAVs include near-field radar jamming, small unit reconnaissance, chemical and biological agent sampling, environmental hazards detection and assessment, drug-enforcement operations, hostage crisis surveillance and/or listening, and other valuable missions.

NRL is a technology leader for MAVs and will be conducting significant Office of Naval Research (ONR)-sponsored research efforts from 1997 through 2001 while concurrently providing technical support for Defense Advanced Research Project Agency-sponsored MAV developments. The NRL effort is being directed by the Tactical Electronic

Warfare Division (TEW) and takes advantage of the multidisciplinary capabilities of the laboratory, in collaboration with five other divisions, to address all aspects in the development of an MAV. The primary Navy interest in MAVs is for radar-jamming missions performed by small unit operations. The NRL-MAV effort will culminate in near-field radar-jamming mission demonstrations in 2001.

System Design Considerations: The research areas being addressed in the NRL-MAV effort are degradation of aerodynamic performance due to low Reynolds number flow conditions; power density and energy density of the energy storage device; the miniaturization of the aircraft avionics, antennas and sensors; heat dissipation; and the development of a radar-jamming payload.

TEW is conducting the air vehicle design, electric propulsion and microfuel-cell research, wind tunnel and flight testing, and overall system integration. The Micro-Tactical Expendable (MITE), a conceptual NRL-MAV baseline vehicle designed to fit within a 15-cm by 15-cm box (shown in Fig. 3), shows some of the size-driven features typical of an MAV. As the wing chord and flight speed decrease, the ratio of fluid inertial forces to viscous forces (Reynolds number) decreases, degrading the aerodynamic performance. Thus, a broad wing chord minimizes the aerodynamic degradation within given size constraints. Also, by increasing the wing area, the wing loading is decreased, which, in turn, reduces the power required to fly. The Laboratory for Computational Physics and Fluid Dynamics is performing advanced computer simulations of very low Reynolds number wing aerodynamics, stability, and control to evaluate competing vehicle designs.

Even with low wing loading, the power required to fly the projected MAV designs is too large for current state-of-the-art batteries. To overcome this deficiency, TEW will be developing micro-fuel cells to provide 20 to 30 min of flight time. Electric propulsion is being pursued because of its reliability, ability to turn on and off during flight, and low audible signature. TEW will sponsor another program with industry to develop a high-efficiency, brushless electric dc motor specifically for MAVs.

In addition to miniaturizing the airframe and optimizing for the unique aerodynamic challenges, the other components of an MAV — such as avionics, antennas, sensors, and payload — must also be scaled down and simplified. The Information Technology Division is developing a range-based vision system to identify ground-based objects for target identification and collision avoidance and will use machine-learning techniques to develop efficient control rules for robust navigation and collision avoidance using minimal information and control requirements. The Condensed Matter and Radiation Sciences Division, working with the University of Michigan, is developing and integrating MEMS temperature, pressure, and acceleration sensors for use on an MAV. Because

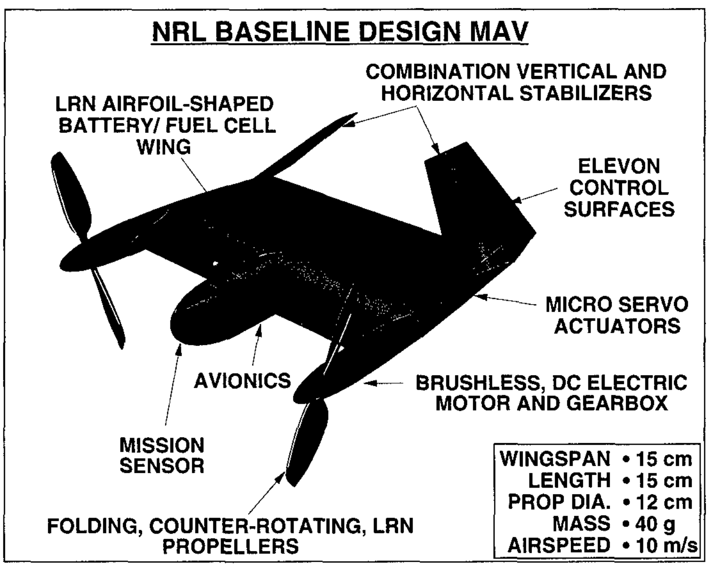

Fig. 3 — The Micro-Tactical Expendable (MITE).

thermal management in the MAV becomes a critical issue as the electronics are miniaturized, the Chemistry Division will investigate the use of diamond applications for lightweight, efficient spreading of thermal loads. The Electronics Science and Technology Division is developing miniature radar-jamming component technologies for operation in the near field of a radar, taking advantage of range losses to build a jammer that requires small jammer output power, thus making the payload suitable for carrying on an MAV.

Summary: Six NRL divisions are collaborating to advance the technologies required to develop and demonstrate a practical micro-air vehicle and mission payload. Technology demonstrations will be performed throughout the effort, culminating with flight and mission demonstrations of prototype MAVs carrying a near-field radar-jamming payload by the year 2001.

[Sponsored by ONR] ■

Nano-Precision Lithography for Nanoelectronics

E.A. Dobisz, C.R.K. Marrian, and M.C. Peckerar
Electronics Science and Technology Division

Introduction: Our ability to pattern finer and finer lines has fueled the "electronics revolution" of the last 2 decades. We are on the verge of reaching feature sizes at which quantum effects in charge transport become evident and important in defining device function. Even a cursory examination of any part of today's Navy reveals the tremendous importance of advanced electronics systems. As we move into the nanoelectronics regime, tomorrow's Navy will need ready access to the resulting increase in device performance and computational functionality. In this article, we review key components to reaching this goal. In particular, we summarize the NRL effort in developing technologies for achieving sub-100-nm feature sizes in future devices.

E-beam lithography has been and remains the workhorse for device fabrication in research and development and mask making for advanced lithographies. The authors have instigated research programs in both e-beam [1] and proximal probe lithographies [2]. Here we focus on a e-beam lithographic processes for making nanoelectronic devices. The requirements of a viable lithographic processes include both high resolution and control of critical dimensions. The e-beam nanolithography research described has been performed at NRL under the DARPA Advanced Lithography Program.

Nanolithography and Nano-Precision: Figure 4 shows an example of high resolution in which 12-nm lines in a 60-nm period grating are patterned in poly(methyl methacrylate) (PMMA) on a W film. This is state-of-the-art resolution for a specialized nanofabrication facility, such as at NRL. It is unique in that it is the finest resolution pattern reported on a high atomic mass substrate, which backscatters a high density of electrons.

The feature size control required in nanolithography is, however, a more difficult issue to solve. If one considers 100-nm critical dimensions

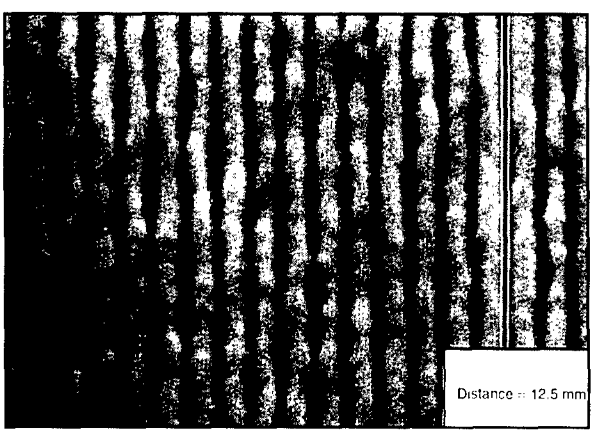

Fig. 4 — 12-nm lines in 60-nm period grating in PMMA on 600-nm tungsten layer on silicon.

(CDs), which are at the large end of the nanolithographic domain and the largest error allowed by device design rules of ±10%, then the tolerance is ±10 nm. Although much effort has been devoted to exploring the resolution limits of e-beam lithography, there has been limited work on modeling electron exposure of resist materials and processing at sub-100-nm dimensions.

Process Latitude for Nano-Precision: To illustrate the challenges of CD control, consider a pattern consisting of two rectangles with a critical dimension gap in the center, as shown in Fig. 5, upper left side. This pattern is similar to the source and drain of a field-effect transistor (FET) pattern. There is a window of dose range and processing range over which the CD can be defined within the allowed error. If the dose/processing window is too narrow, one cannot achieve the correct conditions to define the CDs in the pattern reproducibly, and the yield is very small.

In Fig. 5, the dose latitude window to produce the coded gap width of 500 nm, 200 nm, and 100 nm within ±10% error is plotted vs pad width. Within each graph, the dose latitude exhibits some decrease with increasing pad width. However, when comparing the graphs in Fig. 5, there is a large reduction in dose latitude as the gap width decreases to 100 nm. For the 20 μm pads, a 500-nm gap can be defined with ±32% dose latitude, whereas the 100-nm gap requires better than ±3% dose control. Some of the decrease in the dose latitude window is due to the increased precision. So if a ±10-nm error was also placed on the 500-nm gap, the dose latitude would be reduced substantially but still remains a factor of 2.5 greater than that for the 100-nm gap.

E-beam exposure is modeled by Monte Carlo simulation, which tracks the paths of scattered electrons from a point source and calculates the spatial distribution of the energy the electrons deposit in a resist. At sub-100-nm dimensions, the e-beam is broadened by more than expected from Monte Carlo calculations. The effective width of the beam can be empirically obtained from a measured linewidth, as a function of dose. This is due to an underestimation of the range of the inelastically scattered electrons and the effect of the finite resist contrast after development. The measured linespread for Microposit SAL-601 (™Shipley Corporation) and PMMA are shown in Fig. 6. Here the beam Gaussian widths σ are

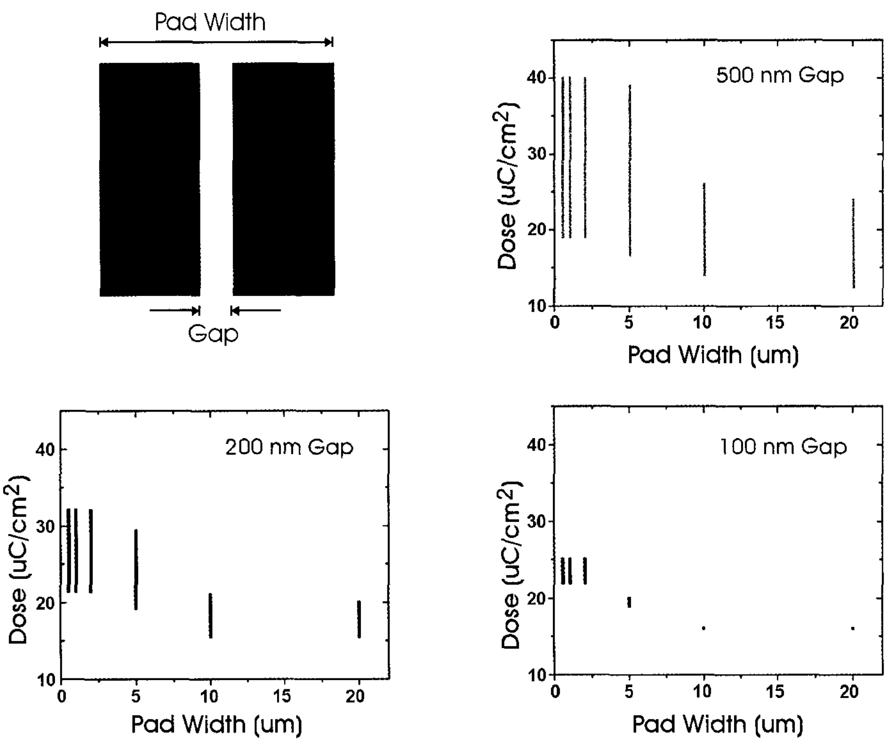

Fig. 5 — Effect of critical dimension gap on dose latitude window. The pattern is shown in the upper left side [4]. Each graph shows the dose latitude window as a function of pad width. The results for 500, 200, and 100-nm gaps are shown.

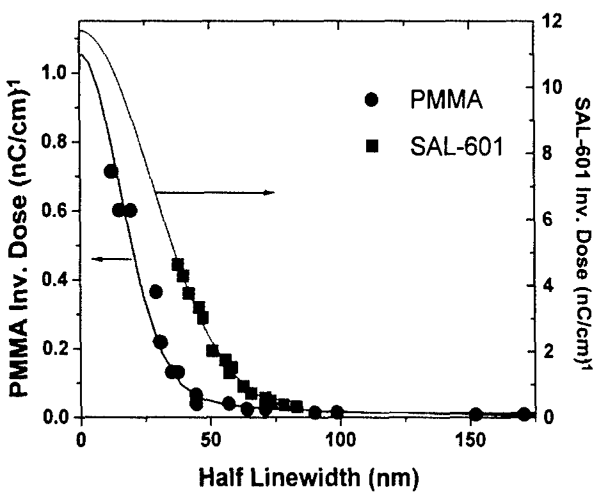

Fig. 6 — Measured linespread widths for SAL-601 and PMMA [4].

27 nm and 19 nm for SAL-601 and PMMA for incident probe σ's of 10 nm and 8 nm, respectively. The results can be integrated to simulate the pad pattern with a gap in the middle, as shown in Fig. 5. The results in terms of energy absorbed by the resist vs distance from the center of the 100-nm gap are shown in Fig. 7 for the measured beam widths in PMMA and Microposit SAL-601 and the Monte Carlo-generated energy deposition function. The region of ±10% error is denoted by the striped box. The dose latitude for a point source with a "Monte Carlo" resist is large. But when a real resist is exposed with a real electron beam probe of finite size, there is little process

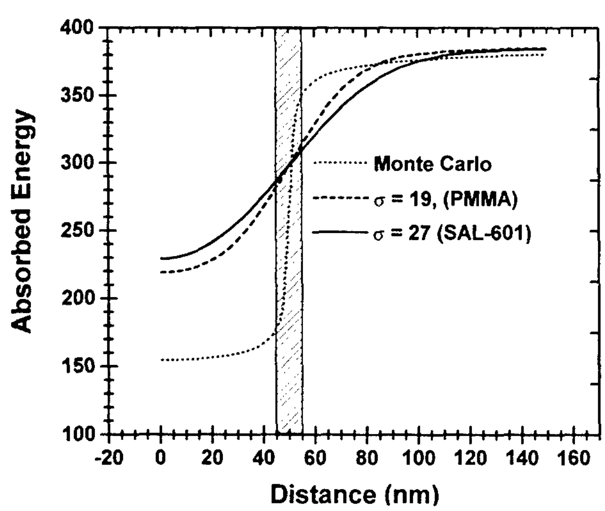

Fig. 7 — Effect of linespread function width on dose latitude for a coded pattern of a 100-nm gap in 20 μm pad. Plotted is the energy absorbed by the resist vs distance from the center of the gap [4].

latitude. However, the exposure profile can be successfully modeled by convolving the Monte Carlo function with an appropriate Gaussian, for example, σ = 15 nm for PMMA.

Summary: The research at NRL in e-beam lithography has been summarized. For sub-100-nm lithography, resolution itself is not the major challenge. Rather it is the necessity to reproducibly define and maintain the critical dimensions of features. Our present understanding of the electron-scattering processes begins to break down as we approach 100 nm. We have shown an empirical modification using measured spread functions in actual resist materials that allows us to extend our models to sub-100-nm dimensions. The work points to the need for finer probe e-beams and new resist systems in which the broadening of the beam is minimized through ultrathin resists or resists insensitive to low-energy electrons. Development of self-assembled monomolecular layer resist systems has already produced sub-10-nm features, using scanning tunneling microscope lithography [3].

[Sponsored by DARPA]

References

1. E.A. Dobisz, C.R.K. Marrian, R.E. Salvino, M.A. Ancona, F.K. Perkins, and N.H. Turner, "Reduction and Elimination of Proximity Effects," *J. Vac. Sci. Technol.* **B11**, 2733 (1993).

2. E.A. Dobisz and C.R.K. Marrian, "Sub-30-nm Lithography in a Negative Electron Beam Resist with a Vacuum Scanning Tunneling Microscope," *Appl. Phys. Lett.* **58**, 2526 (1991); C.R.K. Marrian, E.S. Snow, and E.A. Dobisz, "Apparatus and Method Using Low Voltage and/or Low Current Scanning Probe Microscopy," US Patent # 5,504,338, April 2, 1996.

3. E.A. Dobisz, H.W.P. Koops, F.K. Perkins, C.R.K. Marrian, and S.L. Brandow, "Simulation of Scanning Tunneling Microscope Interaction with Resists," *J. Vac. Sci. Technol.* **B14**, to be published Nov/Dec 1996.

4. E.A. Dobisz and C.R.K. Marrian, "Effects of Post-Exposure Bake Conditions on Performance of SAL-601 at Sub-0.25 μm Dimensions," *SPIE Proc.* **2723**, 383 (1996). ■

Sniper Detection and Counterfire Direction

S.A. Moroz and P.W. Gower
Tactical Electronic Warfare Division

R. Pierson
Maryland Advanced Development Laboratory

Introduction: The rapid detection, verification, and accurate counterfire against snipers is of increasing importance due to the rising prominence of humanitarian and peacekeeping operations conducted by the U.S. military in regions of political instability. While the historically recognized problem of snipers is generally associated with combat situations, in the limited warfare climate, sniping is likely during times of low alert and against exposed civilian as well as military personnel. Detecting and engaging the politically motivated, nonuniformed aggressor or the professional sniper who operates alone among the civilian populace has become a priority problem and serves as the impetus for countersniper system development at the Naval Research Laboratory. The Tactical Electronic Warfare Division's Advanced Techniques Branch, supported by the Maryland Advanced Development Laboratory, has developed the Vectored Infrared Personnel Engagement and Returnfire (VIPER) system to detect and locate sniper rifle infrared (IR) emissions in real time and then rapidly cue countersniper fire to the location.

The IR rifle emission that permits sniper localization is produced from a bright radiation transient caused by temperature, pressure, density, and chemical product composition distributions outside the gun barrel. The barrel effluent contains fuel products such as CO, NO, H, and H_2, which are raised to the ignition temperature from shock heating and/or thermochemistry and are burned during air mixing. The resulting chemoluminescent flash can then be sensed by one or more pixel elements within the detector array of a charged-couple-device (CCD) infrared camera. A digital signal processor (DSP) then receives the camera video and determines the flash location.

System Description and Status: The user interface and many mission-specific design features of the present system were established through discussions with instructors at the U.S. Marine Corps Sniper School, Quantico, Virginia. This user group requires a low-power, compact, and rugged design capable of muzzle flash detection at or beyond the maximum effective range of sniper-class weapons. VIPER meets these requirements and is compatible with point defense/area denial mission scenarios, which are typical of Bosnia, Somalia, and Zaire.

System components comprise: (a) an IR camera for scene monitoring and flash registration, (b) a two-VME-board computer for video signal flash extraction and location, and (c) a rifle-mounted inertial sensor to provide instantaneous rifle orientation for error vector determination. There are two resident user interfaces: (1) a hand-held imaging display showing the local IR scene and superimposed symbology showing locations of sniper weapon flash and counterfire rifle aim points and (2) cueing logic displayed by light-emitting diodes (LEDs) within a laser rangefinder binocular (Fig. 8). In both cases, the observer and shooter of the two-man countersniper team under processor direction align their respective rifle and binocular axes until a boresight match occurs with the threat position. The technology developed in VIPER is to enhance the effectiveness of the countersniper — not to replace the tried and proven. Accordingly, the display for warning, direction, verification, and the return fire direction have been integrated into the observer's binoculars. Using VIPER, sniper location is detected and marked before the bullet has traveled more than 50 to 100 m and time to impact is 0.5 to 2 s. Depending on the user interface chosen

Fig. 8 — VIPER system, clockwise from bottom: binocular, IR camera, computer (rifle inertial sensor on top), and video user interface.

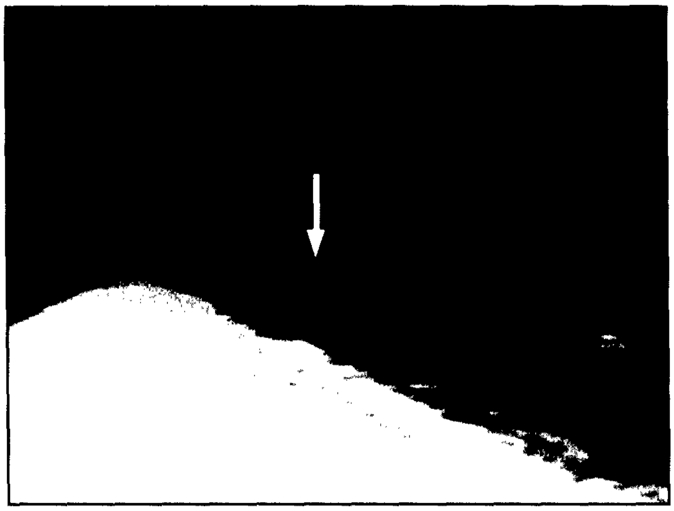

Fig. 9 — Large caliber rifle at range > 1 km (located at arrow).

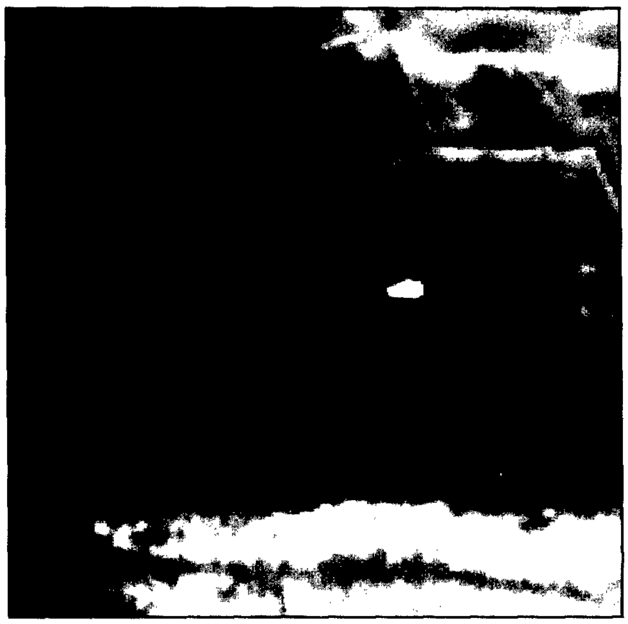

Fig. 10 — Urban detection.

and the degree of concealment of the sniper, counterfire to target can be provided in 1 to 10 s. As an example of the versatility and capability of VIPER, two cases are presented of raw video flash events. These flashes are detected and identified by the flash algorithm within the DSP and passed along with inertial sensor information to the user interface that allows man-in-the-loop verification and counterfire. Figure 9 demonstrates the detection of a large caliber sniper rifle flash against a hot desert background at a range greater than a kilometer. In Fig. 10 of a close quarters urban scenario, the sniper is detected when shooting from a building window.

Several copies of the VIPER system were built and have gone through operator evaluation at the U.S. Army Dismounted Battlespace Battlelab, Ft. Benning, Georgia, as part of an Advanced Concept Tactical Demonstrator.

The technology has growth potential to detect weapons over a wide range of calibers from moving vehicles, air platforms, and full man-portable-on-the-rifle systems.

[Sponsored by DoD and ONR] ■

Energetic Particles, Plasmas, and Beams

ROTHR Ship Detection Improvements through Advanced Signal Processing

B.T. Root
Radar Division

Introduction: ROTHR (relocatable over-the-horizon radar) is the Navy's large-area surveillance radar. By reflecting its beam off the ionosphere, it can see over the horizon and scan a vast area of the ocean's surface. Currently, it is used in the U.S. drug interdiction effort in the Caribbean and South America.

The radar looks primarily for aircraft, which is accomplished with waveforms of a few seconds duration. However, resolving ships from the strong ocean clutter requires longer waveforms of about 30 s. This interferes with the normal operation of the radar. We have devised and simulated advanced signal-processing techniques to detect ships using short waveforms. Some of the algorithms are based on well-known super-resolution techniques, and some are original. The instability of the ionosphere presents a major problem. Computer simulations showed promising results, and recently we have started to collect and examine real in-phase and quadrature (I&Q) radar data. This article examines the application of two algorithms to a sample of radar data.

Figure 1(a) shows how the ROTHR sees thousands of miles over the horizon by reflecting its beam from the ionosphere (a layer of plasma above the Earth's atmosphere). The ionosphere has motion and irregularities that sometime distort the radar signal. Also, there may be multiple modes of propagation that cause confusing "echoes" in the return signal. The radar regularly sees aircraft, whose large Doppler (i.e., radial velocity) places them far from the strong ocean clutter. Ships, however, have velocities comparable to ocean waves, and their return signal is often overpowered by the ocean clutter, especially with short waveforms having low Doppler resolution.

The grid in Fig. 1(b) shows the ROTHR coverage (the area over which the radar scans). A small spot indicates where the radar is looking in this article. The data are high-resolution ship waveforms of 24 s each. One waveform is transmitted every minute for 25 min. The backscattered power is plotted vs Doppler and time, as shown in Fig. 2(a). The radar operating frequency hops between 15 and 16 MHz, which causes the slant range (i.e., time delay or apparent range) to hop back and forth about 6 mi. Hence two different ships from the two ranges are seen as strings of peaks to the right and left of the ocean clutter. Figure 2(b) pairs up peaks from one of the 24-s segments of data into ocean clutter Bragg pairs by using the known precise Doppler separation. The ship peak has no mate, which confirms that it is

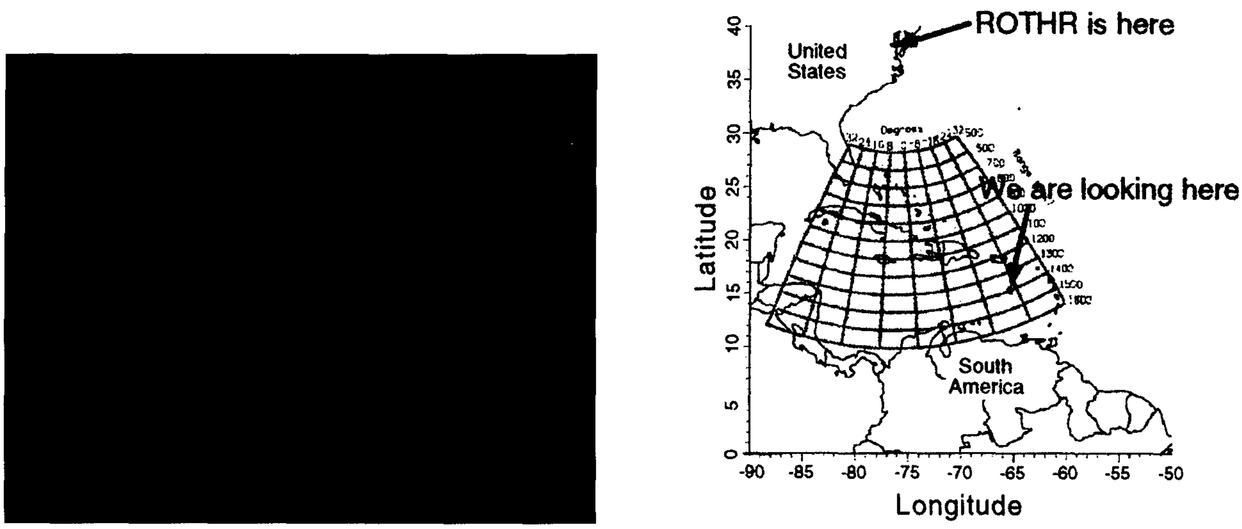

(a) (b)

Fig. 1 — (a) HF radar sees thousands of miles over the horizon by reflecting its beam from the ionosphere. The radar regularly sees aircraft but has more difficulty seeing ships. (b) The ROTHR coverage is shown by the green grid. This article examines a sample of radar data that looks at the indicated spot in the Caribbean.

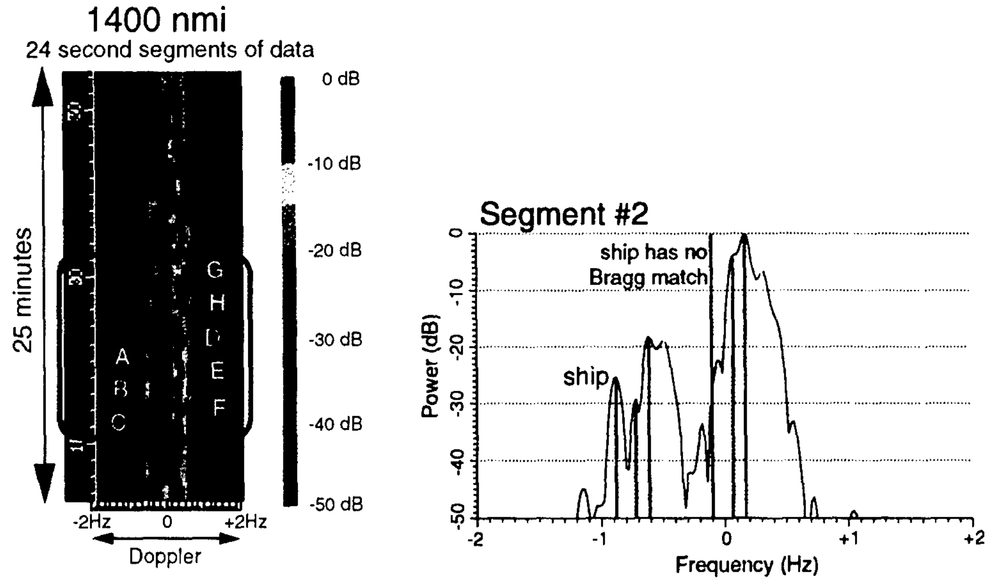

(a) (b)

Fig. 2 — (a) ROTHR backscattered power vs Doppler (velocity) and time. One long 24-s dwell is taken every minute for 25 min. The radar frequency hops between 15 and 16 MHz from dwell to dwell, and the slant range correspondingly shifts by 6 mi. This causes two strings of ship peaks to be seen in alternation at a positive and negative Doppler velocity. (b) This plot verifies that severe multimode exists in the ocean clutter and that the ship peak to the left is not clutter. If it were, it would have a Bragg pair at a precise Doppler shift based on the operating frequency. Many of the peaks can be matched, as shown above, which confirm that they are clutter, but the ship peak has no mate. (The peaks to the right of the clutter in Fig. 2(a) are less distinct, and their identity is less certain but they are still most likely scatter from another ship at the other range.)

not clutter. Also the data have severe multimode, which makes ship detection more difficult, especially with shorter waveforms. Finally, the ship power is much less than the ocean clutter.

The 24-s dwells will now be divided into shorter segments of 6 s each. The ship will no longer be visible with normal Fourier processing. Two algorithms will be examined to retrieve the ship from the shorter data segments.

Algorithm 1: The first algorithm is original and cancels the ocean clutter [1]. The algorithm models the clutter as sinusoidal and proceeds by iteration. At each iteration, the amplitude and frequency of the remaining dominant clutter peak are estimated from the Fourier spectrum. The correct initial phase is found from a search that minimizes the energy of the "error" signal, i.e., the data minus the hypothesized clutter sinusoid. (Note that unlike many current advanced signal-processing techniques, no correlation matrices need be evaluated. This is fortunate, since high-frequency data are highly nonstationary.) Since the clutter is not perfectly sinusoidal and since there will generally be estimation errors, the clutter will not always be perfectly canceled, and some residue may remain. However, this residue will also be canceled at further iterations. The difficult part is determining when a peak at a given iteration is clutter, target, or residue.

Figure 3 shows the result of this algorithm applied to the data in the red box in Fig. 2(a). The data have been divided into 6-s segments (comparable to aircraft waveforms), and the iterations proceed from column to column, going from left to right. The strong red clutter peak is nearly canceled at the first iteration. The ships are not exposed until the sixteenth iteration, since the clutter residue had to be canceled first. Nevertheless, the peaks marked by letters match up with the corresponding peaks in the longer dwells of Fig. 2(a). (Peaks were canceled only in a band where clutter was deemed to exist so that ships would not also be canceled. These ships were nevertheless masked by the clutter mainlobes and sidelobes. Through more involved processing, including peak identification, it might be possible to find ships even when buried under clutter.)

Algorithm 2: The second algorithm is the well-known modified covariance superresolution algorithm, which we call MCV [2]. This algorithm

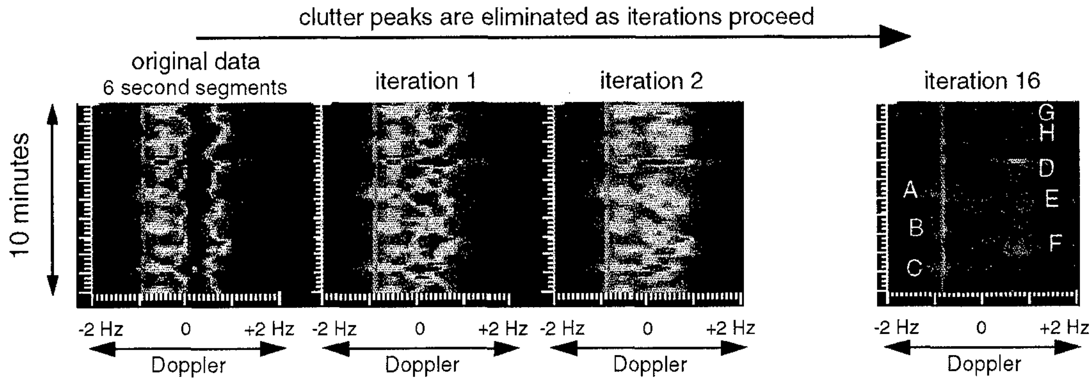

Fig. 3 — Ten minutes of data containing the ship have been extracted from the red box in Fig. 2(a). The data have now been divided into shorter, 6-s segments. The left column is the ordinary Fourier transform, like Fig. 2, but with decreased Doppler resolution due to the shorter data segments. (Note that the red clutter streak is now four times as wide.) The ship peaks in Fig. 2 are no longer evident or, at least, they are distinct from the clutter. Clutter is stripped away one peak at a time (separately in each segment) as the columns proceed to the right. The ship peaks labeled by letters in Fig. 2 are exposed at the last iteration. Many iterations were required due to clutter residue at each iteration.

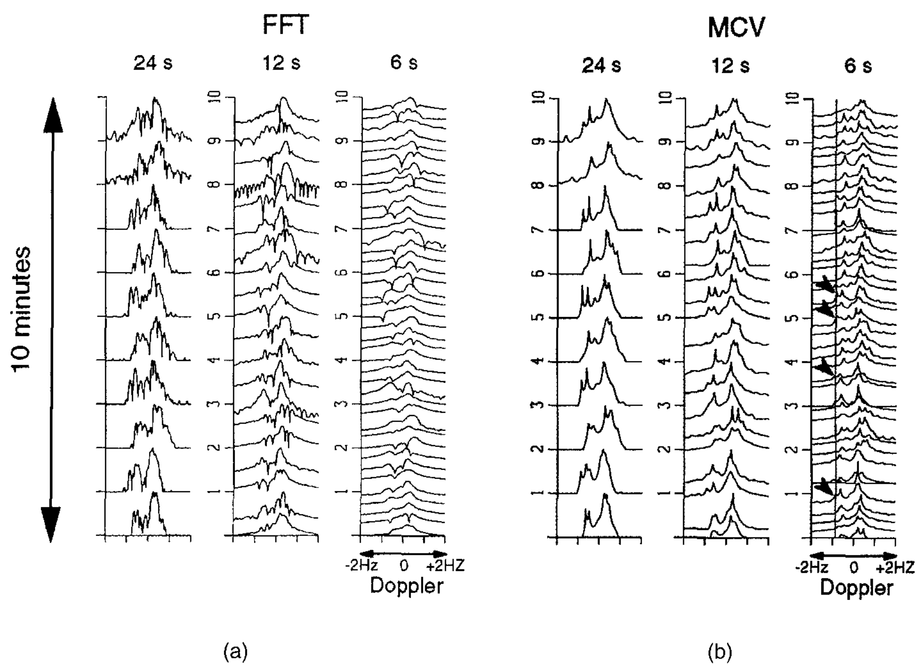

Fig. 4 — (a) The same data as in Figs. 2 and 3 are plotted as line spectra. The data are divided into segments of 24, 12, and 6 s and the Fourier transform (FFT) is taken. The resolution decreases as the segments shorten. (Note that the amplitude scale changes between columns for better visibility.) (b) The same data as in Fig. 4(a) are now processed with the MCV superresolution algorithm, rather than with the Fourier transform as in Fig. 4(a). The increased resolution of the MCV over the FFT is apparent, especially in the 6-s segments in which the ship is again sometimes visible (red arrows).

has resolution properties superior to the classical Fourier transform and comparable to the more sophisticated eigenvector methods (but without their noise and clutter suppression capability). MCV is far less computationally expensive than eigenvector methods — an important consideration for a radar with the massive data flow of the ROTHR. Experience indicates that intelligent postprocessing may be able often to distinguish the targets from the clutter in the superresolution "pseudospectra." (We might also try applying MCV after the clutter cancellation of the previous algorithm.)

Figure 4 shows the performance of MCV on the same data as in Fig. 3. The original 24-s segments have been divided into 12- and 6-s segments to show the progressive deterioration of resolution as the segments become shorter. The Fourier transform (FFT) is applied in Fig. 4(a), and the MCV is applied in Fig. 4(b). One of the ships shows up in some of the 6-s segments of MCV (red arrows), as it did in Fig. 3 with the previous technique. It is not apparent in the corresponding 6-s Fourier transforms. Note that we can also see Bragg structure in the 6-s MCV, which could be useful for remote sensing of the ocean surface with aircraft waveforms.

Conclusions: The ships seem to show up better in our algorithm than in the well-known MCV algorithm. However, it is necessary to track a ship for an extended period of time to confirm that it indeed exists. Ship detection is difficult with HF radar and, hence, the need to explore new signal-processing techniques.

We will continue to examine radar data with these and other techniques to determine their reliability. Plans are currently under way to add Global Positioning Satellite (GPS) data to the ship data, in order to obtain convincing "ground truth." There are also plans to study the distorting effect of the ionosphere on the radar data, using a combination of computer simulations and GPS data and to develop techniques to mitigate this distortion.

[Sponsored by ONR]

References

1. B.T. Root, "Ship Detection with HF Radar: New Signal Processing Techniques," NRL Memorandum Report 5320-96-7838, June 1996.

2. S.L. Marple, *Digital Spectral Analysis*, (Prentice-Hall, Englewood Cliffs, N.J., 1987).■

Nanofabrication with Nanochannel Glass Replica Arrays

C.R. Eddy, Jr.
Condensed Matter & Radiation Sciences Division

R.J. Tonucci and D.H. Pearson
Optical Sciences Division

With continued reduction in the critical dimensions of semiconductor devices, the need for nanometer-scale ($\leq$ 100-nm) pattern generation and transfer methods increases in importance. In addition to the significance in manufacturing semiconductor memories and microprocessors, such methods are vitally important to the development of structures for the study of quantum confinement effects in semiconductors. Nanometer-scale pattern transfer has been demonstrated by many researchers using a wide variety of plasma etching methods. However, the path to development of a massively parallel and economical lithographic technology on the nanometer-scale remains unclear.

To date, optical lithography has provided adequate capability for device structures down to 0.35 μm. This massively parallel, low-cost technique has proven to be easy to use and, accordingly, defines the attributes desired in future lithographic techniques. However, there is some concern about its application to subquarter-micron feature generation. To address these concerns, many solutions have been offered, including electron beam and X-ray lithographies. Both of these technologies are considerably more sophisticated in their application to generate nanometer-scale features. E-beam lithography is currently available but suffers from slow write times (due to its serial nature) and a high cost of ownership. X-ray lithography promises a massively parallel technique similar to optical lithography in application. However, critical components to such a system (i.e., X-ray sources and lithographic masks) are still under development.

Nanochannel-glass-replica (NCGR)-based lithography offers a possible solution to the need for a low-cost, massively parallel technique. This lithography is based on membranes made by a replication technique using thin-film deposition onto wafers of nanochannel glass (NCG). NCG, recently developed at NRL, is a patterned glass

material containing uniform, nanometer-scale capillaries that can be placed in any desired arrangement.

Nanochannel Glass Replica Fabrication: Replica membranes are made of thin metal films (≤ 2000 Å) such as tungsten or platinum, which are sputter- or vapor-deposited onto the NCG. Before the deposition, the NCG is coated with a sacrificial buffer layer, such as aluminum. The buffer layer is dissolved releasing the membrane, which may be floated onto the desired substrate, providing a hole array mask. For dot arrays, this membrane serves as an evaporation mask through which an even thinner (≤ 1000 Å) metal film is deposited, and then the replica membrane is removed. The membranes typically contain approximately 10^6 holes and have been prepared thus far with void diameters as small as 40 nm at packing densities greater than 3×10^9 voids/cm^2 [1].

NCGR technology has a high degree of flexibility that will prove beneficial in lithographic applications. Current NCGR lithographic processes are entirely compatible with other semiconductor processes and pose no harm to the underlying materials.

High-Density Plasma Etching: The high-density plasma etching process is well suited to anisotropic, low-damage pattern transfer. This suitability results from (1) a decoupling of the density and incident energy of the ionic etch species and (2) low process pressures. Thus, high fluxes of directional, low-energy ionic etchants can be directed at the patterned semiconductor surface.

For pattern transfer into mercury cadmium telluride (MCT), we employ hydrogen/argon plasmas with small additions (< 20%) of methane to provide the chemically appropriate etchant flux. Ion energies of 100 eV and room temperature surfaces ensure directional pattern transfer by favoring ion-driven over thermal-etch mechanisms at the surface. These conditions provide directional MCT removal rates of 200 Å/min [2]. Under these conditions, platinum (Pt) NCGRs provided excellent masks with selectivities of MCT:Pt ≥ 10:1. To generate a hole array, 2000 Å thick Pt NCGRs with 600-nm diameter holes were used. As Fig. 5 shows, the pattern is uniform and free of defects, with vertical feature sidewalls.

We have also patterned MCT samples with 250-nm dot arrays using 400 Å thick Pt NCGRs (Fig. 6). These high-fidelity features possess vertical sidewalls and a high degree of uniformity at a "device" packing density of nearly 10^{10}/cm^2.

Currently these processes are used only for generating test device structures but show promising application in generating a variety of quantum devices. We envision the ultimate NCGR-based nanolithographic technique as using NCGR with widely spaced (100-200 nm separation), uniform arrays of small diameter (20-40 nm) channels. This NCGR array will be 10-20 cm in diameter and will be mounted on a piezoelectric driver capable of positioning with a resolution on the scale of angstroms. Using this configuration in a close

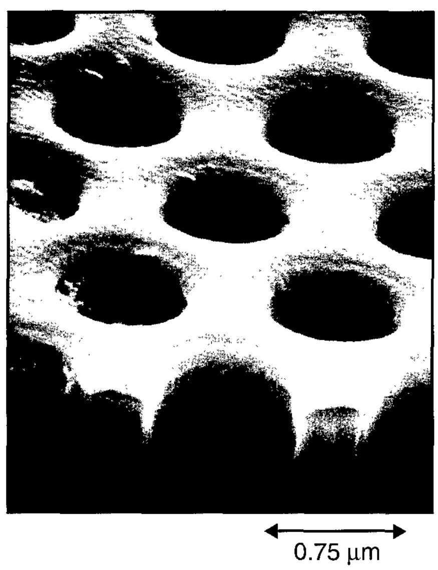

Fig. 5 — SEM image of array of 600-nm diameter holes fabricated in mercury cadmium telluride using Pt NCGR and $CH_4/H_2/Ar$ high-density plasma etching.

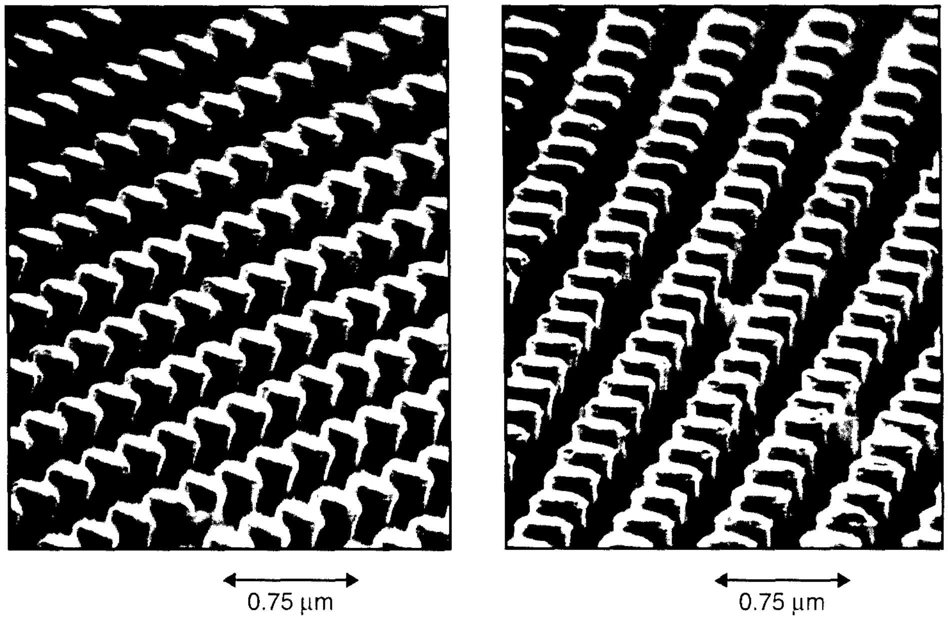

Fig. 6 — SEM images of arrays of 250-nm diameter dots fabricated in mercury cadmium telluride using Pt NCGR and $CH_4/H_2/Ar$ high-density plasma etching.

proximity arrangement, device structures can be directly delineated in a massively parallel fashion using high-density plasma etching.

[Sponsored by ONR and DARPA]

References

1. D.H. Pearson and R.J. Tonucci, "Nanochannel Glass Replica Membranes," *Sci.* **270**, 68 (1995).

2. C.R. Eddy, Jr., R.J. Tonucci, and D.H. Pearson, "Deep Submicron Pattern Transfer Using High Density Plasma Etching and Nanochannel Glass Replica Technology," *Appl. Phys. Lett.* **68**, 1397 (1996). ■

Structural Inhomogeneities in Thin Epitaxial Films and Single Crystals of $YBa_2Cu_3O_{7-\delta}$

S.B. Qadri and E.F. Skelton
Condensed Matter and Radiation Sciences Division

P.R. Broussard, V.M. Browning, and M.S. Osofsky
Materials Science and Technology Division

Introduction: The most widely studied of the high-temperature superconductors (HTS) is $YBa_2Cu_3O_{7-\delta}$ (YBCO). The research responsible for this article has been motivated by hopes of understanding the physics of HTS, as well as potential applications within the Navy and beyond. Significant progress has been achieved in fabricating epitaxial films with superior superconducting properties by a variety of deposition techniques, such as RF sputtering, molecular beam epitaxy, and pulsed laser deposition. Similarly, single crystals of YBCO have been synthesized with "optimal" superconducting properties. To date, unresolved questions concerning the interpretation of many experimental results remain, in addition to an inability to exploit this material for active electronic device applications.

It is widely accepted that the coherence lengths (the decay distance of the superconducting order parameter) of the HTS are short, on the order of tens of angstroms or less. Therefore, sample inhomogeneities (such as cation inhomogeneities, oxygen vacancies, dislocations, and small-angle grain boundaries) on length scales comparable to a unit cell will affect the measured superconductive properties of the system. Nevertheless, it has been generally assumed that sample properties are homogeneous and optimal based on electrical transport measurements. Structural studies, which are rarely reported, provide an independent test of this assumption. We have shown that structural inhomogeneities may exist in YBCO samples (both epitaxial films and crystals) that would be considered homogeneous with optimal transport

properties [1,2]. Highlights of some of these results are given in this article.

Experimental Details: Three different types of X-ray diffraction measurements were used to structurally characterize the HTS samples: high-resolution diffractometer scans, topographs, and energy-dispersive measurements. The first two are carried out using Cu Kα_1 X rays. They probe the entirety of the films and the first micron or two of the surfaces of the single crystals. Very high energy (> 60 keV) X rays are used for the third method. These are generated on NRL's superconducting wiggler beamline (X17C) at the National Synchrotron Light Source, Brookhaven National Laboratory. Because of the extreme brightness of this radiation, a very narrow (< 20 μm) pencil of radiation is all that is needed, thus leading to a high spatial resolution. And because of the greater penetrating power of these high energy X-ray photons, the entire volume of the crystals can be sampled.

Extensive research on bulk ceramic samples by others has led to a quantifiable relation between the X-ray measurements and the oxygen content, that is, the term (7-δ). From the bulk data, we have identified an empirical relation linking the length of the *c* axis of the unit cell with (7-δ) for YBCO crystals. For YBCO epitaxial films, the oxygen stoichiometry is estimated from the ratio of the integrated intensities of the I(005)/I(006) diffraction peaks. For ease of interpretation, it is assumed that only oxygen defects control the value of the *c* parameter. However, it has been shown by others that cation disorder also can alter the X-ray diffraction patterns in a similar manner. This result only changes the details of how the defects affect the measured properties.

The objective of this investigation was to perform the aforementioned X-ray measurements on YBCO samples that were considered "good" based on their transport properties. These are the most extensive structural and electrical transport results on the same crystals reported to date.

Results and Discussions: The crystals studied had low room temperature resistivities and high, sharp T_c's, for example, $\rho = 1.3 \times 10^{-4}$ Ω-cm at 300 K, $T_c > 93$ K, and $\Delta T_c < 300$ mK (Fig. 7). These features alone are often cited as the only evidence for a crystal's quality. The crystal's magnetotransport properties then were measured resulting in a set of data that were identical to those in the literature attributed to "high quality" samples. Nevertheless, the crystals showed compositional variations within a few micrometers of the surface and in the interior (Fig. 8). For the two crystals studied, the variations in the *c* axis on the surface and throughout the interiors indicated that 7-δ ranged between 6.7 and 7.0.

Similar results were obtained in epitaxial films. That is, films that are considered "high quality" with high, sharp T_c's and high, critical current densities J_c at 77 K show measurable structural inhomogeneities. Since large J_c's can result from some types of structural defects, studies are underway to correlate transport properties in epitaxial films with the presence of structural features in hopes of identifying those types of defects that improve the properties as opposed to those that hurt them.

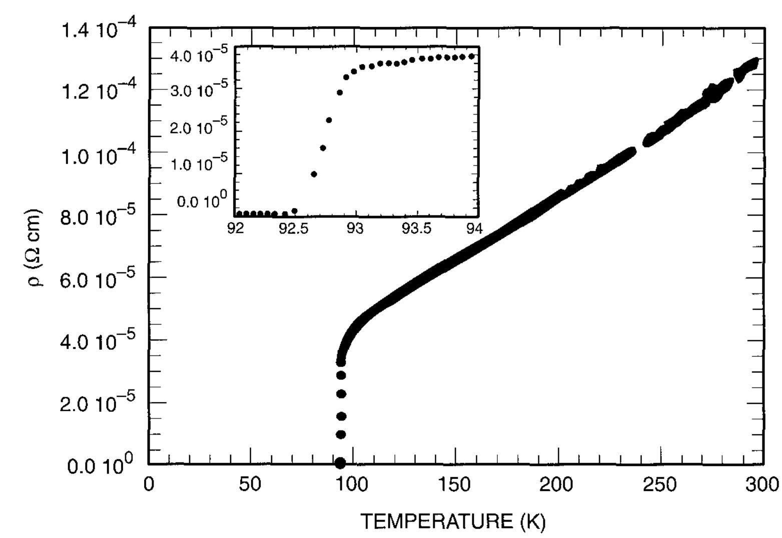

Fig. 7 — Resistivity as a function of temperature for a YBCO crystal.

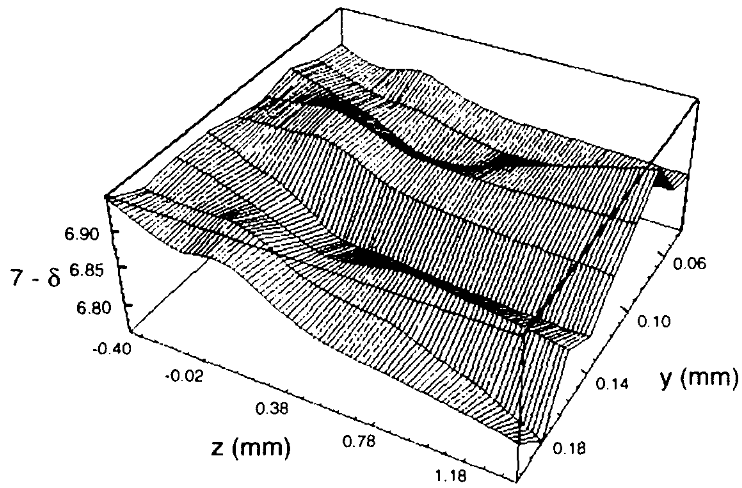

Fig. 8 — Three-dimensional plot of (7-δ) for a YBCO crystal.

In conclusion, both epitaxial films and single crystals, which would be classified as "optimal" based on their transport properties, exhibit structural inhomogeneities when analyzed by sophisticated X-ray diffraction techniques. The presence of these features points out that electrical transport measurements are inadequate for determining sample quality and brings into question whether results of experiments performed on such samples can be attributed to intrinsic behavior. Futhermore, these X-ray techniques can be used to identify helpful and harmful structural features in epitaxial films that will be used in superconducting electronics applications.

[Sponsored by ONR]

References

1. S.B. Qadri, M.S. Osofsky, V.M. Browning, E.F. Skelton, and T.A. Vanderah, "High-Resolution Characterization of Structural Inhomogeneities in $YBa_2Cu_3O_{7-\delta}$ Crystals with Sharp Superconducting Transitions," *Appl. Phys. Lett.* **68**, 2729 (1996).

2. V.M. Browning, E.F. Skelton, M.S. Osofsky, S.B. Qadri, J.Z. Hu, L.W. Finger, and P. Caubet, "Structural Inhomogeneities in $YBa_2Cu_3O_{7-\delta}$ Crystals with 'Optimal' Transport Properties," to be published in *Phys. Rev.* (1997). ■

Tests of HF Radar for Solar Corona Diagnostics

P. Rodriguez
Plasma Physics Division

Historical Context: The possibility of using high-frequency (HF) radars to investigate the solar corona was suggested as early as 1952 by radio astronomers engaged in new experiments with radars [1]. Since this early period, the use of radars to investigate planetary, lunar, and asteroidal bodies has become a highly developed experimental technique. Similar experiments for the solar corona are more difficult because the radar waves interact with a very hot plasma (~1 to 2 million K), with a large density range (10^1 to 10^8 electrons/cm^3), and dynamic time variations. The only series of sustained solar radar experiments was performed in the 1960s by a group from the Massachusetts Institute of Technology led by J.C. James. They built a transmitting and receiving radar array near the town of El Campo, Texas. The experiments consisted of 16 min of transmission at 38.25 MHz, followed by 16 min of "listening" for the reflection. The 16-min period corresponds to the travel time for the radar waves from Earth to Sun and back to Earth. These experiments primarily studied the radar cross-section of the solar corona and its variation with the solar activity.

After 1969, the El Campo antenna array and transmitter were dismantled, and the site no longer exists. This is unfortunate because today it seems that the El Campo experiments were somewhat ahead of their time. A review of the El Campo solar radar results has been published by James [2].

Coronal Mass Ejections: We now think that solar radar experiments can provide unique information on how the Sun's dynamic coronal phenomena can affect the Earth. In recent years, it has become recognized that coronal mass ejections (CMEs) are the drivers for the most intense geomagnetic storms at Earth. Such storms can cause serious problems with electric power grids that provide electric power to homes and industry. Weather and communications satellites in geosynchronous orbit can have their normal operations disrupted and become damaged by such storms. CMEs can be dramatically imaged with coronagraphs, as they move away from the Sun. If we could detect the CME motion toward the Earth, we would gain the ability to forecast the geomagnetic interaction at Earth. The detection of Earthward-moving CMEs is potentially possible with a solar radar [3]. In this application, the radar is used in a manner exactly analogous to the use of traffic radars to catch speeding automobiles. Figure 9 shows an artistic conception of the use of a solar radar to detect an Earth-moving CME.

At the time of the El Campo experiments, coronal mass ejections and their interaction with the Earth was unknown. Today we do not know if any of the early solar radar measurements may have actually detected CMEs. Unfortunately, the original database from El Campo, consisting of about 1000 solar radar experiments, is no longer available for reanalysis in the light of current understanding.

New Solar Radar Experiments: In the summer of 1996, we conducted eight experiments using the Russian Sura radar and the Ukrainian UTR-2 receiving antenna in a "bistatic" configuration that approximates the El Campo radar configuration. Between 9 July and 20 July, noontime experiments involved 16-min transmissions at about 9 MHz followed by 16-min reception intervals. As part of these experiments, the NASA spacecraft WIND received the 9 MHz transmissions and thus confirmed that the radar waves propagated into interplanetary space. Figure 10 shows plots of the wave intensity received by WIND as a function of time. In the first interval of transmission, between Universal Times (UT) of 0911 to 0927, the radar waves were directed to the Sun, while in the second interval, the transmission was directed to WIND itself. The intensity fluctuations at WIND are most probably caused by density irregularities in the Earth's ionosphere. This effect must be taken into consideration in the analysis of the data.

In Fig. 11, we plot the frequency spectrum of waves detected by the UTR-2 antenna array during one of the experiments. The spectrum gives the intensity of received signal as a function of fre-

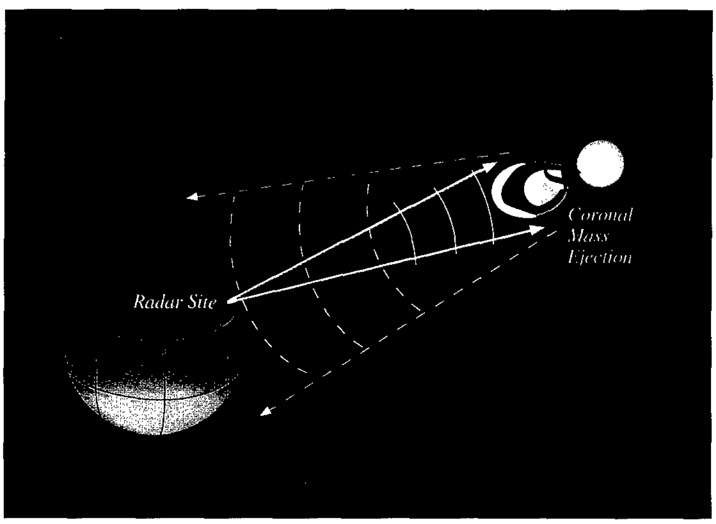

Fig. 9 — An artist's conception of a solar radar transmitting toward the Sun and detecting the signal reflected from an Earthward-moving CME.

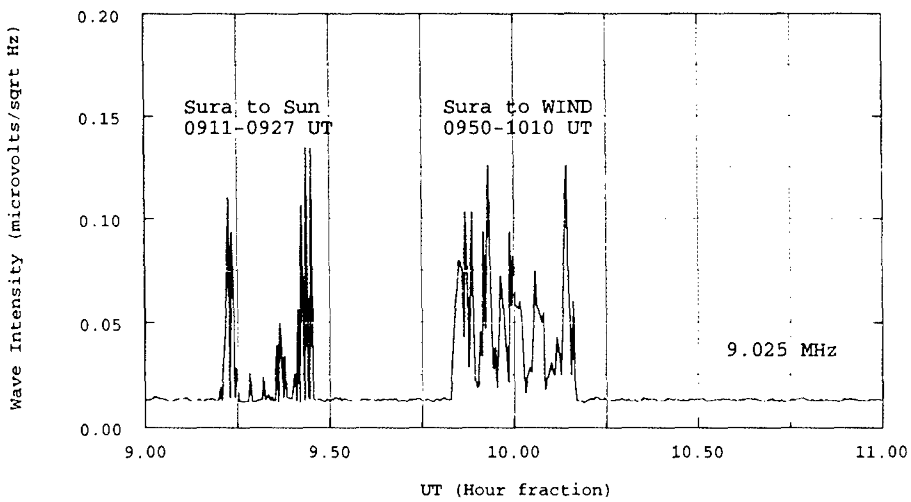

Fig. 10 — Radar waves received by the WIND spacecraft during Sura transmissions to the Sun and to WIND itself (July 12, 1996).

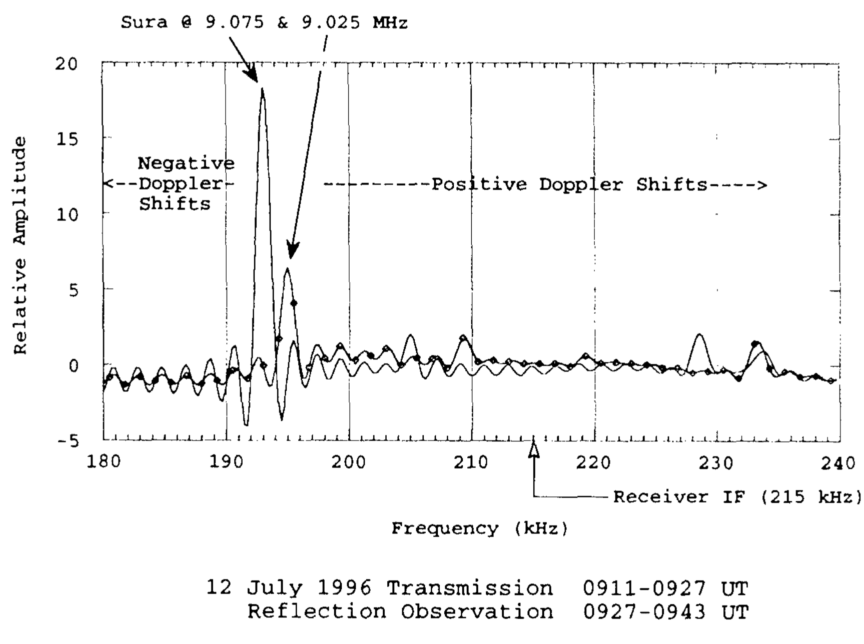

Fig. 11 — The signal frequency spectrum received by UTR-2. The large peaks correspond to Sura transmissions near 9 MHz. The smaller peaks represent possible reflections from the solar corona.

quency. The large peaks correspond to the waves transmitted by Sura. Several small bumps in the spectrum at positive frequencies can be seen, and these signatures are similar to what a CME might provide. However, we cannot state definitively that these bumps result from CMEs; they might be caused by some other noise source. Clearly, it is important to identify all possible sources of noise. We are also using coincident observations of the Sun by other facilities, such as coronagraphs, to provide confirmational data. Our study is in its initial phases, and we expect that as more data and experience are gained, some of the knowledge from the early solar radar experiments will be recaptured, and new information will be derived.

Conclusions: In one respect, we are engaged in an archeological expedition into previous understanding of solar radar experiments. The scientific issues that motivated the original suggestions for solar radars are still relevant. And because we recognize that our Sun is also a star, solar radar experiments can actually provide a unique method of directly probing a true astrophysical object.

Acknowledgments: We thank the Radiophysical Research Institute in Nizhny Novgorod, Russia, and the Institute of Radio Astronomy in Kharkov, Ukraine, for their collaboration on this program.

[Sponsored by ONR]

References

1. F.J. Kerr, "On the Possibility of Obtaining Radar Echoes from the Sun and Planets," *Proc. IRE* **40**, 660-666, 1952.

2. J.C. James, "Radar Studies of the Sun," in *Radar Astronomy*, J.V. Evans and T. Hagfors, eds. (McGraw-Hill, New York, 1968), p. 323.

3. P. Rodriguez, "High Frequency Radar Detection of Coronal Mass Ejections," in *Solar Drivers of Interplanetary and Terrestrial Disturbances*, K.S. Balasubramaniam, S.L. Kiel, and R.N. Smartt, eds. (Astron. Soc. Pacific Conf. Series, Vol. 95, 1996), p. 180.■

Information Technology and Communication

Internet Communication Resistant to Traffic Analysis

D.M. Goldschlag, M.G. Reed, and P.F. Syverson
Information Technology Division

Determining who is talking to whom (called traffic analysis) is an important source of intelligence information. As military grade communication devices increasingly depend on the public communications infrastructure, it is important to use that infrastructure in ways that are resistant to traffic analysis. It may also be useful to communicate anonymously, for example when gathering intelligence from public databases. We describe bidirectional and real-time ANONYMOUS CONNECTIONS [1] that are strongly resistant to eavesdropping and traffic analysis attacks by both insiders and outsiders. If necessary, communication is made anonymous by removing identifying information from the data stream. These anonymous connections have been prototyped in a system that protects the privacy of communication over the Internet and, in particular, the World Wide Web. Anonymous connections can protect both identity and location in many switched communication systems, such as wired, cellular, or satellite phone networks.

The Problem: The Internet and the World Wide Web (Web) have become important parts of modern day communication and commerce. But electronic messages can be easily snooped and tracked, thereby revealing both who is talking to whom and the subject of the conversation. This information may be sensitive: a researcher doing searches on the Web may expect his focus to remain private. The existence of intercompany collaboration may be confidential. Individuals may wish to hide to whom they are sending e-mail.

This article describes a communications technology that provides anonymous connections between two parties. These anonymous connections hide the identities of communicating parties from both the communications network and outside observers. This is protection against traffic analysis. In addition, anonymous connections protect the data being communicated against eavesdropping. Since anonymous connections do not reveal identities, any identifying information must be carried through the anonymous connection. Our implementation of anonymous connections, ONION ROUTING, can be used with a wide variety of unmodified Internet applications, including Web browsing, electronic mail, remote logins, and file transfers.

Who is Talking to Whom? Traffic analysis can be used to infer who is talking to whom over a public network. For example, in a packet-switched network such as the Internet, packets have a header used for routing and a payload that carries the data. The header, which must be visible to the network (and to observers of the network), reveals the source and destination of the packet. Even if the header were obscured in some way, the packet could still be tracked as it moves through the network. Encrypting the payload is similarly ineffective because the goal of traffic analysis is to identify who is talking to whom and not (to identify directly) the content of that conversation.

Making Traffic Analysis Hard: Onion routing works in the following way: instead of making a connection directly to a destination machine, an application makes a connection to an ONION-ROUTING PROXY on a machine (Fig. 1). That onion-routing proxy builds a layered data structure, called an ONION, that defines the route of an anonymous connection through several other

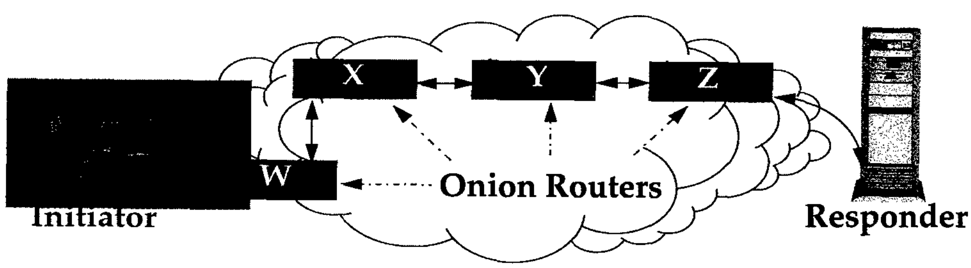

Fig. 1 — Onion routing network configuration: Notice that the onion router labeled W is controlled by the sensitive site. Onion routers W and Z also function as onion routing proxies.

ONION ROUTERS to the destination. The onion is sent along that route. Each onion router can identify only adjacent onion routers along the route. Before sending data over an anonymous connection, the first onion router adds a layer of encryption for each onion router in the route. As data move through the anonymous connection, each onion router removes one layer of encryption, so it finally arrives as plain text (Fig. 2). This layering occurs in the reverse order for data moving back to the initiator. Data passed along the anonymous connection appears different at and to each onion router, so data cannot be tracked en route, and compromised onion routers cannot cooperate. When the connection is broken, even the limited information about the connection is cleared at each onion router.

An onion-routing network can exist in several configurations that permit efficient use by both large institutions and individuals. For example, a site concerned about traffic analysis should control an onion router (Fig. 1). Like an Internet firewall, that onion router is a bridge between the sensitive site and the rest of the Internet. Connections from that onion router to machines in the sensitive site are protected by the site's physical security. Connections to the rest of the Internet are protected by onion routing's anonymous connections. Alternatively, an individual Internet user who accesses the Web through an Internet Services Provider (ISP) may build onions on his own machine and use the ISP's onion router as his entry point to the Internet. In both cases, the local onion router should also route data between other onion routers, to complicate tracking of traffic originating or terminating locally.

Anonymity: Anonymous communication may be layered on top of anonymous connections by removing identifying information from the data stream. For example, in anonymous e-mail, the system's obligation would be to remove identifying headers from the mail message (i.e., the sender's address). The user's responsibility would be to omit or remove any identifying information from the body of the message. The anonymized message can be sent through an anonymous connection.

The sender of an anonymous message can also invite replies by including a REPLY ONION in his message. The reply onion defines an anonymous connection through several onion routers back to the sender. Like an ordinary onion, it is constructed so that each onion router can identify only adjacent onion routers in the route. A reply is sent over that anonymous connection.

Discussion: Onion routers are similar to Chaum MIXES [2], which also reorder and change the appearance of messages to complicate traffic analysis. Mixes have been used primarily for e-mail, notably in anonymous remailers. However, onion routing differs from other anonymity services in two ways: communication is real time and bidirectional. The anonymous connections are application independent, and the onion-routing infrastructure can be used by a wide variety of Internet applications. Onion routing accomplishes this goal by separating identification from routing; connections are made anonymous, although communication need not be. Applications may choose whether to identify their users over an anonymous connection. However, the use of a switched public network should not automatically reveal who is talking to

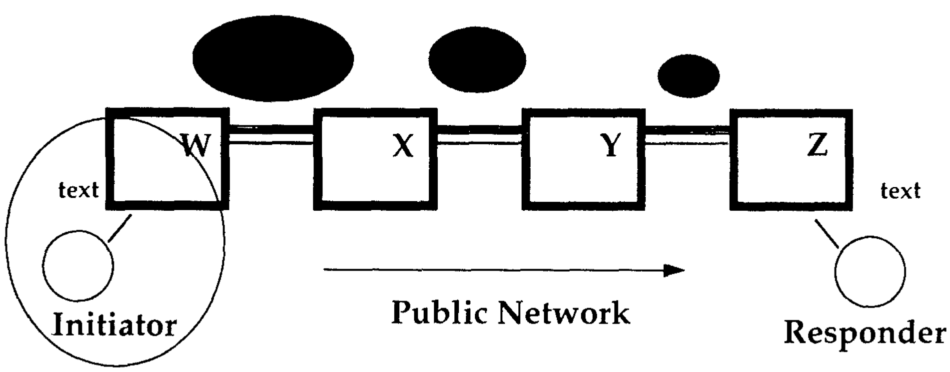

Fig. 2 — Moving data forward over an anonymous connection; as data move forward, layers of encryption are removed. The figure does not reflect that encryption preserves the size of data traveling between onion routers.

whom. This is the traffic analysis that onion routing complicates.

Anonymous connections can also be viewed as a new communications primitive that supports novel and interesting protocols. For example, a cellular phone network can be designed that will hide a caller's location both from outside observers and from the phone network. This reduces the trust one must place in the service provider.

[Sponsored by ONR]

References

1. M.G. Reed, P.F. Syverson, and D.M. Goldschlag, "Proxies for Anonymous Routing," 12th Annual Computer Security Applications Conference, San Diego, CA, December 1996.

2. D. Chaum, "Untraceable Electronic Mail, Return Addresses, and Digital Pseudonyms," *Commun. ACM* **24**(2), 84-88 (1981). ■

Constrained Routing for Strike Aircraft

A. Boroujerdi, J.K. Uhlmann, and M.R. Zuniga
Information Technology Division

Introduction: For the past 3 years, a team at NRL's Information Technology Division has been developing aircraft routing algorithms for the Strike-optimized Mission-planning Module (STOMPM) Project, funded by the Office of Naval Research. The problem involves finding a minimum cost route between two points that are subject to a number of constraints. The cost of a route essentially reflects the probability of failure of the aircraft while flying the route — through clobber, enemy detection, and intersection, etc. The constraints are due mainly to the flight characteristics of the aircraft — maximum rate of ascent, minimum turn radius, and amount of fuel available. The standard approach to the problem is to model the airspace in which routing is to take place as a three-dimensional grid (collection of vertices connected by edges). The problem of computing a route between two points is then reduced to that of finding a sequence of edges between the two corresponding vertices in the grid.

Background: Routing in the absence of constraints is known in the literature as the shortest-path problem: find the shortest path between two vertices of a graph. (Note that "shortest" doesn't necessarily refer to distance; it could mean minimum cost, for example.) The shortest-path problem can be solved very efficiently. In practice, several shortest-path algorithms scale almost linearly. In the presence of certain constraints, however, the problem is more difficult to solve efficiently. Constraints on turn radius and fuel, for example, have a severe impact on efficiency. As a result, existing algorithms for the problem are either inefficient or enforce constraints in an ad hoc manner, which can result in poor routes. We have developed algorithms capable of efficiently enforcing a wide range of constraints without losing optimality. These algorithms enable us to generate high-fidelity routes in real time, paving the way for the complete automation of the routing process.

Enforcing Constraints: To illustrate some of the difficulties involved in constrained routing, let us consider the case where the computed route cannot include turns greater than a given angle θ. One approach to the problem is to transform the original graph G into a new graph G' such that a minimum-cost path in G' corresponds to a minimum-cost path in G that satisfies the turn constraint. The problem can thus be solved by running a standard shortest-path algorithm on G'. The transformation is performed as follows. For each vertex v in G, create d vertices $v(1)$, $v(2)$, ..., $v(d)$ in G', where d is the in-degree of v. Let u be the ith predecessor of v and v be the jth predecessor of w in G (predecessors can be ordered arbitrarily). Introduce an edge from $v(i)$ to $w(j)$ in G' if and only if there exists an edge e from u to v and an edge e' from v to w in G such that e and e' make an angle no less than $\pi\theta$.

It can be proved that a minimum-cost path in G' corresponds to a minimum-cost path in G that does not violate the turn constraint. Thus to compute a minimum-cost path in G that satisfies the turn constraint, we need only compute a shortest path in G'. The drawback of this approach is that the new graph G' is roughly d times larger than the original graph G, where d is the average in-degree of a vertex in G. Running a standard shortest path algorithm on G' would simply take too long for large d. To alleviate this problem, we note that G' has a special structure that standard

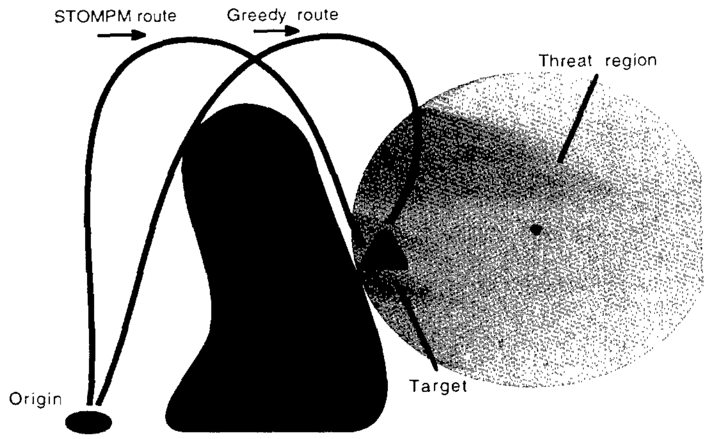

Fig. 3 — A scenario requiring the routing of a strike aircraft from an origin point to a target. The angle of attack required to destroy the target prevents the plane from flying over the mountain (region in black), so any route will have to fly around the mountain. The "Greedy" route simply takes the shortest path around the mountain and then is forced by turn radius constraints to circle around back to the target through the threat region (in red). The STOMPM route, however, is computed in a globally optimal manner that minimizes time spent in the threat region.

shortest-path algorithms were never designed to take advantage of. We have developed considerably faster algorithms suitable for use in real time by taking advantage of the special structure of the graphs resulting from the transformation.

An Example: Since our algorithms guarantee optimality, they do not suffer from the problems that plague existing routers. As Fig. 3 shows, an ad hoc approach to the enforcement of turn constraints may result in a highly suboptimal route. Specifically, the "greedy" route follows the shortest path around the mountain. Once it is around the mountain, however, limitations on the turn radius of the plane forces the route to spend a considerable period of time within the detection region of the threat. The enforcement of turn constraints in STOMPM, however, ensures the selection of the optimal route that minimizes exposure to the threat.

[Sponsored by ONR] ■

Development of an Integrated Object-Oriented Framework for Storage and Query of Multiple Spatial Data Types of Digital Mapping Information

K.B. Shaw, M.J. Chung, and M.A. Cobb
Marine Geosciences Division

Introduction: NRL's Mapping, Charting, and Geodesy Branch is developing an integrated object-oriented framework to allow the naval user to rapidly build an area-of-interest database with vector, raster, and text data types combined. This research is also aimed at developing a conflation process formed on a rule-based expert system to deconflict features within the vector family of data. Currently the National Imagery and Mapping Agency (NIMA, formerly Defense Mapping Agency) is producing discrete vector (vector product format (VPF)), raster (raster product format (RPF)), and text (text product standard (TPS)) databases that present the likely event that a naval user will not have all available digital mapping information that is fully integrated at the data level for a given area and situation. The integrated framework will minimize this possibility by generating on demand any area-of-interest database with combined and deconflicted VPF, RPF, and TPS information from NIMA.

Progress toward this integrated framework is discussed, with attention given to the newly developed composite geographic object concept, a closed-form mathematical expression for query and our expert system developments for conflation.

An Integrated Object-Oriented Framework: The integrated framework is a new approach, developed using Smalltalk programming language for storing all three NIMA data types of information in a single, object-oriented schema, shown in Fig. 4. This allows immediate feature-level updating, grouping of all geographically similar (not just data-type similar) information, and robust query.

One of the key NRL developments that is allowing the combination of multiple data types is the Composite Geographic Object shown in Fig. 5. Frames/subframes of imagery and scanned maps,

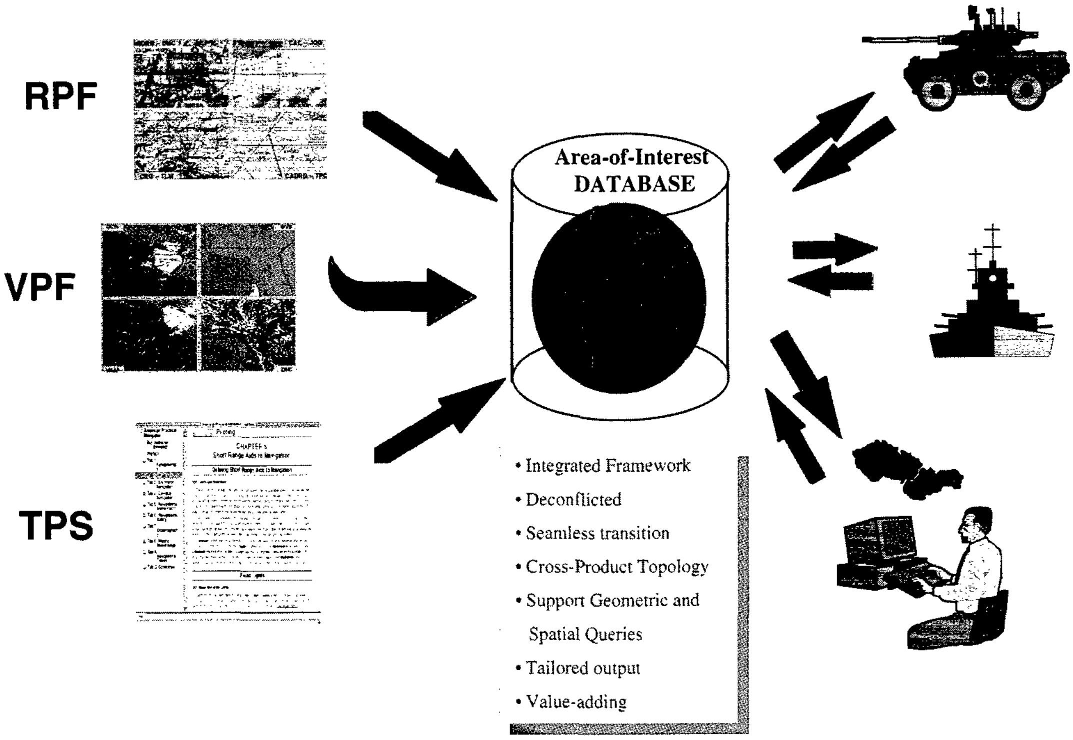

Fig. 4 — Area-of-interest database.

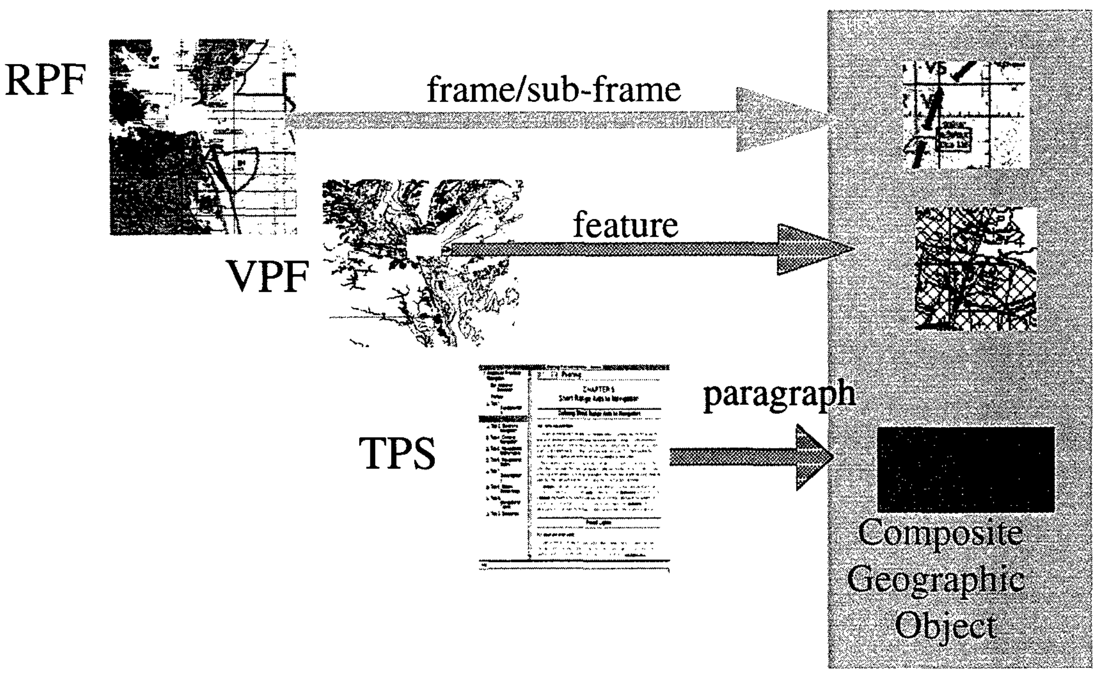

Fig. 5 — Composite geographic object concept.

features from the VPF relational database family, and textual type (or what has been in publication form) are combined by geographic area into a Composite Geographic Object for Area-of-Interest Database query by naval or NIMA users.

Another significant NRL development has been a closed-form equation to describe object-oriented query with constraints on features, attributes, and topology. This equation allows Geographic Information System (GIS)-type queries with no need for the large and expensive GIS layer of software. For example, queries such as "display all hard paved roads with bridges within a 20-mi radius" are readily processed. [1]

Conflation Research: The features that comprise the VPF family of data are repeated within a single product (an individual VPF relational database) and among the multiple VPF products, primarily due to varying sources and scales of sources. These repeats introduce uncertainty and increased decision-making time for naval mission planners and tactical decision makers. Conflation is simply the combination of two or more databases (in this case VPF products) to form "better" information that can be measured in many ways, such as accuracy. An iterative process of feature matching, feature deconfliction of both spatial and attribute information, and positional alignment is performed to produce a "better" mapping information. The first challenge of conflation is determining like features. NRL's Mapping, Charting, and Geodesy Branch has developed an initial approach to feature matching using a four-staged algorithm, shown in Fig. 6. This feature-matching approach is augmented by an expert system that is being loaded with cartographic heuristics to improve the feature-match decision-making process. [2]

Summary of FY 96 Accomplishments: Integrated framework accomplishments include: development of the first object-oriented Text Product Standard prototype and the first object-oriented Raster Product Format prototype; research investigations into and mathematical expression for the following: a feature attribute-based indexing scheme, composite geographic object-creation algorithm, an object-oriented query interface, and the computation of topological relationships. Accomplishments for the conflation segment of the research include: design of an integrated approach to conflation that uses spatial and nonspatial attributes; preliminary implementation of a rule-based system for nonspatial attribute matching; and the development of an algorithm for shape similarity determination.

Significance: NIMA is transitioning their paper charts and publications into digital representations. The integrated object-oriented framework will be useful both at the NIMA (producer level) and the naval users' level. This research and development will allow NIMA and naval users to combine all available digital mapping data regardless of data type and query it by Area-of-Interest. This system will also provide a means for updating the information to retain currency.

Other Related Ongoing Object-Oriented Database Research within NRL's Mapping, Charting, and Geodesy Branch: An Extended Vector Product Format (EVPF) prototype has been developed to combine Triangulated Irregular Networks (TINs) with VPF data content for a three-dimensional (3-D) display for the modeling and simulation community. The EVPF was developed as a relational database and then transformed into

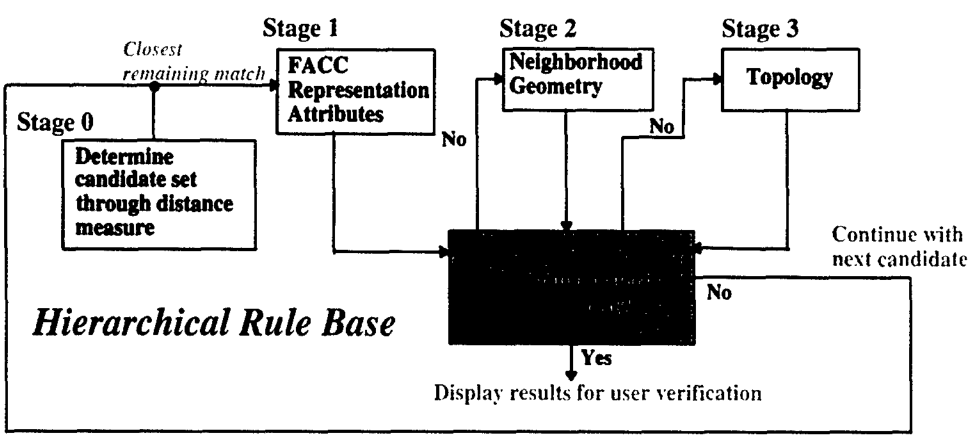

Fig. 6 — Conflation, feature-matching algorithm.

the object-oriented integrated framework prototype to allow for 3-D viewing of Area-of-Interest information. NRL has worked closely with the University of New Orleans in the EVPF development.

Conclusions: Object-oriented approaches for database construction are proving to be beneficial for geospatial (digital-mapping) data. An object-oriented approach has allowed the direct creation of an integrated framework that combines NIMA's primary data types such that the naval user can have all relevant mapping information to make tactical decisions and plan missions at their fingertips. This integrated framework also will empower NIMA and naval users to value-add, update, and tailor digital-mapping information more effectively.

[Sponsored by ONR]

References

1. M. Chung, M. Cobb, and K. Shaw, "Issues Regarding the Combination of Multispatial Data Types for an Improved Digital Mapping Framework," submitted to *Comput. Geosci.*, December 1996.

2. M. Cobb, M. Chung, and K. Shaw, "Issues and Approaches for the Conflation of Vector Product Format (VPF) Data," submitted to *GeoInformatica*, May 1996. ■

The Master Environmental Library (MEL)

R.A. Siquig
Marine Meteorology Division

R.A. Allard
Oceanography Division

J.H. Spencer
Remote Sensing Division

The Need for Authoritative Environmental Data: Modeling and simulation (M&S) have become increasingly important in Department of Defense (DoD) activities, such as training, analysis, acquisition, research and development, test and evaluation, and mission rehearsal because they offer lower-cost, supplemental alternatives to the more traditional approaches to these activities. However, just as in the real world, the natural environment affects platforms, sensors, weapons, systems, war fighters, tactics, and strategy, so too in the simulated world the natural environment must be included in a realistic, physically consistent, correlated way to achieve the full value of M&S. This requirement is formally included as part of the DoD M&S Master Plan [1]. To satisfy this requirement, the Defense Modeling and Simulation Office (DMSO) is funding the Master Environmental Library (MEL) Project, a joint project involving the Navy, Army, Air Force, and National Imagery and Mapping Agency (NIMA), under the leadership of the Naval Research Laboratory.

The Problem of Data Discovery and Retrieval: A problem becomes immediately apparent when trying to locate authoritative environmental data; there is much already available and the amount is increasing rapidly, but the data are provided at various distributed data centers using different databases and are delivered in different formats. Simply getting the data for M&S can be a formidable problem. For geospatial data, which include data of the natural environment such as the ocean, terrain, atmosphere, and near space, a common contents standard for *metadata* (data about data), such as the *Federal Geographic Data Committee (FGDC) Standard* [2], is a powerful key to data discovery and retrieval. With the rapid development of search engines and web browsers on the Internet, it was possible to create a common, consistent, unified interface for browsing metadata at distributed data sites and for ordering the data itself. The actual details of data extraction, encoding in a standard delivery format, and delivery to the user are hidden behind the interface.

Key Components of MEL: The key components of the MEL architecture are shown in Fig. 7. The user no longer has to deal with each provider

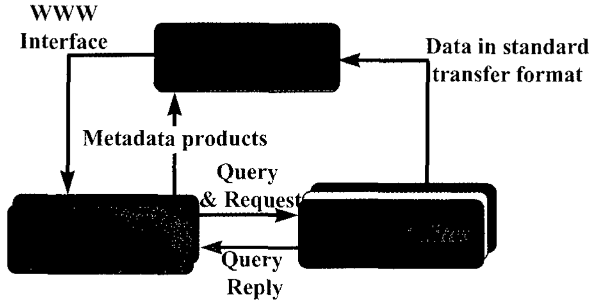

Fig. 7 — Components of the MEL architecture, indicating the key role of the access site as a common interface between the user and the data providers.

separately, thus avoiding a variety of interfaces, methods of data querying and ordering, and different transfer formats. Such local variations are concealed behind the consistent single interface (access site). The data are left under the local control of the provider (regional site), who has only to create and maintain indexed metadata in the standard contents format to be searchable over the library system. The actual details of sending queries and requests from the access site and data extraction and delivery are made generic to the greatest extent possible and customized as necessary for each regional site. Using the fewest and most standard transfer formats possible and providing the corresponding decoders greatly simplifies the effort of the user to work with the data delivered. By using web technologies, MEL exploits the power of the market place for rapid technology development and de facto standards, for both unclassified and classified networks. This is consistent with the DMSO guidelines of reuse and interoperability of systems. As the technology evolves, it is straightforward to incorporate improvements into the basic architecture, such as we have done in providing (in addition to the original hypertext markup language (HTML) interface), a Java interface for data querying and metadata results handling. Furthermore, the architecture is being extended to regional sites that will be computer sites for running models or tool applications.

Significance of MEL: MEL is the first data discovery, retrieval, and delivery system that allows a user to query Navy, Army, Air Force, NIMA, and non-DoD centers [Fig. 8] for the existence of geospatial data that satisfy the user's criteria and to request either archived data or data that can be made available by subscription. The data can be obtained from any of the natural environmental domains of terrain, ocean, atmosphere, and near space. In addition to providing a uniform consistent query and request interface, MEL also provides, as illustrated in Fig. 9, authoritative environmental data and physically consistent scenario databases. Figure 10 shows how atmospheric and ocean models of different length and time scales interact to produce a surf zone data set of high resolution.

The architecture of MEL was implemented for M&S users and will be the environmental library of choice for joint M&S, but it is applicable to a far wider range of uses. In particular, its approach is a powerful paradigm for many joint situations that require the acquisition of data from distributed dissimilar sources and the integration and manipulation of the data for use by decision makers. The MEL system is completely transferable to a classified network that obeys the usual Internet protocols.

Future Plans: MEL funding started in FY 95 and is expected to continue through FY 98. The emphasis in FYs 97/98 will be on increased

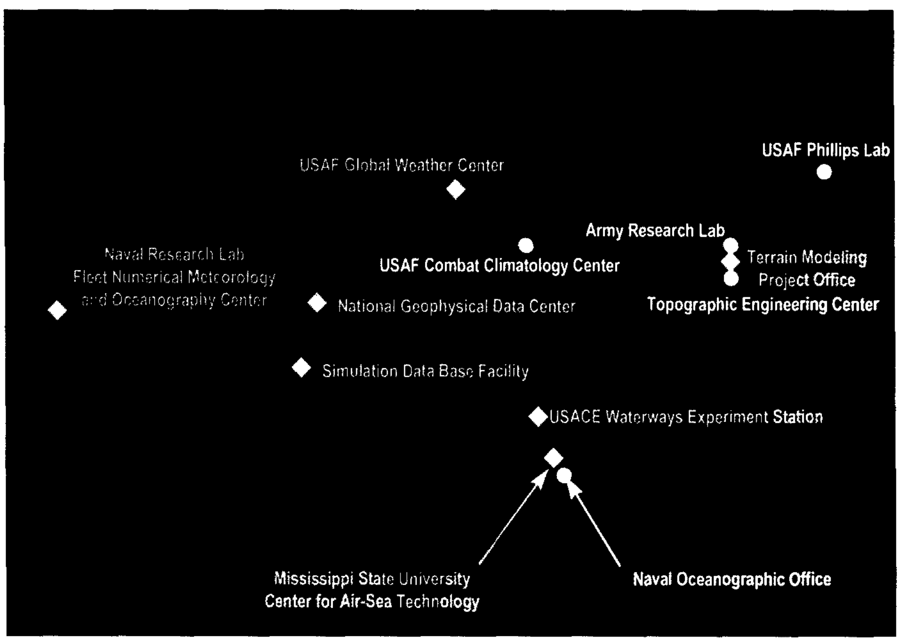

Fig. 8 — Current MEL sites; yellow indicates online sites and white indicates sites not yet online.

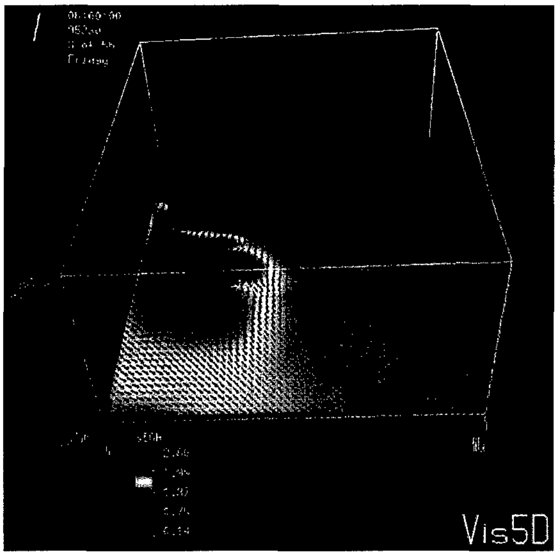

Fig. 9 — A VIS5D example of wave direction and significant height from the wave model (WAM) for the Synthetic Theater of War area in the Southwest U.S.

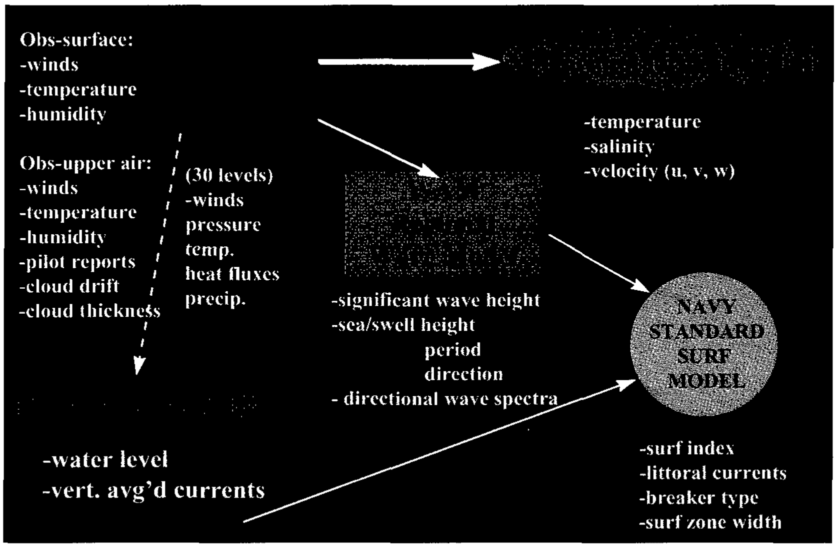

Fig. 10 — The chart illustrates how observations are used to initialize a numerical atmospheric forecast model (COAMPS), which in turn provide input for ocean, tidal, wave, and surf models to develop integrated synthetic scenarios.

robustness of the architectural implementation and transition of tools and other applications to the system, providing enhancements for data manipulation, visualization, distributed computing, and product generators. The project expects to expand its customer base beyond M&S to include joint operational users who require access to distributed sources of geospatial data.

[Sponsored by Defense Modeling and Simulation Office]

References

1. "Modeling and Simulation (M&S) Master Plan," Department of Defense, Under Secretary of Defense for Acquisition and Technology, DoD 5000.59-P, October 1995.

2. "Content Standards for Digital Spatial Metadata," June 8 draft, Federal Geographic Data Committee, Washington, D.C. (1994). ■

Materials Science and Technology

Controlled Structure Technology Yields Unique Composite Capabilities

T.L. Jessen and D. Lewis III
Materials Science and Technology Division

Introduction: The atomic bonding characteristics that allow ceramics chemical resistance and elevated temperature (> 1000° C) structural integrity also make them extremely brittle. In the mid-1970s, continuous fibers were incorporated in ceramics to improve strength and reduce brittle failure. Subsequently, continuous fiber, ceramic matrix composites (CFCMC) have been researched extensively. Significant improvements in strength and fracture resistance have been achieved. CFCMCs are integral materials in a variety of next-generation aircraft engine components (i.e., rotors, stators, combustors, etc.) and as heat exchangers in power plants. Use of CFCMCs can improve fuel efficiencies up to 20% and reduce harmful emissions by increasing operating temperatures beyond those sustainable by other materials.

The improvement in CFCMC mechanical performance has been linked to the strength of the fiber/matrix interface. Weakly bonded interfaces allow redirection of applied stresses to off-axis directions, reducing the effective loading. This discovery in the early 1980s intensely focused CFCMC research on the nature and control of the interface and led to the assumption of microstructure-insensitive CFCMC mechanical behavior, in contrast to the highly correlated structure/mechanical performance relation in monolithic ceramics.

In 1995, a 2-year study investigating the effect of microstructure on CFCMC mechanical performance [1] was concluded. It found strong correlation between intrinsic structural features (matrix-rich regions or channels) in homogeneously distributed CFCMCs and mechanical performance. The orientation of 85-μm-wide matrix channels — features previously thought insignificant — controlled both properties and failure mechanisms. The channels form as a consequence of the fiber coating required to obtain a weakly bonded interface. This NRL-based research received worldwide attention in the CFCMC community. Figure 1 shows an example of the structure sensitivity of

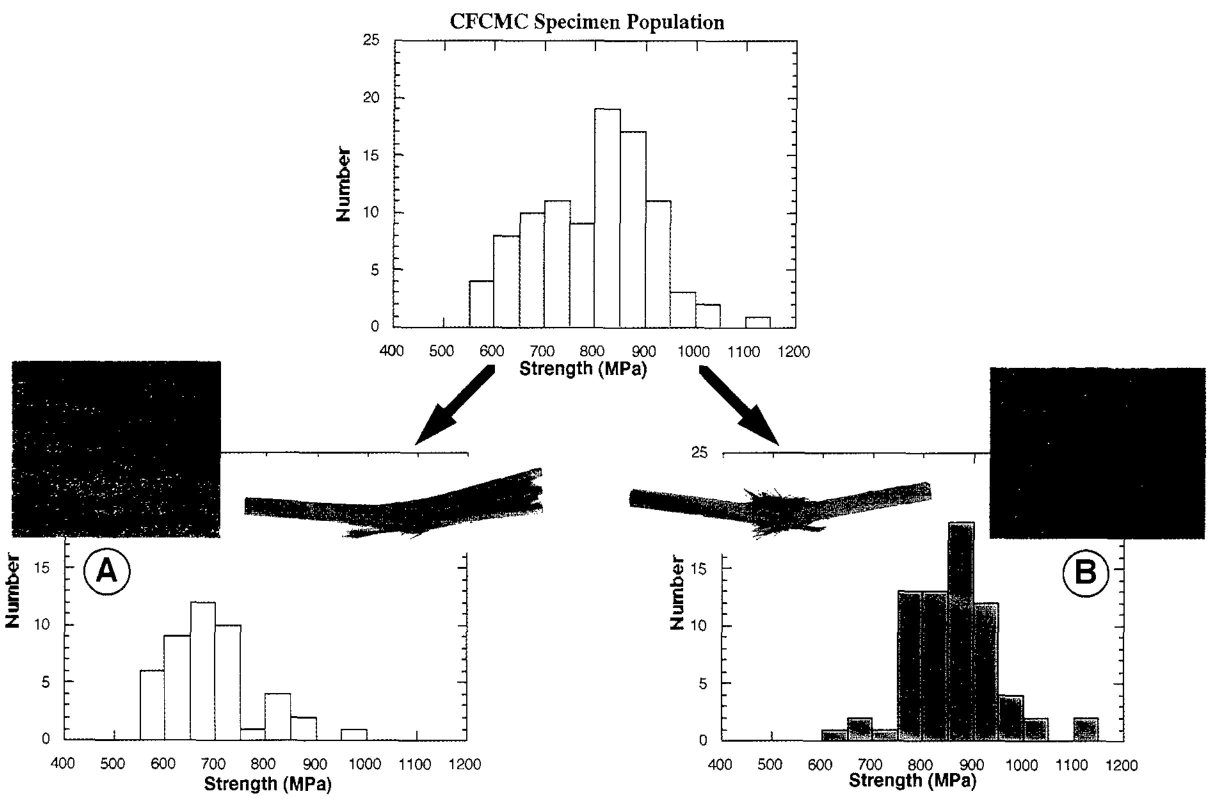

Fig. 1 — Reduction in data scatter and consistency in failure mechanisms when influence of microstructure is considered. The orientation of the matrix channels (dark regions) in the microstructure inserts determines the mechanical behavior.

CFCMCs. The large property scatter of the entire specimen group is significantly reduced when microstructure is considered. More significantly, the failure processes are consistent and predictable within each subgroup combination of microstructural orientation and loading direction (i.e., either Fig. 1(a) or (b)) — an important consideration for use of these materials by design engineers.

Having established the importance of structure (specifically, matrix channels) on CFCMC mechanical behavior, we focused on two important issues in 1996: (1) quantification of the relative importance of microstructure vs interface control and (2) investigation of this behavior for CFCMC performance improvement.

Results: A proprietary process [2], Controlled Structure Technology (CST), was developed to exploit the matrix channel effect on CFCMC mechanical behavior. CST affords the ability to alter selectively the size, spacing, and morphology of the channels. A series of composites were fabricated with varying matrix channel features and a constant fiber/matrix interface condition. Figure 2 summarizes partial results of this unique study. CST provides a 460 MPa improvement in CFCMC strength, as compared with a 330 MPa increase from the use of a weak fiber/matrix interface. These results reinforce the findings of the earlier work [1]. Similar improvements in fracture toughness were also achieved using CST-prepared composites. While these findings have scientific significance in understanding CFCMC behavior, the utility of CST is demonstrated in Figs. 3 and 4.

Figure 3 compares the mechanical behavior of composites prepared with the matrix channels aligned parallel to the applied load. Statistically significant improvements in properties are observed with the CST composites. This improvement was achieved while reducing the fiber reinforcement volume by 15%. Since the fiber cost is typically one-third of composite fabrication cost, these results have important implications in CFCMC usage. Property enhancement is due to the introduction of additional failure mechanisms in the CST composites.

Figure 4 compares the behavior of composites with matrix channels perpendicular to the applied load. While both strength and toughness of the CST composites are reduced due to their exaggerated laminatelike structure, the significant result is the postfracture behavior of the specimens. The

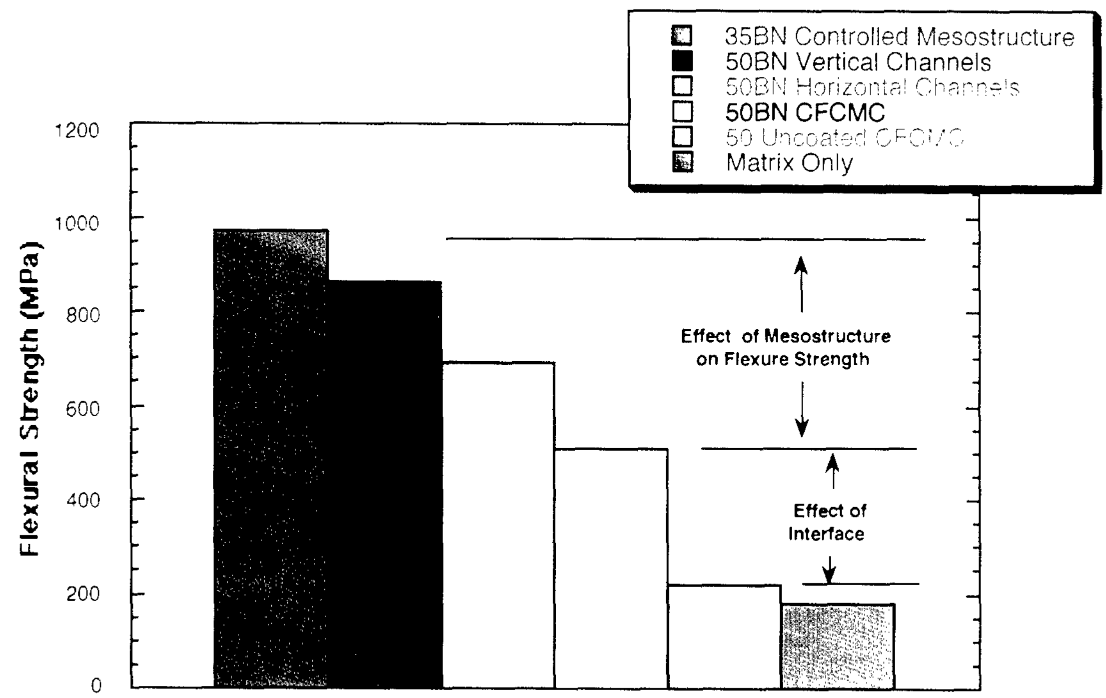

Fig. 2 — Comparison between the effect of fiber distribution and fiber/matrix interface modification on CFCMC mechanical performance.

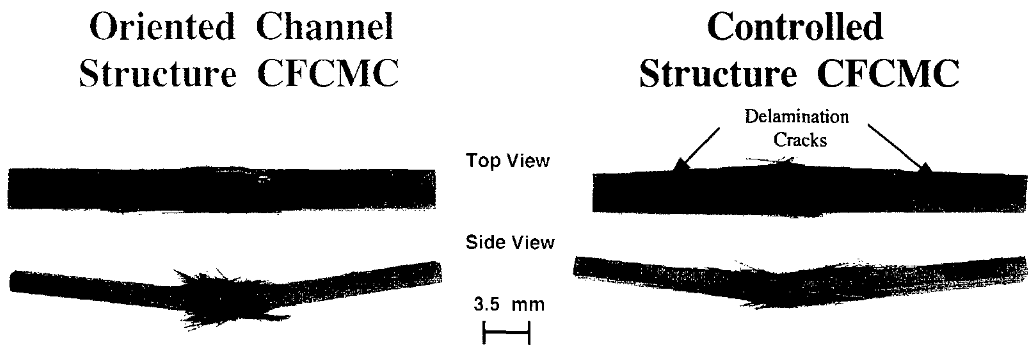

50 %	Fiber Loading	35 %
863	Strength (MPa)	971
1.00	Normalized Toughness	1.49

Fig. 3 — Comparison of failure mechanisms and mechanical properties, which illustrates the improvements possible through control of the composite microstructure. These specimens were tested with the matrix channels *parallel* to the applied load similar to the orientation in Fig. 1(b).

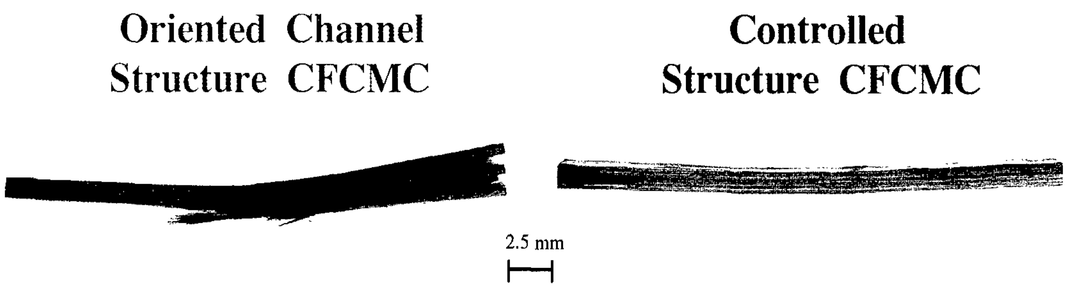

50 %	Fiber Loading	50 %
691	Strength (MPa)	550
1.00	Normalized Toughness	0.92

Fig. 4 — Comparison of failure mechanisms and mechanical properties, which illustrates the retention of postfracture structural integrity possible through control of the composite microstructure. These specimens were tested with the matrix channels *perpendicular* to the applied load similar to the orientation in Fig. 1(a).

CST specimens retain structural integrity following failure. CST samples can carry 50% to 60% of their maximum prefailure load upon reloading, while the other specimens exhibit almost no retained properties. This result is an important consideration for man-rated engines and other failure-critical structural applications. The reason for this unique CST behavior is the uniformly distributed matrix channels, which dissipate energy via microcracking rather than by gross delamination (oriented channel specimen in Fig. 4).

Figures 3 and 4 show the unique tailorability of CST composites for specific system requirements. This fabrication technique, coupled with the behavioral database developed in Ref. 1, also allows property prediction via simple, inexpensive nondestructive evaluation methods. This property prediction is not possible with conventionally prepared CFCMCs.

Significance: CST allows ceramic fiber composites with improved, tailorable, and predictable

mechanical properties to be produced with lower material costs. The importance of CST is that it is dependent strictly on manipulation of the microstructure rather than composition — thus it can be applied to any CFCMC system under development. The process is also adaptable to most commercial CFCMC fabrication processes, including slurry impregnation and chemical vapor infiltration.

Future work in this area includes further property/structure studies and predictive model development.

[Sponsored by ONR]

References

1. T.L. Jessen, "Effect of Microstructural Variability on the Mechanical Behavior of Ceramic Fiber Reinforced Ceramic Matrix Composites," Ph.D. Thesis, Rutgers University, Piscataway, NJ (1995).

2. T.L. Jessen, "Technique for Controllable Mesostructural Development in Continuous Fiber Ceramic Matrix Composites," Application for U.S. Patent, Navy Case No. 77,626 (1996). ■

Micro-Macro Coupling in Solidification Processes

S.P. Marsh
Materials Science and Technology Division

Simulation-based analysis of material processes is a valuable tool for improving the performance and reliability of manufactured components while reducing associated costs and development time. The ability to accurately predict microstructure formation and evolution during materials processing is enhanced by the increased availability of computational resources and improved understanding of the fundamental mechanisms that govern phase transformations and structure formation.

Solidification processing operations, such as casting and welding, involve phenomena that operate over a broad range of length scales. The effects of macroscopic mechanisms, including heat and fluid flows, macrosegregation, and stress/strain development are calculated in discrete simulations using a spatial resolution typically on the order of 10^{-2} to 10^{-3} m. This size scale allows both sufficient detailing of the governing macroscopic fields and reasonable computational times.

Microstructure models, which describe the critical details of evolving material structures, address microscopic and atomic-scale phenomena, including geometrical aspects of evolving phases and defects. These phenomena generally operate at much smaller scales than the resolution of macroscopic simulations and are not amenable to direct numerical calculation over the time and size scales of the overall process. Effective simulation of manufacturing operations requires a bridge between the microscopic and macroscopic phenomena, spanning many orders of magnitude in length scales.

Stereological Modeling: A stereology-based formalism has been developed at NRL that permits incorporation of micromodels into macroscale numerical simulations in a physically consistent manner. Stereological parameters represent spatial densities of geometric properties: common examples include the volume fraction of a given phase V_v and the total surface-area-per-unit volume between two phases S_v. Existing micromodels based on specific morphologies can be translated into an equivalent stereological form, often requiring no more than a simple approximate geometrical model to account for the shapes involved.

The stereological representation of microstructures provides a natural and robust method to bridge the gap in length scales between numerical simulation codes and the microscale phenomena. A unit volume of material is associated with each mesh point in the macroscopic simulation scheme. Macroscopic field variables, such as temperature, serve as global (or average) conditions for each local unit volume. Microstructural models, expressed as simple evolution equations for stereological parameters, are applied to every unit volume over each discrete time step. Calculation of the macroscopic field equations is then performed to determine the local conditions that govern the micromodels over the subsequent time step. This mesoscale approach, linking the microscopic and macroscopic regimes, allows for microstructural gradients on the order of the mesh spacing, consistent with the resolution of the governing macroscopic fields.

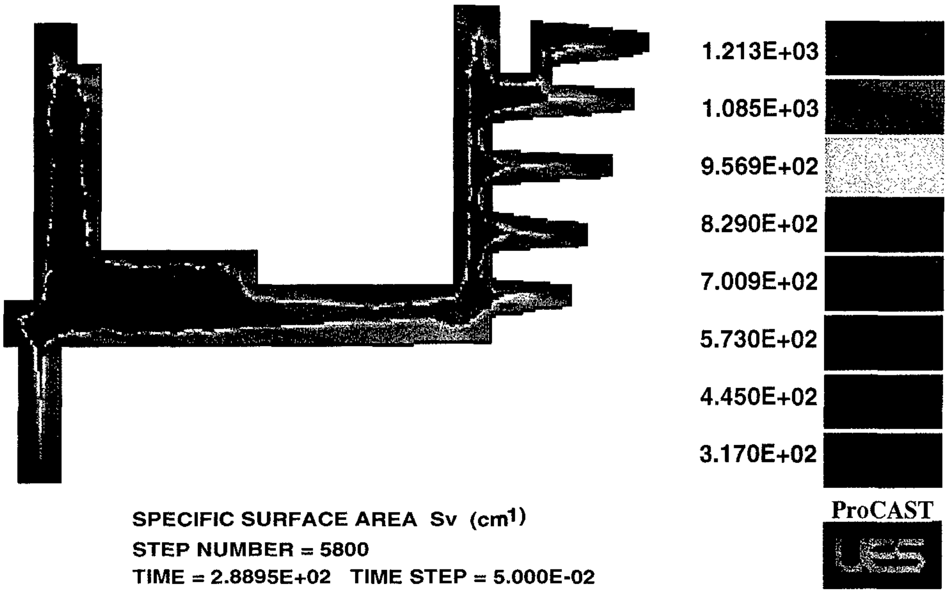

Fig. 5 — Calculated specific surface area S_V for the as-cast structure of an Al-7%Si brake drum casting based on the mesoscale equiaxed solidification model. (Units of S_V in the right-hand scale are cm^{-1}.)

Application to Casting Processes: The mesoscale approach has been used to develop a model for equiaxed dendritic solidification of alloys. A uniform set of stereological descriptors has been used to combine models of nucleation, diffusion-limited growth, temperature-controlled solidification, and structural coarsening. Appropriate transition criteria among these submodels were defined. The entire model was then incorporated into the ProCAST™ simulation code and used to simulate the casting process and resulting microstructure of an Al-7%Si brake drum [1]. Predicted length scales in the casting are shown in Fig. 5. These values agree closely with measured size scales in the casting [2], validating the soundness of the approach and its effectiveness as a predictive tool.

Current Research: The mesoscale approach described here is currently being applied to address the effects of melt convection on solidification phenomena. Specific applications include understanding of flow effects in weld pools, modeling of micro/macro segregation in castings, and prediction of hot tears in honeycomb cast structures. The interaction of interfacial phenomena and flow-fields represents a critical challenge in solidification modeling. The stereology-based approach provides a sound physical and computational basis to address such phenomena, allowing improved design and control of the many manufacturing processes that involve them.

Acknowledgment: The author is grateful to Dilip Banerjee and UES, Inc. for providing access to and assistance with their ProCAST™ simulation code.

[Sponsored by DARPA, ONR, and NASA]

References

1. S.P. Marsh and D. Banerjee, "Micro-Macro Coupling in Casting Simulations," in *Materials Processing in the Computer Age II*, V.R. Voller, S.P. Marsh, and N. El-Kaddah, eds. (The Minerals, Metals and Materials Society, Warrendale, Pa., 1995), pp. 105-116.

2. S.P. Marsh, D. Banerjee, and L.E. Richards, "Stereology-based Modeling and Analysis of Equiaxed Solidification in Casting Simulations," in *Modeling of Casting, Welding and Advanced Solidification Processes VII*, M. Cross and J. Campbell, eds. (The Metallurgical Society, Warrendale, Pa., 1995), pp. 713-720. ■

Three-Dimensional Analysis of Microstructures

G. Spanos, M.V. Kral, and P.G. Moore
Materials Science and Technology Division

An understanding of the three-dimensional (3-D) morphology and distribution of solid-state precipitates is important for control of microstructural evolution and mechanical properties in advanced materials used in a variety of naval and commercial applications. However, conventional optical and electron-microscopy techniques used for microstructural characterization suffer from a serious drawback: results are typically representative of only two-dimensional (2-D) sections. Early studies [1] used serial sectioning in conjunction with optical microscopy to obtain 3-D information, but limited graphical reconstruction methods were employed, and low levels of resolution were available. More recently, serial sectioning techniques in conjunction with scanning electron microscopy and computer-aided reconstruction have been employed to obtain more useful 3-D information [2]. The present research uses serial sectioning techniques supplemented by deep etching to reveal the true 3-D nature of microstructures and thus to provide important new information about the development of solid-state precipitates during the thermomechanical treatment of alloys.

Method: A serial sectioning technique has been developed at NRL that consists of the following iterated steps: incremental polishing through 0.2 µm of material, etching the polished surface, applying fiducial marks with a diamond pyramid microhardness indentor, performing either optical or scanning electron microscopy on selected areas, and using computer techniques to properly align the micrographs from each section. The pyramidal-shaped microhardness indents not only serve as fiducial marks to give the proper registry (translation and rotation) between images in a stack but also provide for a quantitative measure of the depth increments between sections. The series of images are then viewed as both video sequences that "step through" the material slice by slice and as 3-D reconstructions, using advanced computer visualization techniques employing AVS software on a Silicon Graphics Indigo computer. For a limited number of alloy systems, a deep-etching process [3] is also employed to complement the 3-D reconstruction results. With this method, the solid matrix phase is selectively removed by chemical etching, leaving the solid-state precipitates intact for direct observation by scanning electron microscopy. In order to facilitate both techniques, a high purity Fe-1.34 wt. % C-13.1 wt. % Mn alloy has been employed. This alloy was thermally processed in the isothermal heat treatment facility at NRL to produce cementite (Fe_3C) precipitates in an austenite (Fe) matrix. In particular, this alloy system provides for excellent contrast between the cementite and austenite phases for images used in the 3-D reconstruction method, and, during supplementary deep-etching experiments, the austenite matrix is easily preferentially etched away, leaving the cementite precipitates completely intact. Additionally, since cementite is a brittle phase, which when formed in certain morphologies is detrimental to the mechanical properties of alloy steels, the knowledge of its morphological evolution and formation mechanism(s) is important from a practical point of view.

Results: A representative series of nine images taken by optical microscopy at 0.4-µm depth increments is shown in Figs. 6(a) - (i). The cementite phase is in bright contrast while the austenite matrix is gray. In these 2-D sections, the cementite appears to precipitate both *inter*granularly, i.e. on grain or cell boundaries separating austenite grains (austenite "grains" are crystals of austenite within which all of the iron atoms have the same lattice orientation) and *intra*granularly, i.e. inside austenite grains. Some 3-D information can be inferred from such a series of micrographs by tracking the changes in position and shape of the 2-D image of any particular microstructural feature from section to section (particularly by viewing video sequences slicing through such image stacks). Alternatively, the true 3-D microstructure is much more clearly elucidated by combining all of the images into a single 3-D object. Thus, images taken from successive sections at 0.2-µm depth increments were combined and used to reconstruct in 3-D many austenite grains and precipitates. Figure 7 shows one example of a reconstruction from 150 sections of an entire austenite grain and all of the cementite precipitates associated with that grain. In order to facilitate viewing the features within this austenite grain, the top one-half of the grain has been removed in this figure. In addition to revealing "holes" in the grain boundary walls

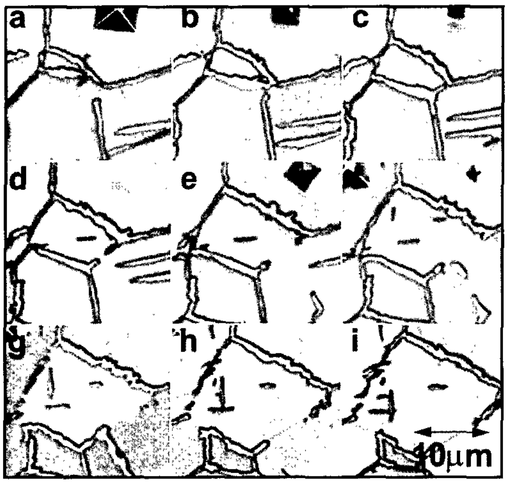

Fig. 6 — A series of optical micrographs of polished and etched sections selected at 0.4-μm depth increments. Cementite appears white and austenite gray.

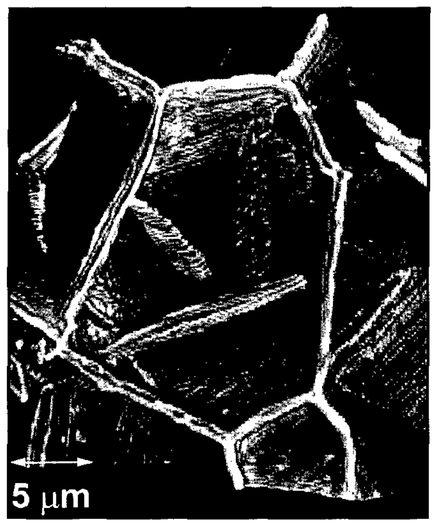

Fig. 7 — A 3-D computer reconstruction of one-half of an austenite grain, showing the coverage of austenite grain boundaries with a cementite film and revealing the 3-D morphology and connectivity of cementite plate and lath-shaped precipitates within the austenite grain. More than 150 sections at 0.2-μm depth increments were used to produce this reconstruction.

that indicate only partial coverage of the austenite grain boundaries by films of cementite, this reconstruction shows elongated lath-shaped (i.e., roughly the shape of a wood lath or a ruler) cementite precipitates within the grain. All of the lath- and plate-shaped cementite precipitates observed in this investigation make contact at some point with the cementite films covering the austenite grain boundaries. Thus, truly *intra*granular cementite precipitates have not been observed in 3-D, in contradiction to what is suggested by observations from 2-D sections. Additionally, at the point of contact between the cementite laths and the cementite film along the austenite grain boundaries, the laths fan out or widen rather than taper down as they enter into the grains. Computer visualization techniques have also allowed these microstructures to be sliced and rotated in 3-D (with documentation on videotape) in order to fully reveal the precipitate and matrix grain shapes and interconnectivities.

To supplement and corroborate the computer-aided 3-D reconstruction results, deeply etched specimens in which the austenite matrix was removed were examined using scanning electron microscopy (which provides for large depths of field) to study the cementite precipitates in 3-D. These studies verify the presence and morphology of the cementite films covering austenite grain boundaries and the cementite laths and plates lying within austenite grains (but making contact with austenite grain boundaries) (see Fig. 8). Deep etching of samples isothermally reacted for shorter times reveals a grain boundary cementite precipitate shape not previously reported: a solid-state fernlike or dendritic morphology (see Fig. 9). At

Fig. 8 — Scanning electron micrograph (SEM) of a single austenite grain in a sample that was isothermally transformed at 650° C for 70 s and then deep etched (to remove the austenite matrix), revealing the cementite grain boundary film structure and cementite sideplates and sidelaths.

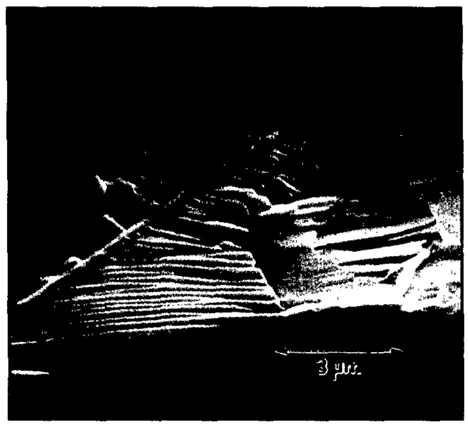

Fig. 9 — SEM micrograph of a sample austenitized at 1100° C, isothermally transformed at 650° C for 10 s and then deep etched. The austenite grain boundaries are partially covered by "fernlike" or "dendritic" cementite precipitates with a central spine and secondary arms.

longer transformation times, these solid-state dendrites grow together, impinge, and overlap, eventually resulting in the contiguous cementite films described earlier.

Conclusions: Serial sectioning and advanced computer visualization techniques, supplemented by deep etching, have been successfully employed to reconstruct microstructures in 3-D and, thus, reveal several new complexities in the morphology and connectivity of cementite precipitates in an Fe-1.34%C-13.1%Mn alloy. Among these findings is the observation that cementite precipitates that appear to form within austenite grains when viewed in a 2-D section are actually revealed by 3-D analyses to be in contact with austenite grain boundaries. A new 3-D morphology not previously categorized under the Dubé morphological classification system has also been reported: solid-state dendrites of cementite formed at austenite grain boundaries. Future plans include extending these studies to ferrite precipitates and other microstructures whose morphologies and distributions are critical in dictating mechanical properties in materials critical to Navy and commercial applications (e.g., in advanced high-strength low-alloy steels).

[Sponsored by ONR/NRL]

References

1. M. Hillert, *The Decomposition of Austenite by Diffusional Processes*, V.F. Zackay and H.I. Aaronson, eds. (Interscience, NY, 1962), pp. 197-237.

2. M.A. Mangan and G.J. Shiflet, *Solid-Solid Phase Transformations*, W.C. Johnson, J.M. Howe, D.E. Laughlin, and W.A. Soffa, eds. (The Minerals, Metals, and Materials Society, Warrendale, 1994), pp. 547-552.

3. M.V. Kral and G. Spanos, "Three Dimensional Morphology of Cementite Precipitates," in press, accepted for publication, *Scripta Materialia* (1996). ■

Metals in Transition Among Metallic, Insulating, and Plasma States

A.N. Mostovych
Plasma Physics Division

At high temperatures and high pressures, there exist regimes where normal metals change from good conductors to insulators as they transition from being a solid to a liquid, plasma, or dense vapor. Good theoretical and experimental understanding of most metals is limited to low temperatures (< 2,000 K), where the metal is in the highly ordered, near-solid-density condensed state, or at very high temperatures (> 10,000 K), where the vaporized low-density metal forms an ideal gas or an ideal plasma. Highly heated conductors in electromagnetic rail guns and in exploding wires or highly shocked metals are examples where this regime may be an issue in military applications. Calculations in the ordered solid phase and the highly disordered gas phase lend themselves to simplifying assumptions, whereas calculations in the liquid phase at elevated temperatures and in the transition liquid-gas, liquid-plasma, and metal-insulator regions are difficult, and there is little experimental data to test the theory. The high-density, high-temperature metals in this special regime can generate pressures in excess of 100,000 atm, making simple experiments impossible.

New techniques that permit controlled dynamic experiments with laser-heated metals have been developed at NRL [1]. Measurements on aluminum samples show a sharp reduction in electrical conductivity and represent the first observations of metal-insulator transitions in aluminum.

Inertial Confinement: To reach the high-density, high-temperature regime, we use a powerful pulsed laser to heat a thin metallic sample but take advantage of inertial confinement to prevent the decompression of the sample during the heating pulse and the time of the experiment. Figure 10 shows the design of our inertial targets and a schematic layout of the experiment. A thin metallic layer is imbedded in the interior of a thick (0.5 mm) substrate of fused quartz and then quickly heated by a laser beam passing through the quartz substrate. In practice, the thin layer of aluminum is only 0.1- to 1.0-μm thick and is vapor-deposited on the fused-quartz substrate. High-quality confinement is ensured by using a fluid gasket of distilled water to completely fill the space between the aluminum layer and the second substrate. The laser is strongly absorbed in the first skin depth of the aluminum layer, heating it to temperatures in the range of 10,000 to 40,000 K. Subsequently, adjoining water layers also ionize and become strongly heated by the laser. This generates a shock wave that quickly pressurizes the target. Heating of

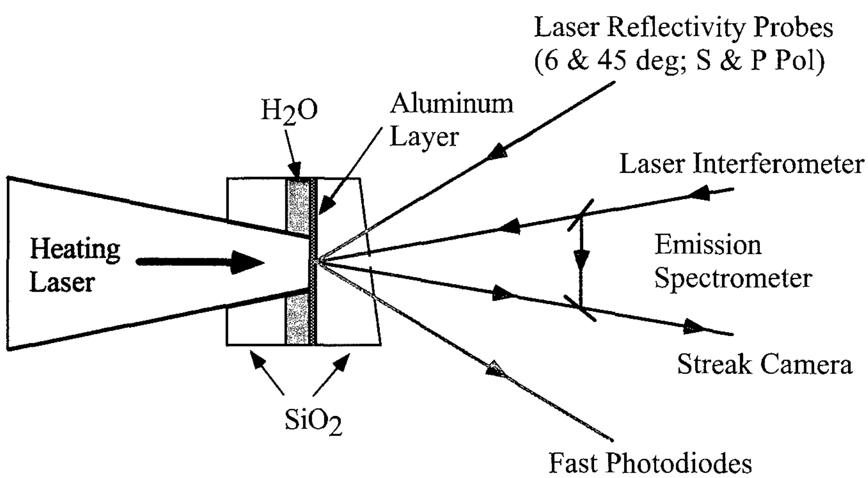

Fig. 10 — Tamped targets and diagnostics. Pulsed laser probes at 6 and 45 degrees measure aluminum layer reflectivity while an absolutely calibrated spectrometer is used to measure the target temperature. Target pressure is inferred from the Al-quartz interface velocity, measured by laser interferometry.

the full aluminum layer occurs by thermal conduction from the very-high-temperature water-aluminum interface.

Diagnostics: The heated aluminum is diagnosed with a multitude of temporally and spatially resolved diagnostics that measure the front (laser-heating side) and rear temperatures, the target pressure, and the reflectivity of the Al-quartz interface. The temperature is determined from the spectral emission from the Al layer. The pressure is deduced from interferometry measurements of the motion of the Al-quartz interface in response to compression of the quartz by the expanding aluminum. For the conditions of this experiment, the temperature at the Al-quartz interface is typically in the range of 3000 to 10,000 K, while the pressure is typically between 30,000 and 100,000 atm.

Conductivity: The small size (0.001 × 1 mm) of the metallic sample and the very short time scales (10^{-8} s) of the experiment make it impractical to measure the electrical conductivity directly. Instead we measure the reflectivity of the hot metal at the Al-quartz interface and take advantage of the property of free electron metals, where the electrical conductivity and the reflectivity of the metal through the high-frequency optical conductivity are related by the Drude conduction model. The reflectivity is measured with a set of 0.527-µm laser probes, which are focused and reflected from the target at 6 and 45 degrees with S and P polarizations. The rear surface of the target is wedged to prevent interference from multiple reflections from the rear surface of the quartz substrate.

Figure 11 displays the measured conductivity values along with predictions of various theoretical models. At low temperatures (~ 3000 K), the measured conductivity is in agreement with standard liquid-metal calculations and lies on the curve (solid line) extrapolated from tabulated conductivities of liquid aluminum from near the melting point. At higher temperatures, the conductivity falls sharply, substantially deviating from current theory, and enters a region associated with a minimum metallic conductivity and the transition between metallic and insulating states [2].

Summary: We have made the first measurements of the electrical conductivity of high-temperature, high-density aluminum in the vicinity of the metal-insulator transition. Comparisons to

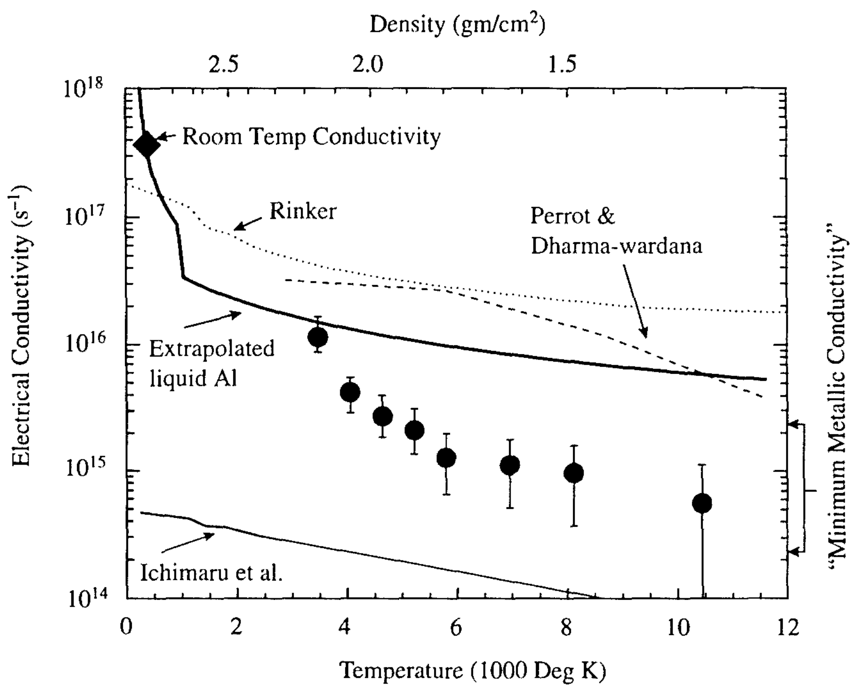

Fig. 11 — Electrical conductivity of heated aluminum as a function of temperature and density. Above 3000 K, the conductivity falls sharply and enters a region associated with the metal-insulator transition and "minimum metallic conductivity" [2].

several theoretical calculations [3,4,5] find major order-of-magnitude disagreements between theory and experiment. This work suggests anomalous behavior for any electrical discharges where the current-carrying conductors are heated beyond the melting point. These new data may explain previous anomalies in rail gun experiments, where high-velocity objectives could not be reached.

[Sponsored by ONR]

References

1. A.N. Mostovych and Y. Chan, "Reflective Probing of the Electrical Conductivity of Hot Aluminum in the Solid, Liquid, and Plasma Phases," submitted to *Phys. Rev. Lett.*

2. N.F. Mott, *Metal-Insulator Transitions* (Taylor & Francis, New York, 1990).

3. G.A. Rinker, "Electrical Conductivity of a Strongly Coupled Plasma," *Phys. Rev.* **B31**, 4207 (1985).

4. F. Perrot and M.W.C. Dharma-Wardona, "Equation of State and Transport Properties of an Interacting Multispecies Plasma: Application to a Multiply Ionized Al Plasma," *Phys. Rev.* **E52**, 5352 (1995).

5. H. Kitamura and S. Ichimaru, "Electrical and Thermal Resistivities in Dense High-Z Plasmas," *Phys. Rev.* **E51**, 6004 (1995). ■

Self-assembled Semiconductor Quantum Dots

B.R. Bennett, B.V. Shanabrook,
R. Magno, and E.R. Glaser
Electronics Science and Technology Division

Over the past 20 years, significant advances have been made in semiconductor electronic and opto-electronic devices by confining electrons in a two-dimensional structure known as a quantum well. Solid-state lasers used today for fiber-optic transmission are an important example of the application of quantum wells in the InGaAsP materials system. Recently, there has been considerable interest in the potential for structures in which electrons and holes are confined in all three dimensions: so-called quantum dots (QDs). The formation of uniform QDs with sufficiently small dimensions (< 50 nm), however, is often beyond the limits of state-of-the-art lithographic techniques.

We have produced QDs without lithography by taking advantage of a naturally occurring epitaxial growth process. This was achieved by depositing thin layers of semiconductors including GaSb, AlSb, and InSb on reconstructed GaAs surfaces. The large difference in lattice constants (7% to 15%) results in the initial formation of a two-dimensional wetting layer, followed by the growth of three-dimensional coherent islands, known as self-assembled QDs.

Growth: We grew samples by solid-source molecular beam epitaxy (MBE) on GaAs(001) substrates. In the MBE growth process, furnaces loaded with Ga, In, Al, As, and Sb are placed in a high-vacuum environment so that beams of atoms (or molecules) emitted from the furnace can impinge on a substrate target and form a semiconductor film. The quality of the QDs depends on the temperature of the substrate during growth, the deposition rate, and the atomic structure of the GaAs surface as determined by its reconstruction. The first step involves preparing a high-quality GaAs surface by growing a 1.0-μm thick GaAs buffer layer at 580° C. Reflection high-energy electron diffraction (RHEED) is used at various stages of the growth to determine the nature of the surface. During the GaAs buffer growth, the RHEED pattern is a streaky (2 × 4) surface reconstruction, indicating that the surface is flat on a molecular scale over lateral dimensions of hundreds of nanometers. At this stage, there is no evidence of transmission spots resulting from three-dimensional islands. Before the growth of the QDs, a 450-s growth interrupt under an As_4 flux is performed and results in sharp diffraction spots along each streak, indicating the formation of large islands. The substrate temperature is then reduced, and the antimonide layer is grown.

As an example, we consider the growth of InSb on GaAs. InSb has a small band gap (0.18 eV at 300 K) and a lattice constant of 0.6479 nm, which is 15% larger than GaAs. During cool-down before the antimonide growth, the RHEED pattern transforms to a centered (4 × 4) reconstruction. After deposition of 1.5-2.0 monolayers (ML) of InSb at 400° C, chevrons and/or transmission spots appear, indicating three-dimensional (QD) growth [1].

Atomic-Force Microscopy: Samples were characterized by atomic-force microscopy (AFM), a technique in which atomic-scale morphology is imaged by detecting the deflection of a microscopic cantilever as it is passed across a surface. AFM scans of our standard GaAs buffer layer reveal 3 Å monolayer steps with a spacing of a few hundred nanometers. The surface remains relatively flat (rms roughness ≅ 1 Å) after depositing 1 ML of InSb at 400° C. After 2 ML, however, isolated QDs are found with a density of about 2×10^9/cm^2, as shown in Fig. 12. Dot heights and diameters are 53 ± 6 Å and 500 ± 80 Å, respectively. Growth of thicker films of InSb (e.g., 4 ML) results in the formation of strain-relieving misfit dislocations within QDs and the coalescence of QDs [1].

Raman Spectroscopy: The small size of the QDs requires unique tools to analyze their chemical composition. We have found that Raman spectroscopy (RS) is useful for this [2]. Raman spectra for four samples are shown in Fig. 13. Sample A consists of a homoepitaxial GaAs layer without QDs; it has a prominent peak at 295 cm^{-1} due to the GaAs longitudinal-optic (LO) phonon and a second weak peak at 271 cm^{-1} due to the GaAs transverse-optic (TO) phonon. Sample B was grown by depositing 3 ML GaSb on GaAs, resulting in 10^{10}/cm^2 QDs with height = 32 ± 9 Å and diameter = 280 ± 40 Å. In addition to the GaAs LO and TO modes, a third peak is observed at 234 cm^{-1}. Because its energy lies between the energies of the LO (238 cm^{-1}) and TO (228 cm^{-1}) phonons in bulk GaSb, we attribute it to vibrational excitations in the GaSb QDs. An AlSb sample, C, was prepared by depositing 4 ML of AlSb on GaAs, and its spectrum exhibits additional scattering at 226 and 331 cm^{-1}. While the high-energy peak in C, which lies between the LO (344 cm^{-1}) and TO (323 cm^{-1}) modes for bulk AlSb, is expected for AlSb QDs, the peak at 226 cm^{-1} is not. This low-energy peak is 8 cm^{-1} below the mode attributed to phonons in GaSb QDs in sample B. Because of the similarity of this two-peak structure to the two-mode behavior observed in the vibrational properties of bulk AlGaSb alloys, we propose that the two peaks represent the two-mode behavior of phonons in $Al_xGa_{1-x}Sb$ QDs. Presumably the alloyed QDs result from Ga segregation from the buffer layer into the AlSb quantum dots during growth. This hypothesis is confirmed by sample D, which is identical to C except that 5 ML AlAs are inserted between the AlSb and the GaAs buffer. The RS spectrum for sample D does not contain a GaSb-like peak near 226 cm^{-1}, indicating the absence of Ga in the QDs. The 5 ML AlAs apparently acts as a barrier, preventing Ga segregation into the AlSb layer. The AlSb-like peak moved to a higher energy (338 cm^{-1}), consistent with a higher AlSb mole fraction.

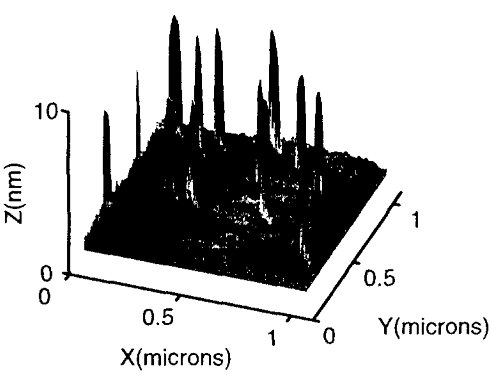

Fig. 12 — Atomic force microscopy image of surface after growth of two monolayers of InSb on GaAs. Self-assembled quantum dots are visible.

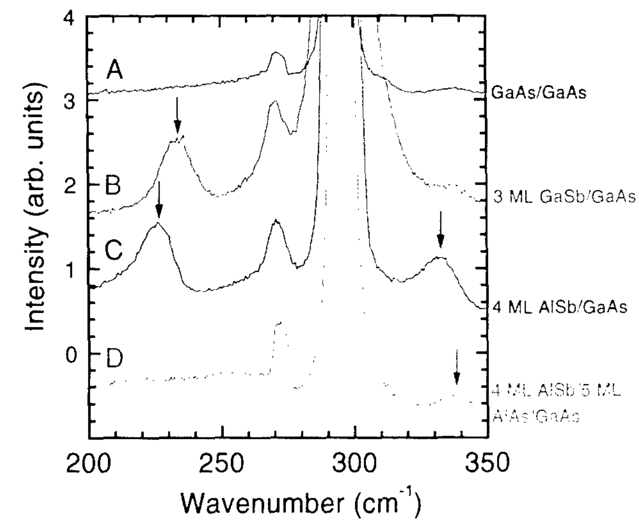

Fig. 13 — Low-temperature Raman spectra for four samples. Scattering attributed to quantum dots is indicated with arrows.

Photoluminescence: Samples used for photoluminescence (PL) studies were grown with the procedures described above except that QD growth was followed by deposition of a GaAs-capping layer. The InSb and GaSb QDs exhibit strong luminescence at 1.13 and 1.16 eV, respectively [3]. The PL peaks occur at energies much larger than the low-temperature bulk InSb (0.24 eV) and GaSb (0.81 eV) band gaps. To understand the origin of the emission, we grew additional samples in which GaSb QDs were clad by $Al_xGa_{1-x}As$. The results,

shown in Fig. 14(a), indicate a shift of QD PL to higher energies with increasing AlAs mole fraction. The shift of 80 meV per 10% AlAs mole fraction is in agreement with an estimate from a type-II band-alignment model. As illustrated in Fig. 14(b), the PL results from the recombination of electrons in the (Al)GaAs cladding layers with holes in the GaSb QDs.

These results aid in understanding the fundamental growth processes involved in the formation of self-assembled quantum dots. This represents an important step toward the goal of 21st century Navy applications, including lasers and electronic devices such as memories based upon single-electron tunneling.

[Sponsored by ONR]

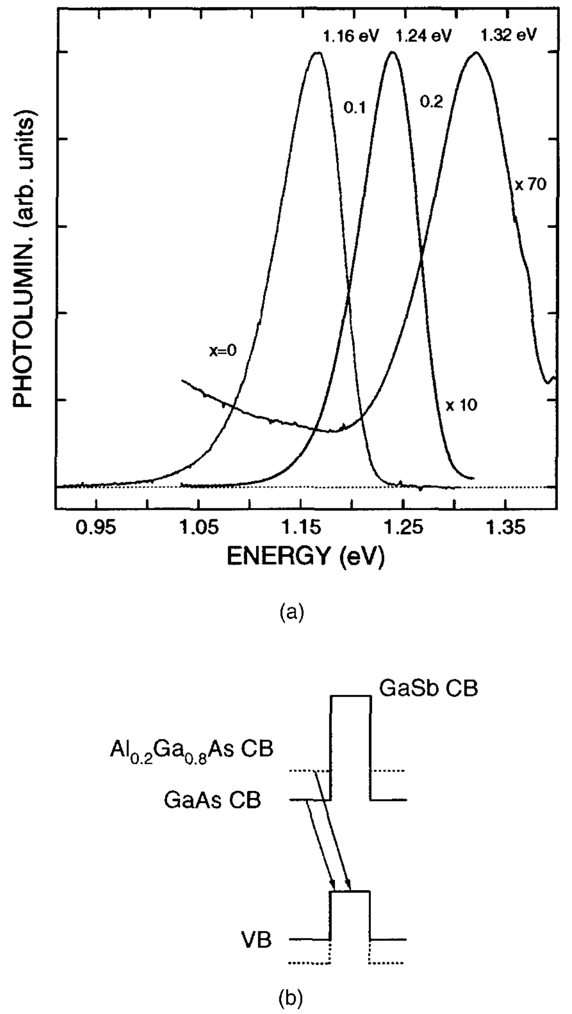

Fig. 14 — (a) Low-temperature photoluminescence for samples consisting of three monolayers of GaSb clad by $Al_xGa_{1-x}As$; and (b) band structure diagram illustrating recombination of electrons in the (Al)GaAs with holes in the GaSb quantum dots.

References

1. B.R. Bennett, R. Magno, and B.V. Shanabrook, "Molecular Beam Epitaxial Growth of InSb, GaSb, and AlSb Nanometer-Scale Dots on GaAs," *Appl. Phys. Lett.* **68**, 505 (1996).

2. B.R. Bennett, B.V. Shanabrook, and R. Magno, "Phonons in Self-assembled (In,Ga,Al)Sb Quantum Dots," *Appl. Phys. Lett.* **68**, 958 (1996).

3. E.R. Glaser, B.R. Bennett, B.V. Shanabrook, and R. Magno, "Photoluminescence Studies of Self-assembled InSb, GaSb, and AlSb Quantum Dot Heterostructures," *Appl. Phys. Lett.* **68**, 3614 (1996). ■

GaN Growth and Characterization for High-Power Device Applications

A.E. Wickenden, D.D. Koleske, R.L. Henry, and J.A. Freitas, Jr.
Electronics Science and Technology Division

The growth of Group III nitride semiconductors, including InN (E_{gap} = 2.0 eV), GaN (E_{gap} = 3.4 eV), and AlN (E_{gap} = 6.0 eV), is the subject of active research in the Naval Research Laboratory's Electronics Science and Technology Division (ESTD). Applications for these wide-bandgap materials range from optical communications and storage to high-speed and high-temperature electronic devices. The ultimate objective of the ESTD wide-bandgap effort is to develop classes of high-speed and high-power integrated-circuit devices for Navy needs, which include instrumentation and controls in harsh and high-temperature environments, microwave radar transmitters, and shipboard power handling. The initial challenge is to achieve a fundamental understanding of the growth of these materials, which facilitates controllable and reproducible growth of electronic device structures.

Growth of Device Structures: The wide-bandgap material GaN is of interest due to its large breakdown field and low charge-carrier thermal-generation rate. Due to the extreme difficulties in the growth of bulk GaN, sapphire is typically used as a substrate for the heteroepitaxial growth of

GaN thin films. The large mismatch in both lattice constant and thermal expansion coefficient between the two materials leads to large strains in the films, which are relieved by the formation of threading defects during the growth process. In addition, the incongruent decomposition of GaN at the temperatures required for thin-film deposition leads to difficulties in achieving stoichiometric growth, and nitrogen vacancies in the GaN lattice may serve to make the film *n*-type. Thick, highly resistive buffer layers are required to separate the silicon (Si)-doped *n*-type channel layer from the highly defective GaN/sapphire interface. NRL is the first to have achieved consistent growth of highly resistive GaN with low compensation levels, using the established metal-organic vapor-phase epitaxy (MOVPE) capability within the ESTD. Field effect transistor (FET) device structures that include a high mobility, Si-doped GaN channel layer ($n = 2 \times 10^{17}$ cm^{-3}, $\mu = 600$ cm^{2}V^{-1} s^{-1}) on a highly resistive buffer layer have been successfully grown.

Characterization of GaN Films: NRL's highly resistive GaN films grown without added dopant have breakdown voltages in excess of 1200 V. The ability to grow high-mobility conductive films by intentionally doping suggests that the resistivity of the unintentionally doped GaN film is not due to heavy compensation by acceptor impurities or defects. Low-temperature photoluminescence (PL) spectra of Si-doped and highly resistive unintentionally doped GaN films are shown in Fig. 15. The inset of the figure shows the high-resolution near-bandedge spectra of both films. The emission bands observed in the highly resistive film are attributed to free exciton recombination, where the lower energy emission peak of the Si-doped film is due to the annihilation of excitons bound to neutral Si donors [1]. The dominance of free-exciton recombination in the spectra of highly resistive films, as well as the presence of very weak emission bands from donor-acceptor pair recombination processes, supports the assumption of low defect or impurity compensation in the films. An interesting feature is the weak, 3 eV emission band that we typically see only in our highly resistive films. This spectral feature may be related to the highly resistive character of the films and is the subject of current PL and optically detected magnetic resonance (ODMR) investigations.

Variable-temperature Hall-transport measurements, illustrated in Fig. 16, have been made on films with very low intentional silicon-doping levels and suggest a compensation ratio < 30%, with a resulting background of compensating centers < 10^{16} cm^{-3}. A secondary ion mass spectroscopy (SIMS) depth profile of the Si concentration of a 3-µm thick Si-doped film grown on an undoped buffer layer, illustrated in Fig. 17, indicates that the Si incorporation is well controlled through the depth of the intentionally doped region of the film and that a sharp interface exists between the

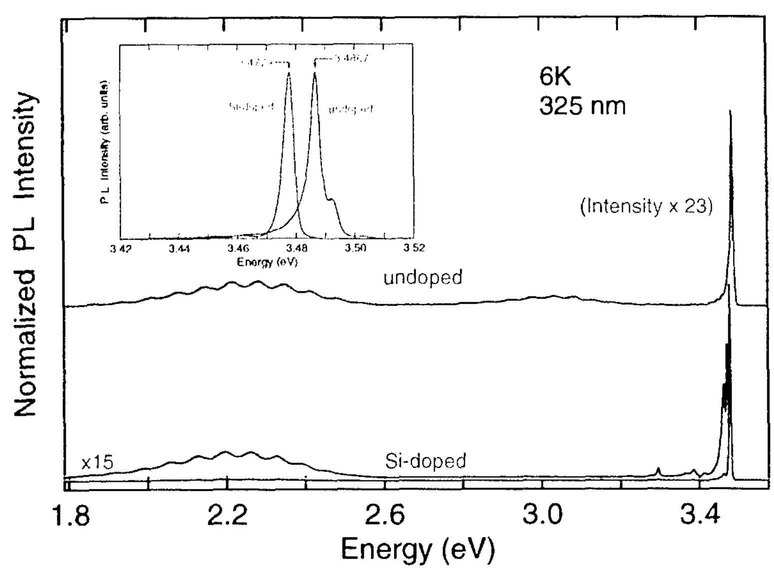

Fig. 15 — Low-temperature photoluminescence spectra of Si-doped and unintentionally doped GaN films. The inset shows the high-resolution near-bandedge spectra of both films.

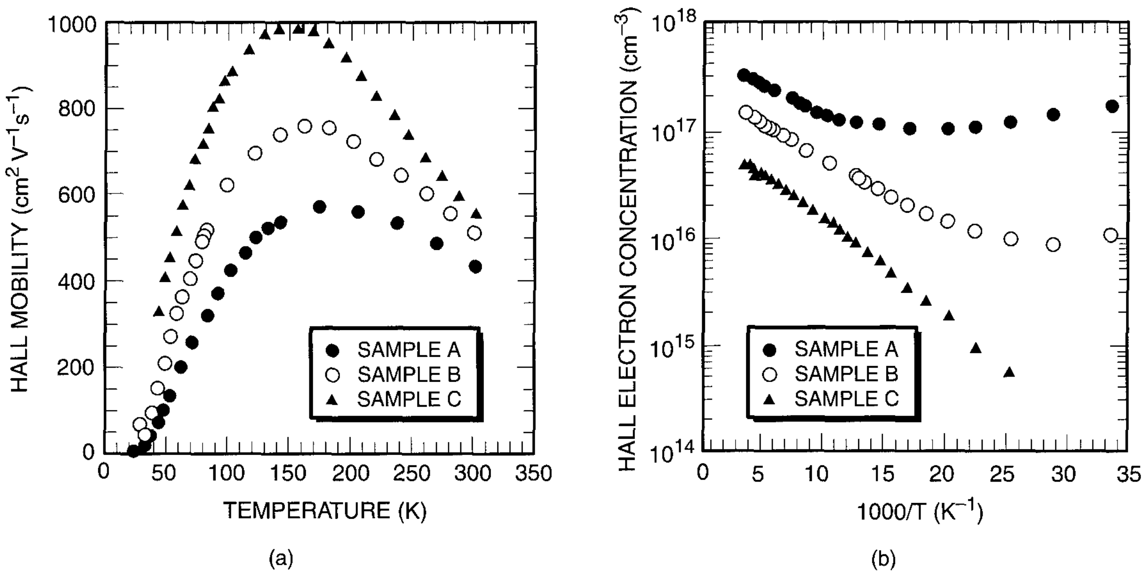

Fig. 16 — (a) Hall mobility vs temperature and (b) Hall electron concentration vs 1000/T for GaN films with varying levels of Si dopant incorporated during growth.

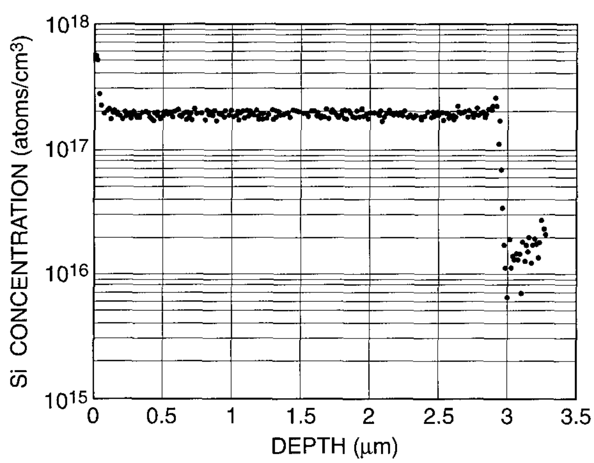

Fig. 17 — SIMS profile of ^{28}Si atomic concentration as a function of depth for a Si-doped GaN film grown on a highly resistive GaN layer.

Si-doped channel layer and the highly resistive buffer layer. These are essential features of a FET structure. The SIMS profile also shows that the Si concentration in the region of the film with no intentionally added dopant is below the SIMS experimental resolution limit of 2×10^{16} cm^{-3}.

High-resolution seven-crystal X-ray diffraction has been employed to characterize the structure of the highly resistive and Si-doped GaN films, as well as the sapphire substrate beneath the films [2]. Figure 18 is a map of the ω- (related to in-plane lattice disorder) and ω/2θ- (related to variation of c-axis lattice spacing) X-ray rocking curves (RC) for a high-mobility Si-doped GaN film and its underlying sapphire substrate. These data show that little variation in lattice spacing occurs in the direction normal to the film, implying that the films are relatively unstrained in this direction. Mosaic structure or curvature, causing in-plane lattice disorder, is known to be present in the GaN film due to low-angle grain boundaries induced by the heteroepitaxial growth. This is evidenced in the broad

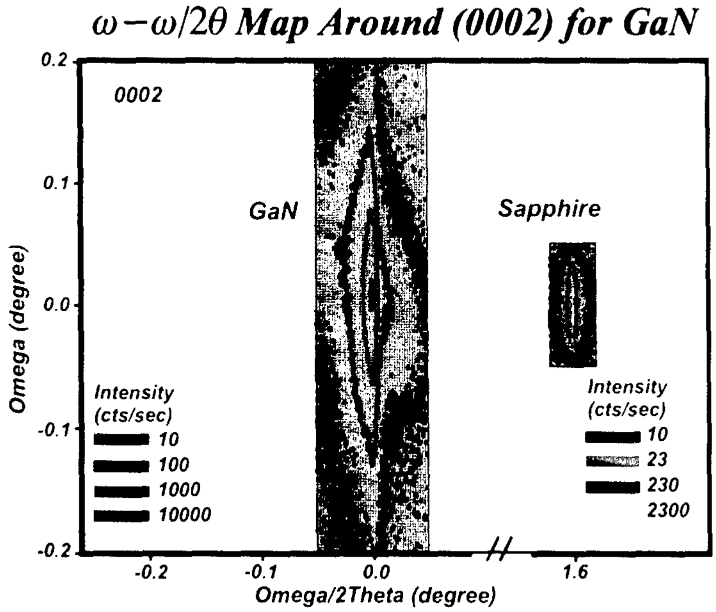

Fig. 18 — High-resolution seven-crystal X-ray rocking-curve map of a high-mobility Si-doped GaN film. The inset shows the map of the underlying sapphire substrate on the same angular scale.

$\omega/2\theta$ – RC of the GaN and is seen to have been introduced into the sapphire substrate due to the presence of the film. We have also observed an increase in diffuse scatter in the $\omega/2\theta$ – RC of a Si-doped GaN film relative to that of a highly resistive film and a related reduction in the full-width, half-maximum of the ω – RC of the Si-doped film. This may suggest that the presence of the Si impurity in the lattice may "pin" the threading dislocations or otherwise influence the degree or type of defect formation in the film, resulting in a slightly more strained film with slightly less mosaic structure.

Summary: Researchers in the ESTD are the first to have controllably grown high-quality, highly resistive films of GaN, which have been doped to form high-mobility channel layers for FET device structures. The materials improvements are of value for improved transconductance, pinch-off characteristics, and frequency response in high-speed GaN devices. Characterization techniques have been used to determine that the films exhibit very low levels of impurity compensation and may be near stoichiometric due to optimization of growth parameters. Growth models are being developed within the ESTD to allow more controlled, reproducible growth of GaN and related alloys [3]. Plans for the ESTD's III-nitride growth effort include the growth of alloyed nitride films for high-electron mobility transistor device structures, other high-power device structures, and novel optical and field-emission device structures.

Acknowledgments: We thank Dr. W.B. Alexander, ASEE Postdoctoral Research Associate, for seven-crystal X-ray experiments. Dr. D.S. Simons and Dr. P.H. Chi, National Institute of Standards and Technology, for SIMS analysis. Dr. D.K. Gaskill, for assistance on variable temperature Hall transport measurements. Mr. S.C. Binari, for device design, fabrication, and characterization, and Dr. E.R. Glaser and Dr. T.A. Kennedy, Jr., for ODMR studies.

[Sponsored by ONR]

References

1. J.A. Freitas, Jr., K. Doverspike, and A.E. Wickenden, "Excitonic Recombination Processes in Undoped and Doped Wurtzite GaN Films Deposited on Sapphire Substrates," in *Gallium Nitride and Related Materials*, Mat. Res. Soc. Symp. Proc. Vol. 395, p. 485-490 (1996).

2. A.E. Wickenden, W.B. Alexander, D.D. Koleske, and J.A. Freitas, Jr., "The Influence of Strain and Mosaic Structure on Electrical and Optical Properties of GaN Films on Sapphire Substrates," *J. Crystal Growth* **5486** (1996) (in press).

3. D.D. Koleske, "GaN Growth Mechanism Formulated to Explain the Large V/III Flux Ratio Used in MOVPE Growth," submitted to *Appl. Phys. Lett.* (1996). ■

Effect of Radiation on Buried Oxides in Silicon-on-Insulator Structures

B.J. Mrstik,[1] P.J. McMarr,[2] H.L. Hughes,[1] and R.K. Lawrence[3]
[1]*Electronics Science and Technology Division*
[2]*SFA, Inc.*
[3]*ARACOR/SFA*

Silicon-on-insulator (SOI) material, which consists of a thin layer of device quality Si on an insulator, has several advantages over bulk Si as substrates for electronic devices. For commercial application, these advantages include the capability of making devices that operate at higher speed and lower power consumption and have higher packing density. SOI material is especially important to the Department of Defense requirements for electronics usable in a radiation environment (including space) because devices fabricated on SOI substrates are 100 times less susceptible to single event upset, which can occur when a charged particle passes through the active layer of a device. The insulating layer of the SOI material can, however, trap charge produced by ionizing radiation. This trapped charge adversely affects device performance by shifting the threshold voltage of the devices. We have been studying the basic mechanisms involved with charge trapping in the SOI insulating layer.

Currently, the two most promising types of SOI material are SIMOX (separation by implantation of oxygen) and wafer-bonded material (BESOI). SIMOX material is formed by implanting a large dose of high-energy (~180 keV) oxygen ions into a Si substrate to form a layer of buried oxide (BOX). After implantation, the material is heated above 1300° C to remove oxygen from the top Si layer. The fabrication method is shown in Fig. 19, which also shows how the material is used to make devices. Wafer-bonded material is fabricated by bonding an oxidized Si wafer to another Si wafer. Strongest bonding occurs at temperatures exceeding 1050° C. After bonding, one of the Si wafers is thinned either by etching or by a controlled cracking process. For both these types of SOI material, the BOX is subjected to high temperatures while confined between Si layers, and, therefore, can be expected to have properties different than thermally grown SiO_2.

Approach: The radiation response of various SIMOX, wafer-bonded SOI, and thermal oxides were measured and correlated with their structural parameters. The radiation response was determined by removing the top Si layer and evaporating Al dots on the exposed oxide to form capacitors. The capacitors were irradiated with 10 keV X rays to a dose of 1 Mrad (SiO_2), while the Al was positively biased so as to maintain a 1 MV/cm field across the oxide. The radiation-induced shift in the flatband voltage ΔV_f was then measured.

The structure of the oxide was determined by using spectroscopic ellipsometry (SE) to determine the optical properties of the BOX/Si substrate structure from 280 nm to 780 nm. The optical properties are described in terms of tanΨ and Δ, the magnitude and phase of the complex reflection coefficient, respectively. The structure of the oxide can be determined by comparing the measured values of Ψ and Δ with values calculated for various trial structures. In this way, it was determined that the BOX consists of a densified form of fused SiO_2, where the density depends on how the BOX is fabricated. Figure 20 shows typical SE data. For

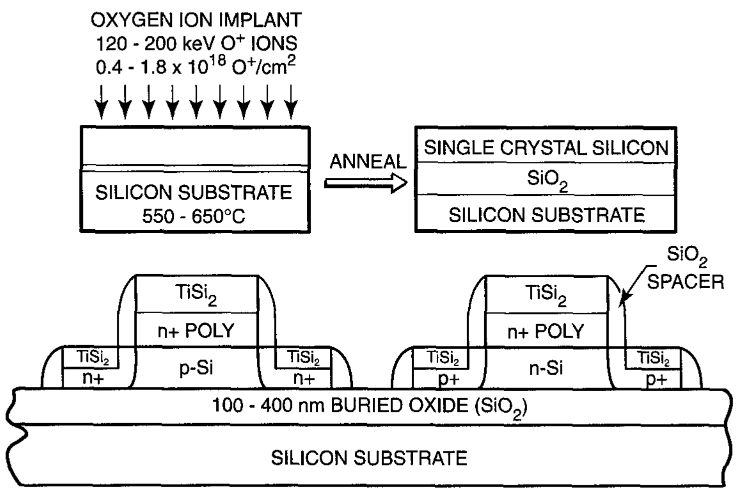

Fig. 19 — Top panel shows process steps used to fabricate SIMOX material. Lower panel shows how SIMOX material is used as a substrate for electronic devices.

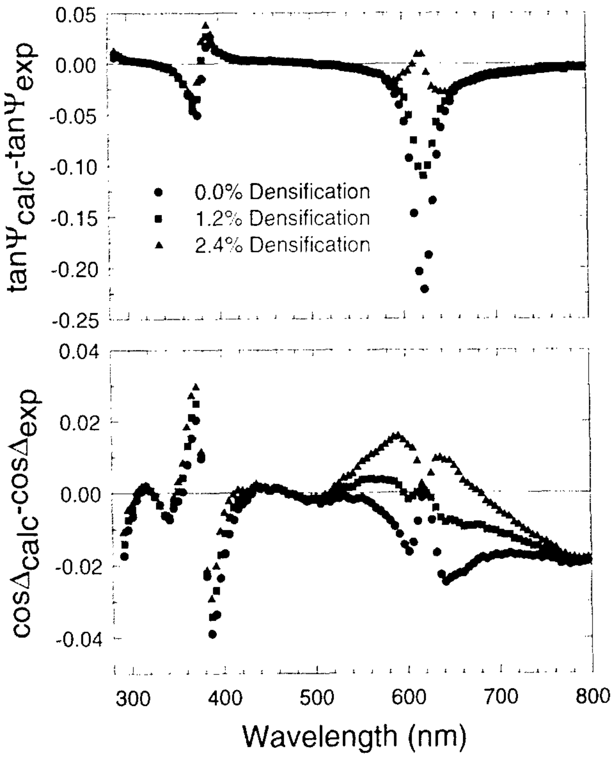

Fig. 20 — Differences between the calculated and experimentally determined values of the spectroscopic ellipsometry parameters tanΨ and cosΔ for an oxide approximately 400-nm thick on a silicon substrate. The calculated values are obtained by assuming that the oxide is densified by either 0.0%, 1.2%, or 2.4%.

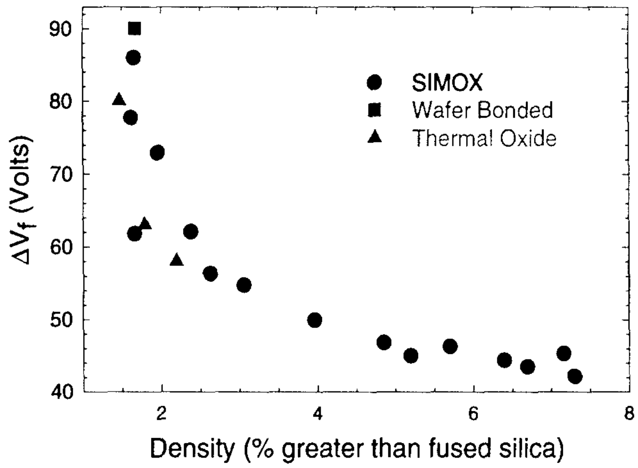

Fig. 21 — Relationship between the radiation response of an oxide and the density of the oxide; values for SIMOX, wafer-bonded SOI, and thermal oxides are shown.

this oxide, deviations between calculated and measured values of Ψ and Δ are minimized by describing the oxide as fused silica densified by about 2.4%.

Results: Figure 21 shows that a clear relationship exists between the radiation response (expressed in terms of ΔV_f) and the density of the BOX of the SIMOX and wafer-bonded SOI samples. The samples shown have BOX thickness ranging from 377 nm to 436 nm, so the values of ΔV_f were normalized to a BOX thickness of 430 nm. The strong dependence of ΔV_f on BOX density is surprising because of the wide variety of conditions that were used to form the SOI material. Even the SIMOX samples were prepared using diverse fabrication conditions, including the use of single and multiple oxygen implantation steps (with a high-temperature anneal between each implant) and the use of "supplemental" oxygen implants, in which a small amount of additional oxygen is implanted after the high temperature anneal.

The broad range of densities observed for the SOI BOX indicates that the size of the Si-O-Si rings in the amorphous oxide can be modified by the fabrication conditions. The results shown in Fig. 21 suggest that the larger rings (corresponding to lower-density oxides) are more prone to breaking and capturing radiation-induced holes during exposure to radiation. To determine whether the radiation response of thermal oxides also depends on the oxide density, we modified the density of thermally grown oxides by using various heat treatments similar to those to which SOI BOX is subjected during fabrication and measured their density and radiation response. The results for these ~ 400-nm thick oxides are shown by the green triangles in Fig. 21. Although these oxides have a smaller range of densities, their radiation response appears to have the same dependence on oxide density as the SOI oxides.

For thermal oxides it is well accepted that the charge trapping occurs at oxygen vacancy defects (the E′ centers, which, before irradiation, are Si atoms bonded to other Si atoms rather than to O atoms). The apparent dependence of hole trapping on oxide density observed here in SOI as well as in thermal oxides was therefore unexpected. Work is continuing on this project to understand how a macroscopic property (density) influences the presence of microscopic defects. The results have already been successfully applied to the development of SIMOX substrates for radiation hard Si devices.

[Sponsored by Defense Special Weapons Agency] ■

Ocean and Atmospheric Science and Technology

Carbon-Dioxide Exchange at the Air/Sea Interface

R.A. Handler, J.R. Saylor,† and R.I. Leighton
Remote Sensing Division
†*NRC/NRL Cooperative Research Associate*

The oceans that cover the Earth's surface have an enormous capacity to absorb heat and dissolved gases. Accordingly, the rate at which heat and mass are transferred across the air/sea interface greatly affects the weather, as well as the long-term status of the environment. Waves play an important role in this transfer process.

Recent concern over global warming has focused attention on greenhouse gases and the transfer of these gases between the air and sea. In the present work, we study the effect of small-scale waves on the transfer of carbon dioxide. CO_2 was chosen for study because of its importance as a greenhouse gas and because of the ease with which it can be measured. Our results are applicable also to the transfer of heat as well as other dissolved gases and have potential applications in developing improved air/sea transport models.

Capillary Waves: It has been suspected for some time that capillary waves (waves having a wavelength $\lambda < 1$ cm) can significantly enhance the transfer of heat and mass through the air/sea interface. On the ocean surface, capillary waves frequently take the form of parasitic capillary waves, which develop on the leading edge of larger gravity waves. A recent three-dimensional simulation by our group (Fig. 1) demonstrates the formation of these capillary waves, with wavelengths from 3 mm to 7 mm on the leading edge of a gravity wave having a wavelength of about 8 cm.

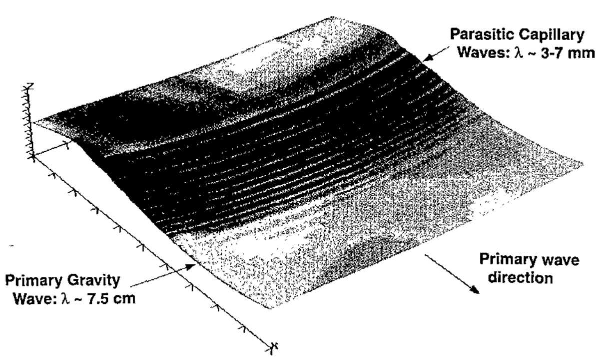

Fig. 1 — Three-dimensional simulation of parasitic capillary waves on the face of a gravity wave.

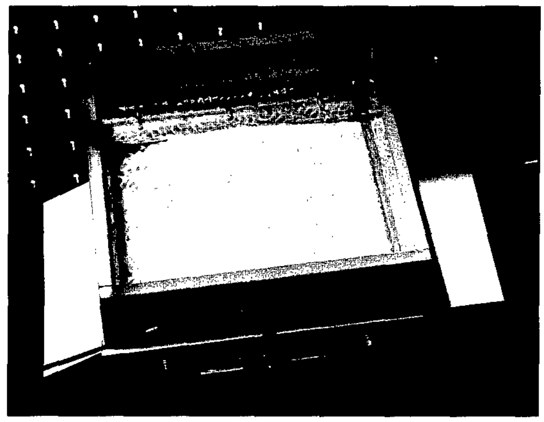

Fig. 2 — Capillary waves generated by vibrating a small water tank at a frequency of 88 Hz. The water has been dyed green to increase the visibility of the waves in this photograph.

These capillary waves are ubiquitous on the ocean surface and are suspected to be important enhancers of heat and mass transfer across the air/sea interface. They are also effective scatterers of microwave radiation, making them important in potential applications such as the remote sensing of high flux regions on the ocean surface.

Isolating Capillary Waves: The ocean surface presents a complicated environment for studying waves because of the large number of phenomena that occur there (turbulence, wave breaking, aerosol generation, etc.). At the NRL Free Surface Hydrodynamics Laboratory, we avoid these problems by isolating capillary waves from all other factors that might affect gas transfer rates. Specifically, we generate capillary waves by vibrating a small tank of water in the vertical direction at a chosen frequency. Figure 2 shows a photograph of a 5 in. × 5 in. tank of water, vibrated at a frequency of 88 Hz. Capillary waves ($\lambda \cong 6$ mm) are readily visible on the surface of the water. These waves are called Faraday waves and provide an excellent platform for studying the parasitic capillary waves that occur naturally on the ocean surface.

Measurement Configuration: Figure 3 schematically shows the facility used to study capillary waves. At the beginning of each experiment, water that has been saturated with CO_2 is poured into the tank. The tank is mounted on an electrodynamic shaker that provides the necessary vertical vibrations. The concentration of CO_2 in the water is monitored by continuously measuring

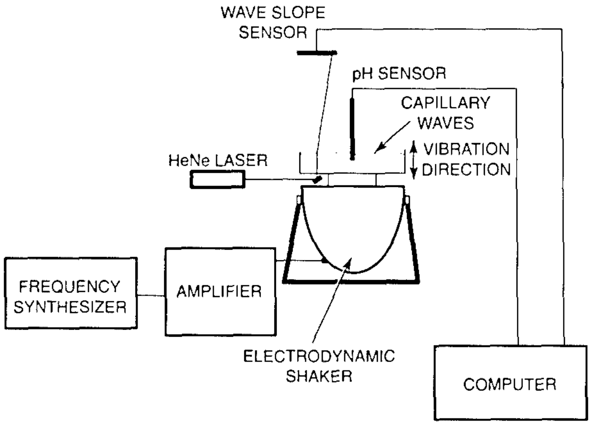

Fig. 3 — Illustration of experimental setup used to study capillary waves.

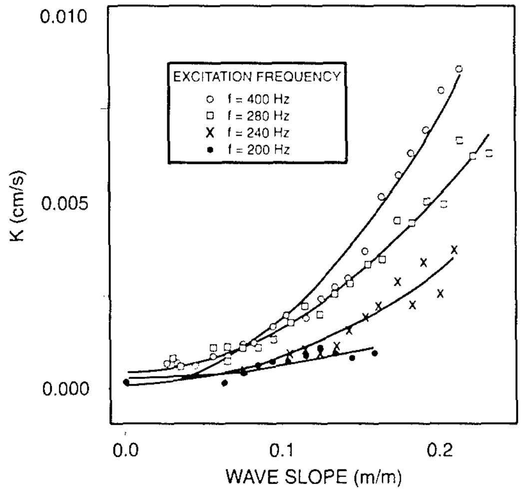

Fig. 5 — Plots of the mass transfer coefficient K vs the average wave slope. Data are provided at f = 400 Hz, 280 Hz, 240 Hz, and 200 Hz, which correspond to wavelengths of 2.3, 2.9, 3.2, and 3.6 mm. The solid lines are second-order polynomial fits to the data.

the pH, which is readily converted to CO_2 concentration. A mass transfer coefficient K, which is a measure of how rapidly CO_2 is transported out of the water, is obtained from the CO_2 concentration vs time data. Figure 4 gives sample time traces of CO_2 concentration for experimental runs at f = 400 Hz. The time traces that show a more rapid decrease in CO_2 concentration represent runs for which K is larger.

We have postulated that the steeper the wave is (i.e., the higher the amplitude of the wave), the larger K will be. Referring again to Fig. 3, the wave slope is measured by directing a laser beam through the transparent tank floor. As the beam travels through the air/water interface, it is refracted in a way that is determined by the wave slope. Data obtained from a detector that senses the laser light spot on the air side of the air/water interface are used to continuously monitor wave slope.

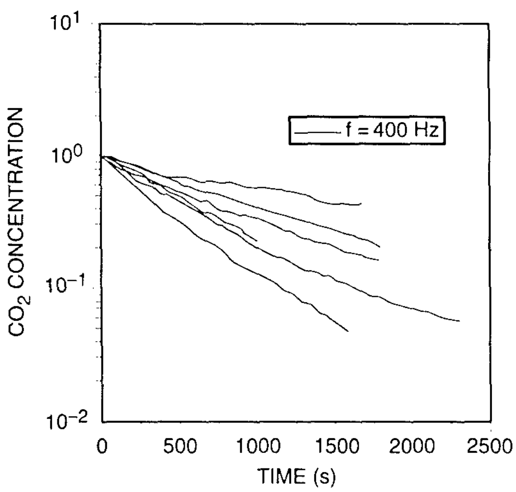

Fig. 4 — Plots of CO_2 concentration vs time. Each time trace corresponds to a different wave amplitude. The excitation frequency was f = 400 Hz. For each run, the CO_2 concentration is normalized to its value at t = 0.

Results: Figure 5 shows the results of our experiments where K is plotted as a function of the average measured wave slope at four different excitation frequencies f. These results indicate that K increases with both increasing wave slope and frequency. The increase in K with wave slope covers almost two orders of magnitude, demonstrating that capillary waves significantly enhance transport across the air/water interface. As f increases, the water wavelength decreases, resulting in a more corrugated interface that provides a larger surface area for gas transfer. This is part of the reason for the increase in K with f. A more important reason is that the concentration boundary layer that exists at the water surface is stretched out during each wave cycle, increasing the rate of gas transfer. It is suspected that these two effects, along with surface currents induced by the capillary wave action, are the physical mechanisms that cause the large mass transfer coefficients observed in Fig. 5. To put these data in perspective, a value of K = 0.01 cm/s typically is not observed until the wind speed exceeds 5 m/s.

These results indicate that capillary waves, while small in size, represent a significant contribution to the total amount of heat and mass transport that occurs across the air/sea interface.

[Sponsored by ONR and NRC] ■

Predictive Modeling of Oceanic Bioluminescence

D.J. Neilson, D.K. Young, and J.C. Kindle
Oceanography Division

Introduction: Bioluminescence (BL), light from living organisms, is one of the most ubiquitous biological processes in the global ocean. Easily stimulated and particularly intense in coastal regions, BL provides insights into the identity and distribution of the organisms living within the world's oceans and can be used as a baseline indicator of the general health of a regional ecosystem. Much of the ocean's expanse, however, has never been measured for BL; information regarding the occurrence and global distribution of BL is based largely on predictive methodologies.

The two primary predictive methodologies are (1) using historical records from random ship sightings to develop a climatology, or (2) assuming BL intensity is proportional to remotely sensed chlorophyll concentrations. The first method does not yield a reliable database for predictive purposes because it relies on isolated BL observations of sufficient brightness to attract the observer's attention; occurrences of low intensity BL, normally encountered in day-to-day ship operations, may not be noticed or recorded. The second method assumes a phytoplankton-based origin to BL and ignores potential changes in trophic structure that can result in the presence or absence of BL organisms other than phytoplankton. The Naval Research Laboratory (NRL) Accelerated Research Initiative, "Forced Upper-Ocean Dynamics" (FUOD), which conducted field work, modeling, and remote sensing of the Arabian Sea in 1994-1995, overcame the shortcomings of the above BL predictive schemes by developing a model that uses spatially and temporally changing hydrodynamic and trophodynamic considerations to predict BL. During FUOD, BL was measured off the Omani coast during the 1995 Southwest (SW) monsoon, 1994 Northeast (NE) monsoon, and 1995 Fall (F) intermonsoon seasons. BL was expected (from historical methodologies and databases) to be most intense during the SW monsoon. Subsequent analysis of field measurements, however, showed BL was brightest during the NE monsoon and dimmest during the SW monsoon, a seasonal pattern reproduced correctly by the numerical model. The model also correctly reproduced the observed geographic variability of BL.

Background: Strong hydrodynamic forcing during the summer SW monsoon creates intense upwelling off the Omani coast. Deep water brought to the surface during this time is rich in basic nutrients, such as nitrate and silicate (Fig. 6). Diatoms, non-BL phytoplankton, take advantage of the "new," previously unavailable nutrients, and a bloom develops. This new production forms the basis of the large phytoplankton bloom seen from satellite color images taken during the SW monsoon, and the dominance of diatoms results in a shortened food chain. As the SW monsoon fades,

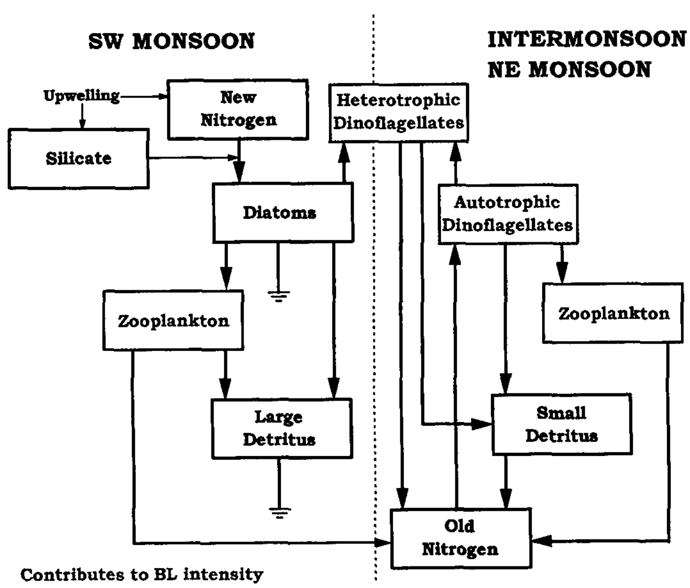

Fig. 6 — Conceptual diagram showing major pathways during the SW monsoon, NE monsoon, and F intermonsoon. Upwelling-based new production is on the left side of the diagram; recycled, old production on the right. Old nitrogen is represented by modeled ammonium and new nitrogen by modeled nitrate. Components containing BL organisms are highlighted in red.

the diatoms deplete available nitrate and silicate and are replaced by smaller phytoplankton species, many of which are BL that survive at the lower, postbloom nutrient levels and use old, recycled nutrients. By the time of the winter NE monsoon, the planktonic community is primarily supported by old production and is characterized by more links in the food chain.

A probable explanation for the seasonal change in Arabian Sea BL intensity is that the diatom-based, relatively non-BL, planktonic community during the SW monsoon is replaced by a dinoflagellate-based, predominantly BL, planktonic community during the NE monsoon.

Method: We embedded an eight-component biological model, representing parallel pathways of diatom- and dinoflagellate-dominated food chains, into a three-dimensional ocean-circulation model. The ocean-circulation model is the NRL reduced-gravity, thermodynamic, layer-averaged model. The biological model consists of components for nitrate (N), ammonium (A), silicate (Si), diatoms (P_{LARGE}), dinoflagellates (P_{SMALL}), diatom-based grazers/predators (Z_1), dinoflagellate-based grazers/predators (Z_2), and detritus (D) (Fig. 7). Nitrate and Si are introduced by upwelling in the physical model. Ammonia is produced by zooplankton excretion and detrital remineralization. Both phytoplankton components can use N and A, but diatoms preferentially take up N while dinoflagellates preferentially take up A. Since diatoms require Si for growth, N uptake by diatoms is subject to a "silicate switch" threshold below which N uptake ceases. Dead phytoplankton (or zooplankton) are added to D, and the portion of D that sinks is permanently lost from the system.

Results: The model reproduces the succession from the SW monsoon, diatom-dominated trophic structure to the NE monsoon, dinoflagellate-based structure as measured during the NRL cruises. The areal and temporal distributions of the modeled plankton also match the field data.

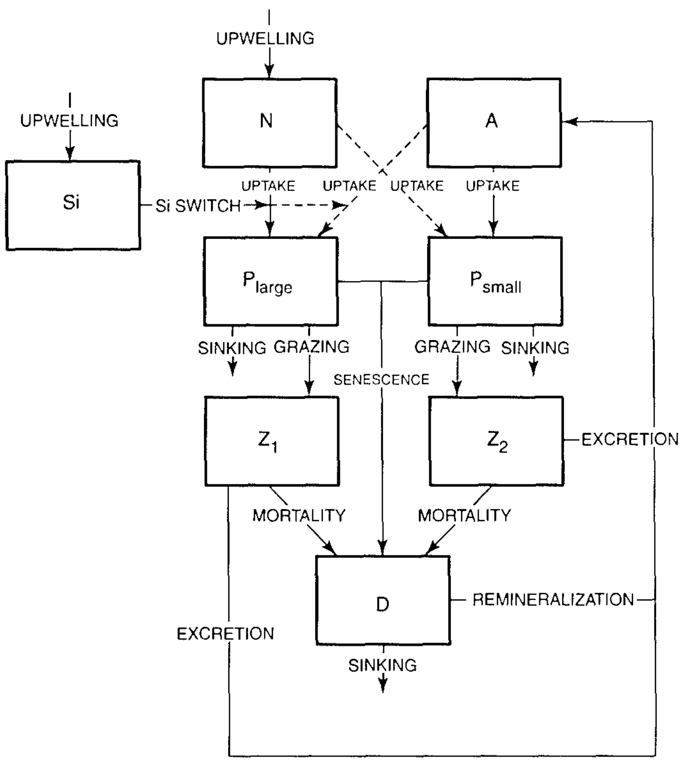

Fig. 7 — Eight-component biological model showing path of nitrogen through components. Bold arrows represent nitrogen paths. Nonbold arrows represent nonnitrogen based, flow control. Solid lines are primary paths, dashed lines are secondary.

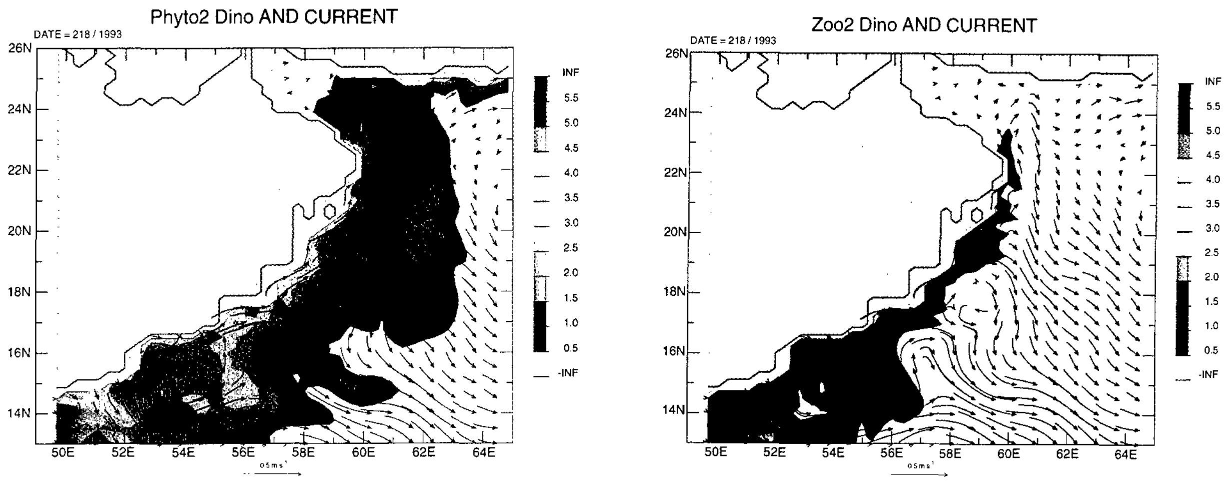

(a) (b)

Fig. 8 — Concentrations (ug-at N1^{-1}) of (a) dinoflagellates (P_{SMALL}) and (b) the associated grazer/predator population (Z_2) off the Omani coast for August 6, 1993 (model date). Together these two components represent the distribution of BL intensity for that particular date. BL intensity is directly proportional to concentrations. Arrows represent surface current direction and intensity.

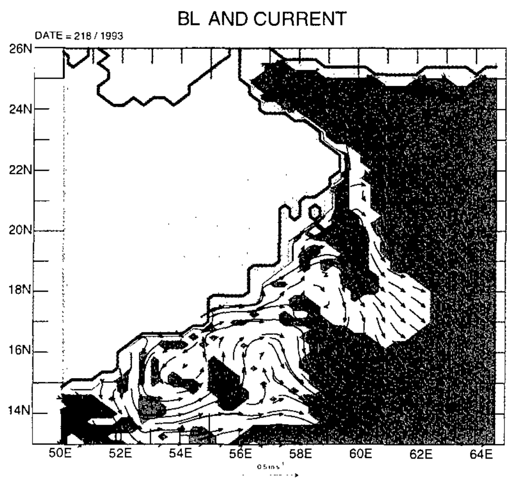

Fig. 9 — Prediction of change in BL intensity between August 6, 1993 and August 9, 1993 (model dates) based on August 9 distributions of nitrate, silicate, and ammonium off the Omani coast. Conditions favorable to increase new production will lead to decreased BL and vice versa. Red = general increase; green = no change; yellow = general decrease. Arrows represent surface current direction and intensity.

Regions and periods of high BL intensities in the Arabian Sea are determined directly from the distributions for dinoflagellates and dinoflagellate-based zooplankton (Fig. 8). Favorability for increased, decreased, or unchanged BL intensity levels can also be predicted (Fig. 9) since nutrient conditions favorable to the dinoflagellate-based model pathway will lead to increased BL in the future. The success of this model in predicting Arabian Sea BL is underscored by its selection for potential transition to the Fleet as an addition to the Navy's suite of oceanographic prediction tools.

[Sponsored by ONR] ■

Optical Science

P-3 Tests of Motion-compensated Multimegapixel Digital Cameras and Image Dissemination

R.B. Brown, J.N. Lee, and D.C. Linne von Berg
Optical Sciences Division

T. Goodrich
Recon/Optical, Inc.

Digital framing cameras have several advantages over film for airborne reconnaissance, both in tactical manned systems, such as Advanced Tactical Airborne Reconnaissance System (ATARS), and unmanned systems with unmanned aerial vehicles (UAVs). Digital imagery can be more easily manipulated for image enhancement and data compression. The electronic sensors can cover more spectral bandwidth than film, for example, additional near-IR response for silicon sensors. Finally, it should be possible to transmit digital data from the aircraft to the users of the imagery; however, several advancements are still needed. First, digital sensors do not yet provide the coverage available with film. Frames in existing film cameras are typically 5 in. square, equal to ~ 100 million pixels (megapixels) (Fig. 1(a)). Frame rates must be high enough to allow stereo photography (56% overlap between successive frames). On high-speed and low-flying platforms, one must compensate for blurring due to aircraft motion. Finally, data delivery to imagery exploitation systems and wide dissemination to users must be low latency. A series of tests on an NRL P-3 aircraft has obtained high-quality 4- and 25-megapixel digital imagery at 2.5 frames/s, with electronic forward-motion correction (FMC) and demonstrated near-real-time dissemination of images via Common Data Link (CDL) RF downlink to terrestrial communication networks. Digital images were compared with images from an operational Fleet film camera, the KS-87, that was flown alongside the charged coupled device (CCD) camera.

Camera Development: NRL and Recon/Optical, Inc. (ROI) have developed CCD cameras with FMC: a 4-megapixel (CA260/4) and a 25-megapixel (CA260/25), 2000 × 2000 and 5000 × 5000 formats, respectively. Additionally, the CA260/25 performs image compression at either 7:1 or 14:1, easing demands on the storage and transmission systems. The cameras are mounted in a body identical to that for the KS-87 film camera and employ the same lens systems, except that lens coatings are enhanced to also pass wavelengths in the 700 - 900-nm near-IR range.

Camera systems currently under development include a 100-megapixel CCD camera and framing cameras in the mid- and long-wave IR.

Data Link: The CDL standard, with up to 274 Mbps capacity, is used by the Department of Defense for RF transmission of raw imagery from airborne platforms. Here a 42.84 Mbps channel was used for imagery transmission and a second such channel used for bit-error-rate (BER) measurements. The airborne CDL hardware and antenna

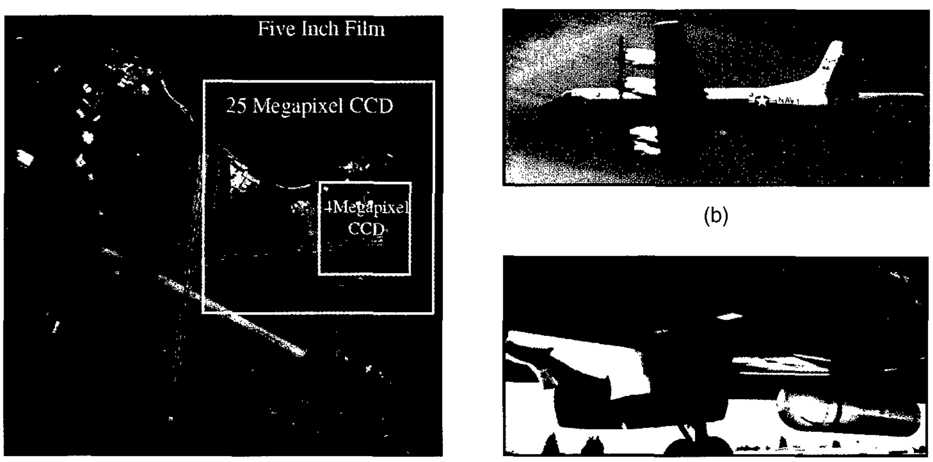

(a) (b) (c)

Fig. 1 — (a) Relative areas recorded by KS-87 film camera and CA-260 EO cameras; (b) NRL P-3 flying pallet containing KS-87 film camera and ROI CA-260 CCD camera; and (c) closeup of bolt-on pallet and CDL pod.

are in an RF-4 ATARS reconnaissance pod, wing-mounted on the P-3 (Fig. 1). The ground-station location is either NRL-Chesapeake Bay Detachment (CBD) or NRL-Washington, DC. A high-gain antenna and low-noise amplifier feed into CDL portable ground-support-equipment (PGSE) modules that reconstitute the original input data stream.

Test Configuration: The CCD and film cameras were mounted nadir-looking on the floor of an NRL-designed bolt-on pallet that replaces the bomb-bay doors of the P-3 (Fig. 1). The film camera operates independently of the CCD camera. The CCD camera, digital tape recorder (DCRSi), navigation (INS-LTN72) and altimeter systems, and CDL hardware were integrated onto the P-3, as seen in Fig. 2. A laptop PC is the controller for the various elements, using communication via a variety of buses. Navigation and attitude data are sent both to the camera, since the velocity-to-altitude ratio is needed for FMC deblurring, and to the CDL hardware to aim the airborne antenna at the ground station. When commanded to operate, the CCD camera feeds into the digital tape recorder. Control of the tape recorder returns to the PC when ready to downlink. A fiber-optic link is needed to carry high-bandwidth digital-image data from the tape recorder through the wing to the CDL pod. The PGSE ground-station output is recorded onto another digital tape recorder. A workstation then forms images from the recorded data and formats them into a standard such as TIFF. The workstation is also connected to Internet and asynchronous transfer mode (ATM) service, for imagery dissemination.

Flight Test Results: Four series of P-3 tests have been flown. Images were obtained of scenery and ground resolution targets at Webster Field (St. Inigoes, Maryland), military targets at Oceana Naval Air Station, Virginia, and urban environments along the East Coast. Imagery data were successfully linked from the P-3 down to the ground station at NRL-CBD at an altitude of 17,500 ft at ranges of > 100 nmi, from the vicinity of Lakehurst, New Jersey, and from the Atlantic, directly east of NRL-CBD. Downlinking sessions were about 30 s (~ 40 transmitted frames). Rewind and search of the ground tape, generation of an imagery frame, and conversion to TIFF image format required about 3 - 5 min. A more powerful workstation would greatly reduce this time. Subsets of frames were transmitted to NRL-DC, the Defense Airborne Reconnaissance Office (DARO), NAVAIR/ATARS, NRaD, and NAVSEA, and timelines were recorded. E-mail latency times ranged from 10 to 35 min; use of switched ATM networks reduced latency to less than 4 mins.

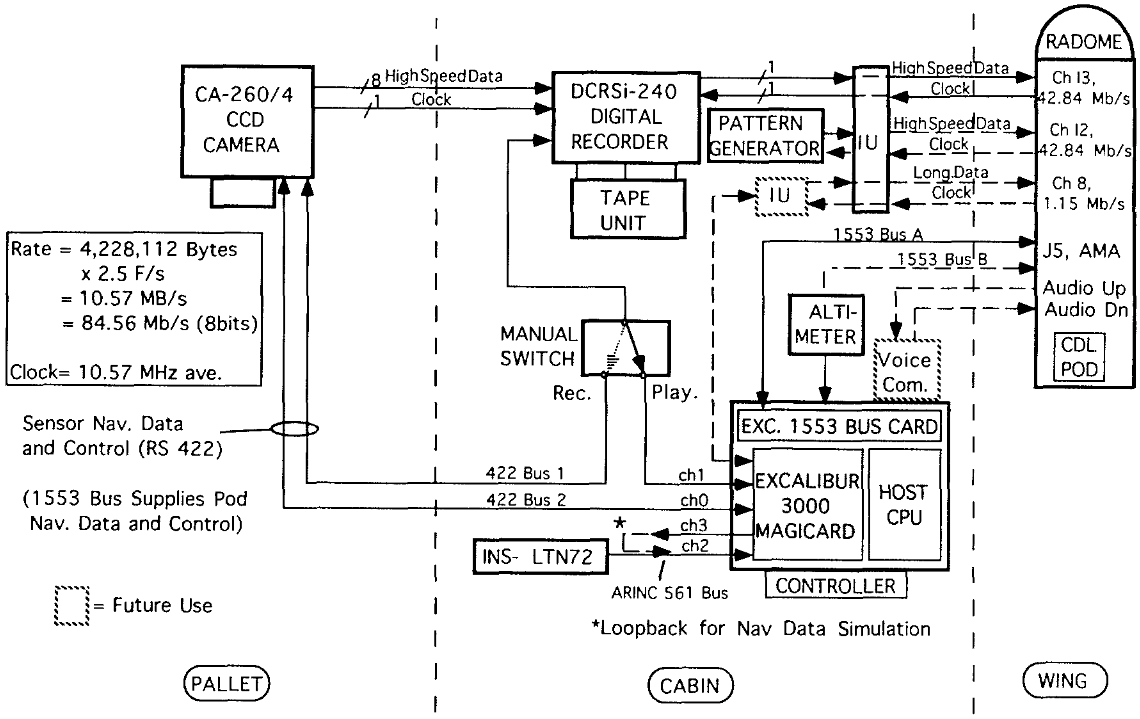

Fig. 2 — Airborne equipment integrated for NRL P-3.

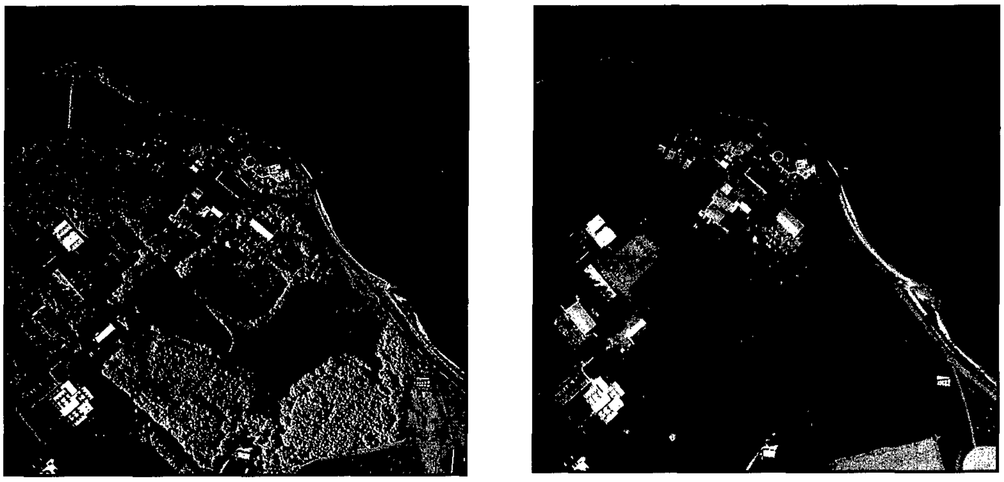

(a) (b)

Fig. 3 — Comparison of (a) full size 2K × 2K CA-260 digital electro-optical image and (b) corresponding cropped target region from 5-in. KS-87 film. Visual differences are a result of the extended spectral response of the digital camera and in differences in CCD/film illumination sensitivities.

Link bit-error rate (BER) and image quality with the CA260/4 were excellent for P-3 ranges < 50 nmi (altitude 17,500 ft). With steady lock-on, BERs of $< 10^{-7}$ were measured regardless of range. BER of 1.4×10^{-8} was measured at 50 - 60 nmi range, 2×10^{-9} at 30 - 45 nmi, and no errors were observed at ranges less than 30 nmi. The latter was verified by subtracting the transmitted and airborne image files. At greater ranges, BER degradation was observed due to Fresnel zone multipath interferences and to low signal levels, leading to link cutoff and, thus, partial frames of image data. The estimated BER at cutoff was 10^{-3}. Pixel dropouts observed at large ranges can be eliminated with the forward-error-correction (FEC) capability available on the 25-megapixel camera.

Film and Digital-Image Comparison: Post-transmission image analyses compared the effective photo resolution and visual quality of the KS-87 5-in. film and CA-260 4-megapixel digital cameras (Fig. 3). Film and digital images were matched frame per frame and analyzed without image enhancement. The CA-260/4 digital camera operates at or near the designed Nyquist sampling rate limit (12 µm/pixel * 2 pixels/line pair)$^{-1}$ = 41.7 line pairs/mm, equivalent to the expected resolution of the KS-87 film camera. There is one important difference between cameras; the modulation transfer function (MTF) of the digital camera has a sharp cutoff as the spatial frequency increases beyond Nyquist. But the roll-off of the film camera is more gradual since the MTF is dependent on the size distribution of the emulsion silver halide grains and not on CCD pixel size.

Due to differences in the spectral responses of the two camera systems, several visual differences between the digital and film imagery are evident. The panchromatic film used in the KS-87 camera has an effective spectral range of 500 - 700 nm, while the spectral response of the CA-260/4 camera is 510 - 900 nm. The most notable visible difference is the change of relative contrast tones between different materials in the image. Because film processing technology has been designed to match the response of the human eye, the tone contrasts of the film prints appear as they would to a human observer viewing the scene directly. With the extended spectral response of the digital camera, several man-made objects (runway, roads, etc.), which appear brighter than the background to the human eye and to film, are darker than the background in the digital print. In addition to tone contrast changes, the extended spectral response of the digital into the near-IR also reduces water-depth perception in shallow-water areas of the digital images relative to the film prints.

Conclusions: Testing of the 4- and 25-megapixel digital framing camera systems was successfully performed, from camera development to digital data transmission and ground-based image quality analysis. Efforts are ongoing to develop and test even larger digital framing camera systems.

[Sponsored by DARO] ■

Charge Trapping in Semiconductor-doped Glasses

A.L. Huston, S. Rychnovsky, and B.L. Justus
Optical Sciences Division

Exposure of a phosphor material to electromagnetic radiation (ultraviolet to γ ray) results in the formation of electron-hole pairs that can recombine and emit visible luminescence. Some electron-hole pairs become trapped and may persist until stimulated to luminesce by the application of heat, light, or electrical current. Optically stimulated luminescent (OSL) phosphors are of significant interest for their potential applications as information storage media in new technologies, such as optical memory systems and digital radiography. Traditional OSL phosphors are typically opaque polycrystalline powders or films that have poor spatial resolution due to excessive light scatter, low brightness, and excessive readout times. We have developed novel, optically transparent glass phosphors that exhibit superior charge trapping and OSL characteristics and have outstanding spatial resolution due to the absence of light scattering. These transparent glass phosphors are fabricated by incorporating small amounts of semiconductor and metal ion dopants into silica glasses. We have exploited the unique information storage capabilities of our phosphor glasses in applications that include radiation protection dosimetry [1], fiber-optic-coupled remote radiation sensing [2], and all-optical data storage [3].

Optically Stimulated Radiation Dosimetry: For many years the Navy has depended on thermoluminescence dosimetry (TLD) to monitor and protect personnel from unnecessary exposure to ionizing radiation. The ionizing radiation dose is determined by measuring the luminescence intensity emitted by a phosphor material as the temperature is raised. As an alternative approach, we have developed an all-optical dosimeter by using our novel OSL glass phosphors. The dosimeter provides superior sensitivity with a wide dynamic range, highly reliable reproducible response when used repeatedly, and excellent storage characteristics. The OSL glass phosphors are manufactured by incorporating transition metal or alkaline Earth sulfides such as zinc sulfide or strontium sulfide activated with metal ions of copper, europium, or samarium into high silica glasses. Ionizing radiation populates traps in the glass that are subsequently read out using a low-power, solid-state diode laser. Figure 4 shows a schematic of the OSL dosimeter. The 807-nm (near infrared) diode laser light stimulates blue OSL emission from the dosimeter, and that emission is collected and detected by a photomultiplier tube. Figure 5 shows a typical OSL signal. In this figure, the diode laser was turned on at $t \sim 1$ s. The signal is read out rapidly and completely, and the dosimeter is ready for reuse. The sensitivity of the prototype OSL dosimeter exceeds that of the current TLD technology, and OSL dosimeter technology is an attractive candidate for the next-generation Navy personal dosimeter.

Remote Radiation Sensing and Dosimetry: A significant advantage of the semiconductor-doped glass phosphors, compared to bulk semiconductor phosphors, is the ability to fabricate the glass in any size or shape, including fibers. We have drawn the OSL glass phosphors into fibers having diameter ~ 200 µm. Short lengths (~ 1 cm) of phosphor fibers are easily fused to long lengths of commercially available multimode fiber. The resulting fiber-optic-coupled sensor can be used to quantitatively monitor radiation levels in difficult-to-access or hazardous locations. The key feature of this remote radiation sensor is the ability to perform dose measurements in situ. A remotely located laser readout unit performs the OSL readout without the need to remove the sensor from its location. Figure 6 shows a schematic of the fiber-optic-coupled remote radiation sensor.

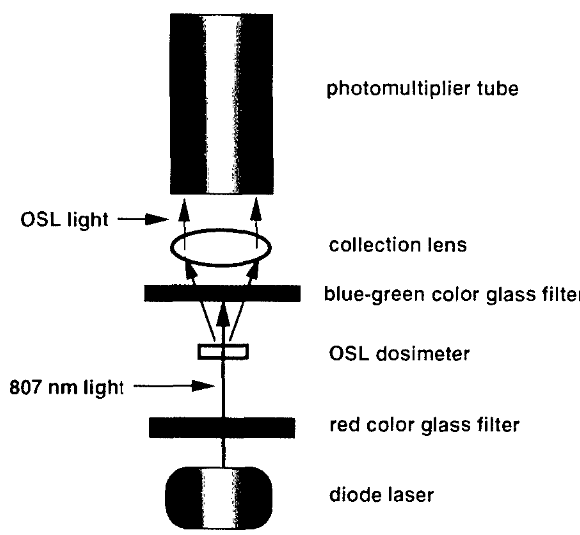

Fig. 4 — An optically stimulated luminescence (OSL) dosimeter system.

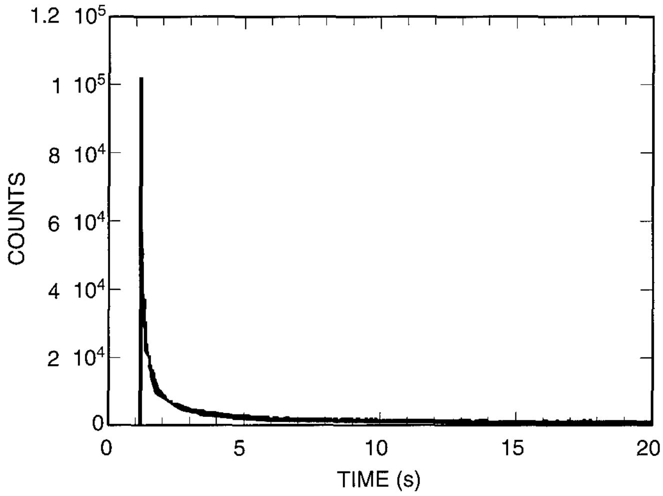

Fig. 5 — Typical signal recorded using the OSL dosimeter system of Fig. 4. The laser was switched on at $t \sim 1$ s.

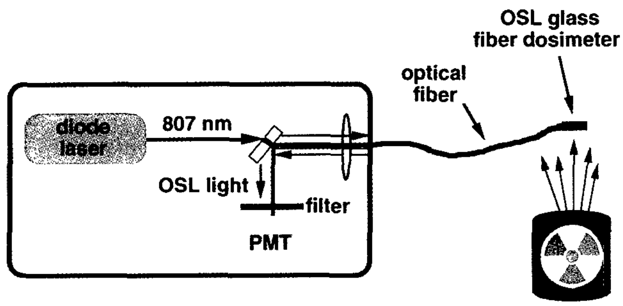

Fig. 6 — A fiber-optic-coupled remote radiation dosimeter.

To read the dose, the diode laser is turned on, and near-infrared light travels down the fiber to stimulate OSL emission from a fiber sensor previously exposed to radiation. The blue OSL emission travels back up the same fiber to be detected by a photomultiplier tube. A prototype remote dosimeter, constructed using a glass fiber weighing only 1 mg, accurately measured cobalt-60 radiation doses from 0.01 Gy to 10 Gy [2]. This range of doses includes all those of interest in medical radiotherapy applications. The use of this remote radiation dosimeter as a patient dose verification system during medical radiotherapy treatments is being studied. Other applications for this technology include environmental monitoring of radioactive contamination from nuclear waste storage sites.

Optical Data Storage: Charges are efficiently trapped in the OSL glass phosphors upon exposure to ultraviolet light, providing the potential to optically write and store information in the glass. We have, in fact, demonstrated two-dimensional storage of data [3] in a sheet of glass that was not only photoinduced but also photoreversible.

Summary: We have developed unique semiconductor-doped glasses that possess superior information storage capabilities. These materials have provided the Navy with superior thermoluminescent and optically stimulated phosphors for use in critical radiation monitoring and data storage applications.

[Sponsored by ONR]

References

1. B.L. Justus, A.L. Huston, and T.L. Johnson, "Laser-heated Radiation Dosimetry Using Transparent Thermoluminescent Glass," *Appl. Phys. Lett.* **68**, 1 (1996).

2. A.L. Huston, B.L. Justus, and T.L. Johnson, "Fiber-optic-coupled, Laser-heated Thermoluminescence Dosimeter for Remote Radiation Sensing," *Appl. Phys. Lett.* **68**, 3377 (1996).

3. A.L. Huston and B.L. Justus, "Photoreversible Birefringence in Doped Vycor Glass," *Opt. Lett.* **20**, 952 (1995). ■

Molecular Organic Light-emitting Diodes

Z.H. Kafafi,[1] H. Murata,[2] D.J. Fatemi,[3]
and C.D. Merritt[1]
[1]*Optical Sciences Division*
[2]*SFA Incorporation*
[3]*NRC/NRL Cooperative Research Associate*

A promising new technology for the 21st century is based on organic light-emitting diodes incorporated in small or large, rigid or flexible, bright and efficient electronic displays. Applications range from hand-held or head-mounted displays to large, flat panel screens that can be rolled up or hung flat on a wall. Commercialization of the first organic emissive displays based on this emerging technology is soon to begin. Highly efficient molecular organic light-emitting diodes (MOLEDs) have been recently developed at NRL.

Structure of an Organic Light-emitting Diode: The essential elements of a MOLED are depicted in Fig. 7. A thin layer of an organic emitter material is placed between a transparent conductor anode and a low work function reflective metal cathode. In forward bias, carriers of opposite sign are injected at the opposing contacts, and organic electron/hole transport materials may be placed between the emitter material and the cathode/anode, respectively, in order to achieve a balanced injection of carriers. The recombination of electrons and holes in the emitter layer results in the formation of both singlet and triplet excitons, and radiative decay from the singlet excited state is usually responsible for the observed electroluminescence. On the basis of spin recombination statistics alone, one out of four excitons produced will be a singlet, and the other three will be triplets. Hence, one can predict the achievable electroluminescence (EL) quantum yield (photons/electrons) to be 25% of the photoluminescence (PL) quantum yield. In view of this theoretical limit, our approach is to develop highly fluorescent molecular composites by dispersing molecules (with a PL quantum yield close to 100%) in a dual-function organic host that is both luminescent and a charge carrier. Enhanced EL can be achieved through energy transfer from host-to-guest molecules and/or the direct recombination of trapped charged carriers at the highly luminescent centers.

Chemical Structures of Light-emitting and Transport Materials: Figure 8 shows the chemical structures of some of the highly fluorescent molecules that are used as dopants. The electroluminescent host materials that are employed in these studies are either good hole or electron transporters. Figure 8 shows an example of a hole and electron transport material, a triaryl amine dimer *N,N'*-diphenyl-*N,N'*-bis(3-methylphenyl)-1,1'-biphenyl-4,4'-diamine (TPD) and a metal complex tris(8-hydroxyquinolinato) aluminum (III) (AlQ_3), respectively. Composite films of highly fluorescent organic molecules dispersed in a dual-function charge transport/electroluminescent host matrix are prepared using high vacuum deposition techniques.

Characterization of Materials and Devices: Figure 9 depicts photoluminescence spectra of films of the pure host materials and composites with various dopants and dopant concentrations. Tunability from the visible blue to orange is clearly achieved by variation of host material, dopant, and dopant concentration. In addition, the spectra of the composite materials are similar to the spectra of the dopant molecules in terms of bandwidth, line shape, and wavelength of emission. The fluorescence quantum yield of the composite materials, which is enhanced upon doping, is studied as a function of dopant concentration. For the optimum dopant concentration, it is enhanced by a factor of three to four relative to that of the undoped material. Light-emitting diodes fabricated using a single-layer organic structure have EL quantum yields that are greatly enhanced when the emitter layer is a molecular composite. For instance, an enhancement by a factor of 30 is measured for a composite of 5,6,11,12-tetraphenylnapthacene (TPN) dispersed in AlQ_3 relative to that of the undoped host. The increase in the EL quantum efficiency is attributed to energy transfer from the AlQ_3 host to the TPN guest molecules and direct recombination of charges trapped on TPN molecules.

Sandwiching the light-emitting molecular composite film between an electron transport and a hole transport layer leads to MOLEDs with high luminance and practical luminous power efficiency due to improvement in the balance of injected electrons and holes and exciton confinement at the emitting layer. Figure 10 shows the current density-voltage-brightness characteristics for a MOLED

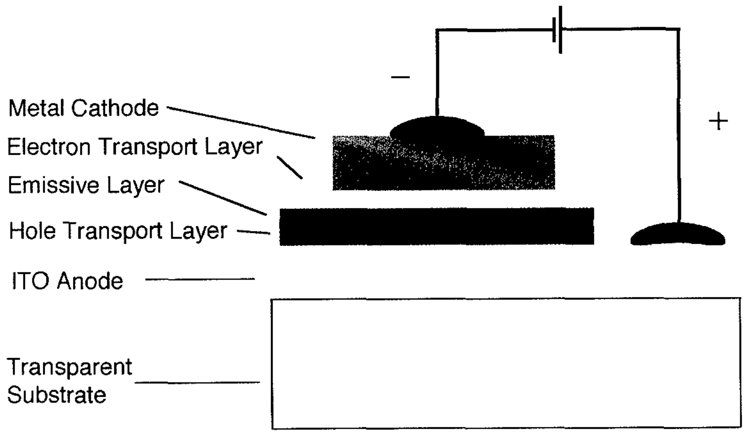

Fig. 7 — The essential elements of an organic light-emitting diode.

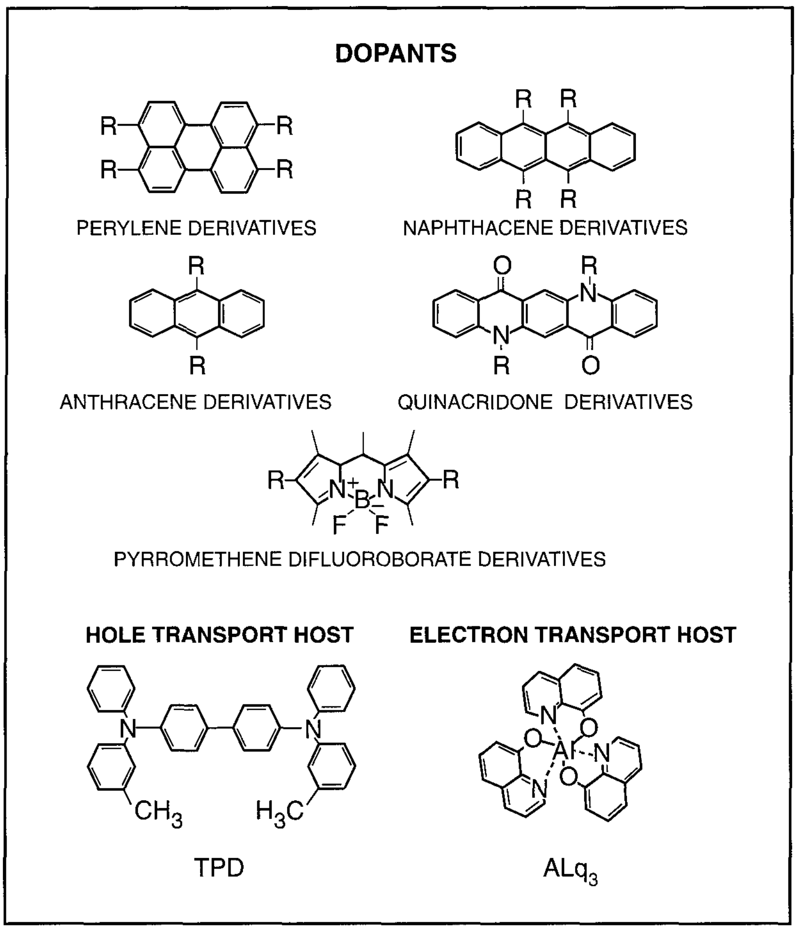

Fig. 8 — Chemical structures of examples of guest and host molecules.

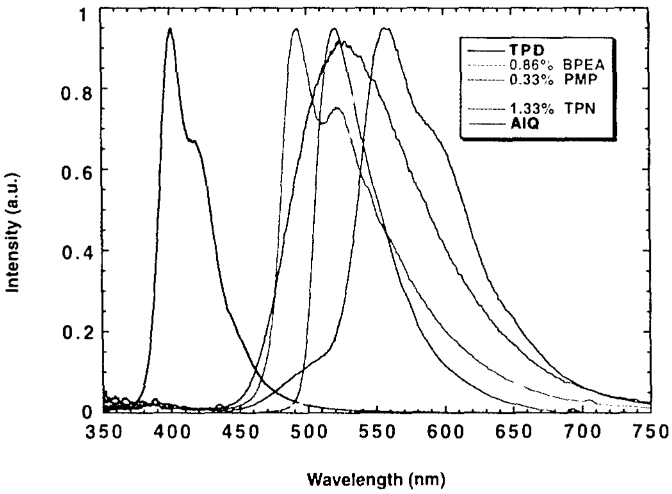

Fig. 9 — Fluorescence spectra of films of TPD, AlQ_3, and molecular composites of AlQ_3 doped with 9,10-bis(phenylethynyl)anthracene (BPEA), 1,3,5,7,8-pentamethylpyrromethene difluroborate complex (PMP), quinacridone (DHQ), and 5,6,11,12-tetraphenylnapthacene (TPN).

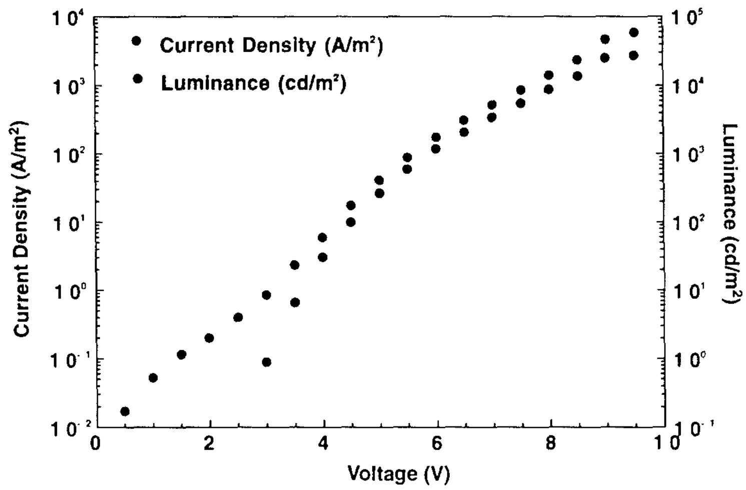

Fig. 10 — Current density-voltage-brightness curves for a MOLED based on a three-layered organic nanostructure.

based on a three-layered organic nanostructure. The emitter layer is a 25-nm thick film of AlQ_3 doped with quinacridone (0.6% mol). This light-emitting composite layer is sandwiched between films of TPD (50 nm) and undoped AlQ_3 (25 nm) used as hole and electron transporters, respectively. Light emission starts (1 cd/m^2) at a current density of 1 A/m^2 when 3 V are applied. The luminance of the light-emitting device increases exponentially as a function of voltage, exceeding 10,000 cd/m^2 below 10 V, comparable to that of a bright moon as seen from Earth. Note that only one-hundredth of this brightness is typical of an electronic display based on a cathode ray tube, such as a computer monitor or a television screen. A luminous power efficiency of 4 lm/W is measured at 100 cd/m^2 and 4.5 V, comparable with state-of-the-art liquid crystal displays. These preliminary results in terms of color tunability, brightness, and power efficiency show great promise for this battery-operated light-emitting device.

[Sponsored by ONR and DARPA] ■

Remote Sensing

Tropical Cyclone Nowcast/Forecast Improvements

J.D. Hawkins and J.S. Goerss
Marine Meteorology Division

C. Velden
Cooperative Institute for Meteorological Satellite Studies (CIMSS), University of Wisconsin

Upper-level wind information is sparse in tropical oceanic regions, which has a negative impact on the Navy's ability to monitor and forecast the track and intensity of tropical cyclones (TCs). Analysts have compensated for the lack of conventional measurements from rawinsondes (balloon-borne instruments) and aircraft by viewing animated loops of sequential visible, infrared, and water-vapor imagery from geostationary satellites, which allows them to infer important wind-flow information at multiple atmospheric levels and visualize the large-scale environment. This limited capability has been enhanced at the operational centers by producing cloud-tracked winds (CTWs) using an automated procedure to track individual cloud targets from sequential images 15 to 30 min apart. The data coverage is still inadequate, however, since the spatial distribution of the CTWs has large gaps in cloud-free areas. Furthermore, upper-level CTWs are particularly difficult to produce, since the clouds are moving rapidly between two consecutive images.

To overcome observational data sparsity over the oceans, efforts were undertaken by NRL, in collaboration with CIMSS, to apply similar tracking procedures to water-vapor images that depict the distribution of water vapor in the upper troposphere (5,000 to 10,000 m) [1]. Tracking gradients in the water-vapor field permits the creation of abundant wind vectors in previous data voids, including most cloud-free regions. Matchups with over 20,000 rawinsonde observations reveal that the water-vapor-tracked winds (WVTWs) are as accurate as the CTW vectors.

Data Products: Figure 1 illustrates the potential of WVTWs in the western Pacific, which is the most prolific region of TC development in the world. This area is monitored by the Joint Typhoon Warning Center (JTWC), Guam, a joint Navy/Air Force command, which issues warnings and forecasts on TCs from the Indian Ocean eastward to the dateline. The WVTWs in Fig. 1 have been plotted in three colors to denote their general altitude (highest - blue: 150-250 mb; yellow: 251-350 mb; lowest - green: 351-500 mb), although each WVTW observation is always assigned a distinct height. A large trough of low pressure is located between 15°N and 32°N around 150°E - 165°E, where the winds dip to the south and then back to the north. Meteorological features such as this tropical upper tropospheric trough (TUTTs) are important in determining the future track and intensity of TCs. TUTTs can dramatically change the course and strength of TCs, depending on their relative locations. Figure 2 maps the WVTW field 48 h later and reveals that the trough has developed into a cutoff low, whose cyclonically rotating winds will likely impact any TCs moving into this region for several days.

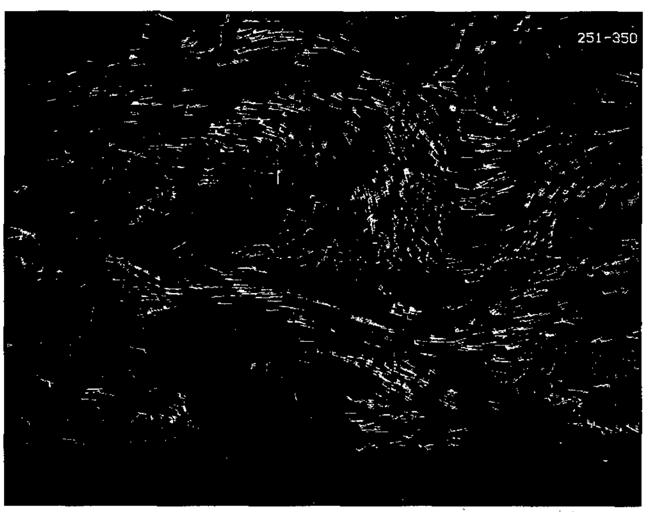

Fig. 1 — Upper-level, water-vapor tracked winds produced using a sequence of water-vapor images from the Japanese geostationary satellite (GMS-5) on 10 June 1996 at ~ 11Z, or 7 a.m. ET. Each full barb at the end of the wind vector represents 10 knot in wind speed and a flag or pennant represents 50 knots.

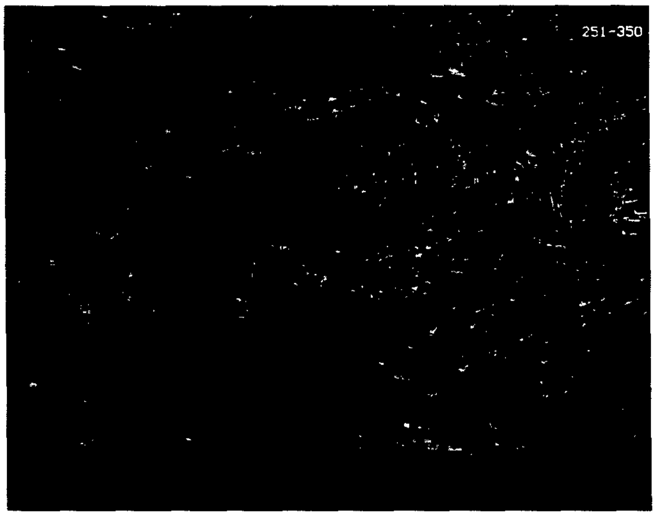

Fig. 2 — Same as Fig. 1, except for 12 June 1996 at ~ 11Z. Note large ridge of high pressure SE of Japan and a closed cutoff low-pressure system rotating cyclonically to the SE of the ridge near 12°N, 152°E.

These upper-level wind fields, available every 6 h, have revolutionized the database available to operational Navy analysts. Real-time use of these winds has dramatically increased the accuracy of JTWC's upper-level wind analyses and subsequent TC forecasts. Excellent knowledge of the meteorological features aloft has assisted the forecasters in issuing their 3 to 5 day track forecasts. Similar positive responses have been received from the Naval Atlantic Meteorology and Oceanography Center (NLMOC), Norfolk. Figure 3 illustrates the WVTWs prior to Hurricane Fran's landfall in North Carolina. WVTWs clearly depict the cyclonic low-pressure system over the eastern U.S., the upper-level outflow associated with Fran (29°N, 76°E), and the intense low-pressure system located southeast of Fran. This ability to visualize the observed wind patterns, in concert with guidance from numerical forecast models, assisted NLMOC in making the correct decision not to send the Fleet to sea in advance of Fran, at an estimated cost savings of $3-5 million.

Numerical Products: NRL also performed sensitivity tests with the Navy Operational Global Atmospheric Prediction System (NOGAPS) to assess whether inclusion of the WVTWs in the operational data-assimilation system would improve the numerical model forecast guidance [2]. Table 1 depicts the results for tropical storm Chantal. The forecasted TC position errors are given in kilometers for the control run (CNTL), the experimental run with WVTWs (EXP), and for Climatology/ Persistence (CLIP), a standard forecast aid based largely on climatology; N represents the number of positions compared for each forecast period.

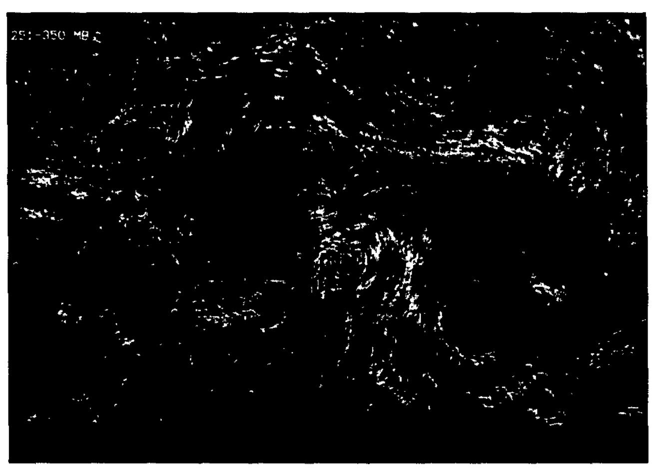

Fig. 3 — Upper-level, water-vapor tracked winds produced using a sequence of water-vapor images from the U.S. geostationary satellite located at 75°W (GOES-8) at 00Z on 5 September 1996. Winds reveal a low-pressure system over eastern U.S., Hurricane Fran off the Florida coast, a low SE of Fran, and the outflow from a developing tropical system to the SE of Fran.

Table 1 — Comparison of Forecast Position Errors (km) for Tropical Storm Chantal.

	N	CNTL	EXP	CLIP
24 h	10	185	148	207
48 h	8	331	229	363
72 h	6	557	448	511

Significant improvement is shown by EXP at all forecast intervals; analyses of the model fields indicate that the model turned the storm more quickly in response to the approaching trough. Major skill enhancements also occurred for Hurricane Iris (Table 2). Improvements of 20% to 30% are evident in the 1-, 2-, and 3-day forecasts, and these improvements are computed from a large number of position comparisons (statistics are significant at the 99% confidence level).

Finally, Table 3 summarizes the results for experiments performed for all storms in the study (Chantal, Humberto, Iris, and Luis). Note the overall 10% improvement in the EXP run compared to the control run and 30% to 50% improvement with the Clipper forecasts. These positive forecast results were the direct outcome of improved initial conditions that better represented the features resolved by the WVTWs, typically upper-level troughs that can rapidly turn tropical cyclones north and northeastward. As a result of this research, the real-time assimilation of WVTWs was implemented operationally in NOGAPS on 24 July 1996. Furthermore, the Navy's positive experiences using this new data source have generated a great deal of interest from other potential users, such as NOAA's Tropical Prediction Center.

Table 2 — Comparison of Forecast Position Errors (km) for Hurrican Iris.

	N	CNTL	EXP	CLIP
24 h	21	163	137	231
48 h	19	290	228	527
72 h	17	355	252	723

Table 3 — Comparison of Forecast Position Errors (km) for all Tropical Cyclones Considered in this Study (Chantal, Humberto, Iris, and Luis).

	N	CNTL	EXP	CLIP
24 h	69	141	122	191
48 h	59	218	192	411
72 h	52	326	287	590

[Sponsored by SPAWAR and ONR]

References

1. C.S. Velden, C. Hayden, S. Nieman, W. Menzel, S. Wanzong, and J. Goerss, "Upper-tropospheric Winds Derived from Geostationary Satellite Water Vapor Observations," accepted for *Bull. Amer. Meteor. Soc.*, Feb. 1997 issue.

2. J. Goerss, C.S. Velden, and J.D. Hawkins, "The Impact of Multispectral GOES-8 Wind Information on Atlantic Tropical Cyclone Track Forecasts in 1995 Part II: NOGAPS Forecasts," submitted to *Mon. Wea. Rev.* (1997).

Inversion Methods for Ultraviolet Remote Sensing of the Upper Atmosphere

J.M. Picone, R.R. Meier, K.F. Dymond, and O.A. Kelley
E. O. Hulbert Center for Space Research
Space Science Division

R.P. McCoy
Office of Naval Research

The Space Science Division of the Naval Research Laboratory has built a number of experimental and operational satellite-borne, ultraviolet (UV) remote-sensing systems that will measure the global composition of the upper atmosphere continuously over the next 2 decades and beyond. The upper atmosphere consists of both a charged component (the "ionosphere") and a neutral component (the "thermosphere"). The ionosphere

is a key environmental factor influencing communications over-the-horizon radar and precision geolocation, including the Global Positioning System. Similarly, thermospheric drag, which depends on the total density, exerts a major influence on satellites in low Earth orbit. Errors in estimating drag are the largest source of uncertainty in orbital tracking software.

How Global UV Remote Sensing Works: Figure 4 shows the geometry of the UV remote sensing systems, which scan or image the "limb" of the Earth. The limb is the atmospheric region seen at the horizon from sea level through about 1000 km. Both the experimental sensors, known as HIRAAS, GIMI, and RAIDS, and the operational Defense Meteorological Satellite Program (DMSP) sensors, designated as SSULI, will view the limb from altitudes of approximately 850 km while in near-polar, circular, Sun-synchronous orbits. The limb-scanning systems will require approximately 100 s to measure the atmosphere over an angular range of 10° to 26.5° below the spacecraft horizontal, with the line of sight confined to the orbital plane. This appears as a light blue area in Fig. 4 and corresponds to observation zenith angles of 100° to 116.5° (from the spacecraft local vertical) and an altitude range of approximately 750 km to 50 km. Each SSULI scan, for example, produces an image of observation angle vs the UV intensity over a wavelength range of 800-1700 Å, as shown by the simulated image in Fig. 5. Vertical lines at specific wavelengths or within wavelength bands in the image provide direct information on the number densities of key upper atmospheric species vs altitude. The most important wavelengths and the corresponding species are as follows:

(1) Dayside Ionosphere (F-layer): 834 Å; atomic oxygen ion (O^+), electron (e);
(2) Nightside Ionosphere (F-layer): 1356 Å, 911 Å, 6300 Å; O^+, e;
(3) Dayside Thermosphere: 1356 Å, 1270 - 2400 Å; temperature T, atomic oxygen (O), molecular oxygen (O_2), molecular nitrogen (N_2).

The SSULI sensors will constitute a vital component of the future Department of Defense system for monitoring and forecasting the near-Earth space environment (often termed "space weather"). Beginning with the first launch in calendar year 2000, SSULI will fly a contiguous series of missions aboard DMSP satellites, each lasting nominally for 3 years. The experimental systems will validate the SSULI concept. The resulting multiyear, continuous global data sets will provide a tidal wave of data from which the scientific community will develop the first deep, comprehensive picture of mechanisms and behaviors of the upper atmosphere.

Extracting the Information: To derive optimal estimates of upper atmospheric composition from the raw spectral data, NRL has developed leading-edge computer software based on

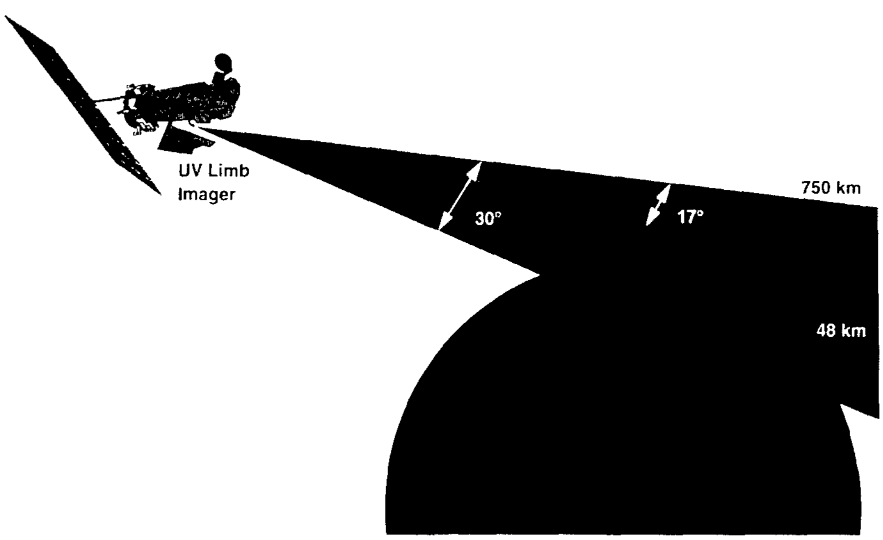

Fig. 4 — Ultraviolet limb imaging geometry.

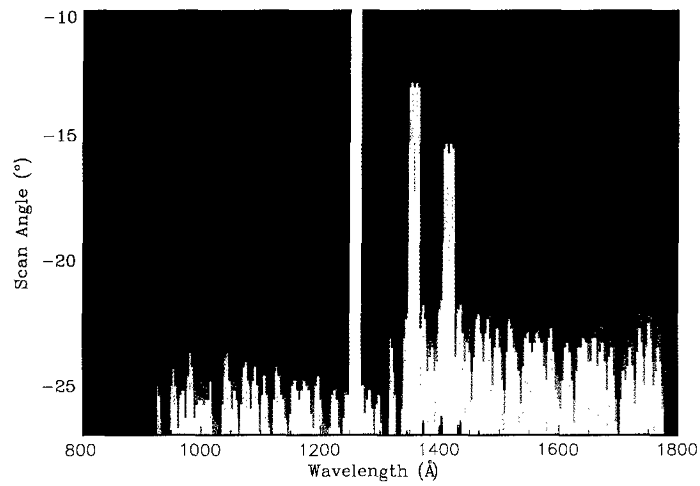

Fig. 5 — Simulated SSULI limb scan image of observation angle vs wavelength.

discrete inverse theory [1-3]. This breakthrough technology forms the core of operational ground data analysis software (GDAS) being developed by NRL for delivery to the USAF 50th Weather Squadron, which disseminates data on and ultimately forecasts of the space environment to the services and defense agencies. The Navy is a major customer for timely information on the ionosphere, and NRL is currently working on applications of SSULI thermospheric data to Navy operations.

The GDAS extracts vertical profiles of the spectral features listed above. As an example [2], Fig. 6(a) shows a simulated SSULI 834 Å intensity profile, indicated by the plus (+) symbols. The presence of statistical noise causes the data to deviate from a smooth profile. The 834 Å intensity at any observation angle relates directly to the concentration of O^+ ions in the ionospheric F layer. For brevity, we denote the concentration (number of particles per cm^3 of species "x" by "[x](z)." In Fig. 6(b), the dotted line gives the true $[O^+](z)$. Given the true $[O^+](z)$, an accurate model of ionospheric 834 Å emissions would produce the solid line in Fig. 6(a). Since O^+ is the dominant positive ion in the F-layer and since the ionosphere is a neutral plasma, the true [e](z) coincides with the dotted line in Fig. 6(b).

Discrete inverse theory uses data like those in Fig. 6(a) to compute $[O^+](z)$ with maximum accuracy. The noise in the data introduces error into

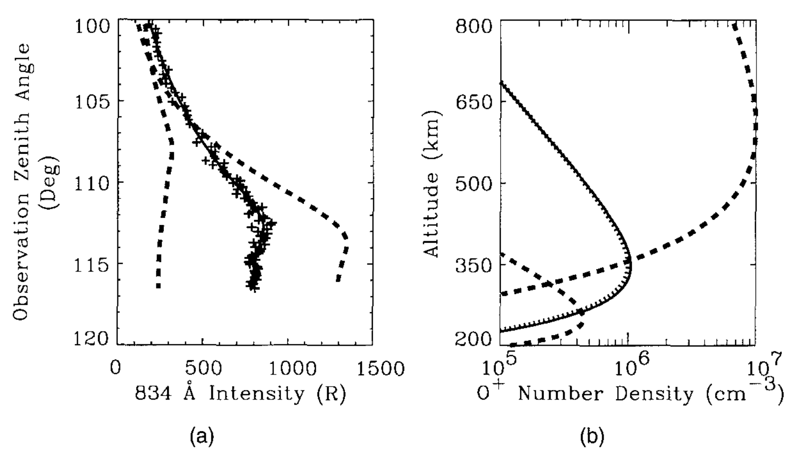

Fig. 6 — (a) Plus signs represent scan angle variation of simulated 834 Å intensity (in Rayleighs) that would be extracted from an image like Fig. 5. (b) Dotted line represents "true" altitude profile of $[O^+]$ and [e]. Solid lines represent optimal discrete inverse theory intensity fit and electron density profile. Dashed lines represent a pair of estimates initializing separate inversion calculations that demonstrate uniqueness of the final result.

the result. However, the NRL inversion method minimizes this error as follows: (1) estimate $[O^+](z)$; (2) use an accurate model to compute an 834 Å intensity profile from the estimated $[O^+](z)$; (3) compare the "model" intensity profile to the data to derive an improved estimate of $[O^+](z)$; (4) repeat steps (2) and (3) until the model intensity profile (like the solid line in Fig. 6(a)) provides the optimal fit to the data. The corresponding $[O^+](z)$, shown as a solid line in Fig. 6(b), is the desired answer, directly specifying $[e](z)$.

The power of discrete inverse theory lies in its ability to compute a unique, optimal profile $[O^+](z)$ from very noisy data and from poor initial estimates of $[O^+](z)$. The dashed lines in Fig. 6(b) show initial estimates of $[O^+](z)$ that are either a factor of 10 high or low in magnitude and whose altitude dependencies differ greatly from the "true" profile (dotted). The corresponding model intensity profiles in Fig. 6(a) differ drastically from the data. However, from either initial estimate, the final results coincide with the respective solid lines in Figs. 6(a) and (b), demonstrating that the answer is unique.

Discrete inverse theory is a key factor in making UV remote-sensing appropriate for operational, global monitoring of the near-Earth space environment. The synoptic data sets of the future will bring a new era of discovery in the science of the upper atmosphere. From these data will follow vastly improved physics-based models for forecasting the evolving state of the space environment, which wields a significant influence over military and domestic operations.

[Sponsored by ONR, USAF/DMSP, USAF/STP, SERDP]

References

1. R.R. Meier and J.M. Picone, "Retrieval of Absolute Thermospheric Concentrations from the Far UV Dayglow: An Application of Discrete Inverse Theory," *J. Geophys. Res.* **99**, 6307-6320 (1994).

2. J.M. Picone, R.R. Meier, O.A. Kelley, K.F. Dymond, R.J. Thomas, D.J. Melendez-Alvira, and R.P. McCoy, "Investigation of Ionospheric O^+ Remote Sensing Using the 834 Å Airglow," *J. Geophys. Res.*, in press (1996).

3. K.F. Dymond, S.E. Thonnard, R.P. McCoy, and R.J. Thomas, "An Optical Remote Sensing Technique for Determining Nighttime F-Region Electron Density," *Radio Sci.*, submitted (1996). ■

Simulation, Computing, and Modeling

Advanced Power Projection Planning and Execution

J.B. Hofmann and F. Segaria
Information Technology Division

Background: Throughout most of the U.S. Navy, operations planning remains a manual and time-consuming process. An NRL in-house study [1] suggested that computer-based automation and visualization could improve the quality and the timeliness of battle planning. This led to the Advanced Power Projection Planning and Execution (APPEX) Project, to significantly increase the state of the art in automated planning tools.

The APPEX Project, commenced in 1994 with a laboratory-based concept demonstration based on an analysis of the current planning process, identified key areas for computer-based solutions [2]. A follow-on effort in 1995 culminated in a successful field test between two sites during the Joint Warrior Interoperability Demonstration '95 (JWID '95). Sites simulating a naval forces command (located inside a mobile command and control van in Point Loma, California) and a Marine forces air combat element (located at Camp Pendleton, California) developed a coordinated attack plan over a wide area network.

In 1996, APPEX team members contacted members of a Carrier Air Wing who were training in preparation for a 1996-1997 deployment. The Air Wing (CVW-3) requested to test APPEX during their Naval Strike Warfare Center training detachment. Developers worked closely with Air Wing members to modify the system to most appropriately fit their needs. Following a successful testing by the air wing, APPEX was installed on the USS *Theodore Roosevelt* (Carrier) in Spring of 1996. Workstation suites were installed in the Carrier Intelligence Center (CVIC) and two squadron ready rooms. APPEX was successfully used in several Fleet exercises and integrated into daily Air Wing operations. In September of 1996, CVW-3 requested to deploy with APPEX and to have an additional suite installed in the E2-C squadron ready room.

Hardware Description: An APPEX workstation suite consists of two networked computers, as shown in Fig. 1. APPEX planning software is hosted on an HP TAC-4 series computer (left) running the naval command and control system commonly known as Joint Maritime Command Information System (JMCIS). This allows for easy access to current naval intelligence and track data, thus streamlining the planning process considerably. The visualization runs on a Silicon Graphics workstation (right). This provides superior graphics performance unavailable on the HP workstation.

In the USS *Theodore Roosevelt* implementation, workstation suites are networked from CVIC to the ready rooms and to various databases over a high-speed network installed by the SPAWAR-NAVSEA Scalable High Performance Local Area Network (LAN) project.

Graphical Mission Entry: Figure 2 displays a screen snapshot of the chart in which missions are entered graphically. The user designates the type of mission and then "points and clicks" the waypoints. This allows for fast entry and early spatial deconfliction.

The user can also adjust the altitude of the mission and obtain additional information regarding the various legs of the mission through use of the vertical profile in Fig. 3. The various waypoints are displayed over a sampled portion of the terrain (the green solid area). The user can select a waypoint, in this case waypoint 11, modify its altitude by dragging the point and receive specific information about that leg of the mission such as length of leg, average measurement above ground level, etc., displayed below the profile graphic.

Timing Coordination: These missions can then be viewed in a timeline (Fig. 4) where the modifiable horizontal axis represents time. The

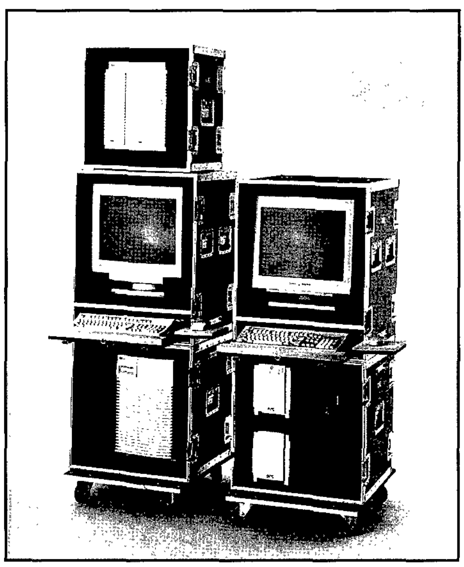

Fig. 1 — APPEX workstation suite as deployed on the USS *Theodore Roosevelt*.

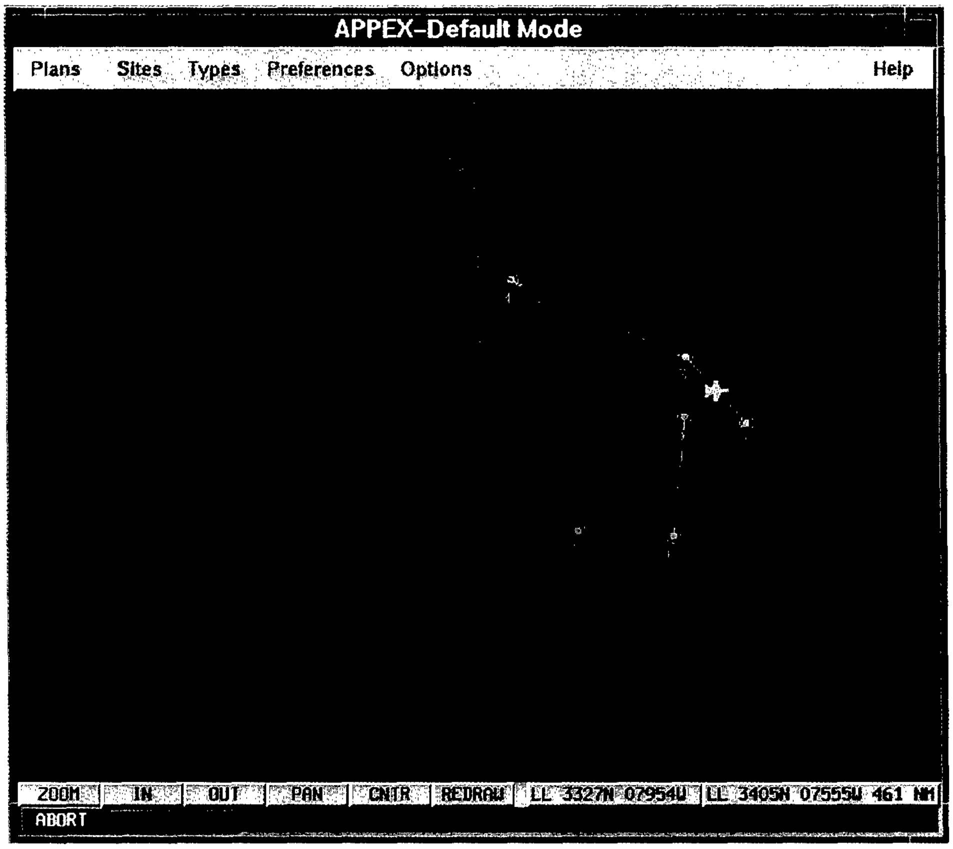

Fig. 2 — APPEX mission entry display (JMCIS-based).

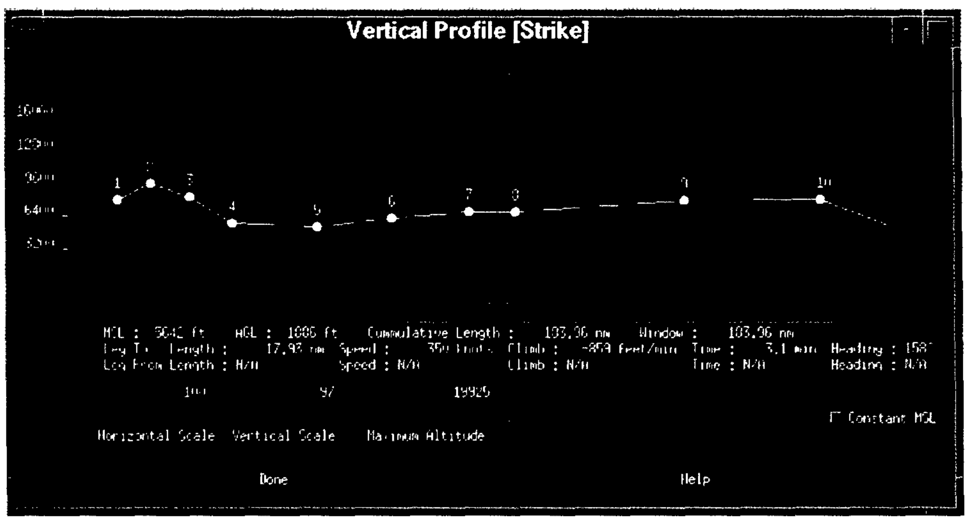

Fig. 3 — APPEX vertical profile display.

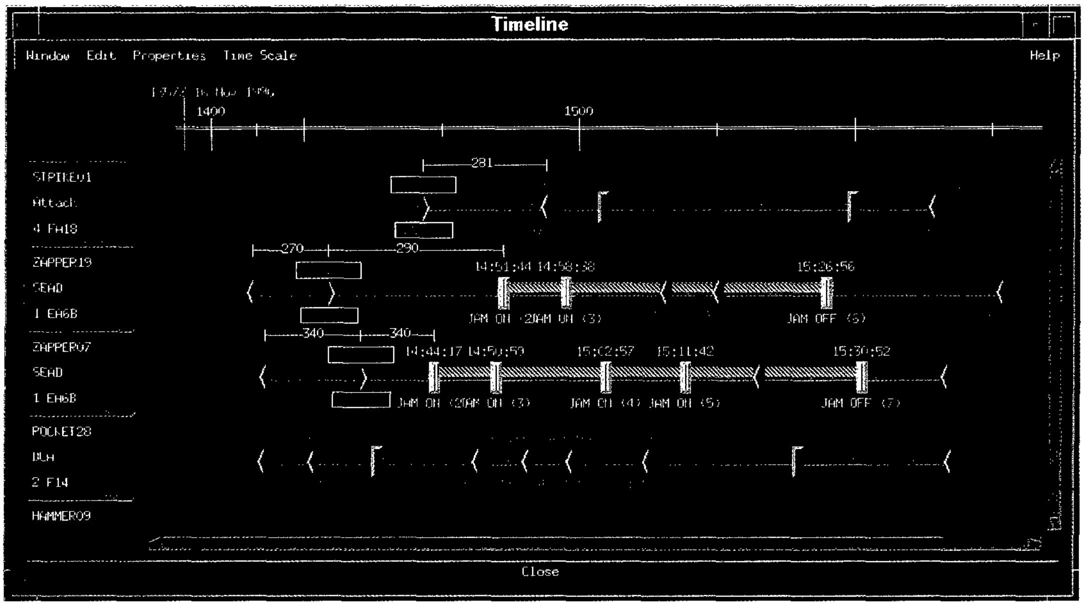

Fig. 4 — APPEX plan timeline display.

Fig. 5 — APPEX plan preview showing radar jamming effects.

vertical axis represents mission packages. In this case, four separate mission packages are displayed. Individual events can be given special symbols to increase plan understanding. For instance, the two missions labeled Zapper19 and Zapper07 are EA6B jamming missions. Note the yellow chevron line indicating when the jamming will occur in time. Other symbols indicate tanking station events, air-to-ground bomb events, and waypoints.

The timeline is also interactive. The user can adjust the events in time by selecting one or more waypoints and moving them forward or backward as desired. The estimated speed of the new leg is displayed above the waypoint legs. Note the speed of 270 knots displayed above the first leg of Zapper19 mission.

Plan Visualization: After developing the plan, the user can then display it in three dimensions, as it is intended to play out in time. Figure 5 shows a "snapshot" of the plan at time 14:41:01. The jammed radar of the two surface-to-air missile sites are displayed in three dimensions. The location of the individual missions are shown by the plane icons. The user can view this picture from any vantage point. This was used extensively by the air wing to brief their plans to the other team members.

Results and Future Plans: Carrier Air Wing Three has stated that APPEX has provided the following advantages: reduced time to plan, allowing more time to develop contingencies, deconfliction of individual plan elements, an "unequaled" situational awareness through the plan preview, and consolidated timeline generation. They also cited the responsiveness of the software developers to perform modifications. Current plans for APPEX include the extension of the planning tools into real-time battle management. Battle management experiments are scheduled with Naval Surface Warfare Center in Dahlgren, Virginia, and the newly named Naval Strike and Air Warfare Center in Fallon, Nevada.

[Sponsored by SPAWAR, ONR, and OPNAV]

References

1. "A Study to Identify Technology Shortfalls in Decision Support for Strike Warfare," Draft Technical Report, Advanced Information Technology Branch, Information Technology Division, NRL Washington, D.C. 20375.

2. J. Hofmann and D. Carroll, "Advanced Technology for Precision Strike Planning," Proceedings of the Military Operations Research Society Symposium (MORSS '94), 6-10 June 1994. ■

Detection of Subpixel Targets in Multispectral Imagery

E.A. Ashton
Optical Sciences Division

The automated detection of small targets under camouflage or concealment in cluttered backgrounds is a topic of great interest for remote surveillance applications. The ability to detect targets that appear in only a few pixels in an image allows surveillance over a wider area and from a greater range than would otherwise be possible. Exploitation of multi- and hyperspectral imagery has been widely accepted as the most likely solution to this problem. Because no knowledge of the target can be assumed, the best way to accomplish such a detection is to form a statistical model of the background and then search the observed data for anomalous pixels. Two novel approaches to background modeling and anomaly detection have been examined in this work. The first involves the separation (segmentation) of an imaged scene into its various terrain types (forest, grass, roadway, etc.) using an iterative, pixel-based algorithm. The pixels of each terrain type are then spectrally decorrelated, a process which highlights pixels that are statistically different from their surroundings. The results are thresholded to provide detection. The second approach also requires segmentation, but the algorithm used is a more sophisticated adaptive classifier. This algorithm allows the direct calculation of a probability for each pixel with respect to an integrated spatial-spectral background model. Pixels that are improbable are likely to be targets.

Background Modeling: Until recently, algorithms for detecting small targets in multispectral data have been limited to linear filtering algorithms, such as the spectral matched filter, and to a few nonlinear variants, such as the RX algorithm of Reed and Yu [1]. These algorithms share a common weakness: they assume that background pixels should be distributed about a locally stationary mean in a multivariate Gaussian fashion. While this assumption holds under some circumstances, it is not generally accurate. Other algorithms have attempted to make use of a linear mixing model (LMM) for background distribution [2]. While this model improves on the multivariate Gaussian approach in some cases, in others, it provides an estimate of background distributions that is even more inaccurate. In this work, a third model has been developed, which assumes that each background pixel should fall into one of several semidisjoint multivariate Gaussian distributions. This model is more flexible than either the LMM or the single Gaussian assumption, and detection algorithms based on the clustering model have been shown to provide superior detection to those based on either the LMM or the single Gaussian assumption in a large majority of cases.

Figure 6 shows scatter plots (plots in which each axis represents pixel intensity values in a single spectral band) of three typical data sets containing tactical targets. The distribution in Fig. 6(c) is nearly multivariate Gaussian and will be well modeled by filtering techniques such as RX, which are very effective on this data set but not on the other two. Background pixels in Fig. 6(b) generally fall into a triangular region (a simplex) and will be well modeled by a LMM. Detection algorithms based on linear mixing will work well on Fig. 6(b) but not on either Figs. 6(a) or (c). The background

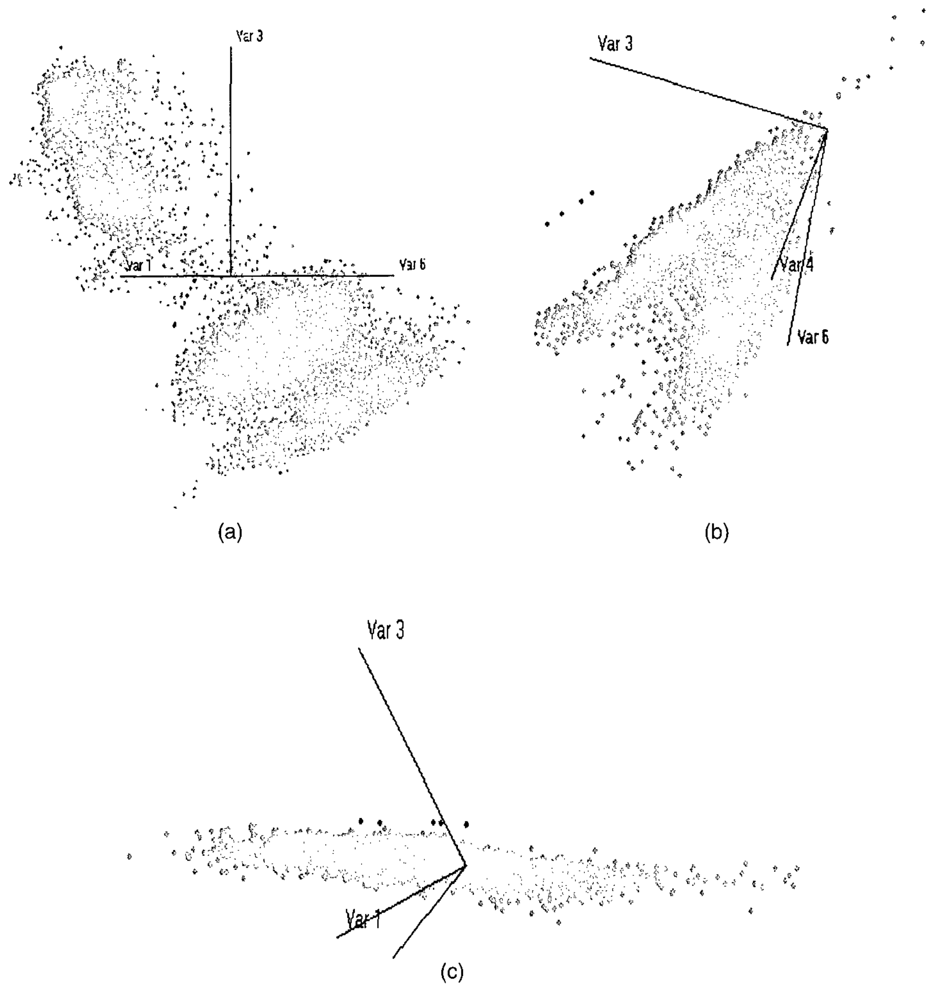

Fig. 6 — Potential distributions of background (green) and target (red) pixels. Detection is predicated on forming a model that includes all background pixels but excludes target pixels: (a) is taken from a visible spectrum image of a forested area near Luray, Virginia. Target pixels are military vehicles. (b) From a long-wave IR image of Kona, Hawaii. Targets are brown metal panels. And (c) is from a long-wave IR image taken over the White Mountains in California. Targets are green metal panels.

pixels in Fig. 6(a) fall into several distinct clusters and will be well modeled by a clustering model with the number of clusters $k = 4$. Moreover, the distributions in Figs. 6(b) and (c) can also be accurately modeled by the clustering algorithm by changing the value of k to 2 and 1, respectively. It is this flexibility with regard to the types of backgrounds that algorithms based on clustering are able to accurately model that gives these algorithms their primary advantage over other techniques.

Detection Algorithms: Once the background pixels have been accurately modeled, it is still necessary to find some way to separate out potential targets. Two approaches to this problem have been explored. The simpler method involves clustering the data using a process known as the k-means algorithm, then spectrally decorrelating (or whitening) the pixels in each cluster. The whitening process is illustrated in Fig. 7. Whitening maps the original multivariate Gaussian distribution into a more nearly circular Gaussian distribution. Once this is done, the targets can be identified simply by thresholding the radii of the pixels from the center of the distribution.

A more complex, but also more robust, approach to the detection problem is to try to identify the first-order statistics (means and variances in each band) of each of the spectral clusters. Once this is accomplished, the probability that

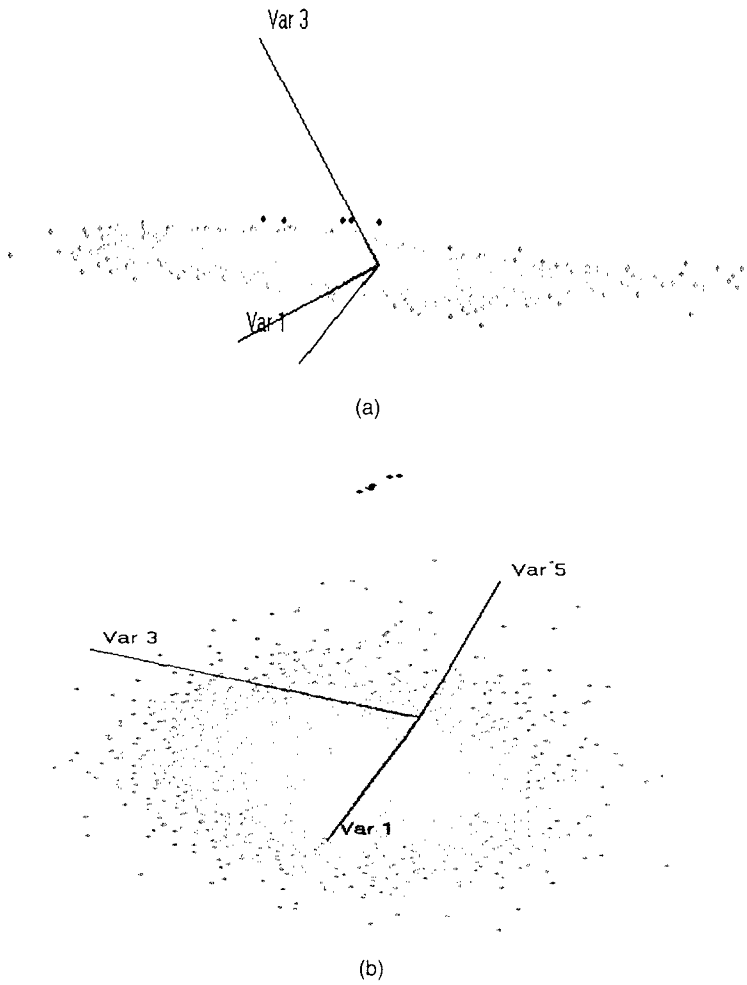

Fig. 7 — (a) Background and target pixels from the White Mountains data set. (b) The same data after whitening by multiplying each pixel vector by the inverse of the spectral correlation matrix. Note that the data take on a more circular distribution and that the targets may be identified by thresholding the radius of each pixel from the center of the distribution.

each pixel truly belongs to the background distribution can be calculated directly. This approach allows the integration of a spatial model to the detection process. It is possible to model the spatial scene as a Gibbs random field, a two-dimensional extension of the causal Markov chain. In essence, this process applies a probabilistic penalty to any pixel that differs significantly from its immediate neighbors. This spatial model helps to regularize the segmentation, in addition to identifying small anomalies.

Experimental Results: Algorithms based on the clustering model have been tested on a number of multispectral data sets. A typical example is given in Fig. 8, which shows a portion of the White Mountains' long-wave IR data set. This is the same data whose scatter plot is given in Fig. 7. Note that these are data that are well suited to the RX algorithm. Even so, both clustering algorithms are able to achieve superior performance. Figure 9(a) shows a plot of false alarms at 100% target detection vs target size as a percentage of a single pixel. Figure 9(b) gives the probability of false alarm vs probability of target detection (the receiver-operator characteristic (ROC) curve). These curves demonstrate that both clustering algorithms consistently out-perform the RX algorithm even when the statistical assumptions of RX are met. The performance differential on data sets seen in Fig. 6(b) is similar, and on data sets seen in Fig. 6(a) is considerably greater.

Figure 10 shows the output from a real-time implementation of the adaptive clustering algorithm. On the left side is shown one band from a multispectral data cube taken using the HYDICE

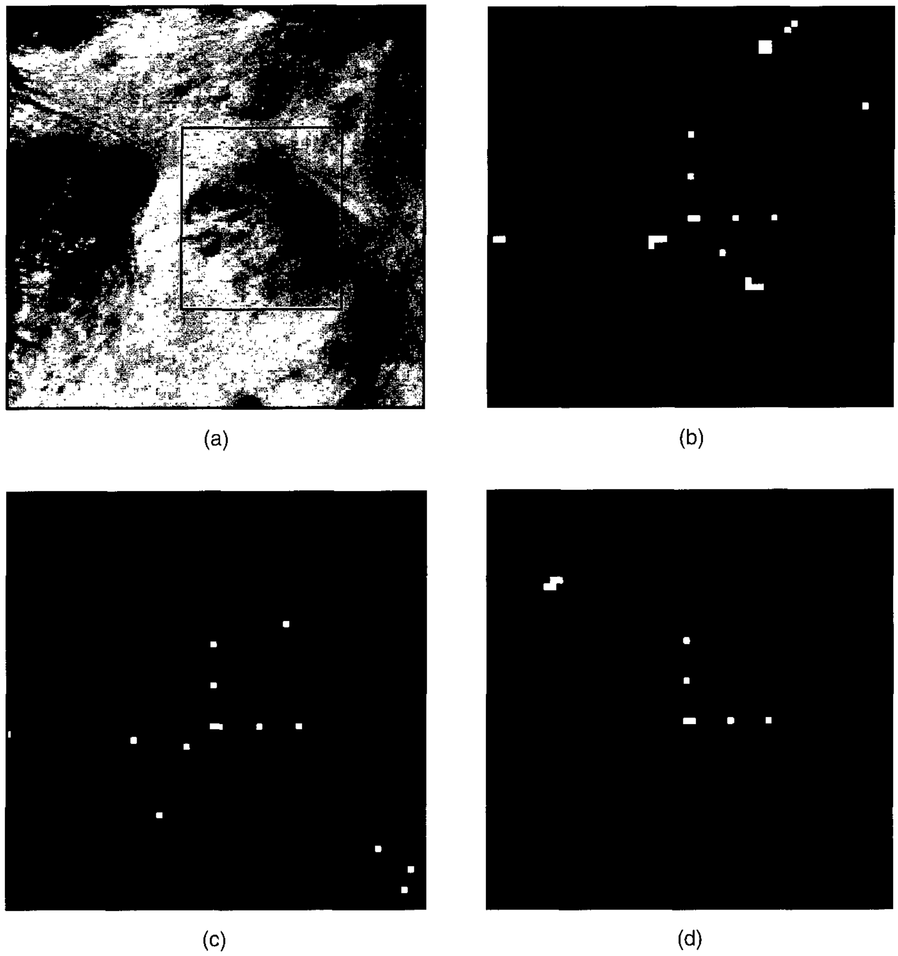

Fig. 8 — (a) A 200 × 200 pixel section from band 1 of the thermal IR multisensor White Mountains image cube. This section contains five targets implanted with a pixel fill factor of 72%. (b) The smaller outlined section of (a) processed using the RX algorithm and thresholded at 100% detection. False alarm rate in this case is 0.56%. (c) Processed data using spectral clustering followed by bin decorrelation. False-alarm rate (FAR) is 0.19%. (d) Processed data using adaptive clustering. FAR is 0.10%.

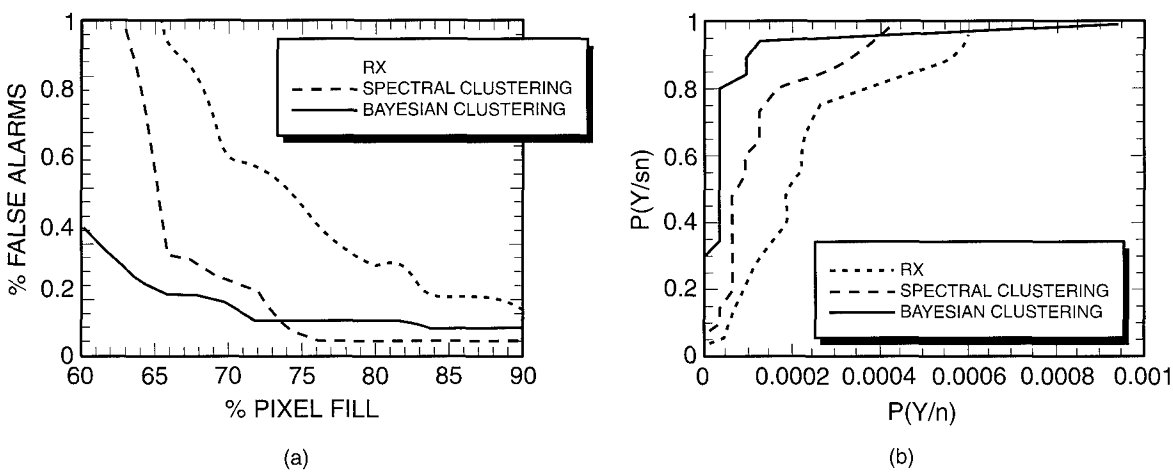

Fig. 9 — Plot of target size (a) as a percentage of one pixel vs false alarm rate at 100% target detection for the TIMS White Mountains' data set; (b) ROC (probability of target detection vs probability of false alarm) curves at a pixel fill factor of 72%. Note that the performance of both clustering algorithms is consistently superior to that of RX.

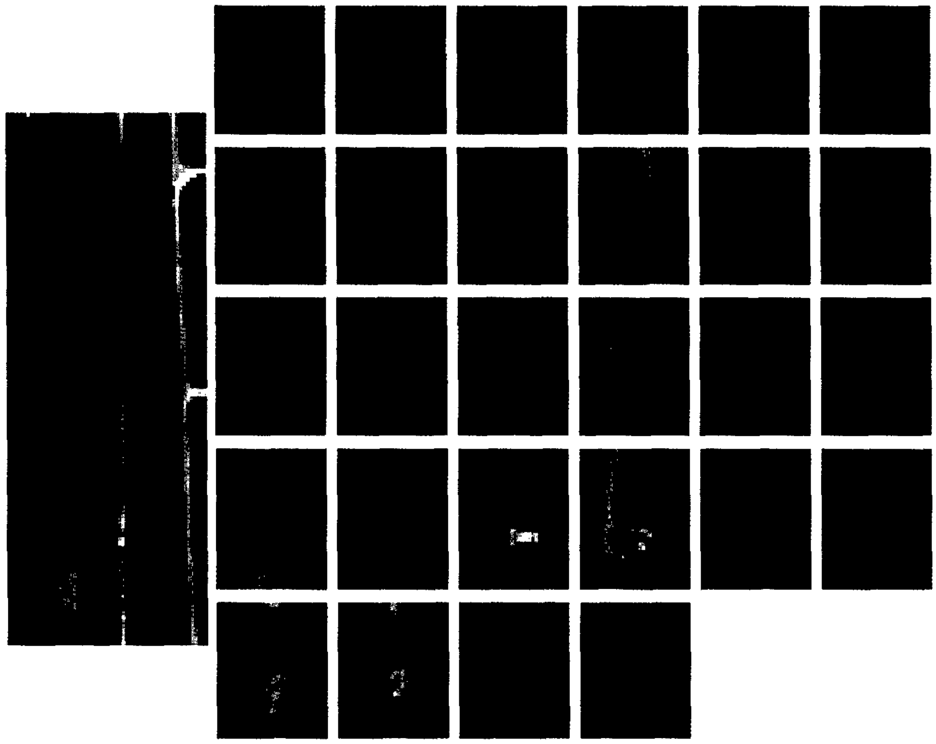

Fig. 10 — Output from a real-time implementation of the adaptive clustering algorithm. The larger image on the left side is one band from a HYDICE data cube containing several military targets. Each red spot indicates a spectral anomaly identified by the algorithm. The smaller images on the right side are high-resolution images of the immediate neighborhood of each spectral anomaly.

sensor. Targets are camouflaged military vehicles. Red spots indicate areas where the clustering algorithm has identified anomalies. Each red spot corresponds to a smaller image on the right side, which is a high-resolution image of the area around each detection. The only areas detected that are not obvious military targets are portions of the road in which the soil has been turned by tank treads. Clearly, this is also a useful detection.

Conclusions: The algorithms developed during the course of this work appear to provide significant improvement in both detection of targets and rejection of false alarms in most cases over the filtering algorithms currently in use. Future work in this area will include code optimization and verification of these results in the field.

[Sponsored by ONR]

References

1. I.S. Reed and X. Yu, "Adaptive Multiple-band CFAR Detection of an Optical Pattern with Unknown Spectral Distribution," *IEEE Trans. Acoust. Speech Sig. Process.* **38**, 1760-1770 (1990).
2. X. Yu, I.S. Reed, and A. Stocker, "Comparative Performance Analysis of Adaptive Multispectral Detectors," *IEEE Trans. Sig. Process.* **41**, 2639-2656 (1993). ■

Numerical Simulations of the Combustion of High-Energy Fuels

K. Kailasanath and E. Chang
Laboratory for Computational Physics and Fluid Dynamics

A new class of high-energy fuels based on strained hydrocarbons such as cubanes is being developed. Because of their structure, these fuels have excess strain energy stored in them. When they burn, this excess strain energy is also available in addition to the heat of combustion. These fuels are also significantly more dense than conventional fuels. Therefore, understanding the combustion of these fuels could lead to a major breakthrough in the quest to attain increased range and speed for missiles and other Navy propulsion systems.

However, several basic issues in the combustion of high-energy fuels need to be resolved before they can be effectively used. Many of these fuels are not in liquid form at standard operating temperatures. If they are diluted in some liquid fuel, we may have to burn a slurry, or if the base fuel quickly vaporizes, we have a gaseous fuel with distributed condensed particles of high-energy fuels. The mixing and combustion characteristics of such a multiphase mixture need to be understood. An additional characteristic common to many of these fuels is a tendency for particles of fuels to disintegrate and rapidly release their energy, a process termed microexplosion. This introduces a new problem because microexploding fuels have not been tested and evaluated in closed combustion systems, such as those relevant to the Navy. For example, the pressure waves generated by the microexplosions could couple with the acoustics of the propulsion system and lead to combustion instability and poor performance or even system failure. Since these fuels are not yet available in large quantities, numerical simulations provide an ideal way to study these basic issues in the combustion of the fuels. However, a suitable computational model was not available, and the first task was to develop such a capability.

Computational Model: A computational model has been developed for the simulation of particle or droplet-laden flows such as occur in the combustion of high-energy fuels. The unsteady gas-phase flow in the combustor is computed by solving the conservation equations for mass, momentum, and energy using the Flux-corrected Transport (FCT) algorithm. The fuel droplets' position in the flow field is computed by solving the Lagrangian equations of motion for the droplets, taking into account the inertial drag force that depends on the droplet size and density. The fuel droplets are considered to be multicomponent, consisting of a solid cubane core surrounded by a liquid-phase carrier. As the droplets are heated, the liquid evaporates for a while, and then the droplets microexplode, rapidly releasing their energy. Factors such as the amount of vaporization before microexplosion have been obtained from single-droplet-burning experiments (conducted at Princeton) but can also be varied parametrically in the simulations to study their effect.

Effects of Droplet Size: Using this newly developed model, simulations have been carried out to address several basic issues (mentioned above) in the combustion of high-energy fuels. The effect of the flow field on the distribution of the fuel droplets of three different sizes is shown in Fig. 11. The flow field itself is dominated by large-scale vortical structures, and if the droplets are very small, they follow the flow and are trapped in these vortical structures. The large droplets do not follow the flow due to inertia, while the intermediate-size droplets interact with the vortical structures and are flung out. This results in a better distribution of the fuel droplets. From such simulations, one can determine the preferred size of droplets for specific

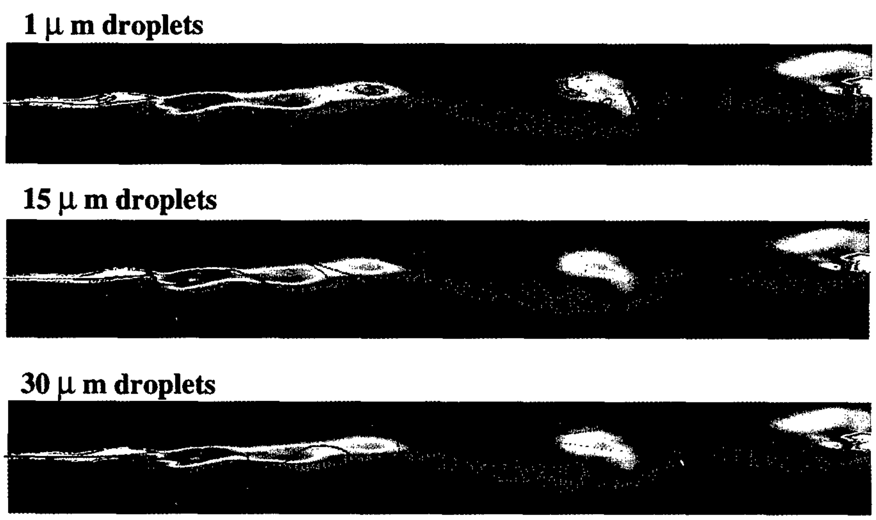

Fig. 11 — The flow field in a ramjet combustor shown along with the distribution of fuel droplets of different sizes. The colors indicate various values of vorticity (blue being the lowest and red being the highest).

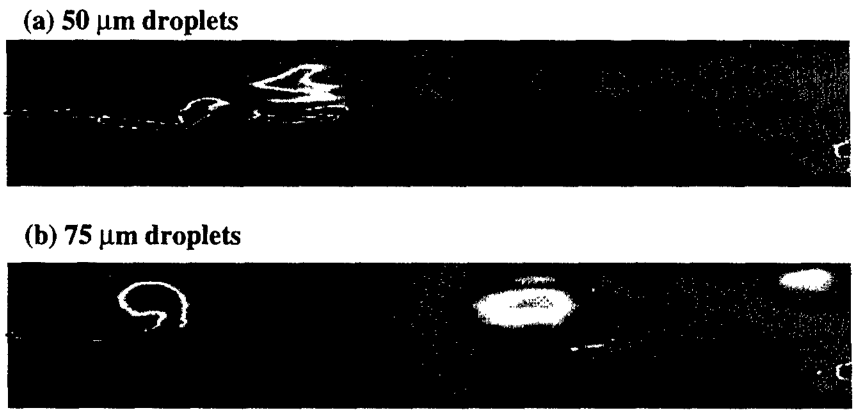

Fig. 12 — Effects of microexplosion on the flow field when droplets of different sizes (a) 50 μm and (b) 75 μm are used.

flow conditions. In the above example, the droplets did not change in size or microexplode. If the temperature of the flow is high enough, significant vaporization will occur, resulting in a change in the size of the droplets and eventual microexplosion.

Effects of Microexplosion: A series of simulations have been carried out to study the effects of microexplosion on the flow field. The time and location where these droplets microexplode depend on the size of the droplets and the core, in addition to the flow environment. When these droplets microexplode and rapidly release their energy, they cause significant disruption of the local flow structures, as shown in Fig. 12. Droplets with an initial size of 50 μm (Fig. 12(a)) vaporize and microexplode in the first half of the combustor while those with an initial size of 75 μm (Fig. 12(b)) are convected significantly further downstream before they microexplode. The microexplosion of the droplets of different sizes has a significantly different effect on the flow field, as shown in the figure. This is because the location of microexplosion affects the coupling between the energy and pressure waves in the system. The first half of the combustor is dominated by vortex shedding and associated high-frequency pressure fluctuations while the second half is dominated by vortex mergings and low-frequency pressure fluctuations. For the simulation shown in Fig. 12(b), the energy released in the microexplosion of the 75 μm droplets couples with a low-frequency pressure oscillation in the system and amplifies it to result in unstable combustion.

Significance: Numerical simulations indicate that microexplosion of the high-energy fuels could lead to unwanted pressure oscillations and combustion instabilities. However, the simulations also show that by suitably choosing the size of the fuel droplets or timing the fuel injection to minimize coupling with the large-scale vortical structures, the tendency towards large pressure oscillations can be minimized. Further simulations using the developed model can have a major impact in the development and potential application of these fuels for Navy propulsion.

[Sponsored by ONR]

References

1. E.J. Chang and K. Kailasanath, "Simulations of Particle Dynamics in a Confined Shear Flow," *AIAA Journal* **34**(6), 1160-1166 (1996).

2. E.J. Chang and K. Kailasanath, "Behavior of Heavy Particles in an Acoustically Forced Confined Shear Flow," *AIAA Journal* **34**(11), 2429-2431 (1996).

3. E.J. Chang and K. Kailasanath, "Dynamics and Microexplosion of High Energy Fuels Injected into a Combustor," to be presented at the 35th Aerospace Sciences Meetings, Reno, Nevada, January 1997 and published as AIAA Paper 97-0126, AIAA, Washington, D.C. (1997). ■

Quasineutral Particle Simulations of Electron Cyclotron Resonance Discharges

M. Lampe, G. Joyce, and W. Manheimer
Plasma Physics Division

For decades now, simulation has been an extremely useful technique for theoretical analysis of plasmas. However, the standard techniques for particle simulation have some serious limitations, which typically restrict their use to microscopic processes rather than global device simulation. Numerical stability requires that time steps be smaller than the plasma period ω_p^{-1} and space steps smaller than the Debye length λ_D; these can be onerous requirements. In quasineutral plasmas, where the electron density is close to the ion density, statistical fluctuations in the charge density pose a nearly insuperable problem. Our work demonstrates a technique for doing full quasineutral particle simulations without such restrictions for the first time [1,2,3]. Furthermore, it provides a self-consistent way of treating plasma sheaths, where quasineutrality does in fact break down.

Fluid Simulations of Quasineutral Plasmas: There are many important examples of quasineutral plasmas in which the shortest relevant time scale is much longer than ω_p^{-1}, and the shortest relevant length scale is much longer than λ_D. Often these plasmas can be simulated with fluid models of the charged species or hybrid models in which one species (usually the electrons) is represented as a fluid, and a particle model is used for the other species. The electrostatic field can then be determined from the electron momentum conservation equation and the requirement of quasineutrality rather than by solving Poisson's equation. This gets around the time and space scale restrictions and the statistical limitations of full particle simulations.

Electron Cyclotron Resonance Processing Plasmas: However, there are many situations in plasma physics where the plasma is quasineutral, but a fluid approximation is not valid for either species. One such example that plays a central role in NRL work on plasma processing is the electron cyclotron resonance (ECR) discharge used in the etching of semiconductors. In this type of device, a magnetized plasma can be sustained at low pressure (below 1 mTorr) by microwaves that are absorbed at a resonant surface where the cyclotron frequency is equal to the microwave frequency. Figure 13(a) shows the ECR reactor in use at NRL. The black cylinders are solenoids, the microwave source is on the right, and the workpiece to be etched is mounted vertically in the stainless-steel

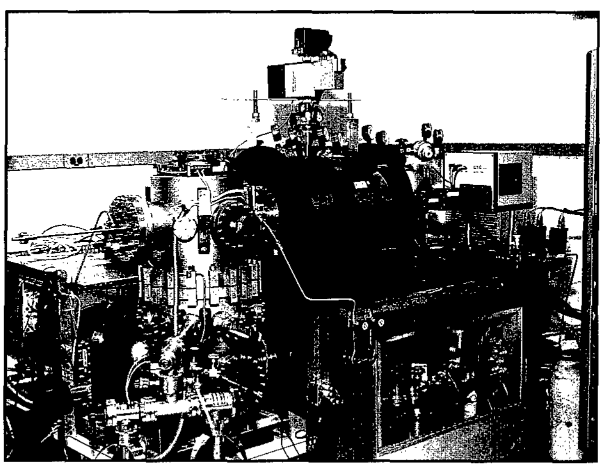

(a)

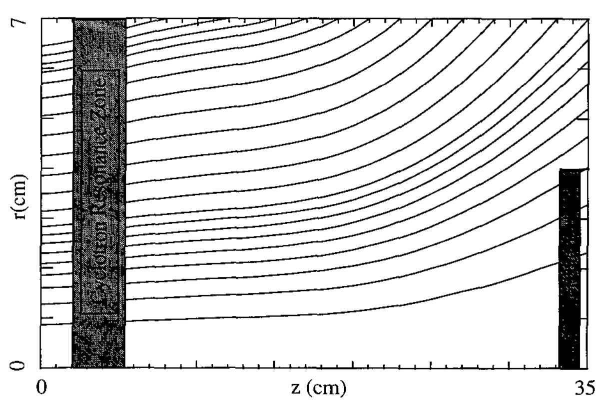

(b)

Fig. 13 — (a) ECR etching apparatus used in NRL research. The microwaves are introduced at the right and absorbed in the resonance region between the two solenoids. Samples are loaded through a load lock at the left and mounted on a movable stage within the plasma chamber. (b) Simulations can be done with the actual reactor geometry, but insight can be developed by using a simplified cylindrical geometry as shown here. The magnetic field lines are seen as the curves which flare out toward the downstream region where the sample is usually mounted. These field lines are used as curvilinear coordinates in the simulation.

vacuum chamber on the left. Figure 13(b) shows a simplified schematic of the magnetic field structure with the cyclotron resonant surface and workpiece highlighted. In this plasma, λ_D is about 10^{-3} cm and the inverse plasma period is about 10^{-11} s. However, the shortest relevant length is the scale length of macroscopic variation, typically several centimeters, and the shortest relevant time scale is the electron transit time over this distance, typically 3×10^{-8} s. The time scale of primary interest is the time to reach equilibrium, typically 10^{-4} s. Simulating the approach to plasma equilibrium for such a reactor in two dimensions (i.e., assuming azimuthal symmetry) with grid spacing 10^{-3} cm and time step 10^{-11} s is an impossible task for today's computers.

Particle Simulations that use Quasi-neutrality to Determine the Electric Field: For this reason, previous simulations have often relied on fluid models. However, the mean free path of both electrons and ions is large (several centimeters) and particle velocity distributions of both species can be non-Maxwellian; thus, a fluid description can be very misleading. Our quasi-neutral particle simulation provides a full kinetic description of the plasma; because macroscopic time and space steps can be used, it is efficient enough to run to equilibrium in a few hours on a workstation. Figures 14 to 16 show results from the simulation of a discharge in argon gas. Figure 14(a) shows the electron density profile along a field line, and Fig. 14(b) shows the average electron temperature on a field line as a function of field line index (roughly speaking, of radial position). The rise in temperature toward the edge, in good agreement with NRL experiments, is a consequence of the more rapid escape of plasma to the walls along the shorter length field lines at the outside. A contour plot of the electrostatic potential, an important parameter of the bulk plasma, is shown in Fig. 15. In semiconductor etching, an important figure of merit is the etch profile, which is controlled by the velocity distribution of the ions bombarding the workpiece. In most cases, the goal is to etch perpendicular to the surface, which requires an ion temperature (in the direction parallel to the workpiece), which is as low as possible. Figure 16 shows a calculation of the ion distribution function at the entrance to the sheath in front of the workpiece.

This simulation scheme, which can calculate plasma properties accurately and inexpensively, is expected to play an important role in the etching of semiconductors at NRL. Applications to other areas of plasma physics are also being explored.

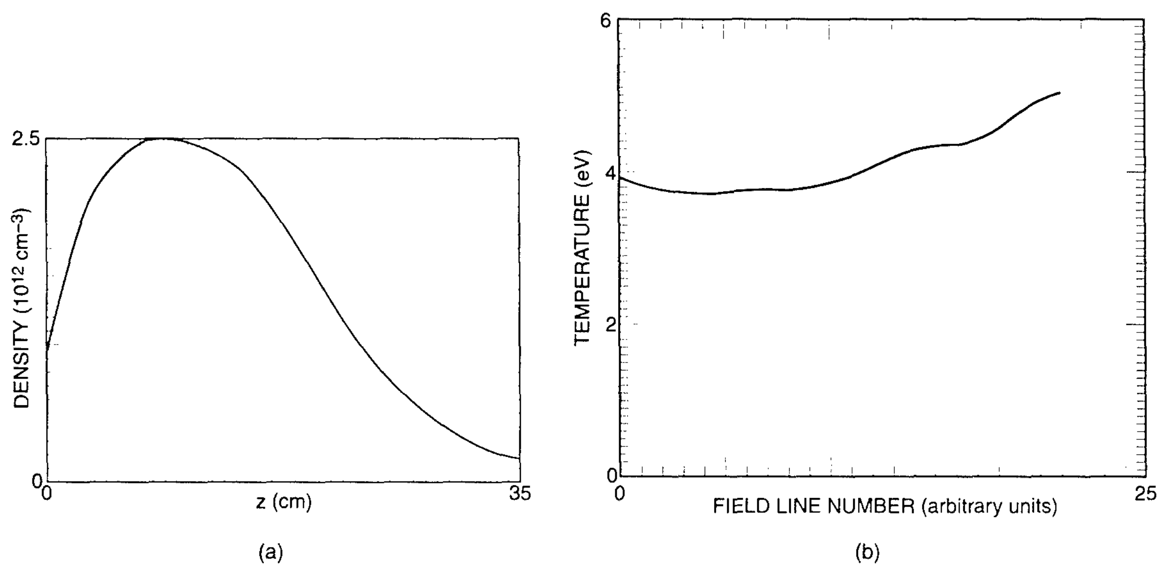

Fig. 14 — (a) Because of the strong magnetic field, electrons are essentially constrained to move along magnetic field lines. A plot of the electron density along one of the field lines as a function of the axial coordinate *z*. (b) This curve gives an indication of the average radial variation of electron temperature. The ordinate is the average temperature of electrons on a field line, and the abscissa is the field line number (see Fig. 13(b)), with field line 0 being on axis.

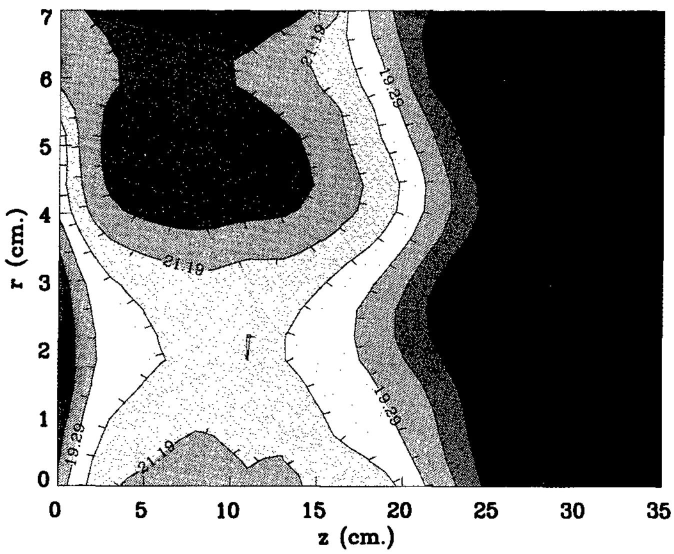

Fig. 15 — The electrostatic potential within the plasma plays a strong role in the dynamics of the electrons and ions. A contour plot of the potential is shown for the geometry of Fig. 13(b).

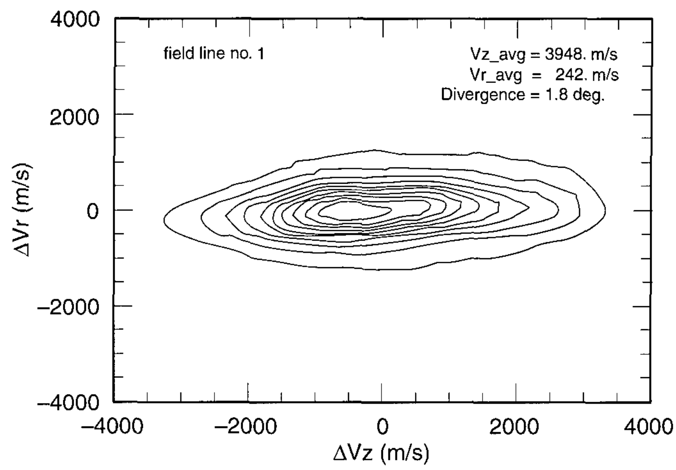

Fig. 16 — A contour plot of the ion velocity distribution $f(v_z, v_r)$ for all of the ions on field line.

Acknowledgment: This work is part of a collaborative effort among the Plasma Physics, Chemistry, Condensed Matter and Radiation Sciences, and Electronics Science and Technology Divisions. S. P. Slinker, C. R. Eddy, S. R. Douglass, and B. V. Weber made important contributions to the work described.

[Sponsored by ONR]

References

1. M. Lampe, W. Manheimer, and G. Joyce, "Quasineutral Kinetic Model of a Magnetized Plasma Discharge," to be published in *Lectures in Plasma Physics and Technology*, V. Stefan, ed. (La Jolla International School of Physics, 1997). Also to be submitted to *IEEE Trans. Plas. Sci.*

2. G. Joyce, M. Lampe, S. Slinker, and W. Manheimer, "Electrostatic Particle in Cell Simulation Technique for Quasineutral Plasma," submitted to *J. Comp. Phys.*, also NRL Memorandum Report 7894 (1996).

3. W. Manheimer, M. Lampe, and G. Joyce, "Langevin Representations of Coulomb Collisions in PIC Simulations," submitted to *J. Comp. Phys.*, also NRL Memorandum Report 7893 (1996). ■

Polarimetric SAR Signatures from Gulf Stream Fronts

J.-S. Lee, R.W. Jansen, D.L. Schuler,
S.R. Chubb, and T.L. Ainsworth
Remote Sensing Division

Introduction: Detecting and understanding ocean current fronts and other ocean surface features using radar measurements are of critical interest to the Navy. The polarimetric synthetic aperture radar (PolSAR) is a superior discriminator in terrain and ice classification, soil moisture measurement, and many other applications when compared with the conventional single-polarization SAR. This study explores PolSAR for a new application: detecting and understanding open-ocean current fronts.

During the recent Gulf Stream experiments, PolSAR imaged the north edge of the Gulf Stream. It was found that when the flight path crosses a convergent current front, the cross-polarization (HV and VH) signal-to-background radar cross-sections from the front are higher (about 2 dB) than the copolarization (VV and HH) signatures. The HV stands for horizontal polarization transmission and vertical reception. In the ambient ocean, cross-polarization radar returns are generally far weaker than copolarization returns. Other polarimetric SAR images from SIR-C and Gulf Stream experiments also confirm this phenomenon. These unusual polarimetric radar signatures are explained by theoretical modeling of radar modulation using an ocean wave model and a composite Bragg-scattering model. Model results agree with the radar measurements at various polarizations and radar frequencies (P-, L-, and C-bands). In addition, a new procedure based on the polarization signature of the Bragg scattering was adopted to measure the slope variation of the front in the azimuthal direction. The surface slope measurement at the front detected a sudden change in slope from positive to negative.

Polarimetric SAR Measurement: The National Aeronautics and Space Administration/Jet Propulsion Laboratory's AIRSAR imaged the north edge of the Gulf Stream with quad-polarization (HH, HV, VH, and VV) at P-band (68 cm), L-band (24 cm), and C-band (5.7 cm) simultaneously. P-, L-, and C-band VV and HV images from a north-south pass across the convergent front near the edge of the Gulf Stream are shown in Fig. 17. The vertical bright line in HV images

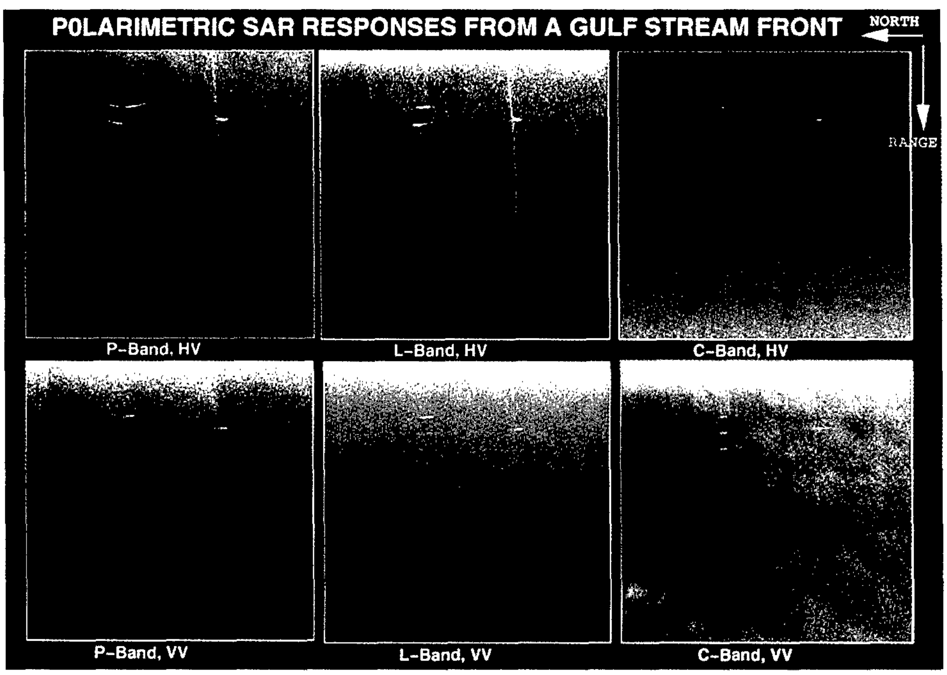

Fig. 17 — HV and VV radar responses of a Gulf Stream front for P-, L-, and C-band are shown here. The PolSAR was flying from south to north (Pass SS360-1). The R.V. *Cape Henlopen* was crossing the convergent front. The HV shows 2 dB signatures at the front, much higher than VV and HH signatures.

corresponds to a surface front having a relatively weak current shear and strong (≅ 20 cm/s) convergence. At the time of the overpass, detailed in-situ measurements were made [1] onboard the research vehicle R.V. *Cape Henlopen*. Figure 17 also shows R.V. *Cape Henlopen* crossing the front. To quantify the radar cross-section, data along a horizontal line across the front were sampled. Fifty samples were averaged to reduce speckle. The results for all three polarizations and bands are shown in Fig. 18. For ambient ocean, cross-sections at VV are the highest, 3-8 dB lower at HH, and 9-18 dB lower at HV. These values are typical for ocean surface returns dominated by Bragg scattering. At the convergent front, however, the HV signal-to-background ratio $\delta\sigma$ is much higher (≅ 2 dB) than those of HH and VV (≅ 0.5 dB). The presence of strong signatures in HV indicates that strong wave-current interaction produces large surface tilts in the along-track direction. Based on the polarimetric analysis of ocean surface Bragg scattering, we have proved that surface tilts in the along-track direction induce higher returns in cross-polarization terms.

Theoretical Modeling: The polarimetric radar signatures near the convergent front and their trends were studied using combined surface-wave propagation and radar-scattering models.

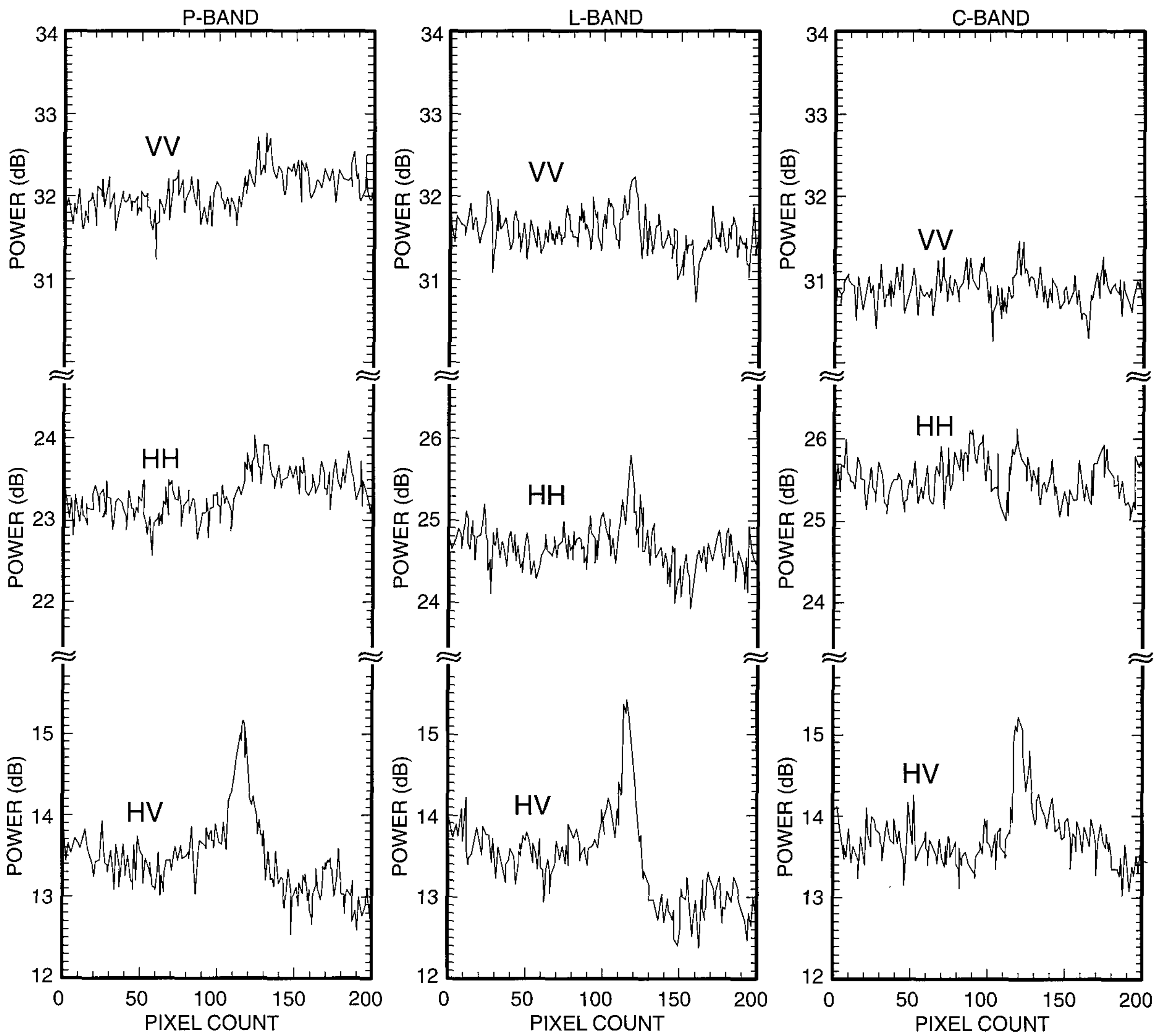

Fig. 18 — To quantify the radar cross-sections of the convergent front in Fig. 17, a cut was made across the front. Fifty samples were averaged to reduce speckle. The radar cross-section $\delta\sigma$ for all three frequencies and for all three polarizations are shown. The distance covered in this plot is 2.4 km (200 pixels). For all three bands, the HV signal-to-background ratio $\delta\sigma$ for the front is much higher (≅ 2 dB) than those of HH and VV (≅ 0.5 dB), and P-band HV has the highest $\delta\sigma$, followed by L-band and C-band.

To incorporate an estimate of the effect of wave breaking to the radar modulation, we use the "sparse breaker" model. In this model, wave-breaking events are assumed to be statistically independent from nonwave-breaking events. Figure 19 shows the theoretical results for the P-band and signal-to-background radar cross-sections $\delta\sigma$ for the cases without wave-breaking and with wave-breaking ($\alpha^0 = 0.25$). The parameter α^0 is the ratio of the ambient wave-breaking to composite-scattering radar cross-sections. Figure 19 reveals that the HV ($\cong$ 2 dB), VV, and HH agree with the observed values as shown in Fig. 18.

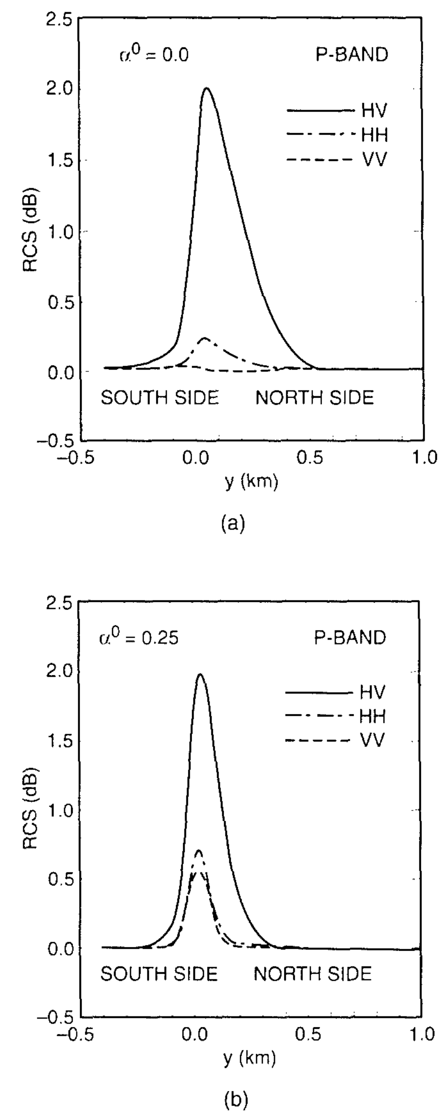

Fig. 19 — Theoretical results for the P-band signal-to-background radar cross-sections $\delta\sigma$ for (a) $\alpha^0 = 0$ (i.e., without wave breaking) and (b) $\alpha^0 = 0.25$ are shown here. The HV (shown in solid line, and $\delta\sigma_{HV} \cong 2$ dB), VV and HH responses are close to the observed values in Fig. 18. With the addition of wave breaking, $\delta\sigma$ increases for HH and VV, while it remains close to 2 dB for HV.

Ocean Surface Slope Measurement: A new technique based on the polarization signature of Bragg scattering has been developed that uses polarimetric SAR to measure the ocean surface slope in the along-track direction. It is an extension of a recently developed technique for terrain slope measurement [2]. The slopes measured are a combination of the mean slope of the ocean near the front and the mean slope caused by the perturbation in the wave structure. Figure 20 depicts the ocean surface slope computed using the P-band polarimetric SAR. To quantify the slope change at the front, a 50-line average below the ship is also plotted in Fig. 20. The estimated slope at the front is dominated by an abrupt change of +0.8° to −0.5°. The strikingly different measured slopes between the left and the right side of the front indicate the strong difference in wave spectra.

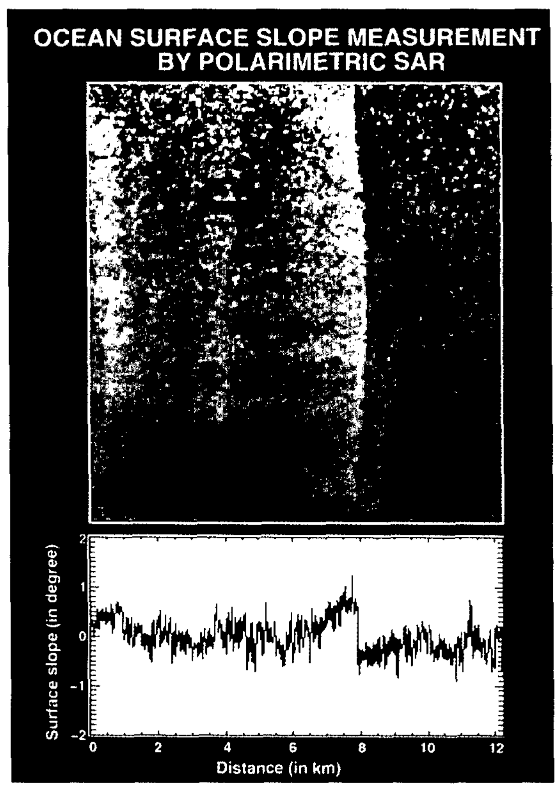

Fig. 20 — Ocean surface slope computed by the new slope estimation algorithm using P-band PolSAR. The top image shows the estimated slopes with gray levels varying between +2 and −2 degrees. The figure below the image shows a 50-line average at a position below the ship. The estimated slope at the front is dominated by an abrupt change of +0.8 to −0.5 degrees.

Significance: Ocean features such as the current front that may be difficult to detect by the conventional copolarization SAR can be observed readily using a polarimetric SAR. The additional advantage provided by the polarimetric SAR is the capability of slope measurement. The technique is also significant for its potential ability to remotely sense and discriminate between classes of ocean features.

Acknowledgment: We thank the NASA/JPL AIRSAR team for collecting and processing the SAR data.

[Sponsored by ONR]

References

1. G.O. Marmorino, et al, "Gulf Stream Surface Convergence Imaged by SAR," *J. Geolog. Res.* **99**(C9), 18315-18328, September 15, 1994.

2. D.L. Schuler and J.S. Lee, "Polarimetric SAR Remote Sensing of Topography," *1996 NRL Review*, pp.147-149. ■

Long-term Simulations with a Coupled Global Atmosphere-Ocean Prediction System

T.F. Hogan and T. Li
Marine Meteorology Division

By the use of a complex atmospheric model, weather can be predicted numerically for a few days. If the same model is coupled to an advanced ocean model, the coupled system may extend current forecast limits from days to weeks and months. The critical feature of any coupled ocean-atmosphere general circulation system is the ability to simulate climatic variability on season-to-interannual time scales. At present, a few such systems are being developed, and they have experienced some degree of difficulty in simulating the observed ocean/atmospheric states.

Statistics of 11 coupled general circulation models reveal a common problem in simulating the climatic asymmetry of relevance to the intertropical convergence zones (ITCZ) [1]. Some of the coupled models produce double ITCZs. A serious problem that has commonly been found is the failure to predict very thin, low-level marine stratus clouds off the coasts of the Americas. These clouds have a fundamental impact on the Earth's energy budget. Some of the coupled models were able to reproduce a reasonable interannual variation when forced by the annual mean solar radiation, but they failed when seasonally varying solar radiation was specified. Other systems simulated the seasonal cycle well, but they simulated interannual variations poorly. The goal of the Naval Research Laboratory's ongoing study is to build a global coupled atmosphere-ocean prediction system and to simulate and predict both seasonal and interannual variability in the coupled system.

System Description: The atmospheric component of the coupled model is the state-of-the-art Naval Operational Global Atmospheric Prediction System (NOGAPS) [2], which was developed by NRL. The oceanic component is the Geophysical Fluid Dynamics Laboratory's Modular Ocean Model (MOM) [3], which consists of full thermodynamics and dynamics with a free surface elevation. A technique has been developed so that different resolution atmospheric and ocean models can be coupled easily through a simple interface, which automatically interpolates and transfers data from each grid. The ocean and atmosphere can be coupled at any desired space or time interval. The atmosphere and ocean interact in such a way that the atmosphere influences the ocean through surface wind stress, radiation, precipitation, and surface heat and moisture exchange, whereas the ocean affects the atmosphere through sea-surface temperature (SST), surface oceanic currents, and moisture and heat fluxes. In the current study, the atmospheric model has a resolution of 3° with 12 vertical levels, and the ocean model has a resolution of 2° in longitude and 0.5° in latitude between 5°S and 5°N, increasing to 2° latitude at 50°N.

Coupling Strategy: A serious problem faced by all coupled air-sea systems today is the climate drift problem. While each component of the system may be good, when they are coupled, they begin to drift to an unrealistic state, typically with a poor simulation of the ITCZ. The common way to lessen the problem is to adopt a flux adjustment method. Many current systems use a time-varying adjustment, which forces the seasonal cycle. In the current work, we adjust only the annual mean SST. This annual mean flux adjustment does not damp the variations of motions, so the system is suitable for extended medium-range and long-range forecasts.

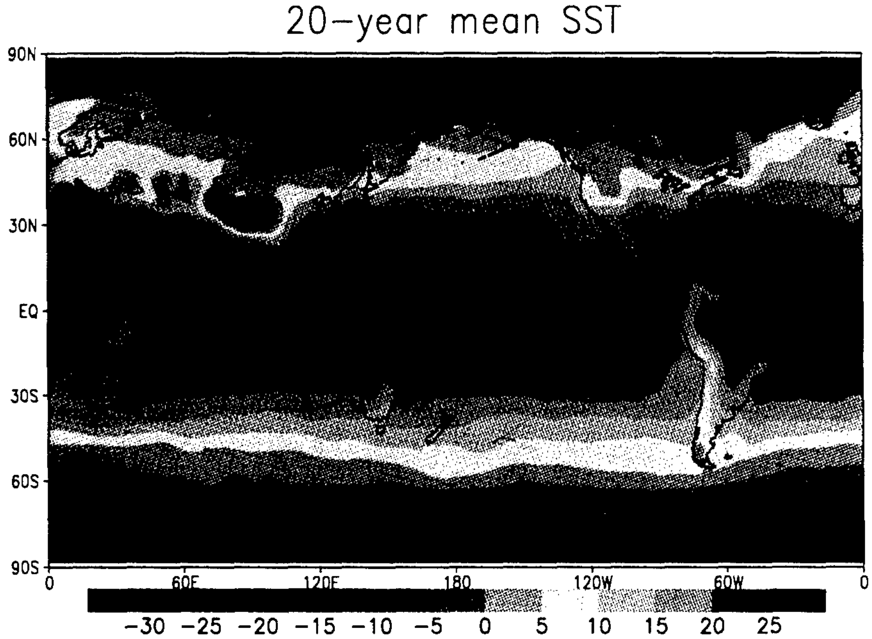

Fig. 21 — The horizontal map of the 20-year averaged ocean and land surface temperature field simulated by the coupled atmosphere-ocean prediction system.

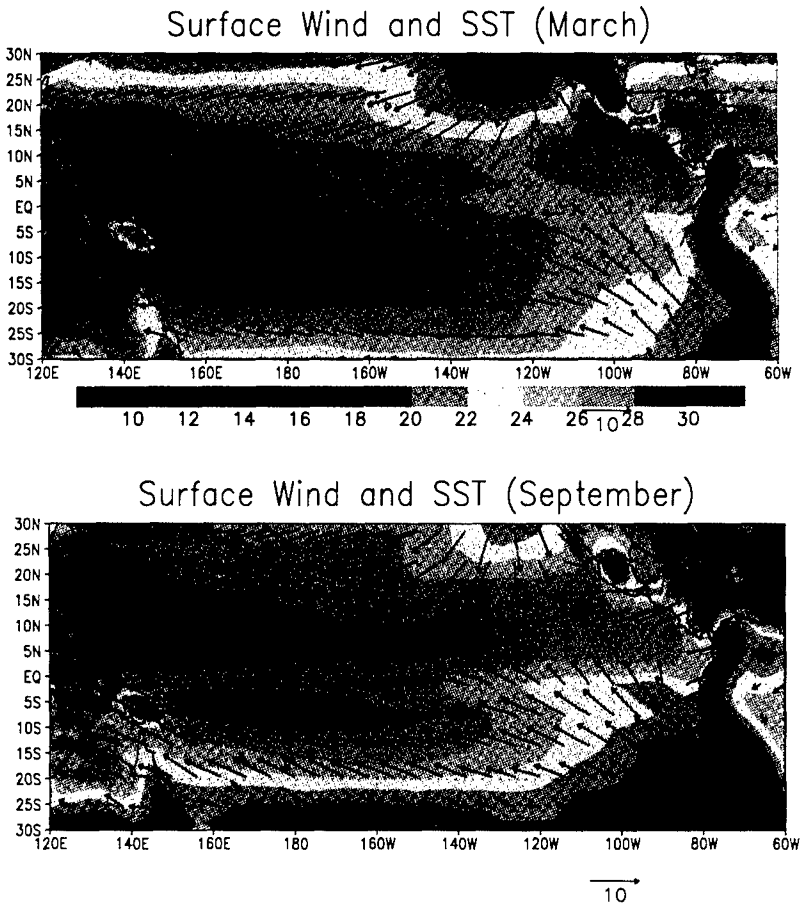

Fig. 22 — The simulated surface temperature and wind fields in two extreme months of the seasonal cycle: (a) March and (b) September.

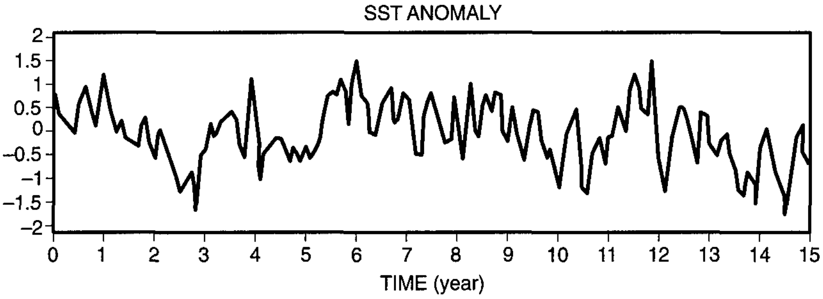

Fig. 23 — Interannual variations of the model simulated sea surface temperatures (during the last 15-year integration) in the equatorial Pacific (130°W-150°W).

System Results: A 20-year integration was performed with the coupled system. Figure 21 illustrates the simulated 20-year mean SST and surface ground temperature field. This time-mean state is close to the long-term observed climatology. There is a east-west asymmetry in SST in the equatorial Pacific and Atlantic, with a warm pool in the west and a cold tongue in the east. There is also a north-south asymmetry, with the warmest water to the north of the equator and very cold water to the south. The seasonal SST variations illustrate a distinctive difference between the western and eastern tropical Pacific. In the western Pacific, maximum SST (as well as maximum rainfall) exhibits a clear north-south movement, closely following the Sun's movement. Therefore, it has a semiannual signal at the equator. In the eastern Pacific, on the other hand, maximum SST moves westward along the equator. An annual signal in both SST and wind fields is observed at the equator even though the solar radiation is dominated by a semiannual forcing (because the sun "crosses" the equator twice a year). Such an annual cycle is attributed to ocean-atmosphere interactions and to the asymmetric time-mean state [4]. The coupled NOGAPS/MOM system is capable of simulating all the above features. Figure 22 shows the simulated surface wind and SST fields in two extreme months of the seasonal cycle — in March when the equatorial cold tongue is weakest and in September when it is strongest. In addition to the seasonal cycle, the coupled system is able to simulate interannual variability. Figure 23 illustrates the interannual signals of modeled SST in the equatorial Pacific. The interannual variations in the model result from the strong coupling between the atmosphere and ocean. The horizontal structure of the anomalous warm (cold) SST resembles well the observed El Niño (La Niña) conditions.

The long-term simulations clearly demonstrate the system's ability to predict climatic variability, such as the El Niño-Southern Oscillation phenomenon, on seasonal-to-interannual time scales in the coupled ocean-atmosphere system. Similar research has most often been accomplished with simplified models. Use of sophisticated primitive equation models for both the ocean and the atmosphere promises to provide new insight into the nature of these strong climatic signals, which will eventually improve the Navy's medium-range forecast skill.

[Sponsored by ONR]

References

1. C.R. Mechoso, A.W. Robertson, N. Barth, M.K. Davey, P. Delecluse, P.R. Gent, S. Ineson, B. Kirtman, M. Latif, H. Le Treut, T. Nagai, J.D. Neelin, S.G.H. Philander, J. Polcher, P.S. Schopf, T. Stockdale, M.J. Suarez, L. Terray, O. Thual, and J.J. Tribbia, "The Seasonal Cycle over the Tropical Pacific in General Circulation Models," *Mon. Wea. Rev.*, in press (1996).

2. T.F. Hogan and T.E. Rosmond, "The Description of the Navy Operational Global Atmospheric Prediction System's Spectral Forecast Model," *Mon. Wea. Rev.* **119**, 1786-1815 (1991).

3. R.C. Pacanowski, "MOM 2 Documentation, User's Guide and Reference Manual," Ocean Technical Report #3, Geophysical Fluid Dynamic Laboratory, NOAA Lab located at Princeton, N.J. (1995).

4. T. Li and S.G.H. Philander, "On the Annual Cycle of the Eastern Equatorial Pacific," *J. Climate*, in press (1996). ■

Space Research and Satellite Technology

A Soft Error Immune GaAs Technology Fabricated with Low-Temperature-Grown GaAs

D. McMorrow, J.S. Melinger, and C.J. Marshall
Condensed Matter and Radiation Sciences Division

Modern satellite systems depend on high-performance microelectronics for communications and the onboard processing of information (such as data encryption/decryption and compression/decompression). The high speed and total dose hardness of GaAs-integrated circuits make them attractive candidates for such space-based applications. A primary limitation of this technology, however, is its high sensitivity to ion-induced soft errors, or single-event upsets (SEUs), such that the SEU performance of the currently available GaAs technology is 5 to 7 orders of magnitude below typical mission requirements. Recent work performed at the Naval Research Laboratory reveals that the incorporation of a low-temperature grown GaAs (LT GaAs) buffer layer beneath the active region of field-effect transistor (FET) gives rise to a GaAs technology that is effectively immune to single-event phenomena, without the performance and cost penalties that are commonly associated with circuit- and system-level hardening methods [1-3]. The results of this work are far reaching and will impact both the commercial and military space electronics industries. The goal of an ongoing joint project involving NRL, the Naval Postgraduate School, and several industrial partners is to develop one or more sources of commercial-off-the-shelf (COTS), state-of-the-art, high-performance GaAs technology that is effectively immune to SEU. Implementation of such a technology will permit the space systems designer access to the complete breadth of designs offered by commercial foundries, resulting in radiation tolerance at low cost with the high density, high speed, low power consumption and software availability that are associated with commercial parts.

Low-Temperature-Grown GaAs: The designation LT GaAs refers to a class of GaAs materials grown in an As-rich environment via molecular beam epitaxy at temperatures below the normal growth temperature of 600° C. The electrical, optical, and mechanical properties of LT GaAs depend, in a sensitive fashion, on the growth and anneal history of each wafer. A commonly implemented form of LT GaAs involves a growth temperature of approximately 200° C, followed by a higher temperature anneal (typically ~ 600° C). The resulting material is highly nonstoichiometric, with an excess As concentration of approximately 2%, a trap density of greater than 10^{18}cm^{-3}, and an excess carrier lifetime as short as 150 fs.

Charge-Collection Measurements: Figure 1 shows a schematic diagram of the cross section of a GaAs heterojunction field-effect transistor (HFET) showing the location of the LT GaAs buffer layer. When an energetic charged particle (such as a galactic cosmic ray) interacts with a transistor, a dense track of electron-hole pairs is created along the ion's path (shown in Fig. 1). The generation, transport, and collection (at the terminals of a transistor) of these carriers are the primary events responsible for the ultimate observation of an SEU in a complex integrated circuit.

Standard methods for hardening GaAs integrated circuits (ICs) to SEUs involve redundancy at the system or circuit level and software-level error detection and correction (EDAC) schemes. Such methods suffer from reduced performance, increased design complexity, increased weight, decreased circuit density, and increased power consumption. The incorporation of an LT GaAs buffer layer into the substrate alleviates the need for such approaches by addressing and effectively eliminating the problem at the transistor level.

Figure 2 shows charge-collection transients measured for GaAs HFETs fabricated with and without an LT GaAs buffer layer for irradiation by 3 MeV α particles at normal incidence. Figure 3 shows the corresponding time-integrated data as a function of gate bias. The short carrier lifetime of the LT GaAs buffer layer leads to a significant

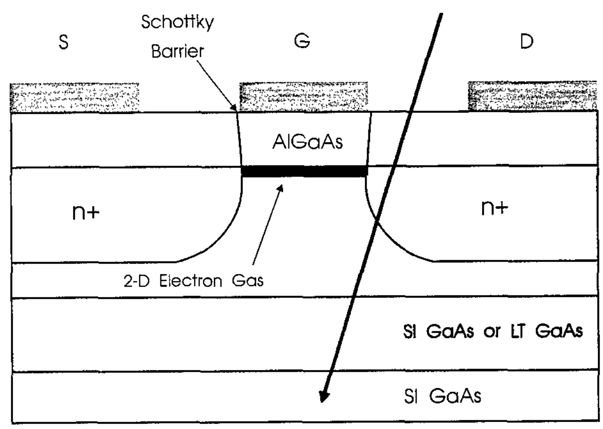

Fig. 1 — Diagram of the n-channel HFET investigated in this study (not to scale).

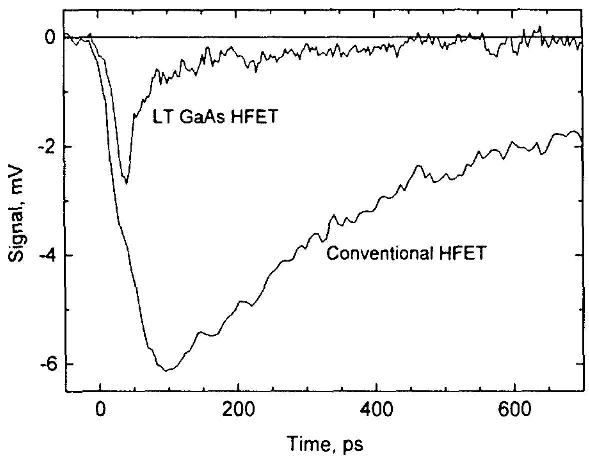

Fig. 2 — 3 MeV α-particle-induced drain charge-collection transients measured for an n-channel HFET device with and without the LT GaAs buffer layer (into a 50 Ω load). $V_G = 0$ V; $V_S = 0$ V; $V_D = 4$ V for the LT device; and $V_D = 1.5$ V for the conventional device.

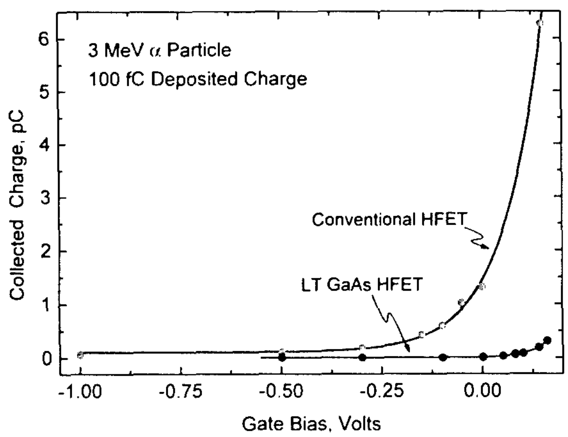

Fig. 3 — Time-integrated charge-collection measurements performed as a function of gate bias for irradiation by 3 MeV α particles. $V_D = 2$ V; $V_S = 0$ V.

reduction in the charge-collection efficiency for the LT GaAs device that is evident for all bias conditions investigated. Charge-collection measurements on individual transistors, such as those of Figs. 2 and 3, provide insight into the mechanisms of carrier transport and collection in GaAs devices. For GaAs FETs, the high density of carriers created by an energetic ion can disrupt the normal operation of the device, leading to a situation in which more charge is collected than the total deposited by the ion (charge enhancement). This charge enhancement is believed to be a primary cause of the poor SEU performance of GaAs FET-based ICs. Following an ionizing event, the short carrier lifetime of the LT GaAs layer rapidly reduces the free carrier density in the device, inhibiting the development of charge-enhancement processes, resulting in a significant reduction in the collected charge.

This effect is illustrated by the two-dimensional computer simulation data shown in Fig. 4, which compares the electron density distribution 100 ps after excitation by a 630-nm optical pulse for metal/semiconductor field-effect transistor (MESFET) devices with and without an LT GaAs buffer layer. The location of the LT GaAs buffer layer is indicated in the figure. As is evident in the upper regions of the device, the electron density is several orders-of-magnitude lower in the LT GaAs device.

SEU Measurements: Heavy-ion SEU measurements were performed at the Brookhaven National Laboratory Single-Event Upset Facility on GaAs-complementary HFET integrated circuits fabricated with and without an LT GaAs buffer layer [2]. Test samples were taken from two separate wafers that were processed together with identical masks. The wafers differed only in that an

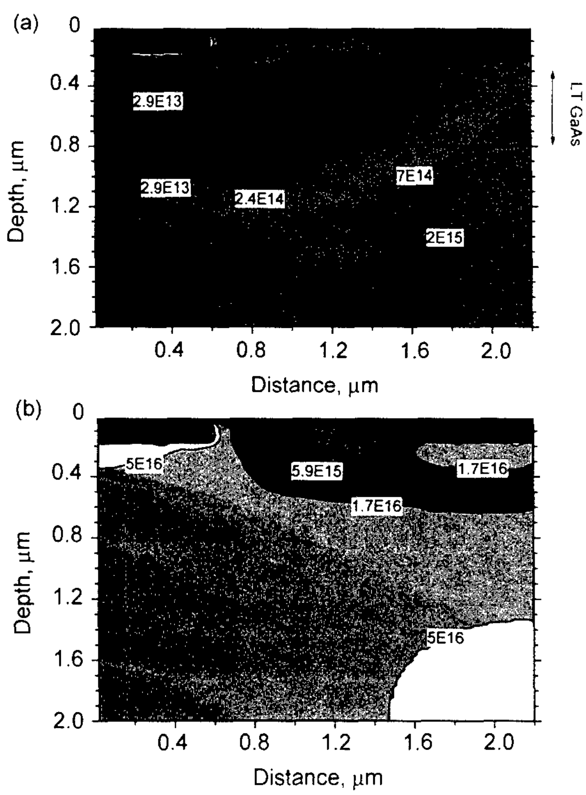

Fig. 4 — Constant electron density contours (cm^{-3}) at 100 ps after the laser pulse for structures (a) with and (b) without a 0.5 µm thick buffer layer with a 1 ps lifetime. $V_D = 2.5$ V; $V_G = 0.05$ V; and $V_S = 0$ V.

LT GaAs buffer layer was grown as part of the epitaxial structure on one wafer. Tests on the conventional (non-LT) parts revealed SEU thresholds in the range of 1 to 3 MeV · cm^2/mg, with a saturated cross section of 10^{-6} cm^2/bit, in agreement with expectations for conventional GaAs ICs. For the LT GaAs devices, which were otherwise identical to the non-LT parts, no upsets were observed for any of the ions tested. These tests involved ions with energy deposition rates ranging from 2.5 to 90.7 MeV · cm^2/mg, with $> 10^7$ particles delivered for each case. The measured SEU threshold of 90 MeV · cm^2/mg renders these parts effectively immune to SEU in the natural space radiation environment (an SEU threshold of > 30 MeV · cm^2/mg typically is considered quite good).

Pulsed laser SEU measurements at 800 nm were performed to provide corroborating evidence of the observed SEU immunity. The conventional (non-LT) circuit upset with an incident laser pulse energy of 6.3 pJ; the LT circuit did not upset for an incident laser pulse energy of 260 pJ. This result, which is consistent with the heavy-ion SEU results, implies a factor of > 40 increase in the SEU threshold for devices fabricated on LT as compared to conventional GaAs substrates.

Conclusions: The results presented here demonstrate that the use of an LT GaAs buffer layer below the active region of a GaAs FET can effectively eliminate the charge-enhancement mechanisms that dominate the charge-collection processes of these devices. The resultant reduction in collected charge gives rise to a significant decrease in the SEU susceptibility of LT GaAs ICs when compared to those of the conventional technology. The heavy ion SEU measurements predict an improvement of eight orders of magnitude in the SEU error rate for geosynchronous orbit — for example, corresponding to an error rate of less than 10^{-10} errors/bit/day. We note that the work described here was performed on research devices. Work in progress is geared toward the development of commercial sources for LT GaAs ICs.

Acknowledgments: The authors acknowledge the contributions of others involved in this work, in particular: Paul Marshall, Todd Weatherford, Lan Huu Tran, Martin Carts, Steve Buchner, Arthur Campbell, and Walter Curtice.

[Sponsored by ONR]

References

1. D. McMorrow, T.R. Weatherford, W.R. Curtice, A.R. Knudson, S. Buchner, J.S. Melinger, L.H. Tran, and A.B. Campbell, "Elimination of Charge-Enhancement Effects in GaAs FETs with an LT GaAs Buffer Layer," *IEEE Trans. Nucl. Sci.* **NS-42**, 1837 (1995).

2. P.W. Marshall, C.J. Dale, T.R. Weatherford, M. Carts, D. McMorrow, A. Peczalski, S. Baier, J. Nohava, and J. Skogen, "Heavy Ion SEU Immunity of a GaAs Complementary HIGFET Circuit Fabricated on a Low-Temperature-Grown Buffer Layer," *IEEE Trans. Nucl. Sci.* **NS-42**, 1850 (1995).

3. D. McMorrow, T.R. Weatherford, S. Buchner, A.R. Knudson, J.S. Melinger, L. H. Tran, and A. B. Campbell, "Single-Event Phenomena in GaAs Devices and Circuits," *IEEE Trans. Nuc. Sci.* **NS-43**, 628 (1996). ■

The Highest Angular Resolution Image Ever Made in Optical Astronomy

D. Mozurkewich and J.T. Armstrong
Remote Sensing Division

J.A. Benson
U.S. Naval Observatory

Atmospheric Turbulence: Astronomers have sought higher angular resolution ever since Galileo first pointed a telescope at the sky. But the turbulence of the atmosphere becomes dominant once the telescope diameter reaches about 10 cm, limiting even large telescopes to a resolution of about 1 arc sec.

In the past 2 decades, three approaches to negating the effects of the atmosphere have developed. The first and most straightforward is to put the telescope above the atmosphere. A second approach, known as "adaptive optics," involves smoothing the distortions in the incoming wavefront with a flexible mirror. But in both of these approaches, the resolution is limited by the size of the primary mirror of the telescope: 2.4 m for the Hubble Space Telescope or 10 m for the Keck Telescopes, the world's largest.

Optical Interferometers: The third approach is optical interferometry. The simplest interferometer consists of two small telescopes that collect light and send it to a central optics laboratory. The typical telescope separations of tens of meters or more provide the resolution of a telescope tens of meters across. In the laboratory, adjustable delay lines compensate for the fact that the atmosphere has retarded the wavefronts arriving at the two telescopes by slightly differing amounts.

The beams are then allowed to interfere with one another. The strength of the interference fringe, along with the known length and orientation of the baseline — the line joining the two telescopes, gives us the amplitude of one Fourier component of the stellar image. Several such observations then permit some reconstruction of the appearance of the star.

In the past decade, two-telescope interferometers have become routine, with several instruments in use [1]. The ongoing program at NRL, which operated the 31.5-m Mark III Interferometer on Mt. Wilson, California, from 1986 to 1992, was particularly successful, producing about half of all the scientific results reported in optical interferometry.

Making an Image: However, a two-element optical interferometer is incapable of making a true image: the atmospheric retardations of the wavefronts completely mask any difference in arrival time that might be due to the shape or position of the star being observed. We can use the amplitude of the interference fringe, but its phase is meaningless.

The only way to make a true image is to observe with three or more telescopes. On each baseline, the fringe phase is due to the difference in atmospheric retardation at the two telescopes forming the baseline, plus a contribution from the structure of the star being observed. If we form the "closure phase" by adding the fringe phases around the triangle of baselines, the atmospheric retardation at each telescope enters once with a plus sign and once with a minus sign. Thus the atmospheric effects cancel: the closure phase is due only to the star itself.

The closure phase idea when applied to radio interferometry was first demonstrated at visual wavelengths by a group led by John Baldwin at Cambridge University [2] using a small test array with telescopes separated by up to 6 m. Six months later, the NRL group succeeded in making three-telescope closure-phase observations, using a full-size array, with the Navy Prototype Optical Interferometer (NPOI).

The NPOI: The NPOI, currently nearing completion near Flagstaff, Arizona (Fig. 5), is a joint project of NRL and the U.S. Naval Observatory (USNO) in cooperation with Lowell Observatory. It is planned to include a Y-shaped, six-telescope imaging array (baseline lengths from 2 m to 437 m) and a four-element astrometric array (18 m to 38 m) that both share an optics laboratory. The maximum resolution will be about 0.0004 arc sec, about 50 times better than that of a 10-m telescope.

Among the optical interferometers being built around the world [1], the NPOI is unique: it will combine light from more telescopes (up to six) and have longer baselines than all but one of its competitors. It already uses a wider optical bandpass (0.45- to 0.85-nm wavelength in 32 channels) than any other current array.

Both the large number of telescopes and the wide bandpass are critical to the imaging capabilities of the NPOI. With 6 telescopes forming 15 distinct baselines, there are 10 independent closure phases compared to only 1 for a 3-telescope, 3-baseline array. The wide multichannel bandpass, in addition to increasing the sensitivity of the interferometer, gives simultaneous measurements of 32 Fourier components of the stellar image on each baseline.

First Results: By early 1996, three telescopes of the astrometric array of the NPOI were

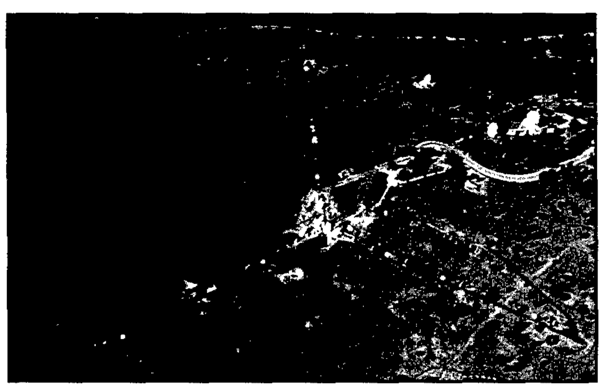

Fig. 5 — An aerial view of the NPOI near Flagstaff, Arizona, taken in October 1996. The optics laboratory is the largest building in the picture, 50 m in length. The small white buildings house the telescopes of the astrometric array. The Y of the imaging array, with arms 250-m long, consists of 30 locations at which the 6 imaging telescopes may be placed.

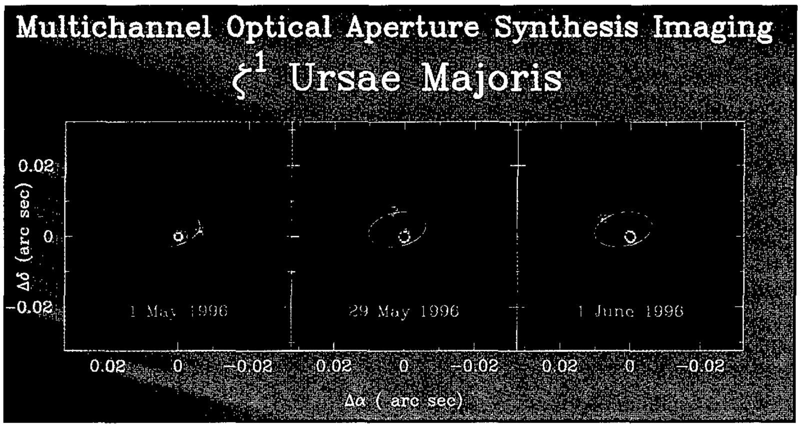

Fig. 6 — The first images obtained with the NPOI, showing the two components of the binary star ζ^1 Ursae Majoris (Mizar A) on three different dates. The primary component is placed at the center of each frame. The ellipse shows the orbit of the secondary relative to the primary, as measured with the Mark III Interferometer — the predecessor to the NPOI.

operational, providing baseline lengths from 18 m to 38 m. We obtained the first images in May and June, observing ζ^1 Ursae Majoris (Mizar A), a spectroscopic binary star with an orbital period of 21 days. These images, with a resolution of 0.002 arc sec, are the highest-resolution images ever made at visual wavelengths, clearly showing the two stars separated by 0.006 arc sec.

Figure 6 shows the first three images, where the brighter component is placed at the center of each frame. The revolution of the two stars about one another is clearly visible from frame to frame. The ellipse shows the orbit of the secondary star around the primary as determined by observations with the Mark III interferometer 6 years earlier. The agreement between the Mark III results and the current data are very good. Since these results were obtained, we have observed Mizar A four more times, sampling a part of the orbit that we missed with the Mark III. We are now revising the Mark III orbit in the light of the new data.

The ability to identify binary stars and precisely locate the photocenters of single stars is an essential part of the USNO astrometry program and will lead to advances in fundamental astrophysics as well.

[Sponsored by ONR and Oceanographer of the Navy]

References

1. J.T. Armstrong, D.J. Hutter, K.J. Johnston, and D. Mozurkewich, "Stellar Optical Interferometry in the 1990s," *Physics Today* **48**(5), 42-48 (1995).
2. J.E. Baldwin et al., "The First Images from an Optical Aperture Synthesis Array: Mapping of Capella with COAST at Two Epochs," *Astron. Astrophys.* **306**, L13-L16 (1996). ■

A Virtual Communications Environment for Remote Management, Command, and Control of Space Systems

S.B. Gardner
Space Systems Development Department

A virtual communications environment (VCE) is a computer-based environment in which multiple participants at remote locations interact within a shared, three-dimensional world. For effective operation of next-generation space systems, system operators at remote locations will need to interact in real time. VCE imbeds peer-to-peer management, command, and control on multiple computers over broadband networks, such as asynchronous transfer mode (ATM). The control paradigm and technology for moving through shared worlds is similar to that of the emerging virtual reality (VR) standards for the Internet.

Introduction: Computers and networks are merging. The ability to manage computer resources independently of network resources is no longer an option. System managers, network administrators, and computer operators need real-

time access and insight into the computer-network system to effectively monitor, interrogate, control, and reallocate resources. Should a bottleneck appear in a network, data rerouting and resource reassignment may be required. Mutual interaction must take place where each of the (spatially distributed) operators can view the same data and be able to interact quickly to determine the best course of action. A related application of VCE is significantly improved training of system operations personnel (for example, remote tutoring). VCE will also contribute to the rapid training of system managers and network administrators.

Program Concept: To date, "traditional" implementations of VR worlds have required computer scientists with experience in object-oriented programming. A primary goal of the VCE program is construction and use by engineers. This includes easy reconfigureability and extensibility. To accomplish this goal, automation of the description and manipulation of three-dimensional (3-D) network components will be required, together with the construction of a complete set of visual software tools and user documentation. The concept will be to furnish end users with a VCE toolkit that contains a standard library of 3-D "clip" objects, such as computers, ATM switches, etc. These library components can be inserted and manipulated dynamically within VCE.

World Representations: The VCE world representations, ways to move among them, and processes that run within them follow the pattern shown in Fig. 7. Note that each world consists of objects with geometries, attributes, and possibly behavior characteristics. Objects communicate among themselves, within a given world, by sending and receiving signals to and from each other. An *avatar*, which represents a remote operator, is another object in the world with behavior that includes moving, grasping, and sending signals to other objects, such as turning switches on and off to activate another process. In addition, an object can respond to real-time data acquisition by altering its behavior or signaling other objects to take action. Note also that World 4 contains two objects, each of which have gateways to other worlds. The mechanism for passing through this gateway is to try to walk through it. This action collides with an *aura* about the object, which triggers a signal to load a new world from file or from another user's memory database, if already populated. Auras are, by definition, objects that respond when other

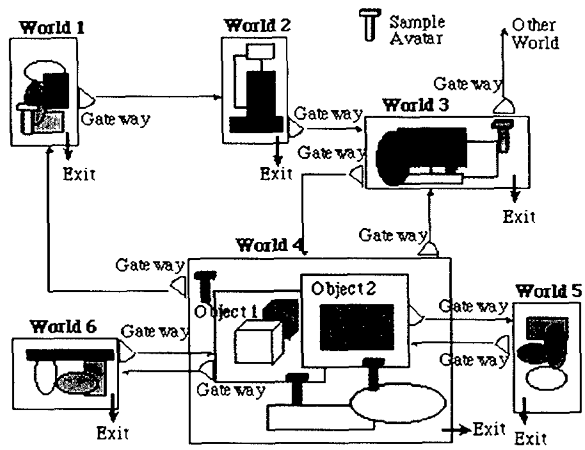

Fig. 7 — World representations.

objects invade their space. In fact, any object can have a defined aura that is of arbitrary geometric shape. This paradigm, in effect, establishes an *awareness* of objects of each other, if defined. Signals are generated at the designer's preference in response to aura invasion.

Operational Demonstration: The VCE project has built and tested an enhanced prototype at an operational site to demonstrate management and control of computer networks. Some of the "World" components, such as a landscape and objects, are illustrated in Figs. 8 and 9. These are screen shots taken from a VCE operational demonstration. Other VCE components such as "Objects/Icons" may be represented by abstractions. Figure 10 shows an abstraction of computer internals represented by CPU, Memory, Network, etc. Clicking on an iconic representation in the abstraction opens a window displaying real-time operations, as shown at the bottom of the figure. The VCE network world is represented by a 3-D network diagram, shown in Fig. 11. The network components — computers and switches — are connected by links shown in green. The component network addresses are shown above the objects.

Summary: VCE is a project to build a set of VR tools that can be used to implement a collaborative environment for management and control of computer networks. These tools, when completed, will provide for the construction by engineers of a virtual communications environment for use by system operators in the management, command, and control of next-generation space systems.

Fig. 8 — VCE screen shot; computer components.

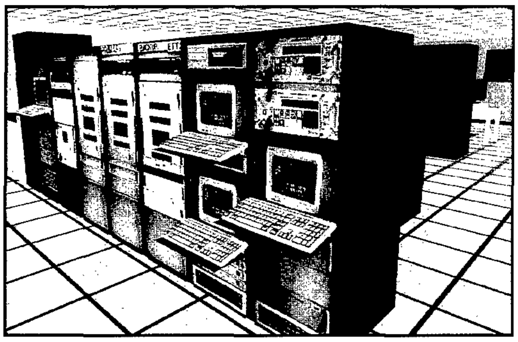

Fig. 9 — VCE screen shot; racks of equipment.

Fig. 10 — Abstractions of computer internals.

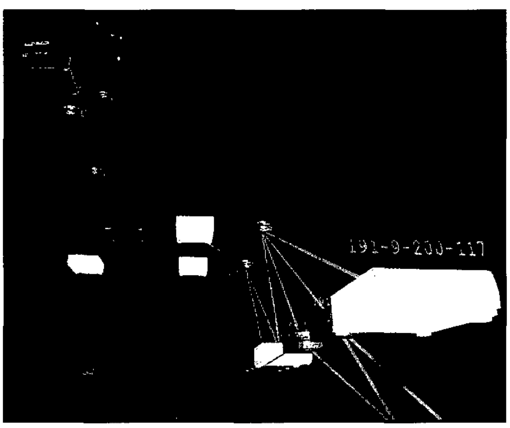

Fig. 11 — Network world.

Acknowledgments: The author acknowledges the encouragement and support of Andrew Fox, William Nead, Vincent Menotti, and George Edwards of NRL. The efforts of John Balash, Mike Saverino, and Hube Callihan of NetSpace Corporation, and Mike Pietrzyk of Advent Systems, Inc., are also acknowledged and appreciated.

[Sponsored by the U.S. Air Force]

References

1. S. Gardner, J. Balash, H. Callihan, and M. Saverino, "A Virtual Communications Environment (VCE) for Command and Control of Complex Systems," 1996 Command and Control Research Symposium, Navy Postgraduate School, Monterey, California, 1996.

2. S. Gardner, J. Balash, H. Callihan, and M. Saverino, "A Virtual Communications Environment (VCE) for Remote Management and Control of Space Systems," 1996 AIAA Space Programs and Technologies Conference, Huntsville, Alabama, Sept. 1996. ■

The Tether Physics and Survivability Spacecraft (TiPS)

S.L. Coffey and W.E. Purdy
Spacecraft Engineering Department
Naval Center for Space Technology

W.J. Barnds
Swales and Associates

Overview: The Tether Physics and Survivability (TiPS) Experiment was conceived as a quick response, simple experiment to study the long-term dynamics and survivability of tethered space systems. The knowledge gained from this experiment will help the Department of Defense and the nation gain experience with tethered systems for eventual use in operational spacecraft. The Naval Center for Space Technology (NCST) designed, built, and now operates the experiment for the National Reconnaissance Office (NRO). The experiment is a free-flying satellite, consisting of two end bodies connected by a 4-km nonconducting tether. In this respect, it is different from other tether experiments (like those flown on the Shuttle) where one end mass was connected to a massive host vehicle.

TiPS was jettisoned from a host spacecraft on June 20, 1996, with the deployment of the tether occurring shortly after jettison. The TiPS tether is intact through this writing (11/14/96), while no other space tether has lasted longer than 5 days. TiPS is the sixth known orbital-tethered system flown to date.

To meet an early launch opportunity, TiPS had to be designed and built in approximately 1 year. Due to a tight budget, the experiment objectives were limited only to those that had the highest payoff: these were (1) long-term orbit and attitude dynamics and (2) tether survivability.

Tether Fundamentals: The on-orbit configuration of TiPS is shown in the artist's rendition of Fig. 12. A tethered system, while in orbit, will behave like a gravity-gradient satellite, orienting the tether along a line through the spacecraft's center of mass and the center of the Earth. About this nominal orientation, the tether system will undergo small oscillatory motion (called libration) about the local vertical. It is this natural alignment with the local vertical that makes tether technology appealing. This may enable or enhance many uses of space by improving spacecraft systems, including: (1) generating electrical power, (2) creating unusual constellation configurations, (3) changing orbit, and (4) stabilizing spacecraft attitude with gravity gradient forces. As with many new technologies, other applications for tethers will likely be discovered as more are built and deployed.

TiPS Hardware: The program constraints of limited time and money dictated that the experiment design be as simple as possible and consist largely of existing component hardware and/or designs. The experimental goals only required a simple electrical power system that used a battery for all its electrical needs. The battery supported initiating deployment, recording data on the deployment characteristics, and transmitting these data to ground stations. TiPS consists of two end bodies — dubbed Ralph and Norton — connected by a 4-km tether. Ralph contains a small, expendable deployer system (SEDS) tether deployer, a battery consisting of 10 lithium thionyl chloride D cells, a timer to initiate deployment, a SEDS data acquisition electronics box, and a transmitter and antennas to downlink the deployment data. The SEDS deployer, electronics, and transmitter were existing spare hardware from the SEDS 2 tether experiment that was successfully flown in space by the National Atmospheric and Space Administration (NASA), who provided this hardware to NRL for the TiPS Program. This was in keeping with the approach of using off-the-shelf components so that tight budgets and short schedules could be met. Norton is an inert body containing the 10 spring cartridges used to rapidly push the two bodies away from each other, pulling the tether out of its deployer, mounted on Ralph. Ralph and Norton each have 18 optical retroreflectors mounted on them. Figure 13 shows the completed satellite without its thermal blankets. In this figure, several of the small, round retroreflectors can be seen.

Fig. 12 — Artist rendition of TiPS in orbit. Ralph is on the bottom. TiPS has been in this orientation since deployment.

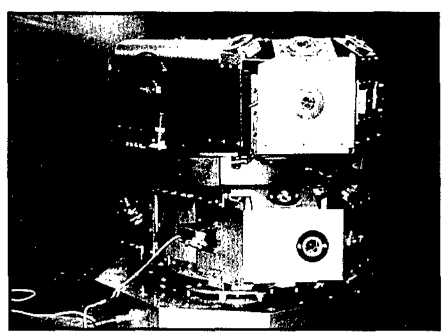

Fig. 13 — TiPS satellite without thermal blankets. The small round objects are the laser retroreflectors.

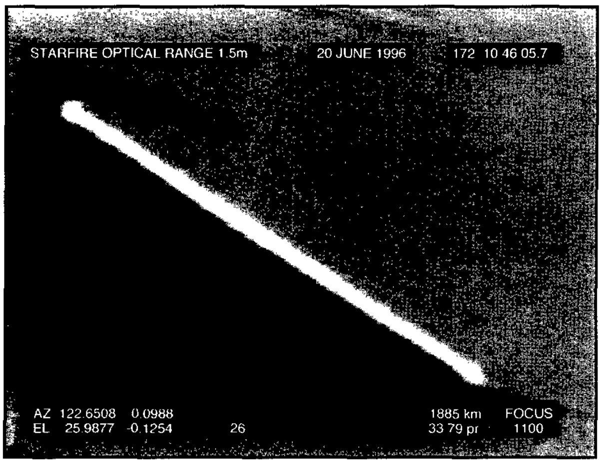

Fig. 14 — Telescope image of TiPS during deployment. Image taken by Starfire Optical Range at the Air Force's Phillips Laboratory.

Satellite Tracking and Dynamics: The motion of the end bodies is observed by a ground-based Satellite Laser-Ranging (SLR) network and by ground based visual observations. Figure 14 is an image of TiPS taken as the two end masses were separating. The tracking data consist largely of range data provided by timing the two-way round-trip delay for a laser bounced off the retroreflectors on the spacecraft. The data are transmitted across the Internet to NASA-Goddard in Greenbelt, Maryland.

The tracking data are analyzed at NRL to determine the dynamic motion of the tethered system. Since there is no object at the center of mass of the tethered system, both the attitude motion and the orbital motion are inferred from observations of the end masses only. This has proved to be a difficult task, requiring frequent observational data and new estimation algorithms that were incorporated in the traditional orbit-determination system used by NASA. The tracking data are also processed to provide updates to the state vector used to predict the motion of the end masses. These predictions are used by the SLR sites for subsequent observations.

The requirement of determining the tether survivability will be met through ground-based radar tracking of TiPS, which will determine when or if the tether is cut.

TiPS Findings to Date: The findings of the TiPS Program are best summarized by saying that they provide confidence that tether technology will be viable for future operational missions. There is still technological development required before operational systems would be ready to incorporate this technology, but TiPS has provided a significant step in that direction. The initial results show that tethers can be made to be survivable. With regard to the librational motion, our estimates now indicate that the tether is librating with a smaller amplitude than at deployment. Visual observations made shortly after the initial separation of the end bodies suggested that the tether was librating with an amplitude of 47 degrees with respect to vertical alignment. Over the course of the next 3 months, we have determined with high confidence that the amplitude of that motion has decreased to approximately 12 degrees. At this lower amplitude, the tether behaves much more predictably. During the month of October 1996, we were able to validate our ability to predict tether motion 6 to 12 h into the future. While these predictions were possible only during a period when an abundance of data are available, they provide confidence in our ability to model tether dynamics.

[Sponsored by National Reconnaissance Office] ■

Special Awards and Recognition

Special Awards and Recognition

NRL is proud of its many distinguished scientists, engineers, and support staff. Here we feature some who have received awards from prestigious institutions, the Department of the Navy, and NRL.

Dr. Herbert Friedman
E.O. Hulburt Center for Space Research

1996 COSMOS CLUB AWARD

Dr. Friedman received this award in recognition of more than 50 years of distinguished scientific achievement and public service. He has conducted or directed programs in metallurgy, electron optics, nuclear radiation, and space research and is nationally and internationally known as a pioneer of X-ray astronomy.

NRL LIFETIME ACHIEVEMENT AWARD

Dr. Friedman is the third recipient of NRL's Lifetime Achievement Award for extraordinary achievement and contributions. It is the highest honor that an NRL Commanding Officer can confer on a civilian employee. Dr. Friedman is widely recognized for developing the science of rocket astronomy, having conducted his first rocket experiment using a captured German V-2 rocket in 1949. Experiments conducted by Dr. Friedman produced the first X-ray photographs of the Sun. In another first, measurements of the ultraviolet fluxes of early-type stars obtained by Dr. Friedman using small mirror telescopes produced the first catalog of bright ultraviolet stars. Through the years, Dr. Friedman has devoted many hours of service to national and international scientific organizations. He holds 50 patents, has authored or coauthored over 300 scientific publications, and has written three books.

Dr. Timothy Coffey
Director of Research

1995 EXECUTIVE EXCELLENCE AWARD FOR DISTINGUISHED EXECUTIVE SERVICE

This award honors career executives "who have made significant contributions to improving the efficiency, effectiveness, and productivity of the federal government, and whose performances have improved the image of the career federal executive service." As NRL's Director of Research, Dr. Coffey directs and manages a research and development program spanning a wide variety of scientific and engineering disciplines. His responsibilities also include the fiscal, personnel, and administrative operations of NRL research facilities located at Washington, D.C. and at sites in Mississippi and California.

CAPT Bruce Buckley, Ms. Deborah Erwin, Deputy EEO Officer, and Dr. Timothy Coffey.

1995 NATHANIEL STINSON EQUAL EMPLOYMENT OPPORTUNITY AWARD (SPECIAL RECOGNITION)

The Nathaniel Stinson EEO Award, the highest EEO award within the Department of the Navy, was originally established in 1989 by the Chief of Naval Operations to honor dedication, commitment, and achievements toward advancing EEO. The award recognizes exemplary achievement of commands and activities to further the Navy's EEO objectives and initiatives. According to the citation, "NRL is recognized for special recognition of support and leadership of the SECNAV 'One Navy' Recruiting Program." NRL, in its leadership role for this Program, coordinated participation of other Navy activities, financed the advertisement of vacancies, and presented workshops at Career Fairs. NRL recruitment initiatives resulted in a marked increase in hires of minorities, women, and people with disabilities.

Dr. Nicholas C. Makris
Acoustics Division

UNITED KINGDOM'S INSTITUTE OF ACOUSTICS A.B. WOOD MEDAL AND PRIZE

Dr. Makris received this distinguished award from the United Kingdom's Institute of Acoustics "for improved theoretical approaches to the understanding of reverberation, scattering and other phenomena in the sea." His work was recognized as "valuable not only in acoustical and optical fields but also in sound perception and psychological acoustics." The award is made in alternate years to persons residing in the United Kingdom, the United States, and Canada.

ONR 50th ANNIVERSARY SYMPOSIUM YOUNG INVESTIGATOR AWARD

Dr. Makris received this award for "pioneering studies on seafloor reverberation." This award is presented to a young, upcoming, promising scientist in ocean acoustics. Dr. Makris was also noted for his physical, analytical critique of the popular concept of "acoustic daylight."

Dr. Bhakta Rath
Associate Director, Materials Science and Component Technology Directorate

THE MINERALS, METALS, AND MATERIALS SOCIETY'S 1996 LEADERSHIP AWARD

The award recognizes individuals who have demonstrated outstanding leadership in the fields of metallurgy and materials. Dr. Rath was recognized for his "outstanding leadership in research planning and guidance and for promoting material science and engineering for national security and society."

Dr. Wallace Manheimer
Plasma Physics Division

THE INSTITUTE OF ELECTRICAL AND ELECTRONICS ENGINEERS' 1996 PLASMA SCIENCE AND APPLICATIONS COMMITTEE AWARD

Dr. Manheimer was given the award "in recognition of his many contributions to plasma science in areas such as basic nonlinear plasma theory, magnetic confinement and laser fusion theory, the theory of intense relativistic beams, and especially in the area of relativistic microwave electronics."

Dr. Stuart Searles
Optical Sciences Division

THE INSTITUTE OF ELECTRICAL AND ELECTRONICS ENGINEERS/LASERS AND ELECTRO-OPTICS SOCIETY'S 1995 WILLIAM R. STREIFER SCIENTIFIC ACHIEVEMENT AWARD

Dr. Searles, a corecipient of this award, was cited "for the demonstration and development of excimer lasers, including the first excimer laser." This award is given annually to recognize an exceptional single scientific contribution that has had a significant impact in the field of lasers and electro-optics in the past 10 years.

1996 INSTITUTE OF NAVIGATION'S THURLOW AWARD

Dr. William Burns
Optical Sciences Division

This award recognizes outstanding contributions to the art and science of navigation. Dr. Burns was cited "for being the first to demonstrate long-term inertial quality performance in a fiber-optic gyroscope, which stimulated intense industrial development of the device, and was a pivotal milestone in its development into a practical, precision inertial-quality navigation instrument."

INDUSTRY WEEK MAGAZINE SELECTION

Dr. Allen Garroway
Chemistry Division

Dr. David Griscom
Optical Sciences Division

Drs. Garroway and Griscom were among the 50 individuals selected whose "achievements are shaping the future of our industrial culture and America's technology policy." Dr. Garroway was recognized for his research, which has led to the development of a new technology, nuclear quadruple resonance (NQR). This technology can be used to detect explosives in a background of benign materials. Dr. Griscom was recognized for being "one of the first to apply electron-spin-resonance spectroscopy to glass materials." His findings have been applied in the fields of optical communication through fiber waveguides and electronics through metal-oxide semiconductor devices.

SIGMA XI 1996 AWARD IN PURE SCIENCE

Dr. Carter White
Chemistry Division

Dr. White was cited for "his original and broad contributions to materials chemistry problems including detonations, carbon nanotubes, semiconductor defects, fullerenes, and nanotribology." Sigma Xi presents this award for outstanding research performed in the past 10 years.

Dr. Joseph Friebele
Optical Sciences Division

SIGMA XI 1996 APPLIED SCIENCE AWARD

Dr. Friebele was cited "for his outstanding contributions in optical materials, especially in the area of radiation effects on optical fibers, which have led to hardening against nuclear radiation by optimizing fabrication parameters and contributions towards the development of novel techniques for writing Bragg gratings in fibers for smart structure applications."

Dr. Stephen Mango
Remote Sensing Division

VICE PRESIDENT AL GORE'S HAMMER AWARD

This award recognizes new standards of excellence achieved by teams helping to reinvent government. Award-winning teams are selected for their significant contributions to the President's National Performance Review principles of "putting customers first, empowering employees, and getting back to basics." Dr. Mango, a corecipient of this award, was recognized as a key member of the Tri-Agency Convergence Transition Team, which combined the separate U.S. military and civil polar meteorological satellite programs into the National Polar-orbiting Operational Environmental Satellite System (NPOESS), a single U.S. national program.

Dr. Paul Natishan
Materials Science and Technology Division

WILLIAM BLUM AWARD OF THE NATIONAL CAPITAL SECTION OF THE ELECTROCHEMICAL SOCIETY

Dr. Natishan is the 18th recipient of the William Blum Award of the National Capital Section of the Electrochemical Society. He was presented this award in recognition of his outstanding contributions to the field of corrosion science and protection, especially in the area of passivity and its breakdown.

Dr. Stuart Wolf
Materials Science and Technology Division

1995 E.O. HULBURT AWARD

This is NRL's highest civilian award for scientific and engineering achievement. Dr. Wolf was recognized for being "engaged in research at the heart of superconductivity—from the start, when he literally established the subfield, which has become known as inhomogeneous superconductivity, to the present, where he has contributed significantly to our understanding of the important superconducting oxides, many of which are superconducting well above liquid nitrogen temperature." According to the award nomination, "working with ARPA and scientists in his branch, Dr. Wolf has established NRL as the major U.S. laboratory for the development of magneto-electronic devices."

Dr. Ben Cantrell
Radar Division

1996 NAVY DISTINGUISHED CIVILIAN SERVICE AWARD

Dr. Cantrell was cited for his "outstanding personal technical contributions and his effective technical leadership that have led to improved capabilities of important operational radars used for shipboard defense against small targets." According to the citation, his "successful basic research and exploratory development relating to waveforms and signal processing for the detection of small targets in severe clutter environments led to an innovative concept, which significantly improves the Navy's ability to counter the small threat. His fundamental contributions also led to the AN/SPS-49 Medium PRF upgrade now being back fitted in Fleet radars to enhance the capability of the Navy by detecting small, high-speed targets in the midst of extensive, heavy clutter."

Mr. John Gallagher
Command Support Division

NAVY MERITORIOUS CIVILIAN SERVICE AWARD

Mr. Gallagher was cited for "exceptionally meritorious conduct in the performance of outstanding service as the Command Support Division's communication security officer from January 1980 until his retirement in February 1996....His performance has made a significant impact on NRL's Communications Center, Communications Security (COMSEC) Material Account, and also in support of NRL's scientific and technical community in mission support."

Mr. Donald Green
Financial Management Division

NAVY MERITORIOUS CIVILIAN SERVICE AWARD

According to the citation, "Mr. Green achieved an unequaled record of excellence in efficiency and productivity in the management of the (NRL) Financial Management Division (FMD). He developed and instituted numerous financial management initiatives and provided professional leadership in transitioning the FMD into one of the best managed financial management organizations within the Navy. His dedication to excellence and professional leadership has made a major lasting and positive impact on NRL's ability to meet its critical research mission requirements and is in keeping with the highest traditions of the U.S. Navy."

Dr. Joseph Leonard
Chemistry Division

NAVY MERITORIOUS CIVILIAN SERVICE AWARD

Dr. Leonard received this award for his "numerous and renowned contributions to the enhanced survivability of Naval ships and personnel through innovative technology." According to the citation, "his prescience on the stratosphere ozone impact of Halon fire-fighting agents led him first to develop substitute materials for testing fire-fighting systems and then to his current contribution to more environmentally acceptable systems, water mist, and compressed air foam. The development and rapid deployment of the Naval Fire Fighters Thermal Imager by Dr. Leonard and his group have resulted in a markedly enhanced capability to 'see through smoke' and to quickly mitigate extensive shipboard damage and personnel loss from fire."

Dr. Russell Groshans
Space Science Division

NAVY MERITORIOUS CIVILIAN SERVICE AWARD

Dr. Groshans was cited for interacting effectively with the technical staff to identify and resolve technical and resource problems and for representing the division to the NRL command and to the division's customers. He is responsible for bringing "insight, innovation, and wit and charm to the working place." The award citation particularly noted Dr. Groshans' skill at dealing with complex programmatic matters. He is credited for bringing Navy responsibility for the Air Force Space Test Program (STP) to NRL and for contributing significantly to the Laboratory's record of success in the program.

Mr. Gary Santerre
Tactical Electronic Warfare Division

NAVY MERITORIOUS CIVILIAN SERVICE AWARD

Mr. Santerre was recognized for his "superb ability, managerial skills, and incisive planning, providing unparalleled support to the command." According to the citation, "he has fostered an alliance among the scientific communities of the Navy laboratories and the operational forces to produce dramatic improvements in Fleet tactical readiness. Through individual energy and dedication, he ensured the Fleet's needs were appreciated by every research scientist, system developer, and program manager with whom he interfaced." He received this award while temporarily assigned to the Naval Surface Warfare Group, in Norfolk, Virginia.

Mr. Frederick Danzy
Space Systems Development Department

NAVY MERITORIOUS CIVILIAN SERVICE AWARD

Mr. Danzy was cited for his "exceptional talent, effort, and dedication throughout his NRL career....Mr. Danzy has made many contributions to the Laboratory through development of numerous laboratory and space-flight electronic packages. His major achievements include development of the atomic clock interface subsystems for the NTS-1 and -2 spacecraft in the 1970s. As an engineer and expert in reliability, he has played a major role in the development of the atomic clocks used in the Global Positioning System....His knowledge and dedication have brought great credit to himself and the Laboratory."

Ms. Judy Watkins-Hope
Supply Division

1996 COMMANDING OFFICER'S AWARD FOR ACHIEVEMENTS IN THE FIELD OF EQUAL EMPLOYMENT OPPORTUNITY (NONSUPERVISORY)

Ms. Hope was cited for her "proactive work in supporting initiatives for the African-American Employment Subcommittee, her tireless efforts on behalf of NRL's Community Outreach Program, and outstanding contributions to the overall EEO Program at NRL."

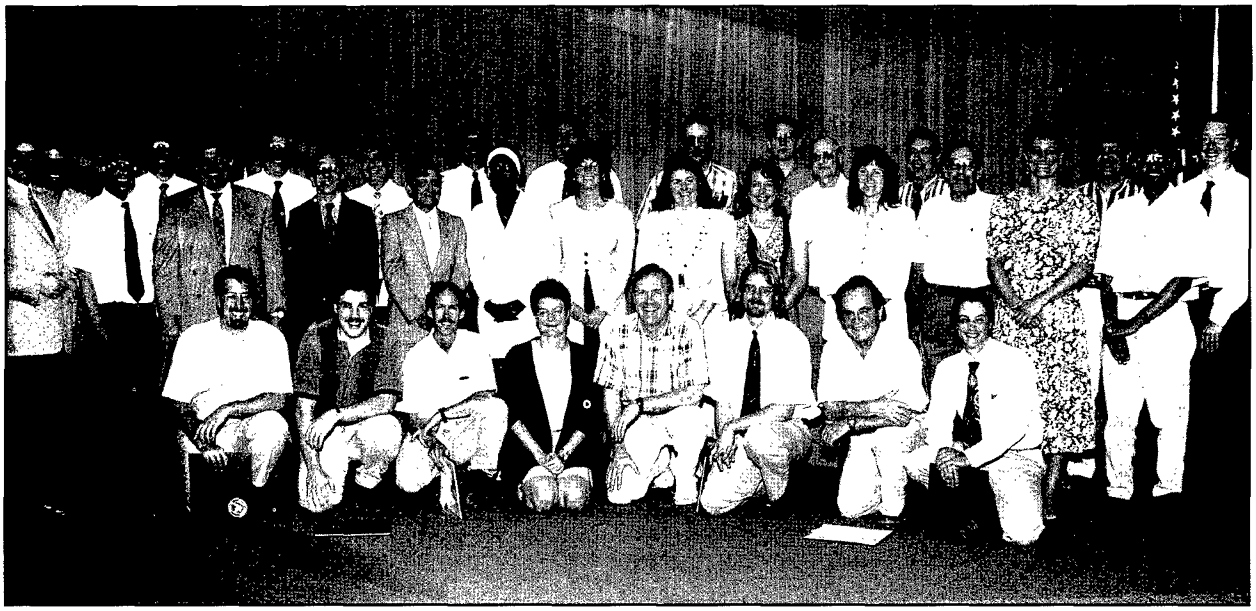

DEPARTMENT OF THE NAVY'S AWARD OF MERIT FOR GROUP ACHIEVEMENT

Naval Center for Space Technology

(Left to right, front row) Rich Menuchi, Jeff Wright, Steve Rauen, Windie Borodin, George Arthur, Mark Lucas, Larry Kegley, and Tom Grove; (Center row) Ken Harringer, George Edwards, Glenn Cooper, Kevin Gish, Art Merat, Brenda Hayes, Jen Willey, Mary Dixon, Mary Tabron, Jan Wilson, Jim McKenney, Bebe Kovel, and Atul Govani; (Back row) Tim Gross, Reed Smith, Ron Fulton, Terry Fisher, Leonard Peterson, Ken Matheny, Ira Levinrad, Rob Daniels, Ken Dehart, Tom Moorehead, Mike Gregory, and Sean McElroy; (Not shown) Curt Eastman, Steve Montgomery, Margie Palumbo, and Carlo Fustini.

The team was cited "for the outstanding work and long hours invested in the concept, design, development, and operations of the ICEBox project." C^4I Branch personnel conceived the ICEBox, an autonomous system that could be deployed anywhere in the world and would relay the critical mission information back to a central location. The ICEBox operates in a remote mode to the central location requiring only minimal remote data updates every 3 days. The few racks of equipment and single antenna replace more than 40 racks of equipment and 4 antennas. Only two support personnel per shift are required and rarely needed, enabling the closure of a major site that previously required hundreds of support personnel, providing cost savings of nearly 100 million dollars a year. This feat was accomplished in just 1 year.

DEPARTMENT OF THE NAVY'S AWARD OF MERIT FOR GROUP ACHIEVEMENT

Radar Division

(Left to right) Mr. Gregory Tavik, Mr. David Cardiel, Mr. Steven Lessin, Ms. Janet Brockett, Mr. Michael Walder, Ms. Linda Schaus, Dr. Ben Cantrell, Ms. Win Jou Cheung, Mr. Brian Connolly, Mr. Michael Rachuba, and Dr. Lawrence Leibowitz.

According to the nomination, "The efforts of the NRL AN/SPQ-9B development team are leading to a low-cost significant ship self-defense capability improvement for the Fleet. The ingenuity, performance, dedication, and hard work of each member in developing the important new AN/SPQ-9B concept and ADM was substantially beyond normal expectations."

NAVAL RESEARCH LABORATORY'S AWARD FOR EXCELLENCE IN SECRETARIAL SUPPORT

(Left to right) Ms. Anne Townes, *Optical Sciences Division*, Ms. Tina Obrebski, *Space Science Division*, and Ms. Tessie Santos, *Plasma Physics Division*

Ms. Townes was described in the award nomination as "a secretary of unequaled excellence...with a near perfect working knowledge of all procedures associated with her job." Ms. Obrebski was recognized as an exceptionally capable and diligent employee. She was cited for routinely solving logistical problems for branch personnel relating to project procurement, travel, and administrative activities. Ms. Santos was recognized for her "exceptional support in maintaining the outstanding safety record for the division and performing additional duties, beyond her grade level, with the highest standards."

NAVAL RESEARCH LABORATORY'S AWARD FOR EXCELLENCE IN MISSION SUPPORT

Human Resources Office

Ms. Janet Deschak, Ms. Lynda Heater, and Ms. Yvonne Fair

Ms. Deschak, Ms. Heater, and Ms. Fair were recognized for their outstanding performance as management advisors during the past 3 years. Their work—advising agency managers in management/employee interaction on sensitive personnel matters—provided cost-effective strategies that reduced the likelihood of negative, time-consuming litigation. Their advice centered on a wide variety of disciplinary and performance issues and the development of cost-effective agency procedures. They earned this award by consistently facilitating cost-effective resolution of complex personnel issues. Further, they were cited for being exceptional representatives of agency management that earned them a high degree of their client's confidence.

NAVAL RESEARCH LABORATORY'S AWARD FOR EXCELLENCE IN MISSION SUPPORT

Contracting Division

(Left to right) Ms. Rosslyn Wallace, Mr. Dan Brinkworth, Ms. Preshema Harris, Ms. Donna Washington, Ms. Lisa Bridgan, Ms. Cheryl Burkhardt, Ms. Jill Burton, Ms. Carol Parnell, Ms. Helen Paul, Mr. Ernest Tunney, and CAPT Buckley; (Not shown) Ms. Tonya Stewart.

According to the citation, Mr. Tunney and members of Contracting Branch No. 2 were cited for "their exceptional performance in support of NRL and its major programs. Mr. Tunney and his staff epitomize the qualities that make a support staff indispensable to an organization. Meeting almost impossible schedules, providing innovative solutions, and delivering authoritative contractual support as a result of sometimes heroic efforts have become commonplace under Mr. Tunney's leadership and guidance."

AWARDS FOR THE *1996 NRL REVIEW* ARTICLES

(Left to right) Dr. Melvin Kruer, Mr. Vincent Rose, Mr. George Price, Mr. Gerald Golba, Mr. Tom Kawecki, Dr. Coffey, Ms. Lisa Shriver-Lake, Dr. Jay Boris, Ms. Sandy Landsberg, CAPT Buckley, Dr. Scott Chubb, Dr. Robert Jansen, Dr. Colin Shen, Mr. Ravi Ramamurti, Dr. Dean Scribner, and Dr. Michael Satyshur; (Not shown) Dr. Bill Sandberg, Ms. Anne Kusterbeck, and Dr. Martin Nisenoff.

Awards for *NRL Review* articles were established to recognize authors who submit outstanding research articles for this scientific publication. The articles are judged on the relevance of the work to the Navy and DoD, readability to the college-graduate level, and the use of graphics that are interesting and informative. The following awards were presented for articles that appeared in the *1996 NRL Review*.

Featured Research Article

"*NRL Advances in Computational Fluid Dynamics: FAST3D and FEFLO*," A. Landsberg, R. Ramamurti, J.P. Boris, and W.C. Sandberg (Laboratory for Computational Physics and Fluid Dynamics)

Directorate Awards for Scientific Articles

Systems Directorate: "*Infrared Color Vision*," D.A. Scribner, M.P. Satyshur, and M.R. Kruer (Optical Sciences Division)

Materials Science and Component Technology Directorate: "*Field Testing of Environmental Immunosensors*," A.W. Kusterbeck and L.C. Shriver-Lake (Center for Bio/Molecular Science and Engineering)

Ocean and Atmospheric Science and Technology Directorate: "*Hydrodynamic and Radar Modeling of Ocean Currents*," R.W. Jansen, S.R. Chubb, and C.Y. Shen (Remote Sensing Division)

Naval Center for Space Technology: "*The High-Temperature Superconducting Space Experiment II*," T.G. Kawecki, G.E. Price, J.A. Golba, V.S. Rose, and M. Nisenoff (Spacecraft Engineering Department)

Alan Berman Research Publication and Edison Patent Awards

The Annual Research Publication Awards Program was established in 1968 to recognize the authors of the best NRL publications each year. These awards not only honor individuals for superior scientific accomplishments in the field of naval research but also seek to promote continued excellence in research and in its documentation. In 1982, the name of this award was changed to the Alan Berman Research Publication Award, in honor of its founder.

There were 247 separate publications submitted by the divisions in 1996 to be considered for recognition. Of those considered, 38 were selected. These selected publications represent 177 authors, each of whom received a publication awards certificate, a bronze paperweight, and a booklet listing the publications that were chosen for special recognition. In addition, NRL authors share in their respective division's monetary award.

The winning papers and their respective authors are listed below by their research units. Non-Laboratory coauthors are indicated by an asterisk.

NRL also recognizes patents as part of its annual publication awards program. The NRL Edison Patent Award was established in January 1991 to recognize NRL employees for outstanding patents issued to NRL by the U.S. Patent and Trademark Office during the preceding calendar year. The award recognizes significant NRL contributions to science and engineering as demonstrated by the patent process that are perceived to have the greatest potential benefit to the country. Of the 15 patents considered for 1996, 4 were selected, representing 12 inventors. They are listed under the NRL Edison Patent Awards.

Command Support Division

Laser-Heated Radiation Dosimetry Using Transparent Thermoluminescent Glass
Tommy L. Johnson, Brian L. Justus, and Alan L. Huston

Radar Division

Automatic Recognition of ISAR Ship Images
Scott A. Musman, David W. Kerr, and Charles McKay Bachmann

Digital and Analog Sidelobe Canceller Performance with the AN/SPS-49(V) Radar
Robert M. Crisler, Pete Hansen, John L. Walters, Kevin Luc,
Donald L. Wilson, William L. Thrift, and David A. Alessio

Information Technology Division

Automated Consistency Checking of Requirements Specifications
Constance L. Heitmeyer, Ralph D. Jeffords, and Bruce G. Labaw

Data-Delay Evaluation in Integrated Wireless Networks Based on Local Product-Form Solutions for Voice Occupancy
Jeffrey E. Wieselthier, Craig M. Barnhart, and Anthony Ephremides*

Optical Sciences Division

Type-II Mid-IR Lasers Operating Above Room Temperature
Jerry R. Meyer, Craig A. Hoffman, Joseph F. Pinto, C.-H. Lin,*
P.C. Chang,* S.J. Murray,* S.-S. Pei,* J.I. Malin,* and C.L. Felix*

Multispectral Field Measurements for the Multispectral Overhead IR/EO Surveillance Program
William A. Shaffer, Alan P. Schaum, Edward A. Ashton,
Martin J. McHugh, and Joseph V. Michalowicz

Tactical Electronic Warfare Division

Numerical Modeling and Coupling-Reduction Techniques for the Improvement of Antenna Isolation on Decoy Platforms
Gary T. Roan, Richard A. Muha, and Armondo D. Elia

Specific Emitter Identification (SEI) Using Massively Parallel Implementations of Neural Networks
Geoffrey L. Barrows, John C. Sciortino, Jr.,
Vijayanand C. Kowtha, and David A. Stenger

Laboratory for the Structure of Matter

Crystal Structure of Cyclo(Adm-Cyst)$_3$:Example of a Topologically Defined Double-Helical Cystine Cyclic Peptide
Isabella Karle, Darshan Ranganathan,* and V. Haridas*

Chemistry Division

Ultrafast Infrared Study of the Ultraviolet Photodissociation of $Mn_2(CO)_{10}$
Jeffrey C. Owrutsky and Andrew P. Baronavski

Improved Tetragonal Phase Stability at 1400°C with Yttria-Stabilized Zirconia
Robert L. Jones and Derek Mess*

Materials Science and Technology Division

Kinetics of Phase Coarsening in Dense Systems
Steven P. Marsh and M.E. Glicksman

Spin Dependent Carrier Localization in Fe-based Semimagnetic Semiconductor Heterostructures
Berend T. Jonker, H. Abad, W.Y. Yu,* S. Stoltz,* A. Petrou,*
J. Warnock, C.D. Poweleit,* L.M. Smith,* and T. Schmiedel*

Laboratory for Computational Physics and Fluid Dynamics

Computations of Enhanced Soot Production to Time-Varying CH_4/Air Diffusion Flanes
Carolyn R. Kaplan, Christopher R. Shaddix,* and Kermit C. Smyth*

Condensed Matter and Radiation Sciences Division

Charge-Collection Characteristics of GaAs Heterostructure FETs Fabricated with a Low-Temperature Grown GaAs Buffer Layer
Dale McMorrow, Joseph S. Melinger, Arthur B. Campbell, Cheryl J. Dale, Todd R. Weatherford,* Alvin R. Knudson,* Steve Buchner,* Lan Hu Tran,* Paul W. Marshall,* Andrej Peczalski,* and Steve Baier*

Applications of a Tight-Binding Total Energy Method for Transition and Noble Metals: Elastic Constants, Vacancies, and Surfaces of Monatomic Metals
Michael J. Mehl and Dimitrios A. Papaconstantopoulos

Plasma Physics Division

Generation of Large Area, Sheet Plasma Mirrors for Redirecting High Frequency Microwave Beams
Joseph Mathew, Richard F. Fernsler, Robert A. Meger, Donald P. Murphy, Wallace M. Manheimer, J.A. Gregor,* and P.E. Pechacek*

Real-time Identification and Prediction of Geoeffective Solar Wind Structures
James Chen, Peter J. Cargill, and Peter J. Palmadesso

Electronics Science and Technology Division

Microwave Channelized Activer Filters—A New Modular Approach to Achieving Compactness and High Selectivity
Christen Rauscher

Fine Structure Splitting in the Optical Spectra of Single GaAs Quantum Dots
D. Gammon, E.S. Snow, B.V. Shanabrook, D.S. Katzer, and D. Park

Center for Bio/Molecular Science and Engineering

Fabrication of Patterned DNA Surfaces
Linda A. Chrisey, Barry J. Spargo, Charles S. Dulcey, Jeffrey M. Calvert, and C. Elizabeth O'Ferrall*

Chiral Molecular Self-Assembly of Phospholipid Tubules: A Circular Dichroism Study
Jonathan V. Selinger, Alok Singh, Joel M. Schnur, Mark S. Spector,* Kalpathy R.K. Easwaran,* and Ghanta Jyothi*

Acoustics Division

The Effect of Saturated Transmission Scintillation on Ocean Acoustic Intensity Measurements
Nicholas C. Makris

AWSUM: A Digital Filter for Achieving Increased Signal-to-Noise Ratio and Other Signal Processor Enhancements
Ronald A. Wagstaff

Remote Sensing Division

LWS Observations of the Colliding Galaxies NGC 4038/39
Jacqueline Fischer, L.M. Shier, M.L. Luhman, S. Satyapal,*
H.A. Smith,* M.A. Greenhouse,* J.W. Miles,* M.G. Wolfire,*
G.J. Stacey,* S.J. Unger,* B.M. Swinyard,* L. Spinoglio,* M.A. Malkan,*
S.D. Lord,* S.E. Church,* M.A. Shure,* P.E. Clegg,* P.A.R. Ade,*
C. Armand,* M. Burgdorf,* A. Di Giorgio,* D. Ewart,* C. Gry,* T. Lim,*
S. Molinari,* M.C. Price,* S.D. Sidher,* A. Smith,* D. Texier,* N.R. Trams,*
G.R. Davis,* I. Furniss,* W.M. Glencross,* and Q. Nguyen-Rieu*

Measurements of Water Vapor in the Middle Atmosphere and Implications for Mesospheric Transport
Gerald E. Nedoluha, Richard M. Bevilacqua, R. Michael Gomez,
William B. Waltman, Brian C. Hicks, D.L. Thacker,* and W. Andrew Matthews*

Oceanography Division

Data Assimilation in a North Pacific Ocean Monitoring and Prediction System
Michael R. Carnes, Daniel N. Fox, Robert C. Rhodes, and O.M. Smedstad*

Evidence for a North Pacific Deep Western Boundary Current
Zachariah R. Hallock and William J. Teague

Marine Geosciences Division

Full Waveform Inversion of Field Sonar Returns for a Visco-Acoustic Earth: A Comparison of Linearized and Fully Nonlinear Methods
Warren T. Wood and Dennis A. Lindwall

Marine Meteorology Division

The Summertime Low-Level Jet and Marine Boundary Layer Structure along the California Coast
Stephen D. Burk and William T. Thompson

Adjoint Sensitivity of an Idealized Extratropical Cyclone with Moist Physical Processes
Rolf H. Langland, Russell L. Elsberry,* and Ronald M. Errico*

Space Science Division

Satellite Measurements of Hydroxyl in the Mesosphere
Robert R. Conway, Michael H. Stevens, Charles M. Brown, Jeff S. Morrill,
Joel G. Cardon,* Scott E. Zasadil,* and George H. Mount *

The Magnetic Nature of Coronal Holes
Yi-Ming Wang, Neil R. Sheeley, Jr., and Scott H. Hawley*

Space Systems Development Department

The High Temperature Superconductivity Space Experiment (HTSSE-II) Design
Thomas G. Kawecki, Gerald A. Globa, George E. Price
Vincent E. Rose,* and William J. Meyers*

Ephemeris Estimation of a Well-Defined Platform Using
Satellite Laser Ranging from a Reduced Number of Ground Sites
Amey R. Peltzer, C. Charmaine Gilbreath,
George E. Price, and W.J. Barnds*

Spacecraft Engineering Department

Spacecraft Attitude Determination Using Gyros and Quaternion Measurements
Glenn Creamer

High Temperature Superconducting Space Experiment II
(HTSSE-II) Cryogenic Design
Thomas G. Kawecki, Scott Chappie, and D.R. Mahony*

NRL Edison Patent Awards

Liquid Crystal Composition and Alignment Layer
Ranganathan Shashidhar, Banahalli R. Ratna,
Jeffrey M. Calvert, and Joel M. Schnur
CENTER FOR BIO/MOLECULAR SCIENCE AND ENGINEERING

Apparatus and Method Using Low-Voltage
and/or Low-Current Scanning Probe Lithography
Christie R.K. Marrian, Eric S. Snow,
and Elizabeth A. Dobisz
ELECTRONICS SCIENCE AND TECHNOLOGY DIVISION

Glass Matrix Doped with Activated Luminescent Nanocrystalline Particles
Alan L. Huston and Brian L. Justus
OPTICAL SCIENCES DIVISION

Sediment Classification System
Frank S. Carnaggio, Douglas N. Lambert, and David C. Young
OCEANOGRAPHY DIVISION

Programs for Professional Development

Programs for NRL Employees

During 1996, under the auspices of the Employee Development Branch, NRL employees participated in 4534 individual training events. Many of these were presented as either videotaped or on-site instructed courses on diverse technical subjects, management techniques, and enhancement of such personal skills as efficient use of time, speed reading, memory improvement, and interpersonal communications. Courses are also available by means of computer-based training (CBT) and live television, for monitoring nationwide.

One common study procedure is for employees to work full time at the Laboratory while taking job-related scientific courses at universities and schools in the Washington area. The training ranges from a single course to full graduate and postgraduate programs. Tuition for training is paid by NRL. The formal programs offered by NRL are described here.

GRADUATE PROGRAMS

• The **Advanced Graduate Research Program** (formerly the Sabbatical Study Program, which began in 1964) enables selected professional employees to devote full time to research or pursue work in their own or a related field for 1 year at an institution or research facility of their choice without the loss of regular salary, leave, or fringe benefits. NRL pays all educational costs, travel, and moving expenses for the employee and dependents. Criteria for eligibility include professional stature consistent with the applicant's opportunities and experience, a satisfactory program of study, and acceptance by the facility selected by the applicant. The program is open to paraprofessional employees (and above) who have completed 6 years of Federal Service, 4 of which are at NRL.

• The **Edison Memorial Graduate Training Program** enables employees to pursue advanced studies in their fields at local universities. Participants in this program work 24 hours each workweek and pursue their studies during the other 16 hours. The criteria for eligibility include a minimum of 1 year of service at NRL, a bachelor's or master's degree in an appropriate field, and professional standing in keeping with the candidate's opportunities and experience.

• To be eligible for the **Select Graduate Training Program**, employees must have a college degree in an appropriate field and must have demonstrated ability and aptitude for advanced training. Students accepted in this program devote a full academic year to graduate study. While attending school, they receive one-half of their salary, and NRL pays for tuition and laboratory expenses.

• The **Naval Postgraduate School** (NPS), located in Monterey, California, provides graduate

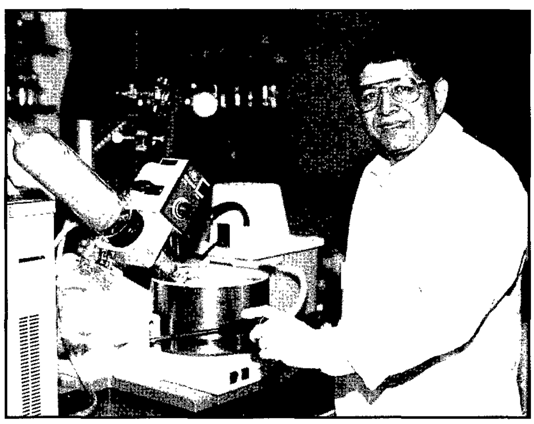

Dr. Alok Singh, of the Center for Bio/Molecular Science and Engineering, recently participated in the Advanced Graduate Research Program at the College de France in Paris.

programs to enhance the technical preparation of Naval officers and civilian employees who serve the Navy in the fields of science, engineering, operations analysis, and management. It awards a master of arts degree in national security affairs and a master of science degree in many technical disciplines.

NRL employees desiring to pursue graduate studies at NPS may apply for a maximum of six quarters away from NRL, with thesis work accomplished at NRL. Specific programs are described in the NPS catalog. Participants will continue to receive full pay and benefits during the period of study.

• In addition to NRL and university offerings, application may be made to a number of noteworthy programs and fellowships. Examples of such opportunities are the **Alfred P. Sloan Fellows Program, Brookings Institute Advanced Study Program**, the **Fellowship in Congressional Operations**, and the **Women's Executive Leadership Program**. These and other programs are announced from time to time, as schedules are published.

• Research conducted at NRL may be used as **thesis material for an advanced degree**. This original research is supervised by a qualified employee of NRL who is approved by the graduate school. The candidate should have completed the required course work and should have satisfied the language, residence, and other requirements of the graduate school from which the degree is sought. NRL provides space, research facilities, and supervision but leaves decisions on academic policy to the cooperating schools.

CONTINUING EDUCATION

• Local colleges and universities offer **undergraduate and graduate courses** at NRL for employees interested in improving their skills and keeping abreast of current developments in their fields. These courses are also available at many other DoD installations in the Washington, D.C. area.

• The Employee Development Branch at NRL offers **short courses** to all employees in a number of fields of interest including technical subjects, computer operation, supervisory and management techniques, and clerical/secretarial skills. Laboratory employees may attend these courses at nongovernment facilities as well. Interagency courses in management, personnel, finance, supervisory development, and clerical skills are also available.

For further information on any of the above programs, contact the Employee Development Branch (Code 1840) at (202) 767-2956.

TECHNOLOGY TRANSFER

• The **Office of Research and Technology Applications Program** (ORTA) ensures the full use of the results of the Nation's federal investment in research and development by transferring federally owned or originated technology to state and local governments and the private sector. (Contact Dr. Richard Rein, Code 1004, at (202) 767-7230).

TECHNOLOGY BASE

• The **Navy Science Assistance Program** (NSAP) establishes an information loop between the Fleet and the R&D shore establishments to expedite technology transfer to the user. The program addresses operational problems, focuses resources to solve specific technical problems, and develops a nucleus of senior scientific personnel

Ms. Sheila McDonnell, of the Marine Geosciences Division, is currently participating in the Edison Memorial Graduate Training Program at George Washington University, Washington, DC.

familiar with the impact of current research and system performance on military operations. The program also provides 2-year science advisor positions in the Fleet.

• The **Scientist-to-Sea Program** (STSP) provides increased opportunities for Navy R&D laboratory/center personnel to go to sea to gain first-hand insight into operational factors affecting system design, performance, and operations on a variety of ships.

For further information on these and other Technology Base Programs, contact Dr. Stephen Sacks, Code 5006, at (202) 767-3666.

PROFESSIONAL DEVELOPMENT

NRL has several programs, professional society chapters, and informal clubs that enhance the professional growth of employees. Some of these are listed below.

• The **Counseling Referral Service** (C/RS) helps employees to achieve optimal job performance through counseling and resolution of problems such as family, stress and anxiety, behavioral, emotional, and alcohol- or drug-related problems that may adversely impact job performance.

C/RS provides confidential assessments and short-term counseling, training workshops, and referrals to additional resources in the community. (Contact Ms. Susan Feldman at (202) 767-6857.)

• A chartered chapter of **Women in Science and Engineering** (WISE) was established at NRL in 1983. Informal luncheons and seminars are scheduled to inform scientists and engineers of women's research at NRL and to provide an informal environment for members to practice their presentations. WISE also sponsors a colloquium series to feature outstanding women scientists. (Contact Dr. Wendy Fuller-Mora at (202) 767- 6207, Dr. Debra Rolison at (202) 767-3617, or Dr. Cha-Mei Tang at (202) 767-4148.)

• **Sigma Xi**, the scientific research society, encourages and acknowledges original investigation in pure and applied science. As an honor society for research scientists, individuals who have demonstrated the ability to perform original research are elected to membership in local chapters. The NRL Edison Chapter, comprised of approximately 600 members, recognizes original research by presenting awards annually in pure and applied science to outstanding NRL staff members. The chapter also sponsors lectures at NRL on a wide range of scientific topics for the entire NRL community. These lectures are delivered by scientists from all over the nation and the world. The highlight of the Sigma Xi lecture series is the Edison Memorial Lecture, traditionally featuring a distinguished scientist. (Contact Dr. David Godbey at (202) 404-1200, Dr. Robert Morris at (202) 767-3845, or Dr. Wendy Fuller-Mora at (202) 767-6207.)

• The **NRL Mentor Program** was established to provide an innovative approach to professional and career training and an environment for personal and professional growth. It is open to permanent NRL employees in all job series and at all sites. Mentorees are matched with successful, experienced colleagues with more technical and/or managerial experience who can provide them with the knowledge and skills needed to maximize their contribution to the success of their immediate organization, to NRL, to the Navy, and to their chosen career fields. The ultimate goal of the program is to increase job productivity, creativity, and satisfaction through better communication, understanding, and training. NRL Instruction 12400.1 established the NRL Mentor Program, and it provides the policy and procedures for the program. (Contact Mr. Dom Panciarelli at (202) 767-2541.)

Mentor Ms. Diane Martin, of NRL's Management Information Systems Staff, and mentoree Mr. Billy Wright, of the Supply Division are one of a number of successful teams participating in the NRL Mentor Program.

• The Charlotte Moore-Sitterly Chapter of **Federally Employed Women, Inc.** (FEW) was chartered at NRL in 1993. FEW is an international organization of federally employed women and men whose purpose is to eliminate sex discrimination and sexual harassment and enhance career opportunities for women in government. FEW works closely with other Federal agencies and organizations, including the Office of Personnel Management, Equal Employment Opportunity Commission, and Federal Women's Program subcommittees. (Contact Dr. Jeanie Osburn at (202) 767-3885.)

• Employees interested in developing effective self-expression, listening, thinking, and leadership potential are invited to join either of two NRL chapters of **Toastmasters International**. Members of these clubs, who possess diverse career backgrounds and talents, meet three times a month in an effort to learn to communicate not by rules but by practice in an atmosphere of understanding and helpful fellowship. NRL's Commanding Officer and Director of Research endorse Toastmasters, and the Employee Development Branch pays for membership and educational materials for those NRL employees whose supervisors see a need for their active training in public speaking or communication skills. (Contact Ms. Kathleen Parrish at (202) 767-2782.)

• An agreement between NRL-SSC and **Mississippi's Alliance for Minority Participation** places students whose background and interests match the Laboratory's field of research with NRL mentors in a 10-week research environment. Together with accomplished senior researchers and faculty advisors, students plan, develop, and conduct a summer research project to include challenging, hands-on experiences with research equipment and principles of modern research. (Contact Mr. George Stanford at (601) 688-5211.)

EQUAL EMPLOYMENT OPPORTUNITY (EEO) PROGRAMS

Equal employment opportunity is a fundamental NRL policy for all persons, regardless of race, color, sex, religion, national origin, age, or physical/mental handicap. The EEO Office is a service organization whose major functions include promoting and practicing affirmative employment efforts, counseling employees in an effort to resolve employee/management conflicts, processing discrimination complaints, providing EEO training, and advising and providing guidance to employees on EEO policy. Additionally, the EEO Office is responsible for the management of the following special emphasis programs:

• The **African-American Employment Program (AAEP)**
• The **American-Indian/Alaskan-Native Employment Program (AI/ANEP)**
• The **Asian-American/Pacific Islander Employment Program (AA-PIEP)**
• The **Federal Women's Program (FWP)**
• The **Hispanic Employment Program (HEP)**
• The **Individuals with Disabilities Program (IWDP)**

Commemorating Black History Month, NRL's African-American Employment Program Subcommittee invited the 54th Massachusetts Volunteer Infantry Company "B" re-enactors to perform a brief weapons drill using authentic reproduction rifle muskets.

Each of these programs has responsibility to identify pertinent areas of concern regarding recruitment, selection, advancement, and retention of employees. They also encourage NRL's population to heighten their sensitivities to others around them as well as to achieve their maximum potential by sponsoring special training and awareness programs throughout the year. (Contact the EEO Office at (202) 767-2486 for additional information on any of its programs or services.)

OTHER ACTIVITIES

• The **Community Outreach Program** traditionally has used its extensive resources to foster programs that provide benefits to students and other community citizens. Volunteer employees assist with and judge science fairs, give lectures, tutor, mentor, coach, and serve as classroom resource teachers. The program also sponsors Black History Month art and essay contests for local schools, student tours of NRL, a student Toastmasters Youth Leadership Program, an annual holiday party for neighborhood children, an annual collection for Children's Hospital, and other programs that support the local community. Also through this program, NRL has active partnerships with four District of Columbia and three Aberdeen, Maryland, public schools. (Contact Mr. Dom Panciarelli at (202) 767-2541.)

• Other programs that enhance the development of NRL employees include four computer user groups (**IBM PC**, **Mac**, **NeXT**, and **Sun**) and the **Amateur Radio Club**. The **Recreation Club** encourages the wide interest of sports for employees with its many facilities and programs, such as a six-lane heated indoor pool; basketball and volleyball court; weight room with qualified consultant, by appointment; table tennis; hot tub and sauna; five martial arts disciplines; aerobics, ranging from low-low to high and step classes; swimming lessons; water walking and exercise; swing dance sessions; softball and basketball leagues; and specialized sports clubs (running, skiing, swimming, biking, and golfing). Sportswear, NRL paraphernalia, discount tickets to amusement parks, and film-developing services are available at the Rec Club office. The **Showboaters**, a nonprofit drama group that presents live theater for the enjoyment of NRL and the community, performs two major productions each year in addition to occasional performances at Laboratory functions and benefits for local charities. Though based at NRL, membership in Showboaters is not limited to NRL employees.

NRL's Meteorology Division, Monterey, California, donated approximately 90 personal computers and printers to the Monterey County Office of Education through NRL's Partnership in Education Program.

Programs for Non-NRL Employees

Several programs have been established for non-NRL professionals. These programs encourage and support the participation of visiting scientists and engineers in research of interest to the Laboratory. Some of the programs may serve as stepping-stones to federal careers in science and technology. Their objective is to enhance the quality of the Laboratory's research activities through working associations and interchanges with highly capable scientists and engineers and to provide opportunities for outside scientists and engineers to work in the Navy laboratory environment. Along with enhancing the Laboratory's research, these programs acquaint participants with Navy capabilities and concerns.

RECENT PH.D., FACULTY MEMBER, AND COLLEGE GRADUATE PROGRAMS

• The **National Research Council (NRC)/ NRL Cooperative Research Associateship Program** selects associates who conduct research at NRL in their chosen fields in collaboration with NRL scientists and engineers. The tenure period is 2 years. The Office of Naval Research offers the associate post-tenure research grants tenable at an academic institution.

• The American Society for Engineering Education (ASEE) administers the NRL/ASEE **Postdoctoral Fellowship Program** that aims to increase the involvement of highly trained scientists and engineers in disciplines necessary to meet the evolving needs of naval technology. Appointments are for 1 year (renewable for a second and sometimes a third year). These competitive appointments are made jointly by NRL and ASEE.

• The American Society for Engineering Education also administers the Navy/ASEE **Summer Faculty Research and Sabbatical Leave Program** for university faculty members to work for 10 weeks (or longer, for those eligible for sabbatical leave) with professional peers in participating Navy laboratories on research of mutual interest.

• **The NRL/United States Naval Academy (USNA) Cooperative Program for Scientific Interchange** allows faculty members of the U.S. Naval Academy to participate in NRL research. This collaboration benefits the Academy by providing the opportunity for USNA faculty members to work on research of a more practical or applied nature. In turn, NRL's research program is strengthened by the available scientific and engineering expertise of the USNA faculty.

• The **National Defense Science and Engineering Graduate Fellowship Program** helps U.S. citizens obtain advanced training in disciplines of science and engineering critical to the U.S. Navy. The 3-year program awards fellowships to recent outstanding graduates to support their study and research leading to doctoral degrees in specified disciplines such as electrical engineering, computer sciences, material sciences, applied physics, and ocean engineering. Award recipients are encouraged to continue their study and research in a Navy laboratory during the summer.

For further information about the above five programs, contact Ms. Leslie Renfro at (202) 404-7450.

PROFESSIONAL APPOINTMENTS

• **Faculty Member Appointments** use the special skills and abilities of faculty members for short periods to fill positions of a scientific, engineering, professional, or analytical nature.

• **Consultants and experts** are employed because they are outstanding in their fields of specialization or because they possess ability of a rare nature and could not normally be employed as regular civil servants.

• **Intergovernmental Personnel Act Appointments** temporarily assign personnel from the state or local government or educational institution to the Federal Government (or vice versa) to improve public services rendered by all levels of government.

STUDENT PROGRAMS

The student programs are tailored to the undergraduate and graduate students to provide employment opportunities and work experience in naval research. These programs are designed to attract applicants for student and full professional employment in fields such as engineers, physicists, mathematicians, and computer scientists. The student employment programs are designed to help students and the educational institutions gain a better understanding of NRL's research, its challenges, and its opportunities. The employment programs for college students include the following:

• The **Student Career Experience Program** (formerly known as Cooperative Education Program) employs students in study-related occupations. The program is conducted in accordance with a planned schedule and a working agreement among NRL, the educational institution, and the student. Primary focus is on the pursuit of bachelors degrees in engineering, computer science, or the physical sciences.

• The **Student Temporary Employment Program (STEP)** enables students to earn a salary while continuing their studies and offers them valuable work experience.

• The **Summer Employment Program** employs students for the summer in paraprofessional and technician positions in engineering, physical sciences, computer sciences, and mathematics.

• The **Student Volunteer Program** helps students gain valuable experience by allowing them to voluntarily perform educationally related work at NRL.

For additional information on these undergraduate and graduate college student programs, contact the Staffing Branch, Code 1810 at (202) 767-8313.

HIGH SCHOOL PROGRAMS

• The **DoD Science & Engineering Apprentice Program** (SEAP) employs high school juniors and seniors to serve for 8 weeks as junior research associates. Under the direction of a mentor, students gain a better understanding of research, its challenges, and its opportunities through participation in scientific programs. Criteria for eligibility are based on science and mathematics courses completed and grades achieved; scientific motivation, curiosity, and capacity for sustained hard work; a desire for a technical career; teacher recommendations; and achievement test scores. The NRL Program is the lead program and the largest in DoD.

For additional information, contact the Employee Development Branch (Code 1840) at (202) 767-2956.

The Marine Meteorology Division in Monterey, California, hosted Ms. Amy Hellam, a summer student from the local Monterey Academy of Oceanographic Science. She completed 90 hours of study, focusing on the evolution of low clouds and fog along the central California coast using real-time Geostationary Operational Earth Satellite (GOES-9) data collected at NRL Monterey.

General Information

Technical Output

The Navy continues to be a pioneer in initiating new developments and a leader in applying these advancements to military requirements. The primary method of informing the scientific and engineering community of the advances made at NRL is through the Laboratory's technical output — reports, articles in scientific journals, contributions to books, papers presented to scientific societies and topical conferences, patents, and inventions.

The figures for calendar year 1996 presented below represent the output of NRL facilities in Washington, D.C.; Bay St. Louis, Mississippi; and Monterey, California.

In addition to the output listed, NRL scientists made more than 1380 oral presentations during 1996.

A complete listing of the publications by NRL authors appears in the *Bibliography of NRL Publications*, a separate annual publication.

Type of Contribution	Unclassified	Classified	Total
Articles in periodicals, chapters in books, and papers in published proceedings	1133	0	1133*
NRL Formal Reports	26	16	42
NRL Memorandum Reports	106	24	130
Books	0		0
Patents granted			62
Statutory Invention Registrations (SIRs)			5

*This is a provisional total based on information available to the Ruth H. Hooker Research Library and Technical Information Center on January 10, 1997. Additional publications carrying a 1996 publication date are anticipated.

Technology Transfer at NRL

There are many ways for private companies to benefit from the technical resources of NRL. Some of these include: (1) entering into Cooperative Research and Development Agreements (CRADAs), (2) obtaining licenses for Navy-owned patents, and (3) consulting with NRL scientists and engineers.

Entering into a CRADA is an excellent way for U.S. companies to gain access to commercially important NRL research and development (R&D) technology. Authorized under the Federal Technology Transfer Act of 1986, a CRADA is an agreement between one or more federal laboratories and one or more nonfederal parties, such as private companies. Designed to encourage and facilitate cooperative R&D, CRADAs can involve research in any area that is consistent with NRL's mission.

Additionally, the Federal Government can license its own inventions. NRL has developed many new technologies and processes in areas as diverse as advanced materials, chemistry, biotechnology, optics, ocean and atmospheric sciences, and electronics. NRL currently has over 500 patents available for license in these fields.

As the Navy's corporate laboratory, NRL draws on the powerful resources of an interdisciplinary combination of scientific expertise and modern facilities. NRL's technical staff is recruited from all disciplines of engineering and the physical sciences and is available to work with private companies to help them solve their technical problems. Many of the staff have received the Award for Excellence in Technology Transfer from the Federal Laboratory Consortium (FLC). This award recognizes employees who have accomplished outstanding work in the process of transferring laboratory-developed technology.

During 1996, new products have been introduced from NRL technology by the private sector. For instance, NRL's Explosive and Contraband Detector was licensed by Quantum Magnetics. This instrument uses nuclear quadruple resonance (NQR) to detect nitrogenous explosives or narcotics carried in luggage, mail, small cargo, or on a person.

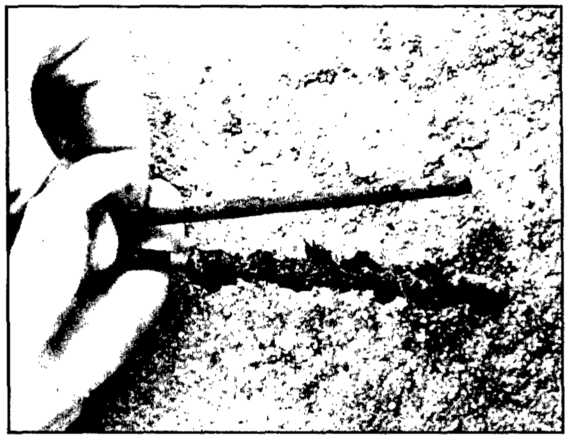

A demonstration of the NRL controlled-release antifouling coating technology. The upper rod is coated with a paint containing the NRL microtubule-based antifouling additive; the lower rod is coated with the same paint, but without the NRL antifouling additive. After extended exposure to a marine environment, the effectiveness of the NRL antifouling additive is clear; the top rod shows little coverage by fouling organisms, and the bottom rod shows extensive coverage.

Biocompatible, LTD, a United Kingdom-based company, licensed NRL's controlled-release antifouling paint additive. The paint additive is microtubles (0.5 micron diameter and 10-150 microns in length), which have proven effective for the controlled release of biocides. The antifouling coatings incorporating this additive rely on the tubule microstructure to both entrap biocides and control their release.

For additional information, contact NRL's Technology Transfer Office, 4555 Overlook Ave., S.W., Washington, DC 20375-5320, or call (202) 404-7920; e-mail: techtransfer@nrl.navy.mil; URL: http://infonext.nrl.navy.mil/~techtran/.

Key Personnel

Area Code (202) unless otherwise listed
Personnel Locator - 767-3200
DSN-297 or 754

Code	Office		Phone Number
	EXECUTIVE DIRECTORATE		
1000	Commanding Officer	CAPT B.W. Buckley, USN	767-3403
1000.1	Inspector General	CAPT R.E. Leonard, USN	767-3621
1001	Director of Research	Dr. T. Coffey	767-3301
1001.1	Scientific Staff Assistant	Dr. K.W. Lackie	767-2880
1002	Chief Staff Officer	CAPT R.E. Leonard, USN	767-3621
1004	Head, Technology Transfer	Dr. R. Rein	767-7230
1006	Head, Office of Program Administration and Policy Development	Ms. L. McDonald	767-3091
1200	Head, Command Support Division	Mr. J.C. Payne	767-3048
1220	Head, Security	Dr. J.T. Miller	767-0793
1230	Public Affairs Officer	Mr. R. Baturin	767-2541
1240	Head, Safety Branch	Mr. K.J. King	767-2232
1400	Head, Military Support Division	CDR R. Francisco, USN	767-2271
1600	Officer-in-Charge, Flight Support Detachment	CDR D.R. Dowell, USN	301-342-3751
1800	Director, Human Resources Office	Ms. B.A. Duffield	767-3421
1803	Deputy EEO Officer	Ms. D. Erwin	767-2486
3204	Deputy for Small Business	Ms. P. Schaefer	767-6263
	BUSINESS OPERATIONS DIRECTORATE		
3000	Associate Director of Research	Mr. R.E. Doak	767-2371
3008	Office of Counsel	Ms. H.J. Halper	767-2244
3030	Head, Management Information Systems Staff	Mr. R.L. Guest	767-2030
3200	Head, Contracting Division	Mr. J.C. Ely	767-5227
3300	Comptroller, Financial Management Division	Mr. D. Therning	767-3405
3400	Supply Officer	Ms. C. Hartman	767-3446
3500	Director, Research and Development Services Division	Mr. S. Harrison	767-3697
	SYSTEMS DIRECTORATE		
5000	Associate Director of Research	Dr. R.A. LeFande	767-3324
5200	Head, Technical Information Division	Mr. P.H. Imhof	767-2187
5300	Superintendent, Radar Division	Dr. G.V. Trunk (Acting)	767-2573
5500	Superintendent, Information Technology Division	Dr. R.P. Shumaker	767-2903
5600	Superintendent, Optical Sciences Division	Dr. T.G. Giallorenzi	767-3171
5700	Superintendent, Tactical Electronic Warfare Division	Dr. J.A. Montgomery	767-6278
	MATERIALS SCIENCE AND COMPONENT TECHNOLOGY DIRECTORATE		
6000	Associate Director of Research	Dr. B.B. Rath	767-3566
6030	Head, Laboratory for Structure of Matter	Dr. J. Karle	767-2665
6100	Superintendent, Chemistry Division	Dr. J.S. Murday	767-3026
6300	Superintendent, Materials Science & Technology Division	Dr. D.U. Gubser	767-2926
6400	Director, Lab. for Computational Physics and Fluid Dynamics	Dr. J.P. Boris	767-3055
6600	Superintendent, Condensed Matter & Radiation Sciences Division	Dr. D.J. Nagel	767-2931
6700	Superintendent, Plasma Physics Division	Dr. S. Ossakow	767-2723
6800	Superintendent, Electronics Science & Technology Division	Dr. G.M. Borsuk	767-3525
6900	Director, Center for Bio/Molecular Sciences and Engineering	Dr. J.M. Schnur	404-6000
	OCEAN AND ATMOSPHERIC SCIENCE AND TECHNOLOGY DIRECTORATE		
7000	Associate Director of Research	Dr. E.O. Hartwig	404-8690
7030	Head, Office of Research Support Services	Mr. G. Bower	601-688-4010
7100	Superintendent, Acoustics Division	Dr. E.R. Franchi	767-3482
7200	Superintendent, Remote Sensing Division	Dr. P. Schwartz	767-3391
7300	Superintendent, Oceanography Division	Dr. W.B. Moseley	601-688-4670
7400	Superintendent, Marine Geosciences Division	Dr. H.C. Eppert, Jr.	601-688-4650
7500	Superintendent, Marine Meteorology Division	Dr. T.L. Tsui (Acting)	408-656-4721
7600	Superintendent, Space Science Division	Dr. H. Gursky	767-6343
	NAVAL CENTER FOR SPACE TECHNOLOGY		
8000	Director	Mr. P.G. Wilhelm	767-6547
8100	Superintendent, Space Systems Development Department	Mr. R.E. Eisenhauer	767-0410
8200	Superintendent, Spacecraft Engineering Department	Mr. H.E. Senasack, Jr.	767-6411

Employment Opportunities for Entry-Level and Experienced Personnel

The *NRL Review* illustrates some of the exciting science and engineering carried out at the Naval Research Laboratory, as well as the potential for new personnel. In this regard, NRL offers a wide variety of challenging positions that involve the full range of work, from basic and applied research to equipment development. The nature of the research and development conducted at NRL requires professionals with experience. Typically there is a continuing need for electronics, mechanical, aerospace, ceramic and materials engineers, metallurgists, computer scientists, and oceanographers with bachelor's and/or advanced degrees and physical and computer scientists with Ph.D. degrees. Opportunities exist in the areas described below:

Ceramic Engineers and Materials Scientists/ Engineers. These employees are recruited to work on materials, microstructure characterization, electronic ceramics, solid-state physics, fiber optics, electro-optics, microelectronics, fracture mechanics, vacuum science, laser physics technology, and radio frequency/microwave/millimeter wave/ infrared technology.

Electronics Engineers and Computer Scientists. These employees may work in the areas of communications systems, electromagnetic scattering, electronics instrumentation, electronic warfare systems, radio frequency/microwave/ millimeter wave/infrared technology, radar systems, laser physics technology, radio-wave propagation, electron device technology, spacecraft design, artificial intelligence, information processing, signal processing, plasma physics, vacuum science, microelectronics, electro-optics, fiber optics, solid state, software engineering, computer design/architecture, ocean acoustics, stress analysis, and expert systems.

Mechanical Engineers. These employees may be assigned to spacecraft design, remote sensing, propulsion, experimental fluid mechanics, experimental structural mechanics, solid mechanics, elastic/plastic fracture mechanics, materials, finite-element methods, nondestructive evaluation, characterization of fracture resistance of structural alloys, combustion, and CAD/CAM.

Chemists. Chemists are recruited to work in the areas of combustion, polymer science, bioengineering and molecular engineering, surface science, materials, fiber optics, electro-optics, microelectronics, electron-device technology, and laser physics.

Physicists. Physics graduates may concentrate on such fields as materials, solid-state physics, fiber optics, electro-optics, microelectronics, vacuum science, plasma physics, fluid mechanics, signal processing, ocean acoustics, information processing, artificial intelligence, electron-device technology, radio-wave propagation, laser physics, ultraviolet/X-ray/gamma-ray technology, electronic warfare, electromagnetic interaction, communications systems, radio frequency/microwave/millimeter wave/infrared technology, and computational physics.

Oceanographers, Meteorologists, and Marine Geophysicists. These employees work in the areas of ocean dynamics, air-sea interaction, upper-ocean dynamics, oceanographic bio-optical modeling, oceanic and atmospheric numerical modeling and prediction, artificial intelligence applications for satellite analyses, benthic processes, aerogeophysics, marine sedimentary processes, and advanced mapping techniques. Oceanographers and marine geophysicists are located in Washington, D.C., and the Stennis Space Center,

Bay St. Louis, Mississippi. Meteorologists are located in Washington, D.C., and Monterey, California.

APPLICATION AND INFORMATION

Interested applicants should submit an Application for Federal Employment (SF-171), an Optional Application for Federal Employment (OF-612), or a resume. The OF-612 and SF-171 can be obtained from local Office of Personnel Management and Human Resource Offices of federal agencies.

Direct inquiries to:

Naval Research Laboratory
Human Resources Office, Code 1810 RV
Washington, DC 20375-5324
(202) 767-3030

Location of NRL in the Capital Area

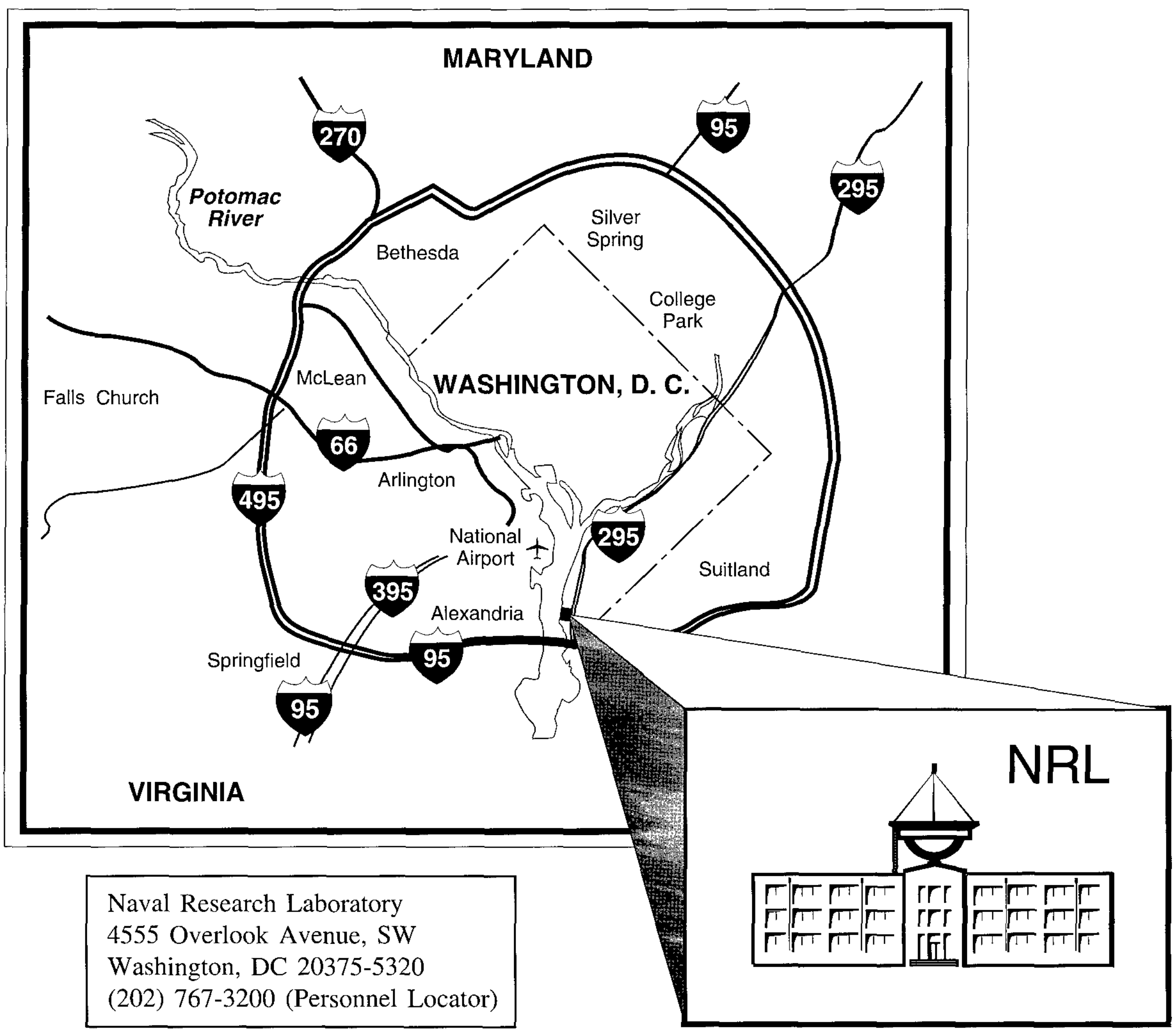

Naval Research Laboratory
4555 Overlook Avenue, SW
Washington, DC 20375-5320
(202) 767-3200 (Personnel Locator)

Contributions by Divisions, Laboratories, and Departments

Subject Index

Author Index

NRL Review Staff

Senior Science Editor:	*Dr. John D. Bultman*
TID Editor:	*Jonna Atkinson*
Assistant TID Editor:	*Patricia Staffieri*
TID Consultants:	*Kathleen Parrish and Timothy Calderwood*

Computerized composition and design: *Donna Gloystein and Judy Kogok*

Graphic support: *Jan Morrow, Jonna Atkinson, Suzanne Guilimineau, Cindy Allen, Carol Hambric, Cathy Johnson, and Darlene DeMarr*

Historical update: *Dr. David van Keuren*

Photographic production: *Richard Bussey, Gayle Fullerton, James Marshall, and Michael Savell*

Production assistance: *Rosie Bankert, Diltricia Montgomery, Leona Sprankel, and Paul Sweeney*

Distribution: *Barbara Jolliffe*

Head, Technical Information Division: Peter H. Imhof

REVIEWED AND APPROVED
NRL/PU/5230--97-320
April 1997

Bruce W. Buckley
Captain, USN
Commanding Officer